



Technische Universität München

Ingenieurfacultät Bau Geo Umwelt

Lehrstuhl für Hydrologie und Flussgebietsmanagement

**Simulating Hydrogeomorphological Processes to
Assess Land Degradation in the Upper Blue Nile Basin
in Ethiopia Using SWAT**

Erwin Isaac Alvarez Polanco

Vollständiger Abdruck der von der Ingenieurfacultät Bau Geo Umwelt der Technische Universität München zur Erlangung des akademischen Grades eines

Doktor-Ingenieurs (Dr.-Ing.)

genehmigten Dissertation.

Vorsitzender: Prof. Dr.sc.techn. Peter Rutschmann

Prüfer der Dissertation:

1. Prof. Dr.-Ing. Markus Disse
2. Prof. Dr.rer.nat. Ralf Ludwig (Ludwig-Maximilians-Universität München)
3. Prof. Dr.Ir. Tammo Steenhuis (Cornell University, United States of America)

Die Dissertation wurde am 10.08.2017 bei der Technischen Universität München eingereicht und durch die Ingenieurfacultät Bau Geo Umwelt am 11.10.2017 angenommen.



Technische Universität München

Ingenieurfacultät Bau Geo Umwelt

**Lehrstuhl für Hydrologie und
Flussgebietsmanagement**

Doktorarbeit

**Simulation von Hydrogeomorphologischen
Prozessen zur Abschätzung der
Bodendegradation im Einzugsgebiet des Oberen
Blauen Nils in Äthiopien mittels SWAT**

Erwin Isaac Polanco

München, August 2017



Technical University of Munich

**Department of Civil, Geo and Environmental
Engineering**

Chair of Hydrology and River Basin Management

Doctoral Dissertation

**Simulating Hydrogeomorphological Processes to
Assess Land Degradation in the Upper Blue Nile
Basin in Ethiopia Using SWAT**

Erwin Isaac Polanco

Munich, August 2017

**Technische Universität München
Ingenieur fakultät Bau Geo und Umwelt
Lehrstuhl für Hydrologie und Flussgebietsmanagement
Prof. Dr.-Ing. Markus Disse**

Simulating Hydrogeomorphological Processes to Assess Land Degradation in the Upper Blue Nile Basin in Ethiopia Using SWAT

Doctoral Dissertation

by
Erwin Isaac Polanco

in partial fulfillment of the requirements for the degree of
Doktor-Ingenieur (Dr.-Ing.)

at
Technische Universität München

Supervisors:
Prof. Dr.-Ing. Markus Disse
(Technische Universität München)
Prof. Dr.rer.nat. Ralf Ludwig
(Ludwig-Maximilians-Universität München)
Prof. Dr. Ir. Tammo Steenhuis
(Cornell University)

DECLARATION OF AUTHORSHIP

I certify that this dissertation is the result of my own work, except where otherwise acknowledged. This doctoral dissertation was not previously presented to another examination board.

Doctoral candidate's signature

Munich, August 1st, 2017

Parts of this dissertation have been published in the following journal article:

Polanco, E. I., Fleifle, A., Ludwig, R., and Disse, M.: Improving SWAT model performance in the upper Blue Nile Basin using meteorological data integration and subcatchment discretization, *Hydrol. Earth Syst. Sci.*, 21, 4907-4926, <https://doi.org/10.5194/hess-21-4907-2017>, 2017.

ACKNOWLEDGEMENTS

I would like to express my sincere gratitude to the government of the Federal Republic of Germany for giving me the opportunity to pursue my doctoral degree. This research has been possible thanks to the financial support of the German Academic Exchange Service (Deutscher Akademischer Austauschdienst-DAAD) and the International Graduate School of Science and Engineering (IGSSE) of the Technische Universität München (TUM). I would also like to thank my supervisors Prof. Dr.-Ing. Markus Disse (TUM), Prof. Dr. rer. nat. Ralf Ludwig (LMU) and Prof. Dr. Ir. Tammo Steenhuis for their close and continuous support, guidance and motivation during my studies.

Moreover, I would like to thank my mother Miriam Polanco Portillo for guiding, advising and encouraging me to continue studying and working hard towards my goals. I would also like to thank my brother Moises Alberto, who have been very important person in my life providing support in my everyday life. Finally I would like to thank all of my friends who have helped me before and during my studies in Germany.

CONTENT

LIST OF FIGURES	i
LIST OF TABLES	v
LIST OF APPENDICES	vii
ACRONYMS AND ABBREVIATIONS	ix
ZUSAMMENFASSUNG	xi
ABSTRACT	xii

1. INTRODUCTION

1.1 Statement of the problem and content of the research	1
1.2 Hypotheses and objectives the research	4

2. DESCRIPTION OF THE RESEARCH AREA AND THEORETICAL BACKGROUND

2.1 The Blue Nile Basin	6
2.1.1 Ethiopia and the Blue Nile River.....	6
2.1.2 Location and political administration of the upper Blue Nile Basin.....	7
2.1.3 Soils.....	10
2.1.4 Land use.....	13
2.1.5 Topography.....	15
2.1.6 Climate.....	15
2.1.7 Irrigation systems, dams and reservoirs.....	20
2.2 Hydrological modelling: Theoretical background	22
2.2.1 Soil and Water Assessment Tool (SWAT).....	22
2.2.2 Spatial representation and basin configuration in SWAT.....	23
2.2.3 The hydrologic cycle, water balance and evapotranspiration processes in SWAT.....	24
2.2.4 Soil erosion.....	31
2.2.5 Soil erosion and sediment estimations in SWAT.....	34
2.2.6 Calibration and validation of hydrological models.....	43
2.2.7 SWAT calibration parameters.....	48
2.2.8 Sediment rating curves.....	49

3. METHODOLOGY

3.1 Input data and SWAT model setup	54
3.1.1 Analysis of the weather datasets, processing and integration...	55
3.2 Effects of different sub-basins and HRUs discretization	

on sediment estimations.....	62
3.2.1 Sub-basins selection and description.....	65
3.2.2 Sub-basin delineations, sediment concentration and sediment yield.....	67
3.2.3 Sediment concentration rating curves for the Blue Nile Basin.....	77
3.3 Weather datasets vs. sub-basins discretization.....	81
3.3.1 Parameterization.....	81
3.3.2 Effects of different sub-basin discretization levels and rain gauge combinations on the water balance of the upper Blue Nile Basin.....	82
3.3.3 Average annual evapotranspiration analysis and the effects of different PET methods.....	86
3.4 SWAT Error Index (SEI).....	89
4. RESULTS	
4.1 Final SWAT model for the upper Blue Nile Basin.....	91
4.1.1 Parameterization, calibration and validation of SWAT at Eldiem and Kessie for the period 1988-1933.....	92
4.1.2 Parameterization, calibration and validation of SWAT at Eldiem and Kessie for the period 1994-2004.....	95
4.1.3 Calibration and validation of SWAT at several sub-catchments of the Blue Nile Basin for the period 1988-2004.....	99
4.1.4 Parameterization and comparison of SWAT sediment concentrations and the sediment rating curves for the period 1988-2004.....	101
4.2 Evaluation of the SWAT Error Index (SEI).....	103
4.3 Erodible areas predicted by SWAT at HRU level.....	106
5. CONCLUSIONS AND RECOMMENDATIONS	
5.1 Major findings and limitations of the study.....	114
5.2 Implications and conservation practices.....	115
5.3 Contributions and final conclusions of the research.....	116
APPENDICES.....	117
LIST OF REFERENCES.....	127

LIST OF FIGURES

Figure 1. Location of Ethiopia.....	6
Figure 2. Administrative regional states in the upper Blue Nile Basin.....	8
Figure 3. Administrative zones in the upper Blue Nile Basin.....	8
Figure 4. Weredas in the upper Blue Nile Basin.....	9
Figure 5. Official sub-basin distribution in the upper Blue Nile Basin.....	9
Figure 6. Soils map of the upper Blue Nile Basin (FAO, 2014).....	11
Figure 7. Land use map of the upper Blue Nile Basin (ILRI, 2004).....	13
Figure 8. Digital Elevation Model of the upper Blue Nile Basin (CGIAR-CSI).....	15
Figure 9. Spatial annual rainfall distribution in the upper Blue Nile Basin (Abtew et al., 2009).....	17
Figure 10. Average monthly precipitation in the upper Blue Nile Basin (Hassan, 2012).....	18
Figure 11. Average monthly minimum temperatures in the upper Blue Nile Basin (Hassan, 2012).....	19
Figure 12. Average monthly maximum temperatures in the upper Blue Nile Basin (Hassan, 2012).....	19
Figure 13. Location of the proposed dam constructions in the upper Blue Nile Basin.....	21
Figure 14. HRU/Sub-basin command loop of the spatial representation in SWAT (Neitsch et al. 2009).....	23
Figure 15: Hydrologic cycle in SWAT (Neitsch et al., 2009).....	25
Figure 16. In-stream processes modeled by SWAT (Neitsch et al., 2009).....	29
Figure 17. Factors contributing to soil erosion by water in the Blue Nile Basin (FAO, 1986).....	32
Figure 18. Types of soil structures in soils (McClellan, 2016).....	37
Figure 19. Workflow diagram.....	53
Figure 20. Weather and hydrometric gauging stations in the upper Blue Nile Basin under two discretization levels, 30 and 87 sub-basins (SWAT30 and SWAT87).....	57
Figure 21. Spatial annual rainfall variation in the upper Blue Nile Basin using the CFSR dataset (Polanco et al., 2017).....	59
Figure 22. Spatial annual rainfall variation in the upper Blue Nile Basin using the Ground dataset (Polanco et al., 2017)	59

Figure 23. Comparisons between the Ground and CFSR weather datasets. A, B and C are average monthly precipitation; D, E and F are average monthly relative humidity; G and H are average monthly maximum temperatures; I and J are average monthly solar radiation; K and L are average monthly wind speed (Polanco et al., 2017)	60
Figure 24. Significance of matching between the Ground and CFSR weather datasets. A, B and C are average monthly precipitation; D, E and F are average monthly relative humidity; G and H are average monthly maximum temperatures; I and J are average monthly solar radiation; K and L are average monthly wind speed (Polanco et al., 2017).....	61
Figure 25. Hydrologic Response Unit (HRU) area distributions and impact of threshold area At on HRU specific sediment yields. a) Distribution of HRUs area in the Upper Danube Basin derived from the initial GIS inputs overlay (initial), and as modeled using one dominant HRU per sub-basin (modeled); b) ratio of HRU mean annual MUSLE specific sediment yields (HSSY; t/ha/year) to mean annual USLE gross erosion (GE, t/ha/year) for the simulation period (1995–2009) at increasing threshold areas At. The gray lines indicate a ratio of 1, i.e. where HSSY and GE are equal (Vigiak et al., 2015).....	64
Figure 26. Location of Gumara, Ribb and Beressa sub-catchments in the Blue Nile Basin.....	67
Figure 27. Sub-basins and HRUs distributions at Gumara catchment: A) 1Sub-71HRUs, B) 5Sub-147HRUs, C) 19Sub-296HRUs, D) 23Sub-356HRUs, E) 33Sub-421HRUs, F) 51Sub-545 HRUs, G) 75Sub-717HRUs, H) 585Sub-2765HRUs.....	71
Figure 28. Results at Gumara catchment for the period 1992-2007: A) Sediment concentration, B) Sediment yield, C) Flow discharge, D) HRUs vs. resolution.....	72
Figure 29. Sub-basins and HRUs distributions at Ribb catchment: A) 3 Sub-112HRUs, B) 13Sub-280HRUs, C) 31Sub-492HRUs, D) 51Sub-625HRUs, E) 75Sub-763HRUs, F) 91Sub-880 HRUs, G) 115Sub-997HRUs, H) 604Sub-2896HRUs.....	73
Figure 30. Results at Ribb catchment for the period 1992-2007: A) Sediment concentration, B) Sediment yield, C) Flow discharge, D) HRUs vs. resolution.....	74
Figure 31. Sub-basins and HRUs distributions at Beressa catchment: A) 7Sub-95HRUs, B) 15Sub-144HRUs, C) 54Sub-332HRUs, D) 56Sub-350HRUs, E) 68Sub-405HRUs, F) 155Sub-741HRUs.....	75
Figure 32. Results at Debre Birhan in the Beressa catchment for the period 1992-2007: A) Sediment concentration, B) Sediment yield, C) Flow discharge, D) HRUs vs. resolution.....	76

Figure 33. Interpretation of the relationship between sediment concentrations and cumulative effective rainfall proposed by Moges et al. (2016)	78
Figure 34. Calibration and validation of SWAT30 at Eldiem. Calibration results achieved R ² and NS values of: Integrated data: 0.88, 0.84; Ground data: 0.86, 0.74; CFSR data: 0.94, -0.51; respectively. Validation results achieved R ² and NS values of: Integrated data: 0.92, 0.91; Ground data: 0.96, 0.45; CFSR data: 0.92, -0.48; respectively (Polanco et al., 2017).....	84
Figure 35. Calibration and validation of SWAT87 at Eldiem. Calibration results achieved R ² and NS values of: Integrated data: 0.92, 0.80; Ground data: 0.92, 0.43; CFSR data: 0.96, -1.54; respectively. Validation results achieved R ² and NS values of: Integrated data: 0.94, 0.91; Ground data: 0.95, 0.85; CFSR data: 0.89, -0.05; respectively (Polanco et al., 2017).....	84
Figure 36. Calibration and validation of SWAT30 at Kessie. Calibration results achieved R ² and NS values of: Integrated data: 0.74, 0.74; Ground data: 0.74, 0.72; CFSR data: 0.87, 0.46, respectively. Validations results achieved R ² and NS values of: Integrated data: 0.76, 0.74; Ground data: 0.78, 0.74; CFSR data 0.86, 0.49; respectively (Polanco et al., 2017).....	85
Figure 37. Calibration and validation of SWAT87 at Kessie. Calibration results achieved R ² and NS values of: Integrated data: 0.77, 0.72; Ground data: 0.77, 0.72; CFSR data 0.77, 0.37; respectively. Validations results achieved R ² and NS values of Integrated data: 0.78, 0.78; Ground data: 0.80, 0.76; CFSR data 0.74, 0.37; respectively (Polanco et al., 2017).....	85
Figure 38. Average monthly evapotranspiration analysis using SWAT with 87 sub-basins and the Hargreaves method, with R ² and NS values of Integrated data: 0.63, -2.32; ground data: 0.60, -1.32; CFSR data: 40, 0.63, -1.20; respectively, compared to the MOD16 data (Polanco et al., 2017).....	88
Figure 39. Average monthly evapotranspiration analysis using SWAT with 87 sub-basins and the Penman-Monteith method, with R ² and NS values of Integrated data: 0.36, -0.02; ground data: 0.34, -0.10; CFSR data: 0.74, 0.03; respectively, compared to the MOD16 data (Polanco et al., 2017).....	88
Figure 40. Flow and sediment gauging stations in the upper Blue Nile Basin.....	92
Figure 41. Calibration and validation results at Eldiem with SWAT99Integrated for the period 1988-1993.....	94
Figure 42. Calibration and validation results at Kessie with SWAT99Integrated for the period 1988-1992.....	95
Figure 43. Calibration and validation results at Eldiem with SWAT99Integrated for the period 1994-2004.....	97
Figure 44. Calibration and validation results at Kessie with SWAT99Integrated for the period 1994-2004.....	99

Figure 45. Calibration and validation results at Gilgel Abay with SWAT99Integrated for the period 1988-2004.....	100
Figure 46. Calibration and validation results at Ardy with SWAT99Integrated for the period 1988-2004.....	100
Figure 47. Sediment concentrations (mg/kg) at Eldiem station.....	102
Figure 48. Sediment concentrations (mg/kg) at Gilgel Abay catchment.....	102
Figure 49. Sediment concentrations (mg/kg) at Ardy catchment.....	102
Figure 50. Flow discharge in the Ribb sub-catchment. Calibration with outflow data achieved R ² and NS values of CFSR data: 0.81, 0.75 and Ground data: 0.85, 0.83; respectively (Polanco et al., 2017).....	104
Figure 51. Average monthly evapotranspiration in the Ribb sub-catchment. Statistical results achieved R ² and NS values of CFSR data: 0.78, 0.47 and Ground data: 0.59, 0.24; respectively, compared to the MOD16 data (Polanco et al., 2017).....	104
Figure 52. Sediment yield in the upper Blue Nile Basin for the period 1988-1990....	112
Figure 53. Sediment yield in the upper Blue Nile Basin for the period 1991-1995....	112
Figure 54. Sediment yield in the upper Blue Nile Basin for the period 1996-2000....	113
Figure 55. Sediment yield in the upper Blue Nile Basin for the period 2001-2004....	113
Figure 56. Slope classes in the upper Blue Nile Basin.....	114
Figure 57. Relative erosion prone areas (predicted sediment yield at each HRU by the SWAT model) for existing conditions in the upper Blue Nile Basin (Betrie et al., 2011).....	115
Figure 58. Average annual soil loss estimated by SWAT for Lake Tana basin between 1997 and 2003 (Konnerth, 2016).....	115
Figure 59. Average annual sediment yield in the upper Blue Nile Basin for the period 1988-2004 without management practices.....	117
Figure 60. Average annual sediment yield in the upper Blue Nile Basin for the period 1988-2004 with management practices.....	117

LIST OF TABLES

Table 1. Official sub-basin distribution in the upper Blue Nile Basin, considering Dinder and Rahad sub-catchments shared with Sudan (MWRI, Addis Ababa, 2006).....	10
Table 2. Soil types and distribution in the upper Blue Nile Basin based on the “Soil and Terrain Database for Northeast Africa” (FAO-UNESCO, 2014).....	11
Table 3. Land cover in the upper Blue Nile Basin (ILRI, 2004).....	14
Table 4. Potential irrigation schemes in the Blue Nile Basin (Hassan, 2012).....	20
Table 5. Existing and proposed dams in the upper Blue Nile Basin	21
Table 6: P_{USLE} factors and slope-length limits for contouring (Wischmeier and Smith, 1978).....	38
Table 7: General performance ratings for the coefficient of determination (R^2), Nash–Sutcliffe efficiency (NS), mean relative bias (PBIAS) and the root mean square error-standard deviation (RSR) for a monthly time step (Moriassi et al., 2007).....	47
Table 8. Average annual water balance components of the upper Blue Nile Basin based on different literature.....	56
Table 9. Sub-basins, HRUs and resolution portion for Gumara catchment.....	69
Table 10. Sub-basins, HRUs and resolution portion for Ribb catchment.....	70
Table 11. Sub-basins, HRUs and resolution portion for Beressa catchment.....	70
Table 12. Calibrated sediment rating curve parameters and the specific dates where the sediment transport ends and the sediment limiting phase starts (Moges et al. 2016).....	80
Table 13. Calibrated sediment rating curve parameters for 7 sub-catchments in the upper Blue Nile Basin.....	80
Table 14. Parameterization of the SWAT models using the SUFI-2 algorithm for the period 1994-2004 (Polanco et al., 2017).....	82
Table 15. Water balance analysis in the upper Blue Nile Basin for the period 1994-2004 (Polanco et al., 2017).....	83
Table 16. Statistical results for the calibrations and validations with outflow data at Eldiem and Kessie gauging stations (Polanco et al., 2017).....	86
Table 17. Factors influencing the main SWAT parameterization changes for different periods in the upper Blue Nile Basin.....	92
Table 18. Parameterization of SWAT99Integrated using the SUFI-2 algorithm	

for the period 1988-1993.....	93
Table 19. Statistical results for the calibration and validation with outflow data at the Eldiem gauging station.....	94
Table 20. Parameterization of SWAT99Integrated for the calibration at Kessie for the period 1988-1993.....	95
Table 21. Statistical results for the calibrations and validations with outflow data at Eldiem and Kessie gauging stations.....	96
Table 22. Parameterization of SWAT99Integrated for the calibration at Eldiem for the period 1994-2004.....	97
Table 23. Statistical results for the calibration and validation with outflow data at Eldiem gauging station.....	98
Table 24. Parameterization of SWAT99Integrated at Kessie for the period 1994-2004.....	98
Table 25. Statistical results for the calibration and validation with outflow data at Eldiem and Kessie gauging stations.....	99
Table 26. Statistical results for the calibration with outflow data at several sub-catchments in the upper Blue Nile Basin.....	101
Table 27. SWAT Error Index results for the upper Blue Nile Basin (Polanco et al., 2017).....	103
Table 28. Statistical results for the Ribb sub-catchment in the Lake Tana region of the Blue Nile Basin (Polanco et al., 2017)	105
Table 29. Soil erosion rates in the Blue Nile Basin grouped by land use, soil type and slope classes for the period 1988-2004.....	106
Table 30. Soil erosion rates in different subbasins of the upper Blue Nile Basin.....	116

LIST OF APPENDICES

Appendix 1. Calibration and validation results at Gumara with SWAT99Integrated for the period 1992-2004. Statistical results achieved R ² values of 0.83 and 0.76 for the calibration and validation, respectively; and NS values of 0.82 and 0.78 for the calibration and validation, respectively.	122
Appendix 2. Sediment concentrations (mg/kg) at Gumara catchment.....	122
Appendix 3. Calibration and validation results at Ribb with SWAT99Integrated for the period 2001-2004. Statistical results achieved R ² values of 0.92 and 0.94 for the calibration and validation, respectively; and NS values of 0.88 and 0.93 for the calibration and validation, respectively.	123
Appendix 4. Sediment concentrations (mg/kg) at Ribb catchment.....	123
Appendix 5. Calibration and validation results at Azuari with SWAT99Integrated for the period 1988-2004. Statistical results achieved R ² values of 0.61 and 0.78 for the calibration and validation, respectively; and NS values of 0.53 and 0.51 for the calibration and validation, respectively..	124
Appendix 6. Sediment concentrations (mg/kg) at Azuari catchment.....	124
Appendix 7. Calibration and validation results at Chena with SWAT99Integrated for the period 1996-2004. Statistical results achieved R ² values of 0.53 and 0.64 for the calibration and validation, respectively; and NS values of 0.40 and 0.47 for the calibration and validation, respectively.	125
Appendix 8. Sediment concentrations (mg/kg) at Chena catchment.....	125
Appendix 9. Calibration and validation results at Muga with SWAT99Integrated for the period 2001-2004. Statistical results achieved R ² values of 0.67 and 0.7 for the calibration and validation, respectively; and NS values of 0.66 and 0.61 for the calibration and validation, respectively.	126
Appendix 10. Sediment concentrations (mg/kg) at Muga catchment.....	126
Appendix 11. Calibration and validation results at Temecha with SWAT99Integrated for the period 1988-2004. Statistical results achieved R ² values of 0.68 and 0.7 for the calibration and validation, respectively; and NS values of 0.46 and 0.57 for the calibration and validation, respectively.....	127
Appendix 12. Sediment concentrations (mg/kg) at Temcha catchment.....	127
Appendix 13. Rainfall data availability for the upper Blue Nile Basin	128
Appendix 14. Temperature data availability for the upper Blue Nile Basin	129
Appendix 15. Relative humidity data availability for the upper Blue Nile Basin.....	129

Appendix 16. Solar radiation data availability for the upper Blue Nile Basin	129
Appendix 17. Wind speed data availability for the upper Blue Nile Basin	129
Appendix 18. Geographic coordinates of ground stations and its respective CFSR stations used in the Integrated dataset.....	130
Appendix 19. Flow discharge data availability for the upper Blue Nile Basin	131

ACRONYMS AND ABBREVIATIONS

ArcGIS	GIS software interface
ARS-USDA	Agricultural Research Service of the United States Department of Agriculture
AGNPS	Agricultural Non-Point Source Pollution Models
ANSWERS	Areal Nonpoint Source Watershed Environmental Simulation
AWC	Available Water Capacity
Bm³	Billion cubic meters
BNRB	Blue Nile River Basin
CEC	Cation Exchange Capacity
CFSR	Climate Forecast System Reanalysis
CGIAR-CSI	Consultative Group on International Agricultural Research-Consortium for Spatial Information
CN	Curve Number
DEM	Digital Elevation Model
DSMW	Digital Soil Map of the World
EARO	Ethiopian Agricultural Research Organization
FAO-UNESCO	Food and Agriculture Organization of the United Nations
GE	Gross erosion rates t/ha/year
GIS	Geographic Information System
GOC	Global Optimization Criterion
GLUE	Generalized Likelihood Uncertainty Estimation
GWh	Gigawatt hours
HBV	Hydrologiska Byråns Vattenbalansavdelning model
HRU	Hydrologic Response Unit
HSSY	HRU specific sediment yields t/ha
IGSSE	International Graduate School of Science and Engineering
ILRI	International Livestock Research Institute
IWMI	International Water Management Institute
ITCZ	Inter-Tropical Convergence Zone
LOADEST	LOAD ESTimator software
m.a.s.l	Meters above sea level
MCMC	Markov Chain Monte Carlo
MoA	Ministry of Agriculture of Ethiopia
MODIS	Moderate Resolution Imaging Spectroradiometer
MoWR	Ministry of Water Resources of Ethiopia
MUSLE	Modified Universal Soil Loss Equation
MWIE	Ministry of Water, Irrigation and Electricity of Ethiopia
NCEP	National Centers for Environmental Prediction
NIMA-NEX	Nile Management-Nexus EXpert Tool
NMA	National Meteorology Agency of Ethiopia
NS	Nash-Sutcliffe efficiency
OF	Objective Functions
OSL	Ordinary Least Squares
ParaSol	Parameter Solution

PBIAS	Percent Bias
PSO	Particle Swarm Optimization
R²	Correlation Coefficient
RMSE	Root Mean Square Error
rRMSE	Relative Root Mean Square Error
RSR	Ratio of the root-mean-square error to the standard deviation of measured data
SCE-UA	Shuffled Complex Evolution method developed at University of Arizona
SCS	Soil Conservation Service
SEI	SWAT Error Index
SHETRAN	Hydrological model developed by the School of Civil Engineering and Geosciences, Newcastle University
SHE	Système Hydrologique Européen
SORTER	Soil and Terrain Database Programme
SRTM	Shuttle Radar Topography Mission
SUFI-2	Sequential Uncertainty Fitting, Version 2
SWAT	Soil and Water Assessment Tool
SWAT-CUP	SWAT-Calibration and Uncertainty Program
SWC	Soil and Water Conservation practices
TUM	Technische Universität München
UNESCO	United Nations Educational, Scientific and Cultural Organization
VSA	Variable Source Area
USLE	Universal Soil Loss Equation
WEPP	Water Erosion Prediction Project Model
WXGEN	SWAT's built-in Weather Generator

ZUSAMMENFASSUNG

Zusammenfassung. Das Einzugsgebiet des Blauen Nils muss sich den Problemen der Bodendegradation, einer unzureichenden landwirtschaftlichen Produktion und einer begrenzten Anzahl von entwickelten Energiequellen stellen. Unter diesen Umständen stellen hydrologische Modelle ein sehr wichtiges Instrument dar, um solche komplexen Systeme besser zu verstehen. Mit Hilfe dieser Modelle können die Ursachen der Probleme identifiziert und quantifiziert werden, um sowohl die Wasserressourcen, als auch die landwirtschaftlichen Praktiken zu verbessern. In dieser Forschungsarbeit wurde SWAT verwendet, um die hydrologischen Prozesse im oberen Blauen Nil zu modellieren. Es wurden Vergleiche zwischen dem Climate Forecast System Reanalysis (CFSR) und einem konventionellen Datensatz mit unterschiedlicher räumlicher Diskretisierung (30 und 87 Teileinzugsgebiete) durchgeführt. Um die räumlichen und zeitlichen Einschränkungen beider Datensätze zu verbessern, wurde ein vernetzter Datensatz erzeugt. Die Ergebnisse verdeutlichen die Unterschiede der Verwendung unterschiedlicher Datensätze mit unterschiedlicher räumlicher Diskretisierung. Datensätze unter 30 Teileinzugsgebiete erreichten NS Werte von -0,51, 0,74 und 0,84 für die CFSR-, die beobachteten und die integrierten Datensätze. Modelle unter 87 Teileinzugsgebiete erreichten hingegen NS Werte von -1,54, 0,43 und 0,80 für die CFSR-, die beobachteten und die integrierten Datensätze. Auf Grundlage der erlangten statistischen Ergebnisse liefert der integrierte Datensatz ein besseres Modell des oberen Blauen Nils.

Häufig können gute hydrologische Kalibrierungen erreicht werden und Annahmen der Qualität der Sedimentschätzungen erfolgen. In SWAT können sich Sedimentkonzentrationen in Abhängigkeit der Anzahl der Teileinzugsgebiete oder HRUs unterscheiden, auch wenn die Wasserabflussschätzungen sehr ähnlich bleiben. Um die Auswirkung von HRUs aufzuzeigen, wurden mehrere SWAT-Modelle von drei Teileinzugsgebieten des oberen Blauen Nils (Gumara, Ribb und Beressa) erstellt, analysiert und die resultierenden Schätzungen der Sedimentkonzentrationen mit den wenigen verfügbaren gemessenen Daten verglichen. Die Ergebnisse der Analysen zeigten, dass bei einer Erhöhung der Anzahl der HRUs, die Sedimentmenge und -konzentration deutlich sank. Dies lässt sich auf die Auswirkung der Hanglängen auf die Konzentrationszeit zurückführen. Deshalb wird in dieser Arbeit empfohlen die Teileinzugsgebiete so zu definieren, dass deren Fläche 0,58% des gesamten Einzugsgebiets des oberen Blauen Nils entspricht. Somit besteht das finale Modell des Einzugsgebiets des oberen Blauen Nils aus 99 Teileinzugsgebieten mit jeweils 100 000 ha und 3466 HRUs.

In mehreren Teileinzugsgebieten des oberen Blauen Nils wurden ebenfalls Sedimentkonzentrationen geschätzt. Um Bodenerosionsanalysen durchzuführen, ist die Kalibrierung mit gemessenen Sedimentdaten ein unentbehrlicher Bestandteil. Allerdings sind nur wenige Sedimentdaten des Blauen Nils vorhanden. Zudem sind diese weder präzise noch wurden sie kontinuierlich gemessen. Daher wurden zusätzliche Sediment-Rating-Curves Parameterwerte für 5 Teileinzugsgebiete festgelegt: Ardy, Azuari, Chena, Muga und Temecha. Beim Vergleich der durch Sediment-Rating-Curves erhaltenen Resultate mit denen mittels SWAT modellierten Ergebnisse zeigte sich, dass diese sehr ähnlich sind. Um darüber hinaus die Zuverlässigkeit der Modelle in Bezug auf unterschiedlichen Diskretisierungsstufen und die Verwendung unterschiedlicher Datensätze zu vergleichen, wurde der SWAT-Error-Index (SEI) verwendet. Der SEI, welcher auf Grundlage von Niederschlags- und Evapotranspirationsdaten basiert, bietet eine Bewertung der Modellqualität. Der SEI zeigte sich als eine zusätzliche, zuverlässige und nützliche Methode um die Fehler von SWAT-Modellen zu messen.

Schlüsselwörter. SWAT, Teileinzugsgebiet Diskretisierung, CFSR, Integrierter Datensatz, SWAT Error Index (SEI).

ABSTRACT

Abstract. The Blue Nile Basin is confronted by land degradation problems, insufficient agricultural production, and limited number of developed energy sources. Under this situation, hydrological models constitute a very important tool to better understand such complex systems, also to identify and quantify the causes of the problem to improve water resources and land management practices. In this research, SWAT was used to model the hydrological processes in the upper Blue Nile Basin. Comparisons between a Climate Forecast System Reanalysis (CFSR) and a conventional ground weather dataset were done under two sub-basin discretization levels (30 and 87 sub-basins) to create an integrated dataset to improve the spatial and temporal limitations of both datasets. The results showed the discrepancies of using different weather datasets with different sub-basins discretization levels. Datasets under 30 sub-basins achieved NS values of -0.51, 0.74 and 0.84; for the CFSR, ground and Integrated datasets, respectively. While models under 87 sub-basins achieved NS values of -1.54, 0.43, and 0.80; for the CFSR, ground and Integrated datasets, respectively. Based on the obtained statistical results, the Integrated dataset provided a better model of the upper Blue Nile Basin.

Often, good hydrological calibrations can be achieved, and assumption about the quality of sediment estimations are done. However, sediment concentrations in SWAT can differ when the number of sub-basins or HRUs are different, even when the flow discharge estimations remain very similar. To demonstrate the effect of HRUs, several SWAT models of three sub-basins: Gumara, Ribb and Beressa in the upper Blue Nile Basin were created, analyzed and their sediment concentrations compared with the few available data. Results of the analyses demonstrated that as the number of HRUs increases, sediment loads and concentrations tend to significantly reduce due to the effect caused by the HRU slope lengths on the concentration time. Therefore, this research proposed a delineation threshold to create sub-basins of 0.58% of the total area of the upper Blue Nile Basin, which corresponded to 100,000 hectares. With this threshold was possible to delineate the final model of the upper Blue Nile Basin that contains 99 sub-basins and 3466 HRUs.

Sediment concentrations at multiple sub-catchments of the upper Blue Nile Basin have also been estimated. Although calibration of models using sediment data is an indispensable process to perform soil erosion analyses, sediment data of the Blue Nile Basin is very limited, not accurate and has not been collected continuously. Therefore, additional values for parameters used in sediment rating curves were defined for 5 sub-catchments: Ardy, Azuari, Chena, Muga and Temecha. Results obtained from these sediment rating curves were compared with those results estimated by SWAT, where both results are very similar. Furthermore, the SWAT Error Index (SEI) was also proposed to compare the reliability of the models under different discretization levels and weather datasets. This index offers an assessment of the quality of a model based on precipitation and evapotranspiration data. SEI demonstrated to be a reliable and useful additional method to measure the level of error of SWAT models.

Keywords. SWAT, sub-basins discretization, CFSR, Integrated dataset, SWAT Error Index (SEI).

1. INTRODUCTION

The Blue Nile Basin has been continuously experiencing a series of noticeable changes associated to land degradation, deforestation, population growth, insufficient agricultural production, urbanization, industrialization, climate change, and also to the increasing political confrontations due to water uses upstream and downstream the river. Nowadays, water resources in Blue Nile Basin have extreme pressure related to the large and fast increasing human population that is living under poor socio-economic conditions. Agricultural production has been intensified with the objective of getting better economic benefits without looking at the environmental suitability. To optimize available fundings for land management and environmental sustainability of the region, a good knowledge of the negative impacts of all these social and environmental changes on the future agricultural production and natural resources is crucial.

1.1 Statement of the problem and content of the research

The most alarming problem in the Blue Nile Basin is the control of the tremendous land degradation due to soil losses. The inadequate management of the natural resources in the Blue Nile Basin are causing serious erosion problems that will soon be directly affecting the agricultural production in the region. Every year millions of tons of soil are lost through water erosion which reduces the quality and productivity of the lands, causes rivers pollution and reduces the storing capacity of reservoirs. The erosion phenomena, is the most significant cause of land degradation and water resources deterioration in the Blue Nile Basin, and although it is a naturally occurring process, it has been accelerated and intensified by human activities such as farming and construction, and also to other characteristics of rainfall, topography and other natural processes (*Pimentel et al. 1995; Yang et al. 2003; Parsakhoo et al. 2009; Kabir et al. 2014*). In severe cases land under erosion is no longer productive and is abandoned. Based on data provided by studies done by the Eastern Nile Technical Regional Office (ENTRO), the Nile River contains approximately 120 million tons of sediment per year, 72% of the total sediment loads are provided by the Blue Nile River and only 3% by the White Nile. These values show the huge erosion problem being confronted in the Blue Nile Basin, hence making the erosion management one of the most important challenges to be addressed in the current research. Most of the erosion problems occur during the rainy season, from July to September when the surface runoff reaches its maximum peaks. Under these circumstances the identification, quantification and understanding of the severity and behavior of the erosion through a hydrological model that can correctly simulate the different hydrological and erosion processes and able to provide more realistic values of the amount of generated sediment is necessary.

Physically based distributed hydrological models have provided a very important and efficient alternative for hydrologist for analyzing multiple hydrological processes, the impact of land management practices on soil erosion and degradation, agricultural production, water allocation and chemical yields (*Setegn et al., 2008*). Several models as the Soil and Water Assessment Tool (*SWAT; Arnold et al., 1998*), Hydrologic Engineering Center River Analysis System (*HEC-RAS; HEC, 1995*), Water Erosion

Prediction Technology (*WEPP; Nearing et al., 1989*), Agricultural Non-Point Source Pollution (*AGNPS; Young et al., 1989*), Erosion Productivity Calculator (*EPIC; Jones et al., 1991*), Chemicals, Runoff and Erosion from Agricultural Environment Systems (*CREAMS; Knisel, 1980*), SHETRAN (Hydrological model developed by the School of Civil Engineering and Geosciences, Newcastle University), Système Hydrologique Européen (SHE) and the Areal Nonpoint Source Watershed Environmental Simulation (ANSWERS), have widely been used to model and calculate water discharges and sediment yields in ungauged watersheds. However, mathematical methods and formulae implemented by hydrological models to simulate and estimate values of the different hydrological processes also have their limitations. Other disadvantages and challenges of using these hydrological models in the Blue Nile Basin are that they have been developed in regions with a semi-arid climates where the main mechanisms governing the runoff process is the infiltration excess unlike the Ethiopian highlands where saturation excess runoff is dominating (*Steenhuis et al., 2009; Bayabil et al., 2010; Tilahun et al., 2013a, b, c*). Additionally, all these models require a lot of detailed information that often has not been measured and is not available in developing countries such Ethiopia. Therefore, it is difficult to simulate the complex interactions of hydrological processes and weather conditions of watersheds without uncertainties.

Due to its versatility and applicability to complex watersheds, researchers have identified SWAT as one of the most intricate, consistent and computationally efficient models (*Neitsch et al., 2009; Gassman et al., 2007*). SWAT has become an international accepted interdisciplinary tool for the watershed modelling and considered one of the most suitable hydrological models to perform analyses, quantify and predict the impacts of land management practices on soils productivity at very large and detailed levels (*Neitsch et al., 2009; Gassman et al., 2007*). Therefore, SWAT has been chosen as the most adequate model to model the Blue Nile Basin.

The following content of this dissertation has been divided into four main chapters. **Chapter 2** provides a detailed description of the soils, land use, topography and climate condition of the Blue Nile Basin. A very comprehensive literature review was also presented in this section, where a theoretical background about SWAT has been given. This section provides a better understating of how the different hydrological processes are simulated in SWAT, helping to understand its pros and cons. Calibration of the models based on sediment data is also an indispensable process to perform soil erosion analyses, however measured sediment data is very scarce in the Blue Nile Basin, therefore a section with an explanation of sediment rating curves was also presented in this chapter.

Chapter 3 describes the methodology followed to define the criteria used before creating the final SWAT model for the Blue Nile Basin. Among all the input parameters of a hydrological model, the meteorological data has the most significant impact on the water balance of a watershed and quality of the simulated outputs. Therefore, the initial step has been the analysis and integration of the CFSR dataset and a conventionally measured Ground dataset to optimize the quality of the dataset used to run SWAT. During this phase multiple graphical and statistical analysis were done on both datasets to determine their limitations and propose a solution. An analysis of the effects of HRUs

on the final sediment estimations was done next, where it was identified that different delineation can considerably affect the sediment estimations performed by SWAT. The effect of different sub-basin delineations on the water balance components was also analyzed and two evapotranspiration methods, Hargreaves and Penman/Monteith, were compared, from which the Hargreaves methods was selected to estimate the evapotranspiration in the upper Blue Nile Basin. An explanation of how the parameters for the sediment rating curves were calculated was also given next. The final part of this chapter proposed the SWAT Error Index (SEI), an index that is intended to be used as an additional tool to measure the level of error of SWAT models.

Chapter 4 presents the final results obtained after applying the previous methodology. Literature documents well the importance of sub-basin delineation on sediment outputs and indicates that sub-basins should not be larger than 2–3% of the entire basin in order to obtain satisfying simulation results (*Jha et al., 2004; Chaplot, 2014; Zhang et al., 2014; Chiang and Yuan, 2014*). Furthermore, this research determined that doing a model delineation (for the Blue Nile Basin) using a portion between 0.4 and 1.3% of the total area of the watershed provides better results, therefore a portion of 0.58% which corresponds to 100,000 hectares was used to delineate the final SWAT model of the Blue Nile Basin. This model provided enough spatial resolution to define 99 sub-basins and locate sub-basin outlets for the 10 calibrated gauging stations. This final model used the Integrated dataset which was the results of the combination of the CFSR and Ground datasets, therefore, hereafter called SWAT99Integrated. This section includes the results for the calibration and validation with outflow data of SWAT99 Integrated which with the objective of obtaining better results was divided into two periods, 1988-1993 and 1994-2004. Comparisons of the sediment concentrations provided by SWAT and the values obtained from sediment rating curves were also done.

This chapter also shows the results obtained from the proposed SEI. The index was tested in two locations, the first test was done at large scale in the Blue Nile Basin and the second test was done in the Ribb sub-catchment which provided better results. After the final model setup, calibrated and validated based of historic data, and evaluated with the SEI; an analysis of how the erosion has evolved in the upper Blue Nile Basin was done. The period under analysis (1988-2004) was divided into four period, and an erosion map for each period was done. These maps showed how the erosion problem has been increasing in the past years.

Chapter 5, the final chapter of this dissertation, makes a compilation of the previous chapters, targeting the main achievements and presenting the main conclusions of the research. Briefly, it also describes and discusses a series of general conservation and management practices that can help to mitigate the erosion and land degradation processes in the Blue Nile Basin.

1.2 Hypotheses and objectives of the research

The general objective of this research has been to perform a comprehensive analysis of the erosion development in the upper Blue Nile Basin, the identification of the most erosion vulnerable areas, and discussion of general conservation practices that can support the mitigation of the land degradation problem. In order to achieve this objective multiple tasks were performed during the process, for instance the optimization of the weather data, definition of a suitable number of sub-basins based on the available weather stations, definition of sediment rating curves to estimate sediment concentration at multiple sub-catchments of the upper Blue Nile Basin, calibration and validation of the SWAT models, an analysis of the water balances components, and finally an analysis of the sediment estimations provided by SWAT.

The *first objective* of this dissertation has been the selection of a reliable weather dataset to setup the SWAT model and the identification of the most suitable number of sub-basins and HRUs for the model. To achieve this objective the first proposed step has been the selection and analyses of different weather datasets at large scale and under different sub-basin discretization levels. The comparison of two datasets, the CFSR and Ground datasets, could help to identify temporal and spatial constraints of both data sources. **Roth and Lemann (2016)** performed a comparison between CFSR and conventional data in small catchments in the Ethiopian highlands, where they showed that the CFSR data provided unreliable results. However, **Roth and Lemann (2016)** made it clear that the CFSR data was tested only in very small catchments ranging from 112 to 477 hectares and not at large scale, also suggesting that CFSR data should be carefully checked and compared with conventionally measured data of similar climatic stations. Therefore, this research intends to propose an integration of CFSR and conventional Ground weather data to be used at large scale in the upper Blue Nile Basin with an area of approximately 202,994 km². Additionally, also a comparison of CFSR stations with conventionally measured data to make sure that degree of matching between the CFSR and the conventional Ground datasets are within acceptable ranges. Secondly, analyses on two SWAT models using different sub-catchment discretization levels have done, 30 and 87 sub-basins, named SWAT30 and SWAT87, respectively. These analyses and comparison could provide a better understanding of the effects of different sub-basins discretization on the total water balance of a watershed and could additionally help to define an optimum number of sub-basins for the upper Blue Nile Basin.

The *second objective* of this research is focused on understanding and assessing how the number of sub-basins and HRUs can affect the final sediment concentration and sediment yield in SWAT. A study done by **Chen and Mackay (2004)** showed the non-linearity relation between the HRU area and its specific sediment yields, demonstrating that decreasing the size of HRUs increased runoff concentration times, leading to lower sediment yields. Other studies have highlighted the importance of the SWAT sub-basin delineation process on sediment outputs and have indicated that in order to obtain satisfying simulation results the threshold should not be larger than 2–3% of the entire watershed (**Jha et al., 2004; Chaplot, 2014; Chiang and Yuan, 2014; Zhang et al., 2014**). Therefore, this objective intends to define the most suitable threshold to create sub-basins for the upper Blue Nile Basin.

Furthermore, since measured sediment data in the Blue Nile Basin is very scarce and available only for few rivers, hydrological models cannot be calibrated based on sediment concentrations. Therefore, this research also intends to apply the methodology used by *Moges et al. (2016)* to create additional sediment concentration rating curves for several sub-catchments in the upper Blue Nile Basin. *Moges et al. (2016)* defined calibrated parameters to be used with the sediment rating curves for Gilgel Abay, Gumara, Ribb, Megech, Maybar, Debre Mawi and Anjeni. Additionally, this research aims to define parameters for other 5 sub-catchments: Ardy, Azuari, Chena, Muga and Temecha. By using these sediment rating curves is possible to estimate sediment concentrations that can be compared with the results provided by SWAT.

Once the most reliable dataset and the most suitable number of sub-basins to be used to model the Blue Nile Basin have been identified, the final SWAT model can be setup. Subsequently, a critical point to determine the quality of a hydrological model is the water balance. Therefore, in addition to graphical assessments, other statistical indicators as Nash-Sutcliffe efficiency (NS), percent bias (PBIAS), and ratio of the root-mean-square error (RSR) to the standard deviation of measured data were proposed by *Moriasi et al. (2007)*. Based on these commonly used statistical indicators most of the SWAT models provide very good results for discharge values at the outlet of a basin (*Griensven et al., 2012*). However, the evaluation of the models based on both evapotranspiration and water balance are not discussed in details, and the evapotranspiration behavior of a catchment is usually not presented. Several published documents could even report unrealistic parameter values (*Griensven et al., 2012*). Therefore, a **third objective** of this research has been to propose an index, the SWAT Error Index (SEI), to quantify the level of error of a hydrological model. The SWAT Error Index (SEI) uses flexible weighting values for the relative Root Mean Square Error (rRMSE) obtained from measured flow discharge data and satellite evapotranspiration data. SEI was tested in two locations, in the first case it was applied to the entire upper Blue Nile Basin, and for the second case was used to evaluate the results of the Ribb catchment in the Lake Tana region.

2. DESCRIPTION OF THE RESEARCH AREA AND THEORETICAL BACKGROUND

2.1 The Blue Nile Basin

2.1.1 Ethiopia and the Blue Nile River

Ethiopia is located in the eastern part of Africa with a total area of approximately 1.13 million km² (*Awulachew et al., 2007*) and located between latitudes 5°N and 15°N, and longitudes 35°E and 45°E (*Yazew, 2005*). Ethiopia shares borders with Eritrea to the north, Djibouti and Somalia to the east, Sudan and South Sudan to the west, and Kenya to the south. Ethiopia has 11 basins: Abay, Ayisha, Awash, Baro Akoba, Denakil, Genali Dawa, Mereb Gash, Ogaden, Omo Gibe, Tekeze and Wabi Shebele (*Figure 1*). Being Abay basin the part of the Blue Nile Basin within the Ethiopian territory.



Figure 1. Location of Ethiopia.

The population in Ethiopia has a very fast growing rate positioning the country as the second most populous in the African continent with approximately 99.39 million inhabitants in 2015. In the past decades the surrounding areas of the Blue Nile River Basin have experienced an exponential increase of population that has been estimated in 44,457,210 inhabitants (*ENTRO, 2006*). Amhara state concentrates most of the population of the Blue Nile Basin with 46% of it, followed by Oromia with 24%, and Benishangul-Gumuz with 2%, in the Ethiopian lands (*Figure 2*), the other 28% of the population is located in the Sudanese lands (*ENTRO, 2006*). Poor living conditions, the uncertainty in the future sustainability and management of the water resources, and the lack of irrigation systems in the region constitute a major concern that could affect the agricultural production in these lands. Therefore, the population is vulnerable to a reduction in the farming and food security. Irrigable areas in Ethiopia are estimated to

be between 1.5 and 4.3 million hectares (*MoWR, 2001; Werfring, 2004; Awulachew et al., 2005 and Makombe et al., 2011*). Nevertheless, the current total extensions of land under irrigation are estimated to be between 160,000 and 200,000 hectares, comprising less than 5% of the total irrigable lands of Ethiopia (*Awulachew et al., 2005 and 2007 and Makombe et al., 2007*).

The Blue Nile River is the major tributary of the Nile River, contributing with approximately 60% of the total water and extending its path along 1,460 kilometers from its origin at the Lake Tana to its confluence with the Nile River in Sudan (*ENTRO, 2006*). The total area of the Blue Nile Basin is approximately 311,382 km² of which Ethiopia comprises approximately 64% and Sudan the remaining 36% (*ENTRO, 2006*). With approximately 800 kilometers within the Ethiopians lands and an average rate of 1,548 m³/s the Blue Nile River has a tremendous potential for irrigation and hydropower generation. The potential for irrigation is 815,581 hectares and a hydropower generation potential of approximately 78,820 GWH/year (*Awulachew et al., 2007*). The Blue Nile River contributes more than half of the total stream flow of the Nile River. During the rainy seasons the capacity of the Blue Nile River increases up to fifty times its normal size. During the less intensive seasons, the soil is rich for farming and it supports intensive crop cultivation. More than 85% of the population are rural and dependent on agriculture and using the surface water of the river to sustain the crop productivity (*Awulachew et al., 2007; MoA, 2011 and Bekele et al., 2012*).

2.1.2 Location and political administration of the upper Blue Nile Basin

The Blue Nile Basin, also known as Abay basin, is located in the northwestern highlands of Ethiopia, approximately between Latitudes 7 40'N and 12 51'N, and Longitudes 34 25'E and 39 50' E (*Figure 1*). The Blue Nile Basin has boundaries to the north, south, east and west with Tekeze, Omo-Gibe, Awash and Baro-Akobo catchments, respectively. Abay basin is administrated by three regional states: Amhara, Benishangul-Gumuz and Oromia (*Figure 2*). Within these states there is an internal division that includes 18 administrative zones: Agew Awi, Assosa, Debub Gonder, Debug Wello, East Welega, Harar, Illu-Aba-Borra, Jimma, Kemashi, Metekel, Mierab Gojam, Misrak Gojam, North Shoa, Semien Gonder, Semien Shewa, Semien Wello, West Shoa and West Welega (*Figure 3*). There is also a third level administrative division called Weredas, including 185 of them in the Abay basin (*Figure 4*). The Blue Nile Basin is officially divided into 14 main sub-basins: Anger, Beles, Beshelo, Dabus, Didessa, Fincha, Guder, Jemma, Tana, Muger, North Gojam, South Gojam, Weleka and Wembera (*Figure 5 and Table 1*). This watershed comprises approximately 179,465 km², additionally a portion of the Dinder and Rahad catchments shared with Sudan and adding an area of approximately 23,529 km², summing up a total area of approximately 202,994 km² within the Ethiopian lands. The Blue Nile Basin at Eldiem, border with Sudan, yields an estimate mean annual flow of 51 Bm³ (*Hassan, 2012*).

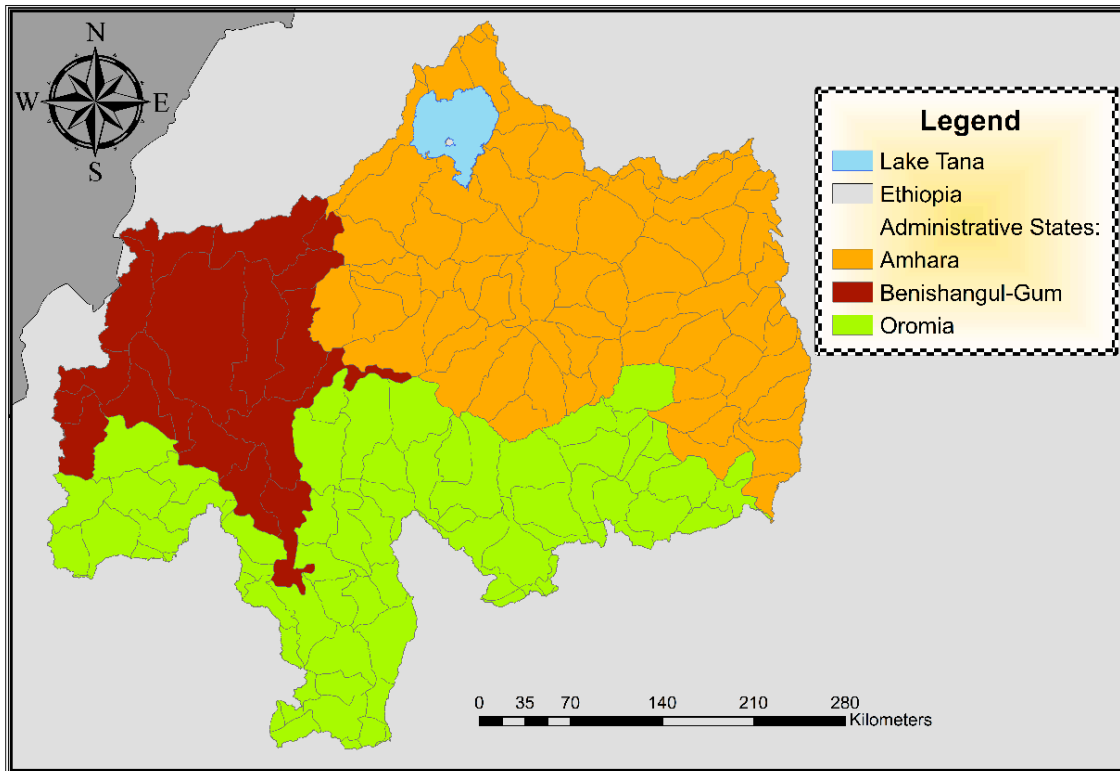


Figure 2. Administrative regional states in the upper Blue Nile Basin.

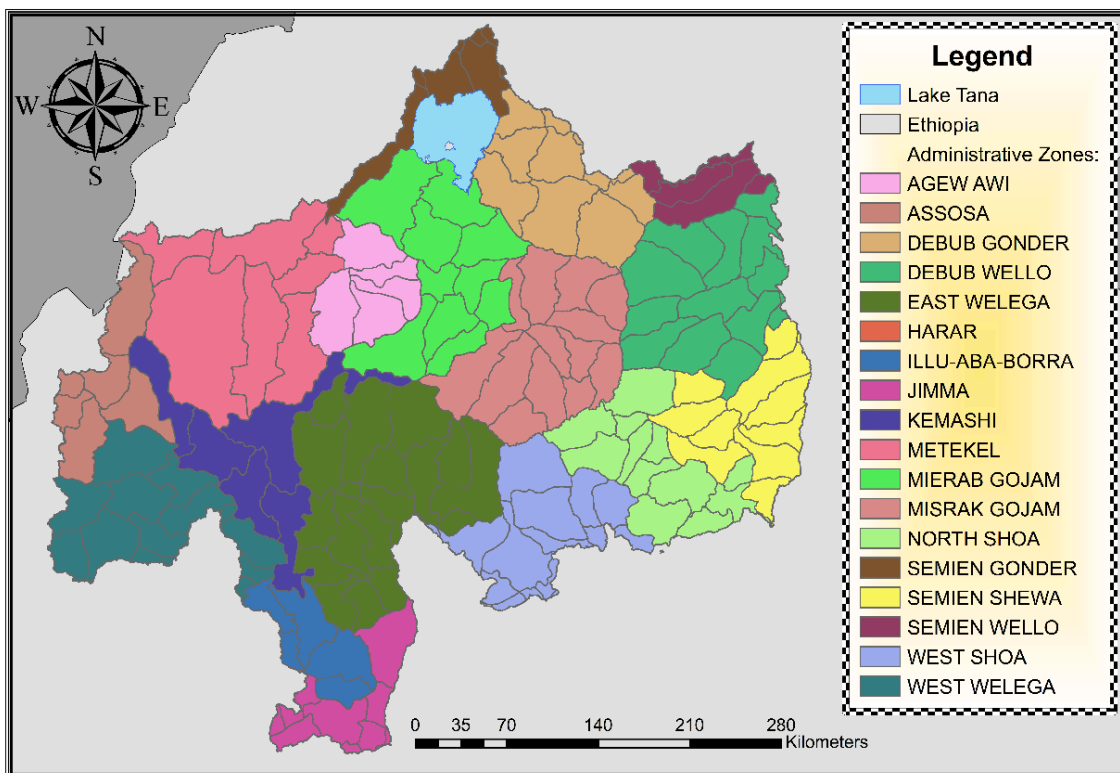


Figure 3. Administrative zones in the upper Blue Nile Basin.

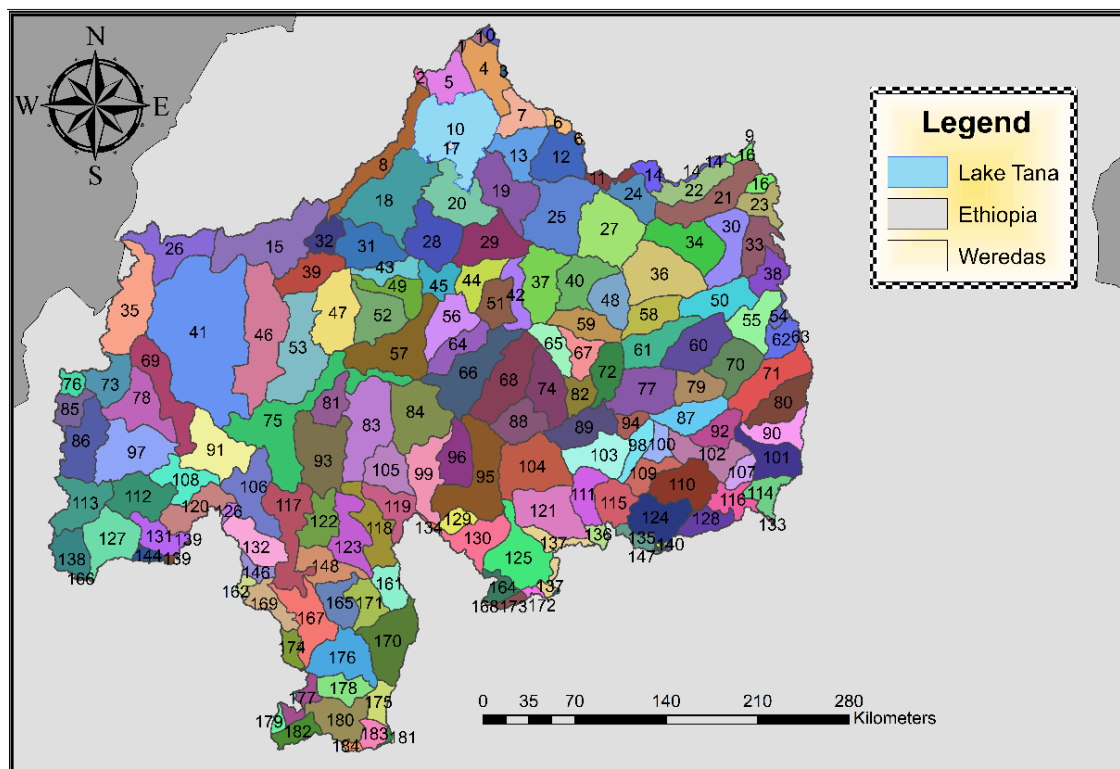


Figure 4. Weredas in the upper Blue Nile Basin.

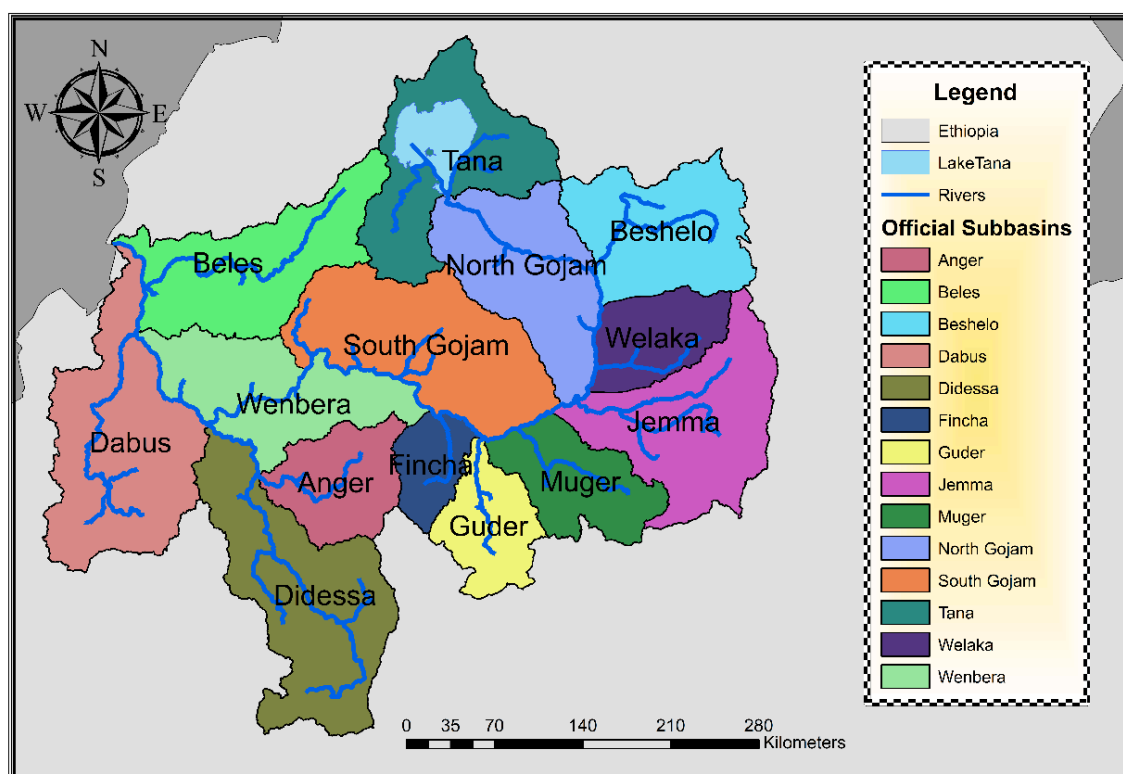


Figure 5. Official sub-basin distribution in the upper Blue Nile Basin.

Table 1. Official sub-basin distribution in the upper Blue Nile Basin, considering Dinder and Rahad sub-catchments shared with Sudan (MWRI, Addis Ababa, 2006).

Sub-basin	Drainage area (km ²)	Gross runoff depth (mm)
Anger	8,027	527
Beles	14,426	378
Beshilo	13,453	455
Dabus	21,367	466
Dedessa	19,943	651
Dinder	15,128	276
Fincha	4,154	450
Guder	7,123	537
Jemma	16,033	422
Lake Tana	15,294	514
Muger	8,318	423
North Gojam	14,618	486
Rahad	8,401	339
South Gojjam	17,029	543
Welaka	6,517	410
Wombera	13,163	410
Total Blue Nile Basin	202,994	

2.1.3 Soils

The wide range of topographic and climatic factors, parent material and land use have resulted in extreme variability of soils in the Ethiopia (FAO, 1984d). Potassium, Nitrogen, Cation Exchange Capacity (CEC) and organic matter contents in most Ethiopian highlands are generally high by international standards (EARO, 1998). However, detailed fertility information of the soils in the Blue Nile Basin is very limited (FAO, 1984d). Nevertheless, it is well known that the phosphorus content is low to very low. Most soils in the Ethiopian highlands are fertile in comparison with the African standard (FAO, 1984c). Soils remain relatively fertile at depth contrary to most other African soils. However, most highland soils are deficient in important nutrients and require fertilizer to sustain crop yields. Researches have indicated that Ethiopian soils are generally low in available nitrogen and phosphorous and cannot produce high crop yields unless these are supplied.

According to the Ministry of Agriculture of Ethiopia (MoA) 19 soil types are identified throughout the country. In the Blue Nile Basin soils are mainly dominated by ten types: Cambic Arenosols, Chromic Vertisols, Dystric Cambisols, Eutric Cambisols, Eutric Fluvisols, Eutric Nitosols, Eutric Regosols, Humic Fluvisols, Orthic Acrisols and Pellic Versitols (FAO, 2014). Eutric Nitosols and Eutric Cambisols dominates most of the eastern highlands while Humic Fluvisols dominate most of the western region (Figure 6 and Table 2).

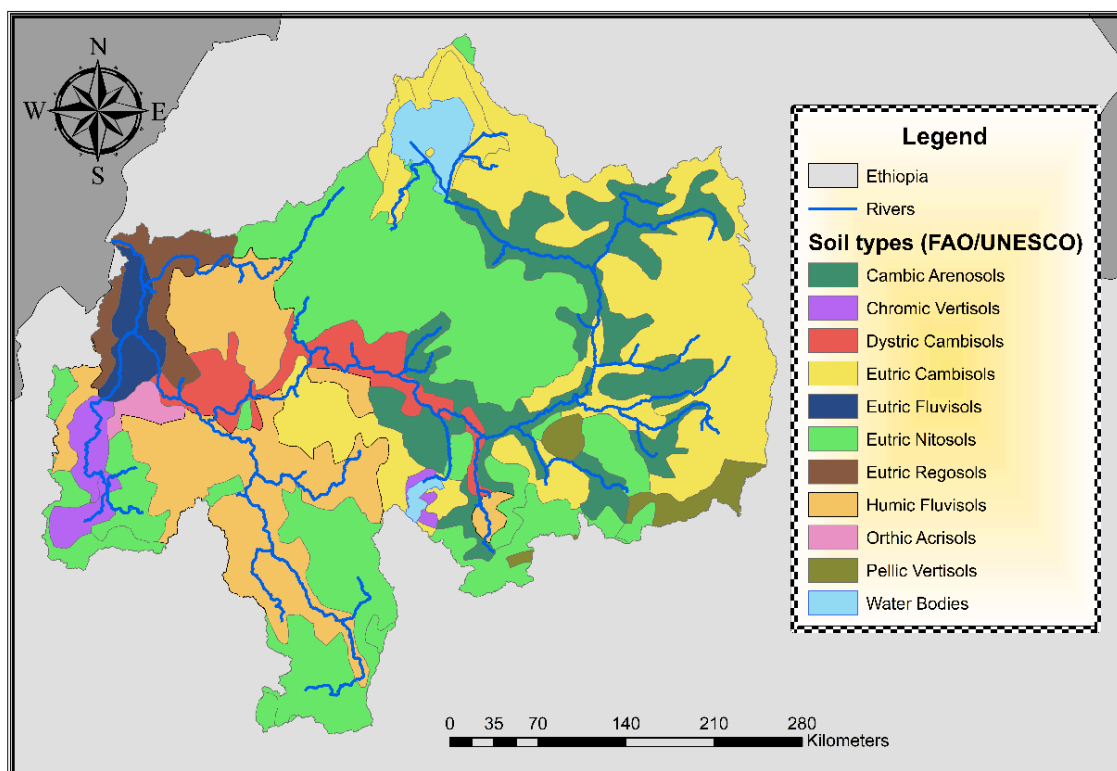


Figure 6. Soils map of the upper Blue Nile Basin (FAO, 2014).

Table 2. Soil types and distribution in the upper Blue Nile Basin based on the “Soil and Terrain Database for Northeast Africa” (FAO-UNESCO, 2014).

Soil Type	Area (Km2)	Area (%)
Orthic Acrisols	598	0.35
Eutric Fluvisols	1,727	1.00
Water Bodies	1,738	1.01
Chromic Vertisols	1,894	1.10
Dystric Cambisols	3,926	2.27
Pellic Vertisols	4,617	2.67
Eutric Regosols	8,595	4.97
Cambic Arenosols	11,417	6.61
Humic Fluvisols	20,293	11.75
Eutric Cambisols	52,869	30.60
Eutric Nitisols	65,094	37.68
Total	172,768	100

Nitisols are the most common soils type in in the Blue Nile Basin. These soils are deep, red and well-drained soils with over 30% of clay content and a block structure (FAO, 2014). Nitisols are formed by fine-textured material weathered from intermediate to basic parent rock and kaolinite, halloysite and ironoxides dominate their clay mineralogy (FAO, 2014). This soil has frequently low phosphorus availability and low base statues. Nitisols are very stable and have high agricultural potential and are often

planted areas. They are found in very extensive areas mostly in the tropics and subtropics. Large extensions of this kind of soils can be found in most tropical highlands of Africa mainly in the Democratic Republic of the Congo, Ethiopia, Kenya, and Cameroon.

Cambisols are the second type of soils with the largest extension in the Blue Nile Basin. Cambisols are soils with a beginning of soil formation. The differentiation of horizons is weak and this is evident from weak, brownish discoloration and structure formation in its soil profile (**FAO, 2014**). These soils are developed in medium and fine-textured materials which are mostly derived from a wide range of alluvial, colluvial and aeolian rocks. Cambisols are good for agriculture and often are intensively cultivated; they are considered the most productive type of soil. These soils are usually not very common in the tropics and subtropics but the reason it exists in a wide range in Blue Nile Basin is because they are commonly found in areas with active erosion which can occur in association with mature tropical soils.

Fluvisols are mostly present in the western region of the Blue Nile Basin and are classified base their texture as sandy loams (**Ayenew, 2008**). These soils have a texture gravely or sandy particles due to high water velocities or turbulent action of the flow. Their characteristics and fertility depend on the nature and sequence of the sediments and soil formation period after or between the flood events. Low velocities or standing water produces fine-textured soils, often mixed with high amounts of organic debris (**Jones et al., 2013**). Their sub-classifications **Eutric Fluvisols** and **Humic Fluvisols** are normally found in the low western lands and wetlands of the Blue Nile Basin (**Abate et al., 2015**).

Regosols are a very weakly developed mineral soil in unconsolidated materials. These soils are mostly spread in lands under erosion, in particular in arid and semi-arid areas and mountain regions (**FAO, 2014**). Some areas with this soil are often used for farming with irrigation, but the most common land use for this soil is the low volume grazing. Regosols can appear in all climatic zones without permafrost and at all elevations. They are particularly common in arid areas, tropics and mountainous regions. These soils can be mostly found in mid-western United States, Northern Africa and Near East Australia.

The Blue Nile Basin also has **Chromic Vertisols** and **Pellic Vertisols** in small extensions that are often used for grazing. These soils have a high content of clay known as montmorillonite that forms deep cracks in dry seasons. After some time, these cracks close and the soils become completely impervious causing significant amounts of runoff (**Abate et al., 2015**). This process facilitates the transfer of material from the surface into the subsoil giving rise to a mixed or churned soil (**Jones et al., 2013**). This soil often mixes itself due to shrinking and swelling conditions that often cause damages to buildings and roads. Vertisols are usually formed by highly basic rocks such as basalt. The texture class of these soils is usually sandy clay (**Ayenew, 2008**). These soils can be found near the equator and some of the major areas are in Africa (Ethiopia, Kenya, Sudan and Chad), Australia, Mexico, southern United States and central India.

2.1.4 Land Use

Current land use maps show that approximately only 40% of the total area of the Blue Nile Basin are covered by vegetation, which includes forests, shrublands, pastures and savannas, while more than 40% correspond to bare lands. Although during the rainy seasons most of the land is green and covered principally by pastures and grass. Studies based on satellite images show that the vegetation cover is rapidly reducing in recent years due to an increasing agricultural expansion. The increase of areas dedicated to agriculture has been estimated in approximately 1.3 million hectares and by 67,000 hectares in urbanization and industrialization. Land cover types are mainly classified as intensively and moderately cultivated, these agricultural practices were quickly intensified and are mostly located in the eastern highlands (*Figure 7 and Table 3*).

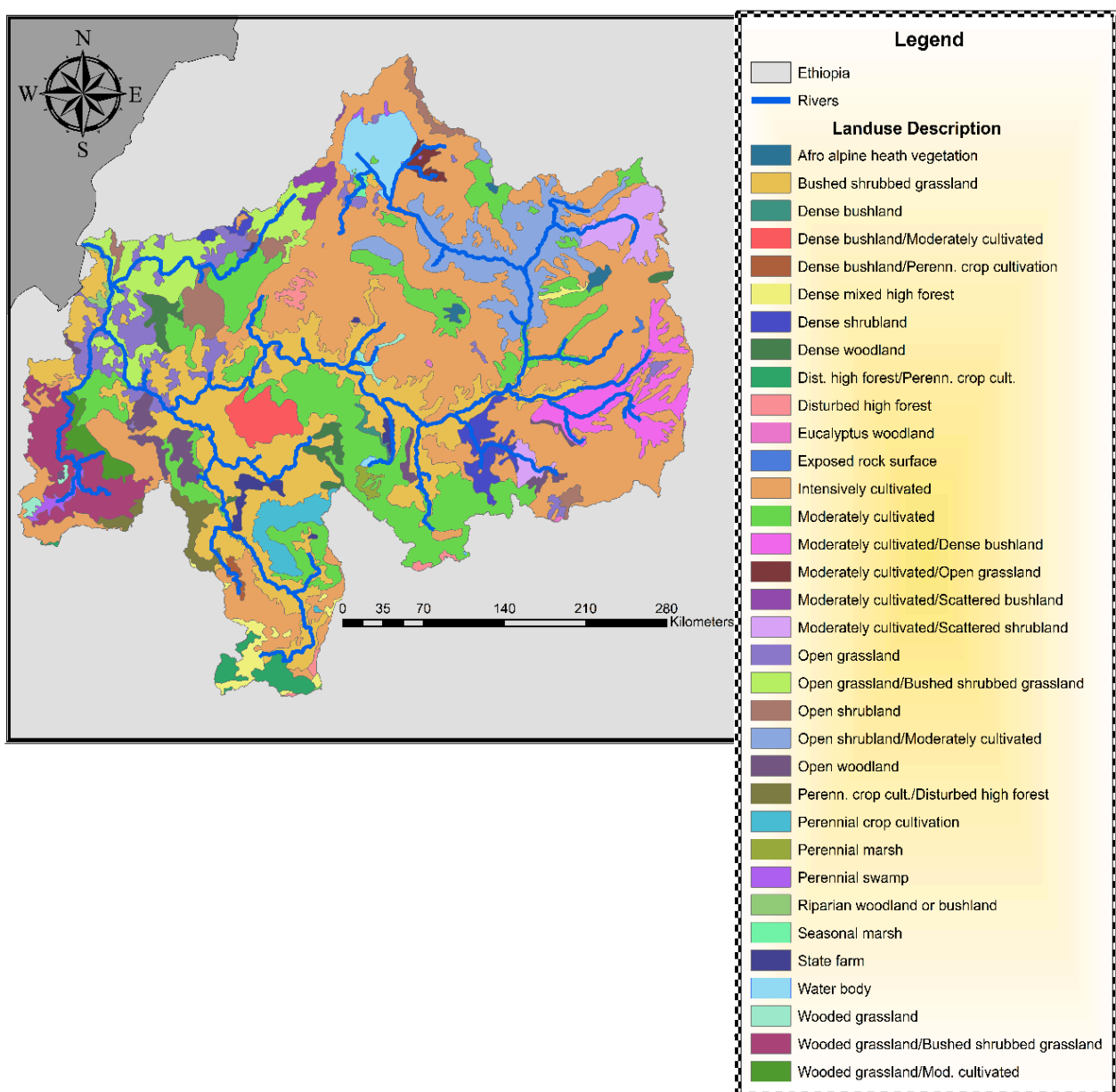


Figure 7. Land use map of the upper Blue Nile Basin (ILRI, 2004).

Table 3. Land cover in the upper Blue Nile Basin (ILRI, 2004).

Land Cover	Area (km ²)	Area (%)
Open grassland/Bushed shrubbed grassland	4.85	0.003
Perennial marsh	5.93	0.003
Wooded grassland/Bushed shrubbed grassland	37.94	0.02
Exposed rock surface	38.66	0.02
Perennial crop cultivation	59.99	0.03
Open shrubland/Moderately cultivated	86.13	0.05
Wooded grassland/Mod. cultivated	102.6	0.06
Dense bushland/Perenn. crop cultivation	131.26	0.08
Seasonal marsh	135.51	0.08
Dense bushland	158.86	0.09
Dense bushland/Moderately cultivated	162.95	0.09
Eucalyptus woodland	224.58	0.13
Afro alpine heath vegetation	330.01	0.19
Riparian woodland or bushland	353.03	0.2
Dense woodland	521.79	0.3
State farm	569.28	0.33
Disturbed high forest	701.69	0.41
Moderately cultivated/Open grassland	744.7	0.43
Open shrubland	749.4	0.43
Open woodland	1361.58	0.79
Moderately cultivated/Scattered bushland	1374.82	0.8
Water body	1829.14	1.06
Perennial swamp	1876.45	1.09
Dist. high forest/Perenn. crop cult.	1904.12	1.1
Perenn. crop cult./Disturbed high forest	3552.66	2.06
Dense mixed high forest	3805.78	2.2
Wooded grassland	5667.13	3.28
Dense shrubland	7304.57	4.23
Moderately cultivated/Dense bushland	10385.98	6.01
Bushed shrubbed grassland	17546.03	10.16
Moderately cultivated	21946.22	12.7
Open grassland	42435.12	24.56
Intensively cultivated	46659.24	27.01
Total	172,768	100

2.1.5 Topography

Elevations in the upper Blue Nile Basin range between 483 m.a.s.l. at the Sudanese border, to 4,248 m.a.s.l. in the eastern highlands (**Figure 8**). This topographic variation together with its near-equatorial location and the rainfall variability leads to the occurrence of different climatic zones within the basin. And although the topographic disparity and variations in altitude may have some impact on the weather, vegetation and soil conditions, this do not represent a significant impact. Rainy seasons are very variable in this watershed, for instance the total discharge peaks at the Eldiem gauging station can reach 7,000 m³/s, and dry seasons can go as low as 100 m³/s.

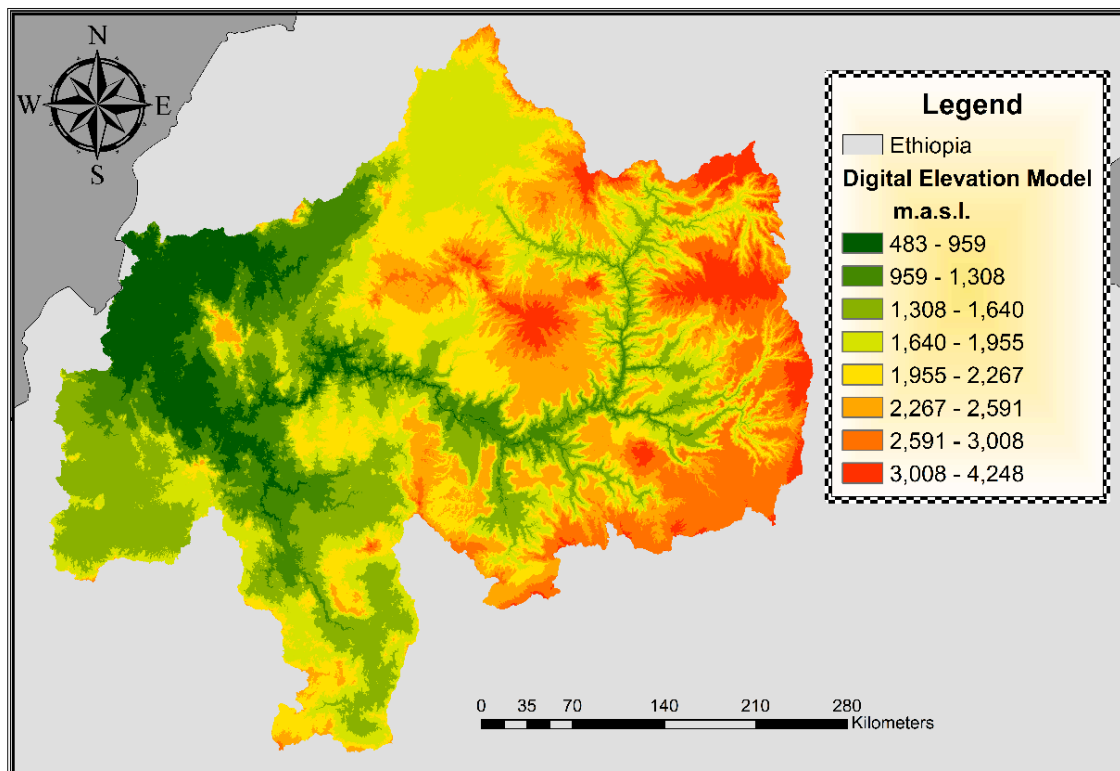


Figure 8. Digital Elevation Model of the upper Blue Nile Basin (CGIAR-CSI).

2.1.6 Climate

The Blue Nile Basin is rich in a variety of local climates, ranging from very hot deserted lands to cold temperatures in the mountain tops. Ethiopia, being near the equator and with extensive altitude differences, has a wide range of climatic features suitable for different agricultural production systems (FAO, 1986). The climate is generally temperate at higher elevations and tropical at lower altitudes (Conway, 1997). The extreme elevation disparities within the basin has a major influence both on human activities and the climate. Average temperatures fall by 5.8°C for every 1000 meters increase in altitude. The traditional classification of climate is based on elevation and recognizes the following zones:

1. Kolla zone: below 1800 m.a.s.l. with mean annual temperature of 20-28°C.
2. Woina Dega zone: between 1800 and 2400 m.a.s.l. with mean annual temperatures of 16-20°C.
3. Dega zone: above 2400 m.a.s.l. with mean annual temperatures of 6-16° C.

Most of the population inhabits the upper two zones which are cooler, healthier and more suitable for agriculture (*Conway, 2000*).

Rainfall

The spatial variation of rainfall over the basin is essential for water resources planning and management. Ethiopia has a strong inter-annual variability rainfall all over the territory. The mean annual rainfall of the area is 1435 mm although there is spatial rainfall variability, with the rainfall ranging from 1200 to 1600 mm (*Nisar, 2016*). According to *Conway (2000)* and *Abtey et al. (2009)* the mean annual rainfall generally declines from south-west to north-east (*Figure 9*). The rainfall is mainly influenced and controlled by the summer monsoon, the movement of the inter-tropical convergence zone (ITCZ) and the moist air from the Atlantic and Indian Oceans in the summer (*Derib, 2013*). ITCZ is basically a strip of low pressure which circles the Earth generally near the equator where the trade winds of the Northern and Southern Hemispheres meet (*SKYbrary Aviation Safety, 2016*). Therefore, the climate of the region can be explained by the ITCZ's change of position and the circulation of trade winds during the year. The rainy season is predominantly under the influence of the ITCZ, the dry season is distinguished by dry trade winds (*Althoff and Förch, 2009*).

Years in the Blue Nile Basin are normally divided into three main seasons: a rainy season from June to September called Kiremt, a dry season from October to January called Bega, and a short rainy season from February to May called Belg (*Mamo and Jain, 2013*). During the Bega season the ITCZ lies in the south of Ethiopia. During the Belg season the ITCZ returns to Ethiopia causing moderate rains in some regions of the basin, particularly in the south-western part of Ethiopia. In June, at beginning of the Kiremt season, the ITCZ moves to the northern part of Ethiopia leading to the main rainy season lasting until September. Therefore, the rainfall in the Blue Nile Basin is very variable, and the Kiremt season makes up to 70% of the mean annual rainfall (*Conway, 2000*), while the remaining precipitation occurs between October and May. Rainfall in Ethiopia is generally correlated with altitude, altitudes above 1,500 meters receive substantially greater falls than do the lowlands, except the lowlands in the western region where rainfall is high. The average annual rainfall of areas above 1,500 meters exceeds 900mm. Lands below 1,500 meters have an average rainfall under 600mm. The average monthly rainfall in the Blue Nile Basin varies from less than 5mm during February up to 170 mm during July (*Figure 10*).

Although a significant part of the Ethiopia gets enough rain for rained crops production, this rainfall variability also makes agricultural planning difficult (*FAO, 1984b*). The lowest rainfall data detected during the current research period (1984-2004) corresponds to the eastern region, for the subbasins of Beshelo, North Gojam, South

Gojam, Welaka, Jemma, Muger, Guder and Fincha; where the precipitation drops below 900 mm per year. While the highest precipitation ranges belong to the western region: Didessa, Wenbera, Anger, Dabus and Beles; with precipitations above 1700 mm per year. As consequence of the rainfall variability, inundations constitute a serious problem at the confluence of the rivers in Khartoum as well as in the upper course of the Blue Nile River. Periodic flooding significantly affects a number of households residing in the floodplains of Fogera, Dembia, and Bichign around Lake Tana. The combination of temperature and rainfall with topography and soils determine the moisture availability which determines vegetation and agricultural productivity. Ethiopia has enough moisture for annual crops and another 16 percent is thought to be reliable for perennial crops (*FAO 1984a*).

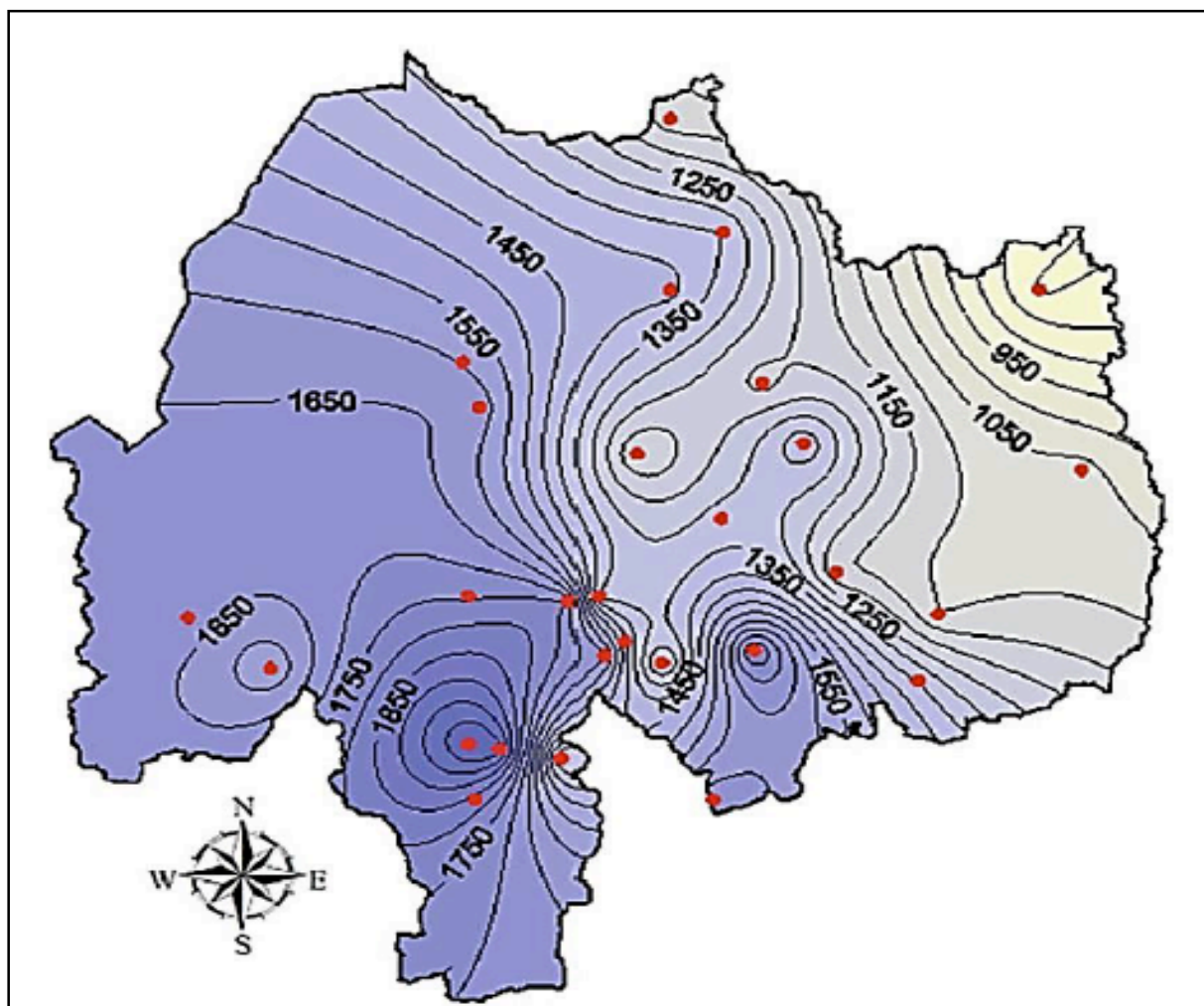


Figure 9. Spatial annual rainfall distribution in the upper Blue Nile Basin (*Abtew et al., 2009*).

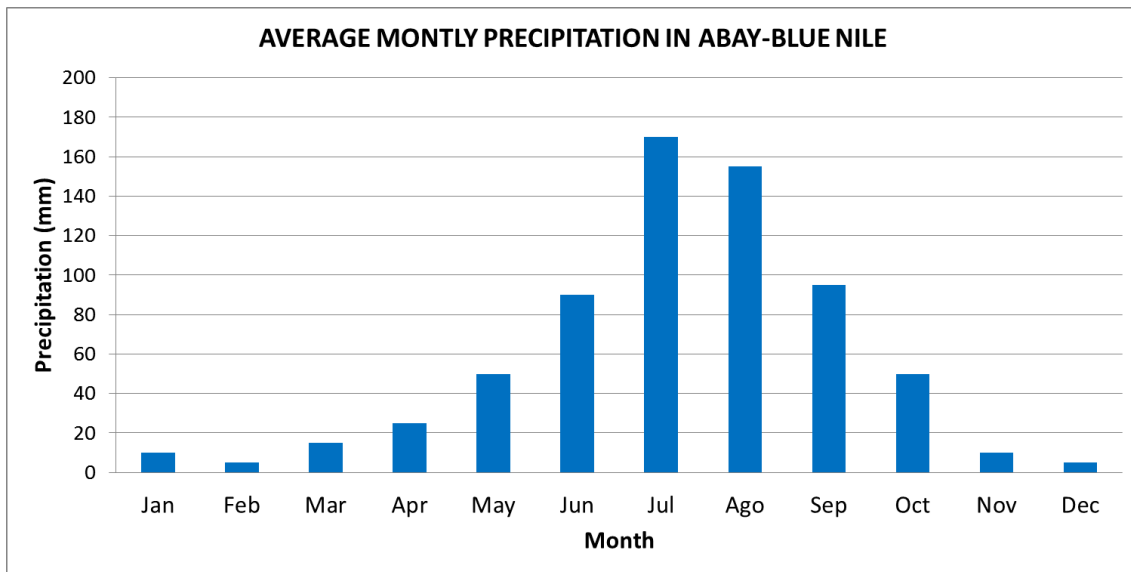


Figure 10. Average monthly precipitation in the upper Blue Nile Basin (*Hassan, 2012*).

Temperature

Air temperature is a crucial parameter influencing numerous natural processes, for instance the plant growth, evaporation rates, wind movement, precipitation patterns and evapotranspiration variations. The highest average air temperatures in the Blue Nile Basin occur between March and June, while the lowest average air temperatures occur in December. During the summer, between July and September, high temperatures are reduced because the rainfall, cloudy conditions and energy used for evapotranspiration occur when the highest temperatures are typically expected. Thus, the hottest period is experienced between March and May, before the major rainy season (*Conway, 2000*).

The climate in the Blue Nile Basin oscillates from humid to semi-arid and it is substantially dominated by latitude and altitude, with temperatures ranging from 13°C in the south eastern regions to 33°C in the south western regions (*Figure 11 and Figure 12*). The Blue Nile Basin shows a good correlation between temperature, altitude and evapotranspiration. The mean annual temperature in altitudes over 2300 m.a.s.l. is estimated to be between 17°C-19.5°C. Approaching the Sudanese boarder where the altitude is lower than 1000 m.a.s.l. the temperature ranges approximately between 24°C-26°C. In the surrounding areas of Khartoum the altitude is below 500 m.a.s.l. and the average temperatures range between 28.5°C-30.5°C. The mean annual potential evaporation ranges from below 1,500 mm at Fiche station located in the highlands at approximately 2,300 m.a.s.l. to more than 1,800 mm in the north eastern part of the basin (*ENTRO, 2006*).

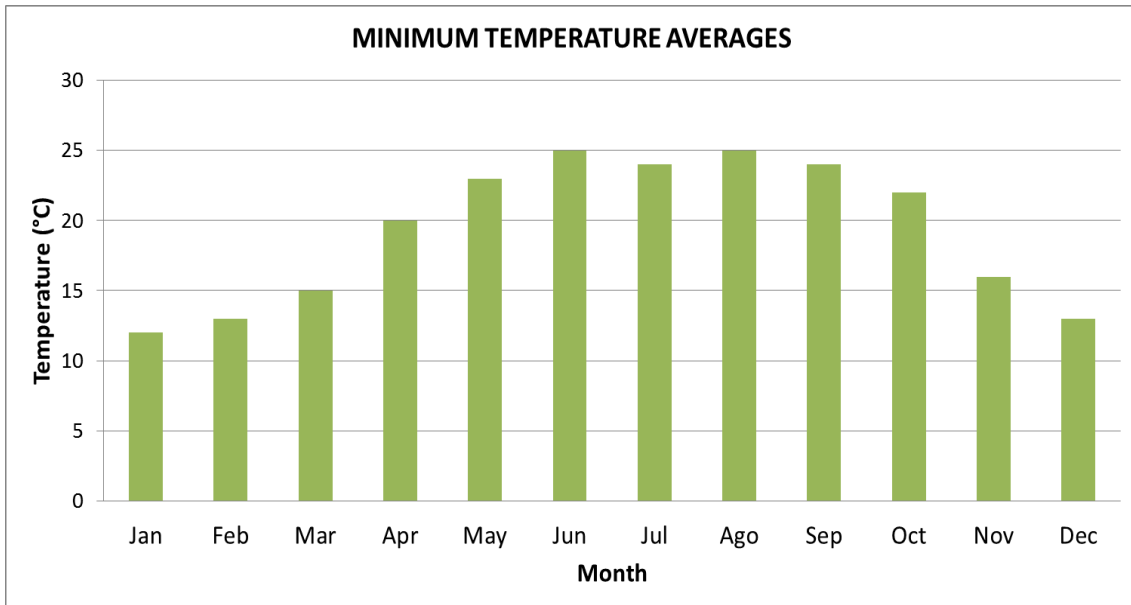


Figure 11. Average monthly minimum temperatures in the upper Blue Nile Basin (Hassan, 2012).

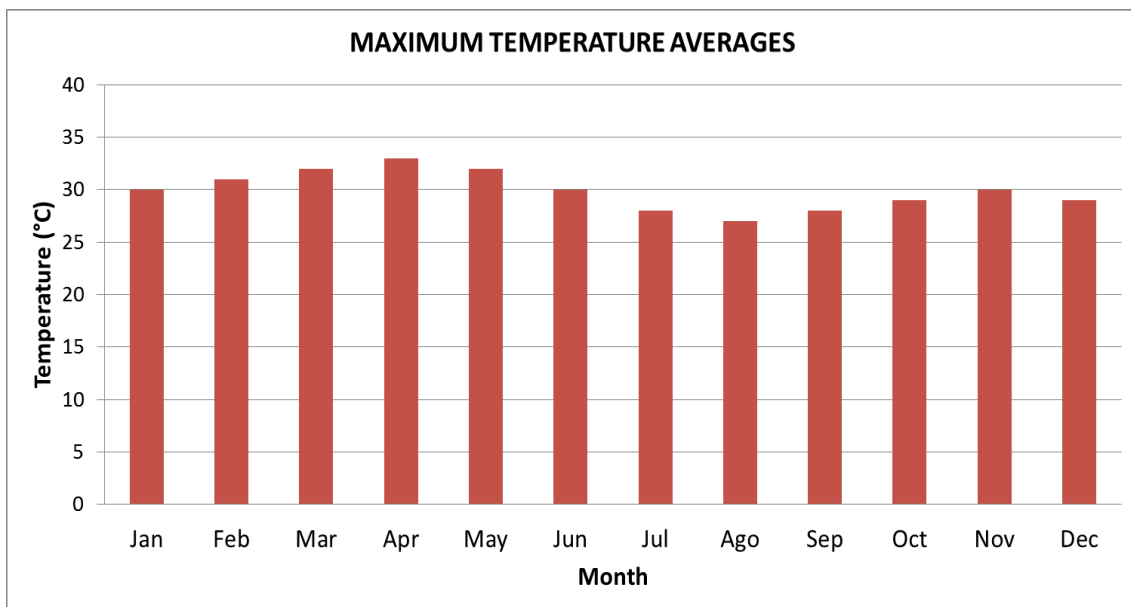


Figure 12. Average monthly maximum temperatures in the upper Blue Nile Basin (Hassan, 2012).

2.1.7 Irrigation systems, dams and reservoirs

Currently, approximately 644,087 hectares are under irrigation systems in the upper Blue Nile Basin depending of 9 irrigation schemes (**Table 4**). These systems yield to a water demand for potential irrigation of approximately 4.87 km³ in Ethiopia (**Hassan, 2012**). However, **Hassan (2012)** mentioned that the upper Blue Nile Basin has a potential of approximately 1,364,639 hectares, which has led to an initiative for building new dams for irrigation purposes, where the irrigated lands are expected to be expanded by 200,000 hectares in the near future. Most of these irrigation dams and other projects are located or dependent on the main stream of the Blue Nile River.

Table 4. Potential irrigation schemes in the Blue Nile Basin (**Hassan, 2012**).

Potential Irrigation Schemes						
Sub-basin	Scheme	Capacity			Type	Irrigation area (ha)
		High	Medium	Water Demand (km ³ /year)		
Lake Tana	Megech		X	0.33	Gravity	7,300
	Magech	X			Pump	24,510
	Ribb	X		0.15	Gravity /Pump	19,925
	Gumera	X		0.15	Gravity /Pump	13,976
	Gigel Abbay	X		0.10	Gravity /Pump	12,852
	NW Tana		X	0.08	Pump	6,720
	NE Tana		X	0.06	Pump	5,745
	SW Tana		X	0.09	Pump	5,132
Beles	Upper and Lower Beles	X		2.73	RoR	53,700
Didessa	Didessa Pump and Didessa Dam	X			Gravity	14,280
Rahad-Dinder and Blue Nile	Anger and Nekemte	X		0.12	Gravity /Pump	25,670
	Dabana		X			
	Negeso		X			
	Rahad and Galegu in Ethiopia	X			Gravity	55,029
	Upper and Lower Dinder in Ethiopia	X			Gravity	49,550

Although the upper Blue Nile Basin already has several dams distributed in different regions around the basin, only a few dams are under operation. However, several other dams are being constructed for irrigation and hydropower purposes (**Table 5**). The four proposed dam constructions are: Karadobi, Mabil (Beko Abo), Mandaia and the Renaissance dam at the border (**Figure 13**).

Table 5. Existing and proposed dams in the upper Blue Nile Basin.

Existing Dam								
Name	Type	Installed Capacity MW	Reservoir size (km ³)	Height (m)	Irrigation area (ha)			
Tis Abay I+II	RoR/Pump	84.4	River		11,300			
Fincha	Gravity/Pump	134	0.65	20	8,145			
Amerti-Neshi	Gravity	97	0.15	38	12,700			
Roseires	Gravity	1800	7.4	78	-----			
Koga	Gravity	43	0.0831	21	7,000			
Proposed Dams (Block et al., 2007)								
Name	Mean flow (Mm ³)	Flow at Design Head (mm ³)	Reservoir elevation	IC MW	E GWh	Structural elevation (m)	Crest Length (m)	Reservoir capacity (billion m ³)
Karadobi	16,570	948	1,175	1,580	6,920	252	980	32.5
Mabil		1346	-----	-----		171	856	13.6
Mandaia	35,310	1758	750	1,700	6,750	164	1134	15.9
Renaissance	48,493	2378	600	6,000	7,800	84.5	1200	11.1

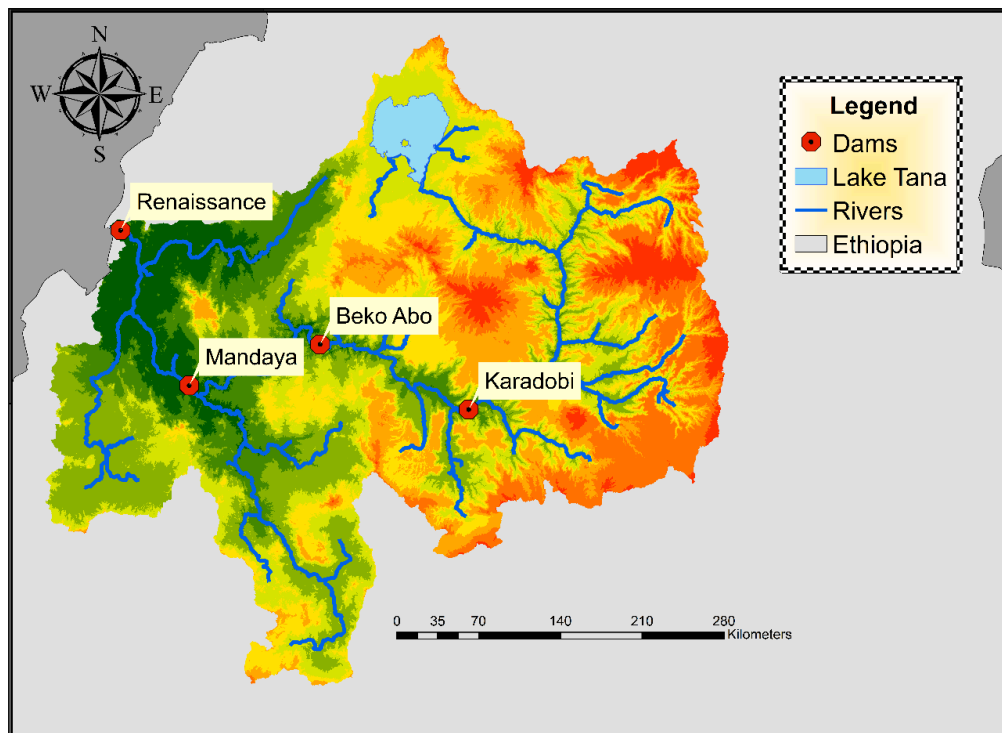


Figure 13. Location of the proposed dam constructions in the upper Blue Nile Basin.

2.2 Hydrological modeling: Theoretical background

2.2.1 Soil and Water Assessment Tool (SWAT)

The Agricultural Research Service (ARS) of the United States Department of Agriculture (USDA) has been developing SWAT for over 30 years. The hydrological model SWAT has been designed to simulate the influence of land management practices on water, sediment and chemical cycles of large catchments. SWAT is a basin-scale, physically based and time continuous model that runs on a daily time step and is capable of predicting the effects of land use and land management practices on the hydrological cycle. SWAT can simulate long periods of time in daily steps, it is also capable of incorporating multiple soils, land use and management conditions in complex watersheds. These characteristics make it a very useful tool to perform research in many fields including hydrological modeling, agriculture production, climate change impact, among others. Complementary available model components include plant growth, nutrients, pesticides bacteria and pathogens. Its computational efficiency makes possible to process all this information at high speed (*Gassman et al., 2007*). SWAT also has a great flexibility that allows the simulation and evaluation of multiple hydrological processes, for instance the prediction of water, sediment, nutrient and pesticide yields with reasonable accuracy on large and ungauged watersheds on a daily time step (*Chandra et al., 2014*). Recent studies are a prove that SWAT has become internationally and interdisciplinary accepted for modeling large and small watersheds (*Malunjar et al., 2015; Me et al., 2015; Emam et al., 2016; Wang and Sun, 2016*). SWAT also has the advantage to have been developed to analyze the interaction of several hydrological parameters and the impact of land management practices specifically for large and complex basins, thus a good model to be applied in the Blue Nile Basin. However, due to the lack of a unifying theory to accurately model the interaction of the hydrological processes, complex models suffer from over-parameterization and high predictive uncertainty (*Sivapalan, 2006*).

Although SWAT is with no doubt a powerful tool for modelling, it is also important to highlight some of its limitations. SWAT is not able to simulate non-field sources of sediment, for instance streambanks, bluffs and ravines (*Folle, 2007*). Stream channel degradation and sediment deposition processes are simplified in the model and are under development and continuous improvement (*Folle, 2007*). Nevertheless, the main limitation of SWAT that will be affecting the results obtained in this research is related to the fact that SWAT cannot simulate the Variable Source Area (VSA) hydrology with excessive overland flow saturation, which is common in humid climates like in the Blue Nile Basin. This problem causes that SWAT estimates more erodible areas in high slopes, when in reality most erodible areas are the product of the high runoff occurring in saturated areas with gently slopes. Additionally, since the model was developed in the USA its database has been specifically created for North America. Therefore, the lack of data for African watersheds is constantly a major issue regarding the use of SWAT. The majority of the databases available for SWAT are for North America and Europe. Hence, before using SWAT these databases should be modified and additional data containing soil and land use information specifically for the African continent should be integrated.

2.2.2 Spatial representation and basin configuration in SWAT

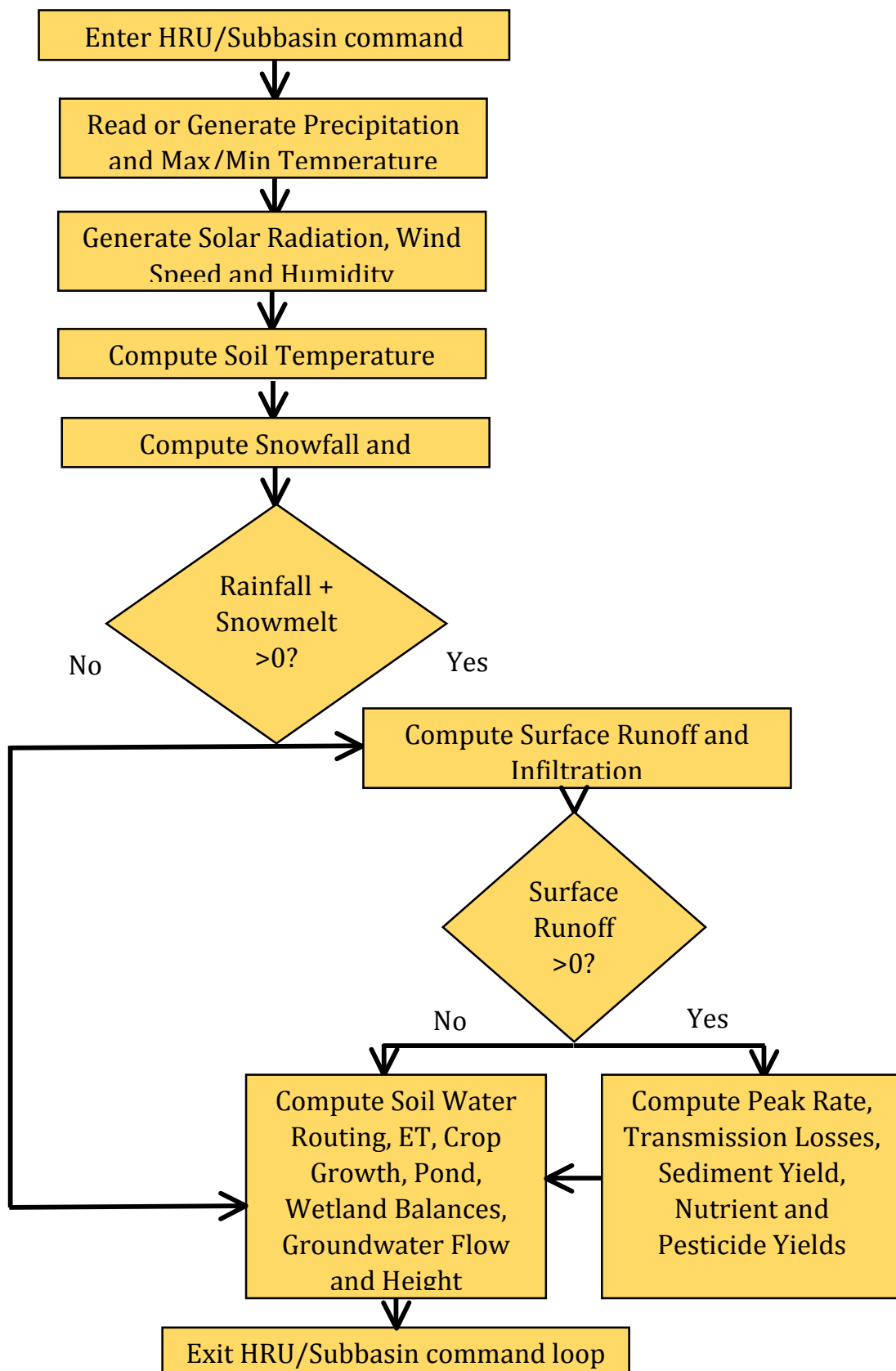


Figure 14. HRU/Sub-basin command loop of the spatial representation in SWAT (Neitsch et al. 2009).

SWAT is a semi-distributed hydrological model where the input data processing and the hydrological estimations are done at two levels of discretization, sub-basins and Hydrologic Response Units (HRUs). Sub-basins are geographically bordering areas, at this level SWAT processes different information defining the climate conditions, groundwater and the main channel draining the sub-basin. Sub-basins are spatially distributed and are interconnected by reaches where they drain to. Dividing the watershed into sub-basins facilitates the stream channel routing within SWAT, which is important when modeling watersheds with a hydrological delay greater than the model time step, daily or monthly (*Fuka et al. 2013*). These sub-basins are divided into HRUs, which are the smallest spatial units in SWAT. HRUs are not functionally defined in space, but conceptually correspond to small catchments homogeneous in land use, soil and slope classes, and are simply aggregated for the calculation of sub-basin outputs (*Neitsch et al., 2009*). All the input data is grouped into HRUs, except from the weather data which is grouped for each sub-basin. HRU's are not spatially distributed, contrary to the sub-basins which are geographically connected, this means that no flow occurs between different HRUs. Runoff processes and sediment yields are estimated separately at HRUs level. HRUs also allow the model to reflect differences in evapotranspiration and other hydrologic conditions for each crop and soil type. These two levels to simulate the different hydrological processes become important particularly when different areas of the watershed are dominated by land uses or soils different enough to affect the hydrological processes.

2.2.3 The hydrologic cycle, water balance and evapotranspiration processes in SWAT

The driving force for all the hydrological processes happening in the watershed is the water balance. The movement of the sediment particles, nutrients or pesticides is heavily related to the changes in the hydrological cycle. SWAT divides the hydrologic cycle into two major parts (*Neitsch et al. 2009*):

1. The land phase of the hydrologic cycle: This cycle is the responsible for the movement of water from the land into the main channel, which involves the sediment nutrients and pesticides.
2. The routing phase of the hydrologic cycle: This cycle contains the movement of water, sediments and constituents through the reach network to the output of the catchment.

Land phase

The main factor governing the hydrological cycle in SWAT is the water balance of the watershed. The water balance is also one of the most important factors used to determine if a model is good enough for any particular application. Hence, analyses of the processes involved in the estimation of the water balance of a watershed can provide more details about the hydrological behavior of a watershed and can be used to understand the interaction of main hydrological processes (*Zhang et al., 1999*). The

hydrological processes involved in the water balance include: precipitation, evaporation and transpiration, revap from shallow aquifer, surface runoff, lateral flow, return flow, water infiltration to the root zone and vadose zone, percolation to shallow aquifer, recharge to deep aquifer and flow out of the watershed (**Figure 15**). The water balance in SWAT is calculated for each HRU using the following formula (**Neitsch et al., 2009**):

$$SW_t = SW_0 + \sum_{i=1}^t (R_{day} - Q_{surf} - E_a - W_{seep} - Q_{gw})$$

Equation (1)

where SW_t is the final soil water content (mm), SW_0 is the initial soil water content on day i (mm), R_{day} is the amount of rainfall on day i (mm), Q_{surf} is the amount of surface runoff on day i (mm), E_a is the amount of evapotranspiration on day i (mm), W_{seep} is the amount of water entering the vadose zone from the soil profile on day i (mm), and Q_{gw} is the amount of return flow on day i (mm).

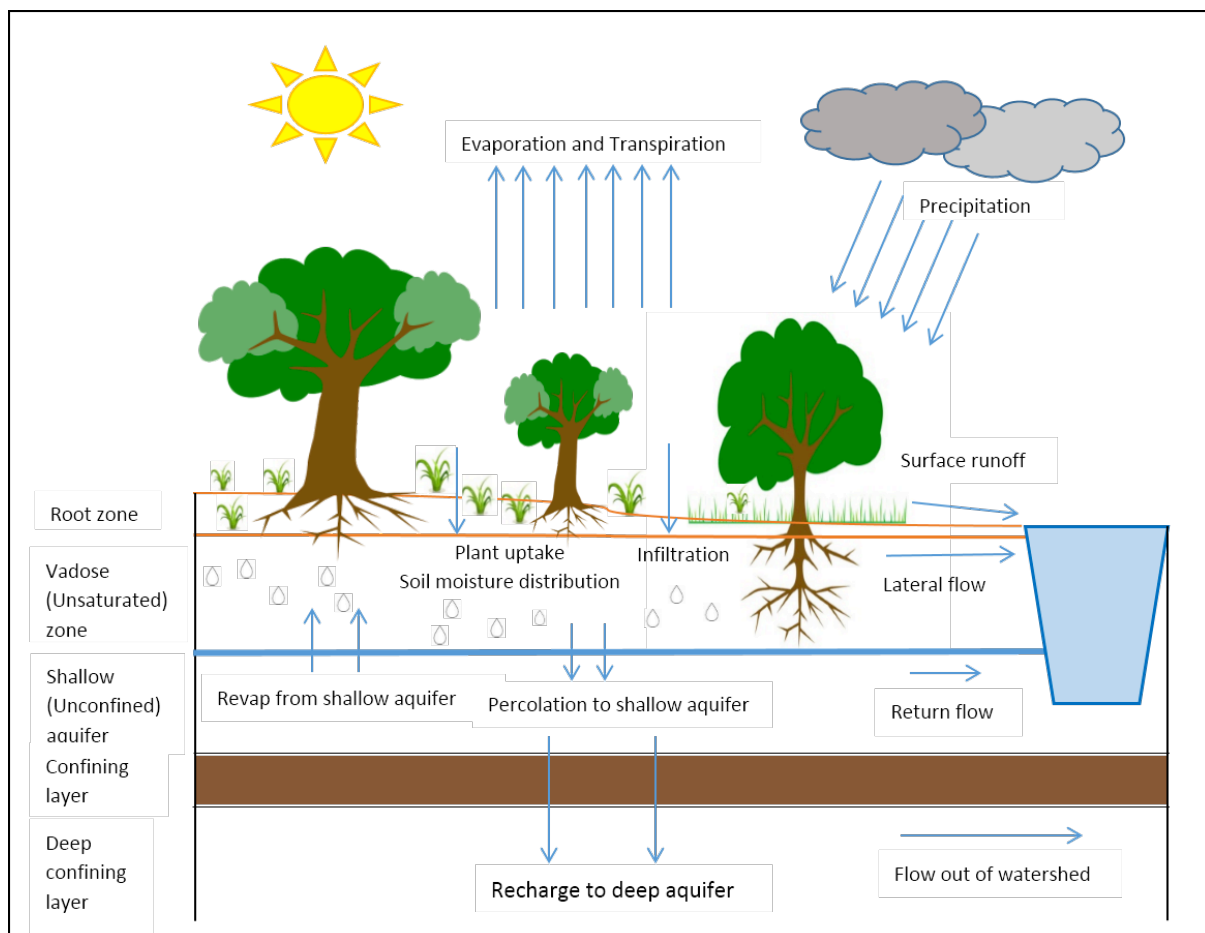


Figure 15: Hydrologic cycle in SWAT (Neitsch et al., 2009).

Evapotranspiration

SWAT can estimate the evapotranspiration using several methods: Priestly-Taylor, Penman/Monteith and Hargreaves. The Hargreaves method calculates the potential evapotranspiration using minimum and maximum daily temperature as input data (**Hargreaves and Samani, 1982**). This method was chosen as a better option for the Blue Nile Basin due to the data scarcity of the meteorological stations in the basin. Hargreaves equation can be used with the sole input of temperature data, while Penman/Monteith requires more data, for instance wind speed, solar radiation and relative humidity. Hargreaves method has been recommended for computing potential evaporation in cases when only the maximum and minimum temperatures are available (**Allen et al., 1998**). A study from **Tekleab and Uhlenbrook (2011)** was also able to successfully use the Hargreaves equation to calculate the potential evaporation in the Blue Nile Basin. Several improvements were made to the original equation since 1975 (**Hargreaves and Samani, 1982 and 1985**). The final form of the Hargreaves equation used in SWAT and published in 1985 (**Hargreaves and Samani, 1985**) is as follows (**Neitsch et al., 2009**):

$$\lambda E_0 = 0.0023 * H_0 * (T_{mx} - T_{mn})^{0.5} * (\bar{T}_{av} + 17.8)$$

Equation (2)

where λ is the latent heat of vaporization (MJ kg^{-1}), E_0 is the potential evapotranspiration (mm d^{-1}), H_0 is the extraterrestrial radiation ($\text{MJ m}^{-2}\text{d}^{-1}$), T_{mx} and T_{mn} are the maximum and minimum air temperature for a given day ($^{\circ}\text{C}$), respectively, and \bar{T}_{av} is the mean air temperature for a given day ($^{\circ}\text{C}$).

The evaporative water demand after the evapotranspiration of free water in the canopy has occurred is calculated with the following formula:

$$E'_0 = E_0 - E_{can}$$

Equation (3)

where E'_0 is the potential evapotranspiration adjusted for evaporation of free water in the canopy ($\text{mm H}_2\text{O}$), E_0 is the potential evapotranspiration on a given day ($\text{mm H}_2\text{O}$), and E_{can} is the amount of evaporation from free water in the canopy on a given day ($\text{mm H}_2\text{O}$).

Following the potential evapotranspiration, the actual evapotranspiration must be calculated by removing water from different components of the model. Initially, SWAT calculates the evaporated water intercepted by the canopy, then, maximum transpiration and soil evaporation are calculated. Evaporation from canopy is very significant in forested areas and in several cases can be higher than transpiration. Transpiration for the Hargreaves equation is calculated as (**Neitsch et al., 2009**):

$$E_t = \frac{E'_0 \cdot LAI}{3.0}$$

Equation (4)

where E_t is the maximum transpiration on a given day (mm H₂O), E'_0 is the potential evapotranspiration adjusted for evaporation of free water in the canopy (mm H₂O), and LAI is the leaf area index.

Evaporation from the soil on a given day is calculated with following equation (**Neitsch et al., 2009**):

$$E_s = E'_0 \cdot cov_{sol} \quad \text{Equation (5)}$$

where E_s is the maximum soil evaporation on a given day (mm H₂O), E'_0 is the potential evapotranspiration adjusted for evaporation of free water in the canopy (mm H₂O), and cov_{sol} is the soil cover index.

The maximum soil evaporation is reduced during periods of high plant water use with the relationship (**Neitsch et al., 2009**):

$$E'_s = \min \left[E'_s, \frac{E_s * E'_0}{E_s + E_t} \right] \quad \text{Equation (6)}$$

where E'_s is the maximum sublimation/soil evaporation adjusted for plant water use on a given day (mm H₂O), E_s is the maximum sublimation/soil evaporation on a given day (mm H₂O), E'_0 is the potential evapotranspiration adjusted for evaporation of free water in the canopy (mm H₂O), and E_t is the transpiration of a given day (mm H₂O).

Surface Runoff

The Soil Conservation Service (SCS) runoff curve number (CN) method and the Green & Ampt infiltration method are the two methods incorporated in SWAT for the estimation of the surface runoff process of a watershed. The SCS curve number is an empirical model developed in the 1950s. The surface runoff factor included in the MUSLE equation was developed to provide soil loss estimations under different land uses and soil types (**Neitsch et al., 2009**). The SCS CN equation to estimate the surface runoff created in 1972 and used by SWAT is:

$$Q_{surf} = \frac{(R_{day} - I_a)^2}{(R_{day} - I_a + S)} \quad \text{Equation (7)}$$

where Q_{surf} is the accumulated runoff or rainfall excess (mm H₂O), R_{day} is the rainfall depth for a day (mm H₂O), I_a is the initial abstraction which includes surface storage, interception and infiltration prior runoff occurs (mm H₂O), and S is the retention parameter (mm H₂O) which can change depending on types of land use, soils,

management practices and slope, and temporally also due to changes in the soil water content.

The retention parameter S is calculated as follows:

$$S = 25.4 \left(\frac{1000}{CN} - 10 \right)$$

Equation (8)

where CN is the curve number for the day.

CN is a parameter defined by the initial soil water conditions, the soil permeability and landuse. This number has been empirically determined for many different land uses depending on the permeability of the soil and precedent soil water conditions and can be found on SWAT: Theoretical Documentation (**Neitsch, 2009**).

The peak runoff rate is the maximum runoff flow rate that can occur during a rain. Peak runoffs are the maximum indicator of the erosive power of a rain and is used to predict sediment yields. In SWAT the peak runoff rate (m^3/s) is estimated using the modified rational method which is also widely used for designing ditches, channels and other water control systems. The formula included in SWAT is as follows (**Neitsch et al., 2009**):

$$q_{peak} = \frac{\alpha_{tc} * Q_{surf} * area_{hru}}{3.6 * t_{conc}}$$

Equation (9)

where q_{peak} is the peak runoff rate (m^3/s), α_{tc} is the fraction of daily rainfall that occurs during the time of concentration, Q_{surf} is the surface runoff ($\text{mm H}_2\text{O}$), $area_{hru}$ is the HRU area (km^2), t_{conc} is the concentration time for the HRU (hr), and 3.6 is a unit of conversion factor.

Since the curve number is adapted at a daily time step to the moisture conditions of the soil, the available water capacity (AWC) is another important factor influencing the surface runoff and can be calculated by subtracting the amount of available water at permanent wilting point from that present at field capacity with following equation:

$$AWC = FC - PWP$$

Equation (10)

where AWC is the plant available water content, FC is the maximum water capacity that the soil can hold over a longer period, and PWP is the water content that is not available for plants due to the high matrix potential. SWAT calculates FC and PWP , based on the soil available water capacity, bulk density ρ_b and clay content m_{clay} of a soil.

The daily curve number oscillate within the bounds of the three curve numbers: *CN1* (dry conditions – wilting point *PWP*), *CN2* (average conditions) and *CN3* (wet conditions – field capacity *FC*). *CN1* and *CN3* are calculated from *CN2*. *CN2* can also be adjusted on a daily basis for different land use classes through the introduction of management procedures such as tillage or harvest, for which a specific curve number *CNOP* can be defined by the user. The CN method can be adjusted to define exactly the portion of a watershed responsible for the surface runoff generation (*Steenhuis et al., 1995*). It has also been proved that this portion of the watershed can be accurately modeled by spatially connecting the CN with the Topographic Index (TI), in a similar way as it is done in TOPMODEL (*Beven and Kirkby, 1979; Lyon et al., 2004*).

Routing phase

Once the water distribution, sediment loads, nutrients and pesticides have been estimated, these are routed through the channel network (*Figure 16*).

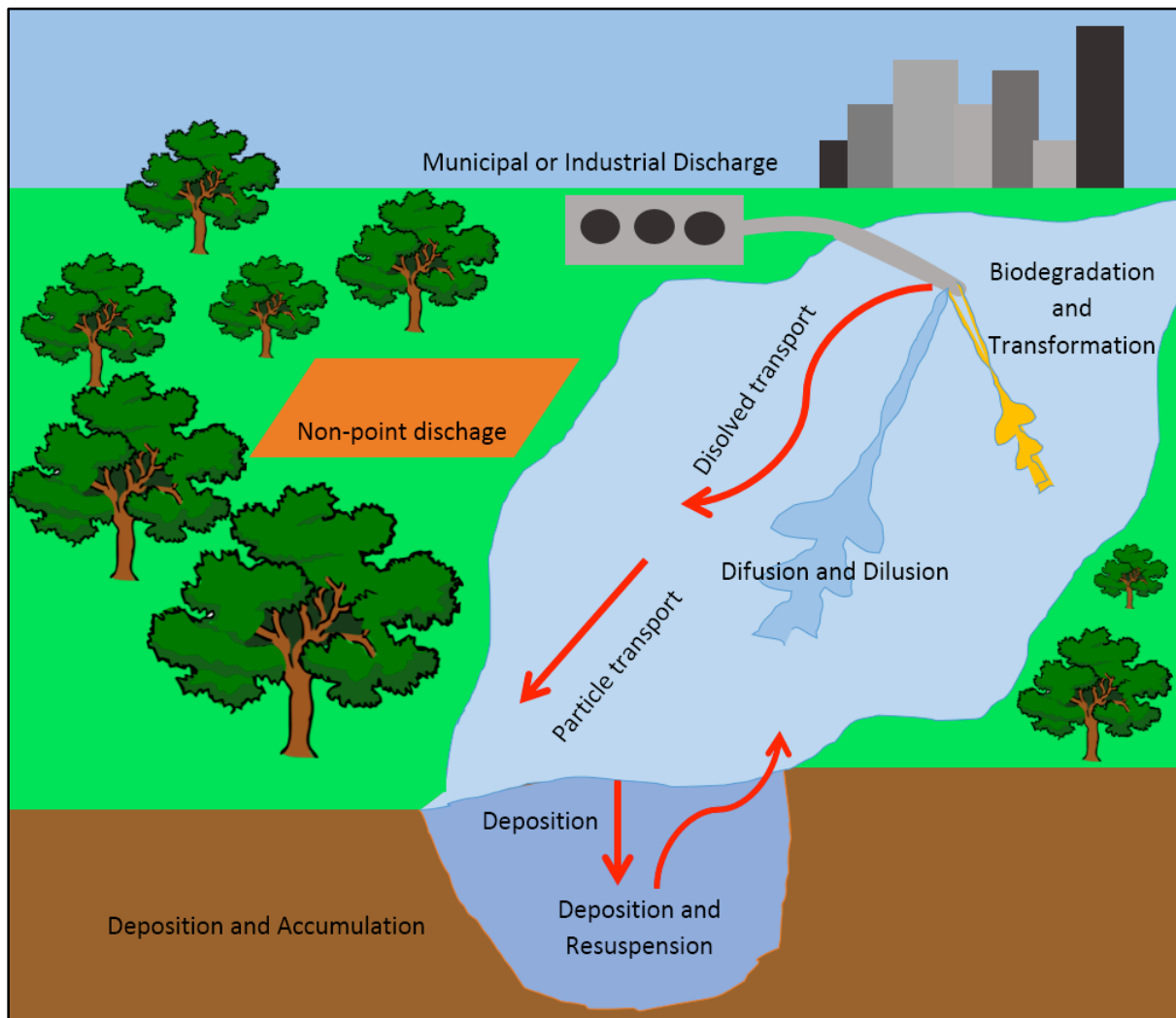


Figure 16. In-stream processes modeled by SWAT (Neitsch et al., 2009).

Some of the aspects and formulae governing the water routing process are:

- The Manning's equation is used to estimate rates and velocity of constant flows.
- For this type of uniform dimensions, the main channel has a trapezoidal shape and the channel characteristics can be set to remain.
- Flood routing is done in volumes and estimated with a variable storage method. The Muskingum routing method is also an additional option.
- During the routing process the gains and losses from the main channel can occur from precipitation, evaporation, transmission losses, bank storage losses or returns and diversions.
- During the flood routing process, losses can be caused by transmissions through the channel bed, evaporation and anthropological removals.
- Water inclusion can occur through precipitation or point source discharges.

Flood routing

Flood routing estimations are used to predict hydrograph shape variations where water moves through a reservoir, basin or a river. It can also be very advantageous to design reservoirs, river channels, watershed simulations and floodplain studies (**Beven, 2012**). These models require large amount of data related to the river's geometry and morphology and can consume a lot of computer resources to solve the numerical equations (**Beven, 2012**). The equations used are the Saint-Venant equations which are based on hydraulic principles but they are clearly an approximation to the fully three-dimensional flow processes in any stream channel (**Beven, 2012**). The two main solutions are the diffusion wave approximation and the kinematic wave approximation:

$$\frac{\delta A \rho g h}{\delta x} = \rho g A (S_o - S_i)$$

Equation (11)

$$\rho g A (S_o - S_i) = 0 \quad S_o = S_i$$

Equation (12)

where A is the cross-sectional area, ρ is the local hydrostatic pressure, h is the average depth of the flow, x is the distance downslope or downstream, S_o is the channel bed slope, and S_i is the friction slope which is a function of the roughness of the surface or channel.

Hydrological routing also employs the continuity equation for hydrology where the inflow to the river reach is equal to the outflow of the river plus the change of storage:

$$I = O + \frac{\Delta S}{\Delta t}$$

Equation (13)

where I is the average inflow to the reach during Δt , O is the average outflow from the reach during Δt and S is the current storage water (water in the reach).

Additionally, hydrological routing requires the estimation of hydrological parameters using measured data in both upstream and downstream regions of the rivers and the application of complex optimization techniques to solve the one-dimensional equation for conservation of mass and storage-continuity (**Barati, 2011**). However, semi-distributed models are often based on simple physical concepts and common river characteristics such as the reach length, slope and the roughness coefficients, and geometry of the channel. Altogether, these models can efficiently be used to estimate the model parameters without complex and expensive numerical solutions. A common example of this type of models are the ones based on Hydrological Response Units, for instances SWAT (**Beven, 2012**).

2.2.4 Soil erosion

The erosion is a naturally occurring process where water and wind contributes to a significant amount of soil loss each year. Soil erosion can be a slow or fast process that can occur an unrecognized or at an alarming rate causing loss of the soil's top layer. Some of the causes leading to an accelerated increase of the erosion rate are related to human activities such as deforestation, cultivation and livestock farming. The soil loss can be reflected in a reduction of the crop production, low water quality and damage of drainage networks. Prevention of soils loss through sustainable conservation practices is the main approach that can limit the erosion in vulnerable lands. The Food and Agriculture Organization of the United Nations in the "Ethiopian highland reclamation study" distinguishes six different categories of erosion (**FAO, 1986**):

Water erosion

This is the most severe erosion process and mainly caused by the raindrop splash on the land cover and the water runoff. The intensification of its effect depends on the characteristics of the land, where slopes have to be sufficient and soil configuration favorable in order to transport the water efficiently. Six types of rainfall erosion processes can be identified:

1. *Sheet erosion*: also called splash erosion, is almost a uniform removal of soil over the land surface (**FAO, 1986**). This type of erosion is caused by the runoff energy and the force of the raindrops impacting on bare soil and removing particles of soil (**Ellison, 1944**). Thus, the aggregate stability is a very important factor in the control of splash erosion (**Farres, 1987**). Sheet erosion is mainly dependent to the maximum intensity, energy and duration of the rain (**Hudson, 1973**).
2. *Rill erosion*: evolves from sheet erosion when rills are formed due to water concentrations down a slope. Rills are narrow and shallow channels which are eroded into vulnerable soil by hill slope runoff. The erosion process begins when water breaks the soil particles freely and carries them down the slope (**Torri, 1987**). Rills are capable of washing away archeological sites and eroding agricultural areas by decreasing large amount of organic content (**Fullen, 1987**).

3. Gully erosion: takes place when rills are widened and deepened until they are too wide to be removed from cultivation. Gully erosion happens until the vegetation cover can stabilize the slopes of the gully. For this kind of erosion to take place significant amount of water flow rates should exist (**Costard, 2002**).
4. Ban/Bed erosion: is the detachment and transportation of sediment particles alongside the riverbed due to water runoff (**FAO, 1986**). This process can significantly increase the erosion creating thinner soils as the channel adjusts to the increase of the flow creating complex erosion in the stream bed (**Garcia, 1991**).
5. Tunnel erosion: is caused by water eroding the soils under the surface. This erosion is common to soils that are rich in smectites (swell and shrink clays, associated with Vertisols) which cause a low permeability (**Miserez, 2016**). Once tunnels are formed they continue to enlarge during successive wet periods. If the tunnel reaches a point where the roof collapses it can result in the formation of a gully erosion (**Miserez, 2016**).
6. Landslides: are a massive movement of soil, usually generated by intense rainfalls. This is the most rapid and risky forms of soil erosion and riverbanks erosion (**FAO, 1986**). Landslides can occur when slopes change from stable to unstable conditions due to different natural or anthropogenic causes, for instance earthquakes, volcanic eruptions, deforestation, vibration of machinery, constructions, among others (**FAO, 1986**).

The governing erosion factors that contribute to most of the soil degradation by water in the Blue Nile Basin is the land use, followed by land slope, erodibility and erosivity (**FAO, 1986**) (**Figure 17**).

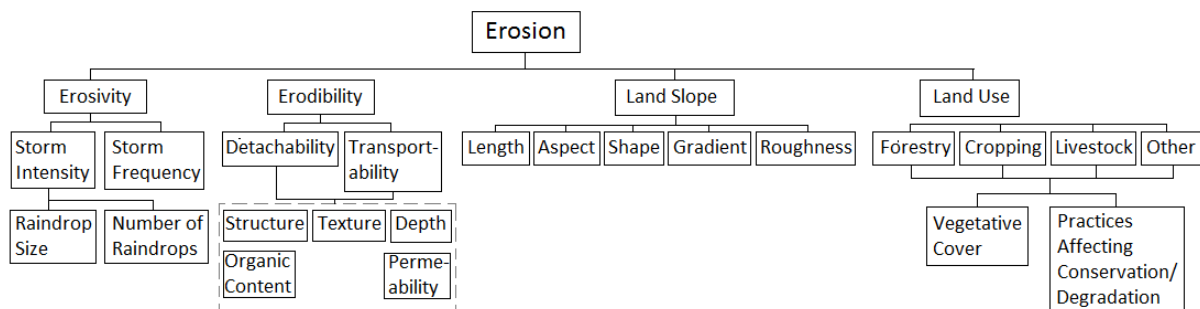


Figure 17. Factors contributing to soil erosion by water in the Blue Nile Basin (**FAO, 1986**).

1. Erosivity: is the potential capacity of a rainfall to cause erosion. It depends on the rainfall amount, intensity, frequency and drop size. Since rainfall in Ethiopia tends to happen in short periods of time, soil erosivity is an important aspect of water erosion (**FAO, 1986**).

2. ***Erodibility***: is defined by the predisposition of the soil to be degraded and transported. The distribution and size of the pores and the initial pore water content determines the rate at which the water can infiltrate the soil during a rain event (permeability) and how much water can be stored by the soil. High concentration of clay content can have adverse effects on erodibility: organic matter dependence on clay and soils with low organic matter content are high susceptible to erosion (**Luk, 1979**).
3. ***Topography***: slope and the length of the slope are the governing factors for rainfall erosion. The slope can directly affect the runoff velocity and thus the transport capacity of the runoff (**Ali et al., 2012**). Slope length also affects the runoff concentration and the formation of rills and gullies (**Julien and Simons, 1985**).
4. ***Land use***: Soil is usually protected from erosion by a vegetation cover under natural conditions. Plants and crops protect the soil from the harmful force of raindrops and from drying effects of wind and sun. Roots bind the soil together and create pores in the soil that increase the drainage capacity. Water uptake and transpiration of the plants also reduces the soil water content and enhance to increase the capacity of the soil to absorb rain. Plant and crop layer not only covers and protects the soil, but is also necessary for the development of organic matter, a crucial component of a resistant soil.

Wind erosion

Wind causes the detachment and transportation of soil particles as well as the abrasive effects of sediment particles as they are moved. Wind erosion usually carries the finest particles in particular organic matter, clay and loam. Different factors like the aridity of the climate, soil texture, and soil structure, state of the soil surface, vegetation and soil moisture can affect the extent of wind erosion. To control this type of erosion different methods can be used such as reducing the wind speed at ground level, increasing the soil cohesion and improving the soil resistance to the wind by increasing the land cover (**Heusch, 1988**).

Physical Degradation

This degradation can be caused by deforestations, inappropriate irrigation, urban sprawl, vehicle off-roading, and monoculture and dumping of non-biodegradable trash such as plastics. This process involves changes of the physical characteristics of the soil such as porosity, permeability, bulk density and structural stability. Land degradation is affected by a combination of human induced processes that acts upon the land (**Conacher, 1995**).

Chemical Degradation

This is the decomposition of the soil due to chemical processes. Although the use of pesticides and other chemicals used on crops have helped farmers to increase yields, the overuse of these chemicals can change the soil composition and disturb the balance

of microorganisms in the soil (*Ritter 2012*). Additionally, soil nutrients and other surface-applied chemicals can be transported with oil particles, contributing to off-site impacts.

Salinization

This process represents the impact of salt content in the soil. Salty soils present particular challenges because they tend to have very poor structure which limits the water infiltration and drainage. In dry regions salts may accumulate, leading to naturally saline soils. Salinization can occur when the water is between two and three meters from the surface of the soil (*FAO, 1988*). Salinization can also occur due to irrigation, since almost all water contains some dissolved salts. When the plants stop using the water the salt are left behind in the soil and eventually begin to accumulate and can also be greatly increased by poor drainage (*FAO, 1988*).

Biological Degradation

This type of degradation represents the reduction of biological activity in and on the sediment particles.

2.2.5 Soil erosion and sediment estimations in SWAT

In SWAT the erosion process caused by rainfall and runoff is calculated with the Modified Universal Soil Loss Equation (MUSLE). This equation was developed by *Williams (1995)* who modified the Universal Soil Loss Equation (USLE) of *Wischmeier and Smith (1965, 1978)*. The differences between the USLE and the MUSLE equations is that the modified equation predicts the average annual gross erosion as a function of runoff while the USLE replaces de runoff factor with the rainfall energy. The MUSLE equation is focused on the elimination of the need to deliver ratios and improves the sediment yield prediction.

MUSLE

Soil erosion occurs during the hydrological cycle on the land phase and water phase (streams if channel degradation is active). The land phase erosion, which is the erosion caused by the precipitation and runoff, is calculated for each HRU based on the MUSLE method (*Neitsch et al., 2009*). This equation estimates the sediment concentration as a function of runoff instead of rainfall as it was done with the USLE method developed by *Wischmeier and Smith (1965, 1978)*. The MUSLE formula developed by Williams in 1995 (*Williams, 1975*) is as follows:

$$sed = 11.8 * (Q_{surf} * q_{peak} * area_{hru})^{0.56} * K_{USLE} * C_{USLE} * P_{USLE} * LS_{USLE} * CFRG$$

Equation (14)

where sed is the sediment yield on a given day (metric tons), Q_{surf} is the surface runoff volume (mm H₂O/ha), q_{peak} is the peak runoff rate (m³/s), $area_{hru}$ is the area of HRU (ha), K_{USLE} is the USLE soil erodibility factor (0.013 metric ton m² hr/(m³-metric ton cm)), C_{USLE} is the USLE cover and management factor, P_{USLE} is the USLE support practice factor, LS_{USLE} is the USLE topographic factor and $CFRG$ is the coarse fragment factor.

The surface runoff Q_{surf} is estimated with the SCS curve number method and the peak runoff rate q_{peak} is estimated with a modified rational method (*Neitsch et al., 2009*). In the modified rational method runoff peaks are made on the idea that a rainfall of certain intensity begins and continues indefinitely, and the runoff rate will increase until the time of concentration. In this method the runoff increases until the entire sub-basin area contributes to the discharge at the outlet. The time of concentration is estimated from the HRU area and the overland flow velocity is estimated with the Manning's equation. In the modified rational method, the peak runoff is dependent on the proportion of the daily rainfall. The time of concentration is a function of overland and channel flow.

The surface runoff volume is calculated with the following formula:

$$Q_{surf} = \frac{(R_{day} - I_a)^2}{(R_{day} - I_a + S)}$$

Equation (15)

where Q_{surf} is the accumulated runoff or rainfall excess (mm H₂O), R_{day} is the rainfall depth for a day (mm H₂O), I_a is the initial abstraction which includes surface storage, interception and infiltration prior runoff occurs (mm H₂O), and S is the retention parameter (mm H₂O) which can change depending on types of land use, soils, management practices and slope, and temporally also due to changes in the soil water content.

The equation used to calculate the peak runoffs rate is:

$$q_{peak} = \frac{\alpha_{tc} * Q_{surf} * area_{hru}}{3.6 * t_{conc}}$$

Equation (16)

where q_{peak} is the peak runoff rate (m³/s), α_{tc} is the fraction of daily rainfall that occurs during the time of concentration, Q_{surf} is the surface runoff (mm H₂O), $area_{hru}$ is the HRU area (km²), t_{conc} is the concentration time for the HRU (hr), and 3.6 is a unit of conversion factor.

The MUSLE method contains several factors (K_{USLE} , C_{USLE} , P_{USLE} , LS_{USLE} , $CFRG$) for which empirical formulas have been developed:

K_{USLE} is the soil erodability factor which is defined as the soil loss rate per erosion index unit for a specified soil as measured on a unit plot (**Arnold et al., 2012**). This factor can be determined by field measurements or with help of various empirical equations. These equations determine erodability based on soil texture, structure and organic matter content which can be assessed from soil samples. The USLE_K factor (so named in SWAT) is defined for each soil type and layer in SWAT. The soil type usually becomes less erodible with the decrease in silt fraction; thereby the corresponding increase in the sand or clay fraction does not necessarily matter (**Wischmeier and Smith, 1978**). This formula is applicable when the very fine sand and silt content makes up less than 70% of the soil particle size distribution (**Wischmeier et al., 1971**). The formula for the erodability factor K_{USLE} is:

$$K_{USLE} = \frac{0.00021 * M^{1.14} * (12 - OM) + 3.25 * (c_{soilstr} - 2) + 2.5 * (c_{perm} - 3)}{100}$$

Equation (17)

where M is the particle-size parameter, OM is the percent of organic matter (%), $c_{soilstr}$ is the soil structure code used in soil classification, and c_{perm} is the profile permeability class.

The particle-size parameter M , is given by:

$$M = (m_{silt} + m_{vfs}) * (100 - m_c)$$

Equation (18)

Where m_{silt} is the silt content (0.002-0.05 mm diameter particles) in %, m_{vfs} is the percent of very fine sand content (0.05-0.10 mm diameter), m_c is the percentage of clay content (< 0.002 mm diameter particles).

The organic matter content, OM , in percent is given by:

$$OM = 1.72 * orgC$$

Equation (19)

where $orgC$ is the percent of organic carbon content of a soil layer.

$c_{soilstr}$ is the soil structure codes characterized by the class and the type of soil structure present in the layer. Soil structure is the arrangement of soil particles into groupings, which are called either peds or aggregates. There exists four primary types of structure (**Figure 18**):

- Platy, with particles arranged around a plane, generally horizontal.
- Prismatic, with particles arranged around a vertical line and bounded by relatively flat vertical surfaces.

- Blocky or polyhedral, with particles arranged around a point and bounded by flat or rounded surfaces which are casts of the molds formed by the faces of surrounding peds.
- Spheroidal or polyhedral, with particles arranged around a point and bounded by curved or very irregular surfaces that are not accommodated to the adjoining aggregates.







		
<p>Granular. Resembles cookie crumbs and is usually less than 0.5 cm in diameter. Commonly found in surface horizons where roots have been growing.</p>	<p>Blocky. Irregular blocks that are usually 1.5-5.0 cm in diameter.</p>	<p>Prismatic. Vertical columns of soil that might be a number of cm long. Usually found in lower horizons.</p>
		
<p>Columnar. Vertical columns of soil that have a salt “cap” at the top. Found in soils of arid climates.</p>	<p>Platy. Thin, flat plates of soil that lie horizontally. Usually found in compacted soil.</p>	<p>Single Grained. Soil is broken into individual particles that do not stick together. Always accompanies a loose consistence. Commonly found in sandy soils.</p>

Figure 18. Types of soil structures in soils (McClellan, 2016).

C_{USLE} is the cover and management factor which reflects the protection of the soil by canopy and plant residue cover for a specific crop and vegetation type. It is defined as the ratio of soil loss from a specifically cropped land to the soil loss from a clean tilled plot. Since this factor changes during the growing period, $USLE_C$ is updated daily by SWAT. The user input for $USLE_C$ represents the maximum protection that can be provided by a full-grown plant of the crop/vegetation type. It is calculated by:

$$C_{USLE} = \exp([\ln(0.8) - \ln(C_{USLE,mm})]) * \exp[-0.00115 * rsd_{surf}] + \ln[C_{USLE,mm}]$$

Equation (20)

where $C_{USLE,mm}$ is the minimum value for the land cover and management factors of the land cover, and rsd_{surf} is the amount of residue on the soil surface (kg/ha).

The minimum value for cover and management factor is estimated from a known average annual C factor and given by:

$$C_{USLEmn} = 1.463 * \ln[C_{USLE,aa}] + 0.1034$$

Equation (21)

Where C_{USLEmn} is the minimum value for the land cover and $C_{USLE,aa}$ is the average annual C factor for the land cover.

P_{USLE} is the support practice factor which represent the conservation practices such as contour tillage and terracing. It is defined as the ratio of soil loss from a field where certain support practices are used to soil loss from an up-and-down slope tilled field. The support practice factor differs for different practices. **Table 6** shows the factor values for contouring, i.e. plowing across the slope following its contour lines depending on the land slope (**Minnesota Department of Agriculture, 2016**).

Table 6: P_{USLE} factors and slope-length limits for contouring (Wischmeier and Smith, 1978).

Land slope (%)	P_{USLE}	Maximum length (m)
1-2	0.60	122
3-5	0.50	90
6-8	0.50	61
9-12	0.60	37
13-16	0.70	24
17-20	0.80	18
21-25	0.90	15

The topographic factor LS_{USLE} is the soil loss per unit area from a field slope and is calculated with the following formula:

$$LS_{USLE} = \left(\frac{L_{hill}}{22.1}\right)^m * (65.41 * \sin^2(\alpha_{hill}) + 4.56 * \sin \alpha_{hill} + 0.065)$$

Equation (22)

where L_{hill} is the slope length (m), m is the exponential term, and α_{hill} is the angle of the slope.

The exponent m is calculated from the average HRU slope as follows:

$$m = 0.6 * (1 - \exp[-35.835 * slp])$$

Equation (23)

CFRG is the coarse fragment factor which is calculated from the rock content of the top soil layer as:

$$CFRG = \exp(-0.053 * rock)$$

Equation (24)

The MUSLE does not include losses from gully erosion, only rill and sheet erosion.

Sediment estimation at HRU level

In SWAT each hydrological process is independently calculated for each HRU, which can be distributed or divided into several parts within a sub-basin. Sediment calculations are done at HRUs level, where the erosion process is calculated based on runoff. The fraction of daily rainfall used in the modified rational method is calculated by SWAT as a function of the fraction of daily precipitation falling in the half-hour highest intensity rainfall and is given by the formula:

$$\alpha_{tc} = 1 - \exp[2 * t_{conc} * \ln(1 - \alpha_{0.5})]$$

Equation (25)

where α_{tc} is the fraction of daily rainfall during time of concentration, t_{conc} is the concentration time of a HRU (hr), $\alpha_{0.5}$ is the fraction of daily rainfall happening in the half-hour of highest intensity rainfall

Since larger HRUs have longer slope lengths, this will have an impact on the runoff concentration time, hence an impact on the total sediment load estimations. The runoff concentration time from the place where the rainfall occurs to the point where the sub-basin outlet is located, is calculated as follows:

$$t_{conc} = t_{ov} + t_{ch}$$

Equation (26)

where t_{conc} is the concentration time of a HRU (hr), t_{ov} is the overland flow time of concentration (hr), and t_{ch} is the channel flow time of concentration (hr).

The overland flow concentration time can be calculated using the equation:

$$t_{ov} = \frac{L_{slp}}{3600 * v_{ov}}$$

Equation (27)

where L_{slp} is the average HRU slope length (m), v_{ov} is the overland flow velocity (m³/s), and 3600 is a unit of conversion factor.

The overland flow velocity however, is estimated from the Manning's equation:

$$v_{ov} = \frac{q_{ov}^{0.4} * slp^{0.3}}{n^{0.6}}$$

Equation (28)

Where q_{ov} is the average overland flow rate (m³/s), slp is the average slope in the HRU, n is the Manning's roughness coefficient for the HRU

Although SWAT is not showing the channels at HRU level, they do exist as artificial channels to calculate the concentration time. This channel flow concentration time is estimated using the equation:

$$t_{ch} = \frac{L_c * \left(\frac{Area_{hru}}{Area_{subbasin}} \right)}{3.6 * v_c}$$

Equation (29)

where L_c is the average flow channel length for the sub-basin (km), v_c is the average channel velocity (m s⁻¹), and 3.6 is a unit of conversion factor.

The average channel length is then estimated with the equation:

$$L_c = \sqrt{L * L_{cen}}$$

Equation (30)

Where L is the channel length which defines the longest path from the most distant point to the sub-basin outlet (km), L_{cen} is the distance along the channel to the sub-basin centroid (km). The centroid of the sub-basin is the average, the "center" position of the area.

The length L is derived from the longest tributary channel length. Tributary channels are minor channels, most of them branches of main channels in sub-basins. Each tributary channel drains a fraction of the sub-basin and is not affected by the groundwater.

The slope of the channel is the difference in elevation of the watershed outlet and the most distant point in the sub-basin, divided by the length of the longest tributary channel. The average slope of the channel is dependent on the channel length, which in SWAT is the longest tributary channel.

Once the sediment loads caused by the surface runoff have been calculated with the previously mentioned formulae, the amount of sediments able to reach the main stream after the sediment lag is calculated with the following formula:

$$sed = (sed' + sed_{stor,i-1}) * \left(1 - \exp\left[\frac{-surlag}{t_{conc}}\right]\right) \quad \text{Equation (31)}$$

where sed is the amount of sediment discharged to the main channel on a given day (metric tons), sed' is the amount of sediment load generated in the HRU on given day (metric tons), $sed_{stor,i-1}$ is the sediment stored or lagged from the previous day (metric tons), $surlag$ is the surface runoff lag coefficient, and t_{conc} is the time of concentration for the HRU (hrs).

Sediment routing

This is the sediment erosion that happens in the reach network and therefore, in the water phase of the hydrological cycle. The sediment routing is dependent on two processes happening at the same time: deposition and degradation. They can take place in the channel depending on the stream power, the exposure of the channel sides and the characteristics of the reach bank and sediment. Sediment transport in the channel is separated into two phases: the transport of eroded sediments from the land phase and the eroded particles from the channel bed and banks. The components eroded from the land phase involve all the sediment particles coming into the reach calculated by the MUSLE equation (deducting the lag in grassed waterways, vegetative strips or ponds). The actual sediment concentration (Mg sed/m³ H₂O) in the surface runoff for each HRU is calculated by the equation:

$$conc_{sed,surq} = \frac{sed}{10 * area_{hru} * Q_{surf}} \quad \text{Equation (32)}$$

where sed is the sediment yield on a given day (metric tons) estimated by MUSLE equation, $area_{hru}$ is the HRU area (ha), Q_{surf} is the surface runoff on a given day (mm H₂O).

The default method for sediment routing is based on the Bangold's equation for stream power. The method determines the maximum amount of sediment that is transported from a reach segment as a function of the peak channel velocity. In this method different particle sizes of the sediment are not tracked. Consequently, all sediment appears as silt in the SWAT output table. The maximum concentration transportable $conc_{sed, ch, mx}$ is then compared to the concentration of sediment in the water at the beginning of the time step. The formula in SWAT is:

$$conc_{sed, ch, mx} = c_{sp} * v_{ch, pk}^{spexp}$$

Equation (33)

where $conc_{sed}$ is the maximum sediment concentration that can be transported by the water, $v_{ch, pk}$ is the peak channel velocity (m/s), c_{sp} and $spexp$ are coefficients defined by the user. The $spexp$ coefficient is used in the original stream power equation and is only an exponent parameter to calculate sediment retained in the channel sediment routing process. However, it has a great impact on sediment estimations in SWAT, where its higher values generate larger amounts of sediment. This exponent is extremely sensitive and sediment calibrations can easily be done by adjusting this parameter. An increase of the $spexp$ value reduces the amount of sediment deposition in the channel and increments the sediment transport capacity of the channel. $spexp$ varies from 1.0 to 2.0 and was set at 1.5 in the original equation (**Arnold et al., 1998**), however this range and its adjustments are totally empirical and lack of physical meaning because no measurements have been done to estimate specific values of certain channel conditions. The default $spexp$ value in SWAT does not represent erosive channels, therefore it has to be adjusted to match measured sediment data of rivers with high erosive processes. Additionally, due to its sensitivity, erosion estimations can easily be manipulated to obtain good fitting values, which raises questions about how realistic is the representation of the erosion processes in SWAT.

The total amount of sediment deposited in the watershed is calculated by:

$$sed_{dep} = (conc_{sed, ch, i} - conc_{sed, ch, mx}) * V_{ch}$$

Equation (34)

Where sed_{dep} is the total amount of sediment degraded in the reach sector (metric tons), $conc_{sed, ch, i}$ is the initial sediment concentration at the beginning of the time step (t/m^3), $conc_{sed, ch, mx}$ is the maximum amount transportable sediment by water, V_{ch} is the volume of water in the reach sector (m^3).

The total amount of suspended sediment in the reach is calculated after degradation and deposition and estimated as follows:

$$sed_{ch} = sed_{ch, i} - sed_{dep} + sed_{deg}$$

Equation (35)

where sed_{ch} is the total amount of suspended sediment in the reach sector (metric tons), $sed_{ch, i}$ is the quantity of suspended sediment at the beginning of the time step

(metric tons), sed_{dep} is the quantity of sediment deposited in the reach segment (metric tons), sed_{deg} is the quantity of sediment degraded in the reach sector (metric tons).

Once the suspended sediment in the reach has been calculated, the total amount of sediment transported out of the reach is calculated with the following equation:

$$sed_{out} = sed_{ch} * \frac{V_{out}}{V_{ch}}$$

Equation (36)

where sed_{out} is the amount of sediment transported out of the reach sector (metric tons), sed_{ch} is the amount of suspended sediment in the reach sector (metric tons), V_{out} is the volume of outflow during the time step (m^3), V_{ch} is the volume of water in the reach segment (m^3).

Sediment yield in lateral and groundwater flow

Unless the return flow is very high, the sediment concentrations caused by lateral flow or groundwater does not contribute significantly to the final sediment yields of a HRU. The estimation of sediments to the main channel caused by lateral and groundwater flows are done with the following formula:

$$sed_{lat} = \frac{(Q_{lat} + Q_{gw}) * area_{hru} * conc_{sed}}{1000}$$

Equation (37)

where sed_{lat} is the sediment load in lateral and groundwater flow (metric tons), Q_{lat} is the lateral flow for a given day ($mm\ H_2O$), Q_{gw} is the groundwater flow for a given day ($mm\ H_2O$), $area_{hru}$ is the area of the HRU (km^2), and $conc_{sed}$ is the concentration of sediment in lateral and groundwater flow (mg/l).

2.2.6 Calibration and validation of hydrological models

The inaccurate input data quality and limitations in the capabilities of a model to represent the complexity of the hydrological processes often constitute obstacles. Therefore, models must be calibrated, and a statistical analysis is also required to see how reliable the results of the model are prior to their applications (**Bastidas et al., 2002**). Calibration is the process of adjusting the model parameters and force them within the margins of the uncertainties. The calibration main objective is to obtain a model representation of the processes of interest that satisfies a pre-agreed criteria. The main approach of the calibration is the improvement of the model by developing correction factors that can be applied to generate predicted values and can improved the model description. The reliability of a model depends on the degree of matching of

simulated results with the observed values from the stream outflow or sediment measurements. The calibration and validation of SWAT models can be done manually within SWAT ArcGIS interface or automatically through the SWAT-CUP interface.

Semi-automatic calibration with SWAT-CUP

The automated model calibration process is SWAT-CUP requires the selection of the hydrological parameters to be systematically changed and input of measured data, based on which the model will compare the simulated data and will perform different statistical analyses. SWAT-CUP can enable sensitivity analysis, calibration, validation and uncertainty analysis of SWAT models. Packages like SWAT-CUP can help decrease models uncertainty by removing sources of modeling and calibration errors. SWAT-CUP allows a diverse amount of available statistical algorithms to perform the calibration and validation of SWAT:

1. Sequential Uncertainty Fitting II (*SUFI-2; Abbaspour et al. 2004 and 2015*).
2. Particle Swarm Optimization (PSO).
3. Generalized Likelihood Uncertainty Estimation (*GLUE; Beven and Binley, 1992*).
4. Parameter Solution (*ParaSol; Van Griensven et al. 2003 and 2006*).
5. Markov Chain Monte Carlo (*MCMC; e.g., Kuczera and Parent, 1998; Marshall et al., 2004; Vrugt et al., 2003; Yang et al., 2007*).

The **Sequential Uncertainty Fitting II (SUFI-2)** is a sequential parameter estimation method that operates within parameter uncertainty domains (*Tanveer et al. 2016*). SUFI-2 performs several iterations, where each iteration provides better results than the previous iteration and reduces the parameters ranges. In SUFI-2 the objective is to capture most of the observed values within the 95PPU (95% prediction uncertainty) range at the same time that thinner 95PPU range is preferable. The 95PPU represents the uncertainty in the model outputs. Therefore, the simulation starts assuming large and physically meaningful parameter ranges, so that the measure data falls within the 95PPU, and continuously decreases the ranges of the 95PPU and produces better results. The final 95PPU is the 95% of the observed data captured within the final 95PPU band, which is defined by the final parameters intervals. Therefore, the best simulation is the best iteration within the 95PPU, and considering that is difficult to claim a specific parameter range for a certain watershed, then any solution within the 95PPU should be an acceptable solution. The fit of simulated results within the 95PPU is quantified through the p-factor and r-factor. The p-factor is the percentage of observed data falling within the 95PPU and ranges from 0 to 1, while r-factor is the thickness of the 95PPU band and ranges from 0 to the infinity. The quality of a calibration and the prediction uncertainty are judged based on how close p-factor is to 1 and how close r-factor is to 0 (*Yang et al., 2007*). A p-factor of 1 and r-factor of 0 represents the measured data. As the number of iterations increases SUFI-2 continues to reduce the 95PPU thickness and produces smaller values for p-factor and r-factor, trying to find a better combination of the parameter values. The uncertainty in SUFI-2 is expressed as an uniform distribution of parameters ranges, and parameters uncertainties are considered for any possible source in variables, for instance model inputs, model structure, model parameters and also measured data (*Abbaspour et al., 2015*). The

uncertainties in the outputs are expressed as the 95PPU. The uncertainty analysis in SUFI-2 is based on the concept that a single parameter value generates a single model response, while a parameter range or propagation of the parameter uncertainty leads to the 95PPU.

The **Particle Swarm Optimization (PSO)** is a population based stochastic optimization technique developed by *Eberhart and Kennedy (1995)*. Social behavior of bird flocking or fish schooling are the inspiration for this algorithm. The PSO simulates the scenario of a group of birds (called particle) randomly searching food in an area. PSO is initialized with a group of random particles (solutions) and then searches for optimum values by updating generations.

The **Generalized Likelihood Uncertainty Estimation (GLUE)** was introduced partly to allow for the possible non-uniqueness (or equifinality) of parameter sets during the estimation of model parameters in over-parameterized models. In the case of large over-parameterized models, there is no unique set of parameters, which optimizes goodness of fit-criteria. For the GLUE analysis the only formal requirements needed are that the likelihood measure should increase monotonously with the increase of the performance and to be zero for models considered as unacceptable or non-behavioral.

The **Parameter Solution (ParaSol)** method aggregates objective functions (OF's) into a global optimization criterion (GOC). This method minimizes these functions (OF's and GOC) using the Shuffle Complex (SCE-UA) algorithm and performs an uncertainty analysis while choosing between two statistical concepts. SCE-UA has been widely used in hydrological model calibrations and other areas of hydrology such as soil erosion, subsurface hydrology, remote sensing and land surface modeling (*Duan, 2003*).

The **Markov Chain Monte Carlo (MCMC)** method generates samples from a random walk which adapts to the posterior distribution (*Kuczera and Parent, 1998*). The sequence Markov Chain is constructed as follows: an initial starting point in the parameter space is chosen and a candidate for the next point is proposed by adding a random realization from a symmetrical jump distribution.

Performance evaluation of hydrological models

Graphical techniques and quantitative statistics have been used for evaluation the model. The graphical model evaluation technique is used to see a visual comparison of simulated and measured constituent data and a first overview of model performance. The graphical evaluation is essential for determining an appropriate model evaluation (Legates and McCabe, 1999). The quantitative statistical evaluation of a calibrated model is normally performed based on four objective functions (*Table 9*):

1. Nash-Sutcliffe efficiency (NS)
2. Coefficient of determination (R^2)
3. Mean relative bias (PBIAS)
4. Ratio of the RMSE to the standard deviation of measured data (RSR)

The **coefficient of determination (R²)** describes the proportion of the variance in the observations explained by the model. R² is a measure of how well the regression line represents the data and the proportion of the fluctuation of a variable that is predictable from another variable. The values for this coefficient denote the strength of the linear relation between Q_m and Q_s , representing the percentage of the data closest to the line of best fit. The range of R² are from 0 to 1 where values closer to 1 give less error variance and values greater than 0.5 are considered as acceptable range (**Santhi et al., 2001 and Van Liew et al., 2003**). This coefficient measures only the deviation from the best fit line. The R² objective function provided in SWAT-CUP is as follows:

$$R^2 = \frac{[\sum_{i=1}^n (Q_{m,i} - \bar{Q}_m)(Q_{s,i} - \bar{Q}_s)]^2}{\sum_{i=1}^n (Q_{m,i} - \bar{Q}_m)^2 \sum_{i=1}^n (Q_{s,i} - \bar{Q}_s)^2}$$

Equation (38)

where Q are discharge values, m and s stand for observed and simulated values, respectively, and i is the i^{th} measured or simulated data.

The **Nash-Sutcliffe efficiency (NS)** is a normalized statistics method widely used as goodness-of-fit indicator that expresses the potential predictive ability of a hydrological model (Nash and Sutcliffe, 1970). NSE determines a comparison of the relative magnitude of the residual variance and the measured data variance (**Nash and Sutcliffe, 1970**). NS indicates how well the plot of observed versus simulated data fits the 1:1 line (**Moriasi, 2007**). An NS value of 1 indicates a perfect fit between observed and simulated data. The Nash-Sutcliffe objective function provided in SWAT-CUP is as follows:

$$NS = 1 - \frac{\sum_{i=1}^n (Q_m - Q_s)_i^2}{\sum_{i=1}^n (Q_{m,i} - \bar{Q}_m)^2}$$

Equation (39)

where Q are discharge values, m and s stand for observed and simulated data, respectively, and the bar stands for the average values.

The **Percent Bias (PBIAS)** measures the average tendency of simulated data to be larger or smaller than the observed data, where a PBIAS of 0 represent a perfect match between simulated and observed data. Negative PBIAS values represent an overestimation of the simulated data while positive values represent an underestimation of the simulated values (**Gupta et al., 1999**).

$$PBIAS = \left[\frac{\sum_{i=1}^n (Q_m - Q_s)}{\sum_{i=1}^n (Q_m)} \right] * 100$$

Equation (40)

where Q are discharge values, m and s stand for observed and simulated data, respectively.

RSR standardizes the RMSE using the observation standard deviation. RSR is the **ratio of the Root Mean Square Error (RMSE)** to the standard deviation of measured data (*Moriasi et al., 2007*). RSR is calculated by applying the ratio of the root mean square error (RMSE) between simulated and observed values to the standard deviation of the observations. RSR varies from 0 to large positive values, being the lower values a better fit of a model (*Moriasi et al., 2007*). The lower the RSR means the lower the RMSE therefore the better the model simulation performance is.

$$RSR = \frac{\sqrt{\sum_{i=1}^n (Q_m - Q_s)^2}}{\sqrt{\sum_{i=1}^n (Q_m - \bar{Q}_m)^2}}$$

Equation (41)

where Q are discharge values, m and s stand for observed and simulated data, respectively, and the bar stands for the average values.

Table 7: General performance ratings for the coefficient of determination (R^2), Nash–Sutcliffe efficiency (NSE), mean relative bias (PBIAS) and the root mean square error-standard deviation (RSR) for a monthly time step (*Moriasi et al., 2007*).

Objective Function	Performance
$R^2 = \frac{[\sum_i^n (x_{obs}(i) - \bar{x}_{obs})(y_{model}(i) - \bar{y}_{model})]^2}{\sum_i^n (x_{obs}(i) - \bar{x}_{obs})^2 \sum_i^n (y_{model}(i) - \bar{y}_{model})^2}$	$R^2 > 0.5$ Satisfactory
$NSE = 1 - \left[\frac{\sum_{i=1}^n (x_{obs}(i) - y_{model}(i))^2}{\sum_{i=1}^n (x_{obs}(i) - \bar{x}_{obs})^2} \right]$	$0.75 < NSE < 1.00$ Very Good $0.65 < NSE < 0.75$ Good $0.50 < NSE < 0.65$ Satisfactory $NSE < 0.50$ Unsatisfactory
$PBIAS = \left[\frac{\sum_{i=1}^n (x_{obs}(i) - y_{model}(i))}{\sum_{i=1}^n (x_{obs}(i))} \right] * 100$	$PBIAS < \pm 10\%$ Very Good $\pm 10\% < PBIAS < \pm 15\%$ Good $\pm 15\% < PBIAS < \pm 25\%$ Satisfactory $PBIAS > \pm 25\%$ Unsatisfactory
$RSR = \left[\frac{\sqrt{\sum_{i=1}^n (x_{obs}(i) - y_{model}(i))^2}}{\sqrt{\sum_{i=1}^n (x_{obs}(i) - \bar{x}_{obs})^2}} \right]$	$0.00 < RSR < 0.50$ Very Good $0.50 < RSR < 0.60$ Good $0.60 < RSR < 0.70$ Satisfactory $RSR > 0.70$ Unsatisfactory

2.2.7 SWAT calibration parameters

SWAT provides a very wide range of parameters to work with, allowing users to analyze several hydrological processes. The parameters adjustment for the calibration is a crucial that will determine several characteristics of the watershed, for instance the amount of water content in the soil, of water available during rainy and dry seasons, of water in the shallow and deep aquifer, runoff, and others. All these parameter are divided into several groups in SWAT for instance soils, HRUs, groundwater and management parameters. Although SWAT provide several dozens of parameters to work with, a selection of the most influencing parameters for a specific watershed is always recommended. Therefore, the main parameters used during this research have been the following:

ALPHA_BF: the baseflow alpha factor is a recession constant that represent the groundwater flow changes resulted from recharge. Values in SWAT range from 0.1 to 1.0, where values above 0.9 are for fast response lands and values below 0.3 correspond to low response lands (*Arnold et al., 2012*).

CANMX: is the maximum canopy storage (mm H₂O), this parameter represents the amount of rainfall intercepted by the canopy of the plants. This parameter is calculated as function of the plant cover density and morphology of existing vegetation (*Arnold et al., 2012*).

CN2: is the initial runoff curve number for moisture conditions II. This will represent the initial conditions and will not change during the simulation period. CN2 values have an enormous effect in the watershed runoff hence in the total water outflow rate during rainy and dry seasons (*Arnold et al., 2012*). Two points to consider when modifying the curve number II are that:

- By increasing CN2 values the amount of water discharge during rainy seasons will increase and during dry seasons will decrease.
- By decreasing CN2 values the amount of water during rainy seasons can be decreased, peaks will be reduced allowing less runoff and more water availability during dry seasons.

ESCO: is the soil evapotranspiration compensation factor. This factor ranges between 0.01 and 1.0 in SWAT and can be used to determine the depth distribution of the soil to reach its evaporative demand. With lower values for this factor, SWAT will be able to extract more water content from the lower layers to compensate the evaporative demand (*Arnold et al., 2012*).

EPCO: is the plant uptake compensation factor. This factor corresponds to a function between the water needed by the plants and amount of water available in the soils. This value can range from 0.01 to 1.0, and as the value of EPCO increases to 1.0 the model is able to compensate the water uptake needs with available water in the lower layers of the soils (*Arnold et al., 2012*).

GWQMN: is the threshold depth of water in the shallow aquifer needed for the return flow to occur. This parameter will limit the amount of groundwater in the shallow aquifer to be returned to the river. The return flow will occur only if the amount of water in the shallow aquifer is equal or higher than the GWQMN value (*Arnold et al., 2012*).

GW_DELAY: is the groundwater delay time (days). This parameter represents the required time for the water to move from the surface of the soil to the lowest soil layers by percolation. This parameter account for the days needed for the water to flow through the vadose zone until it recharges the shallow aquifer. Values for this parameter will depend on the hydraulic properties of the vadose and groundwater zones (*Arnold et al., 2012*).

GW_REVAP: the groundwater revap coefficient determines how feasible is for the water to move from the shallow aquifer to the root zone, the higher this value is the higher the potential evapotranspiration factor will be (*Arnold et al., 2012*).

REVAPMN: is a threshold to the depth of water in the shallow aquifer for revap or percolation to the deep aquifer to occur. This parameter has great impact in the total water amount going to the deep aquifer or to the shallow aquifer, following the amount of water transferred to the shallow aquifer comes the GW_REVAP coefficient which will determine the potential evapotranspiration (*Arnold et al., 2012*).

SOL_AWC: the available water capacity of the soil layer (mm H₂O/mm soil) is determined by the amount of water in situ field and the permanent wilting point (*Arnold et al., 2012*).

2.2.8 Sediment rating curves

Sediment concentration data of rivers is very important to calibrate hydrological models that will be used to perform land degradation and reservoir analyses. However, few rivers have continues measured sediment data, and developing countries usually have only few measured data that have been taken only on random days without continuity. Sediment loads are frequently modelled using empirical relations such the rating curves (*Asselman, 2000*). Sediment rating curves describe the average relation between the water discharge and the sediment concentration for a certain location (*Asselman, 2000*). The most commonly used sediment rating curve is a power function (*Walling, 1974, 1978*).

Sediment rating curves can constitute a good approach that can be used to estimate sediment rates for ungauged catchments and also sediment loads over a period of time, hence the impact of land use changes and watershed management practices on sediment yield. However, it is important to note that some studies have shown that they can provide inaccurate values that underestimate the actual sediment loads (*Walling, 1977b; Walling and Webb, 1981; Ferguson, 1986; Thodsen et al., 2004*). Rating

curves obtained from a logarithmic transformation by using the least squares regression has been proved to underestimate the sediment estimation by 10-50% (**Asselman, 2000**). These inaccuracies and differences in the shapes of the fitted rating curves are usually associated to the watershed characteristics (**Asselman, 2000**). However better results can be obtained if a non-linear least squares regression is applied. Since watershed will have different hydrological conditions, a general and universal method to develop accurate sediment rating curves cannot be proposed. However, some researchers have proposed a statistical bias correction to reduce the degree of underestimation (**Duan, 1983; Ferguson, 1986**).

Typically, sediment rating curves plot water discharge and sediment concentration on a log-log graph where a straight line is drawn. The power function is then log transformed and a linear regression is applied to estimate the parameters.

Large scatter in point between discharge and sediment concentration normally occur because soil erosion rates in a watershed are different during different seasons. When scatter in points are too large, developing separate rating curves for different seasons, for instance for rainy and dry seasons, could provide more accurate results.

A common method to develop sediment concentration rating curves is the use of intermittent sediment data with continuous flow discharge data (**Walling, 1977b; Ferguson, 1986**) and commonly presented in the relation sediment concentration/flow discharge (**Campbell and Bauder 1940; Walling, 1977b; Asselman 2000**). Suspended sediments moves approximately at the same velocity as the water flow (**McMahon et al. 2004**). Since the suspended sediment load is a function of water discharge, many studies have used flow discharge data to estimate the sediment loads or sediment concentrations (**Leopold and Maddock 1953; Walling, 1977b; Ferguson 1986; Walling and Webb 1988; Sickingabula 1998; Asselman 2000; Horowitz 2003; Hu et al. 2011**). In this relation, the power function between water discharge and suspended sediment is solved with a logarithmic transformation through the Ordinary Least Squares (OLS) regression to fit a straight line through the scatter of points (**Walling, 1977b**). In this method the geometric mean of the antilog is always smaller than the arithmetic mean of the load in log form, which causes an underestimation of the real sediment values (**Ferguson 1986; Ferguson 1987**). The relation has been classified based on the temporal resolution of the data as daily, monthly, annual and flood period curves, although they can also be classified based on the particle size as clay-silt and sand-sized (**Colby, 1956**).

The original form of sediment rating curves was developed by **Leopold and Maddock (1953)** for suspended sediment load (*Load*) and water discharge (*Q*):

$$Load = aQ^b$$

Equation (42)

where *a* and *b* are empirical parameters.

In the same way, sediment rating curve can also be developed for suspended sediment concentration (*C*) and water discharge:

$$C = aQ^{b-1}$$

Equation (43)

where C is the suspended sediment concentration (mg/l), Q is water discharge (m^3/s), and a and b are regression coefficients.

This equation covers the effect of increased stream power at higher discharge and also the extent to which new sediment sources are available in weather conditions that cause high discharge (*Asselman, 2000*). Multiple studies have used the previous equation to develop the sediment rating curves (*Walling, 1977b; Thomas 1988; Asselman 1999; Hu et al. 2011; Zhang et al. 2012*). Additionally, several other forms of sediment rating curves have been developed for different watershed to account for the effect of different hydrological characteristics of the watershed and enhance the accuracy of load estimates (*Crawford 1998 and Morehead et al. 2003*).

Although it has been found that the rating parameters are also linked to factors such as river channel morphology, surface air temperature, and basin relief (*Syvitski et al. 2000; Yang et al. 2007*). Some researchers have considered that the parameters a and b have no physical meaning (*Colby 1956; Ferguson 1986*), while others sustain an opposite interpretation (*Asselman 2000; Morehead et al. 2003L Morgan, 1995; Peters-Kümmerly, 1973 and Walling, 1974*). Nevertheless, the coefficient a is influenced by the soil erodibility and suspended sediment input in the basin upstream of the gauging station (*Morgan 1995; Asselman 2000*). Therefore, it can be considered an index of erosion severity that represents the sediment concentration at the unit discharge, this makes it dependent of the availability of sediment in the region contributing to the measurement and also of whether the sediment can be easily eroded and dragged by the stream flow (*Tran, 2014*). The rating coefficient a has multiple units and varies with the value of the exponent b : $(\text{kg/s})(\text{s/m}^3)^b$. The parameter b represents the erosive power of a river (*Peters-Kümmerly, 1973*), therefore it can be considered as an indicator of the changing rate of the sediment load per change of unit of the flow discharge (*Tran, 2014*). Large values of this coefficient would indicate that a small increase in water discharge could result in a strong increase of the erosive power of the river (*Peters-Kümmerly, 1973*). Frequently, values for the exponent b could be underestimated because plots of discharge and suspended sediment loads have a high degree of scatter due to the augmentation of external factors during periods of high discharge. The possible ranges for the values of this parameter can be (*Asselman 2000; Morehead et al. 2003*):

1. $0 < b < 1$: Sediment rating curves with this range have a concave shape. The suspended load increases in a diminishing rate with the increase of flow discharge. The sediment transport in these rivers is constricted by the amount of available sediment (*Hickin, 1995; Meade and Moody, 2010*).
2. $b = 1$: In this case the suspended sediment load increases in a linear way with the increase of the water discharge. A rating curve with this exponent value is represented by a straight line.
3. $b > 1$: Having a convex shape, in this rating curve, the suspended load increases at an increasing rate with the increase of discharge. This kind of rivers are expected to have limited transport capacity (*Asselman, 2000*). This condition is likely to happen in a river with coarse material (*Hickin, 1995*).

The influence of the channel geometry and the climate and land use changes in the availability of sediment sources make the behavior and interaction of sediment particles a complex process (**Tran, 2014**). Additionally, since the flow discharge is used as an alternative for the measure of shear stress and stream power, load estimation using a sediment rating curves can have some errors when disparities between discharge and stream power exist (**Hickin, 1995**). These inequalities happen under sudden turbulence distortions and changes in the channel bed's forms (**Tran, 2014**). Although, the majority of rivers transport sediment particles according to the sediment supply (**Tran, 2014**). However, for a flood event during the peak raining seasons, sediment load and water discharge can more precisely be described as a loop instead of a single rating curve. This is caused by the difference of sediment availability before and after the peak discharge (**Horowitz 2003; Morehead et al. 2003**). Sediment concentrations are frequently higher during the rising period of hydrograph (when sediments sources are still available) than on the falling period (**Pye, 1994**).

3. Methodology

This chapter comprises a detailed explanation of all the steps done before the setup, calibration and validation of the final model used to perform the erosion analyses in the Blue Nile Basin (**Figure 19**). The most relevant procedures have been:

- The preprocessing and integration of conventional Ground data with CFSR data.
- An analysis of the effects of the number of sub-basins and HRUs on the sediment estimations done by SWAT
- Definition of parameters for the sediment rating curves for several sub-catchments in the Blue Nile Basin.
- Analysis of the effects of different data sources and number of sub-basins in the water balance of the Blue Nile Basin, where the proper number of sub-basins to be used in the final SWAT model was defined.
- Development of the SWAT Error Index (SEI) as an additional tool to evaluate hydrological models.

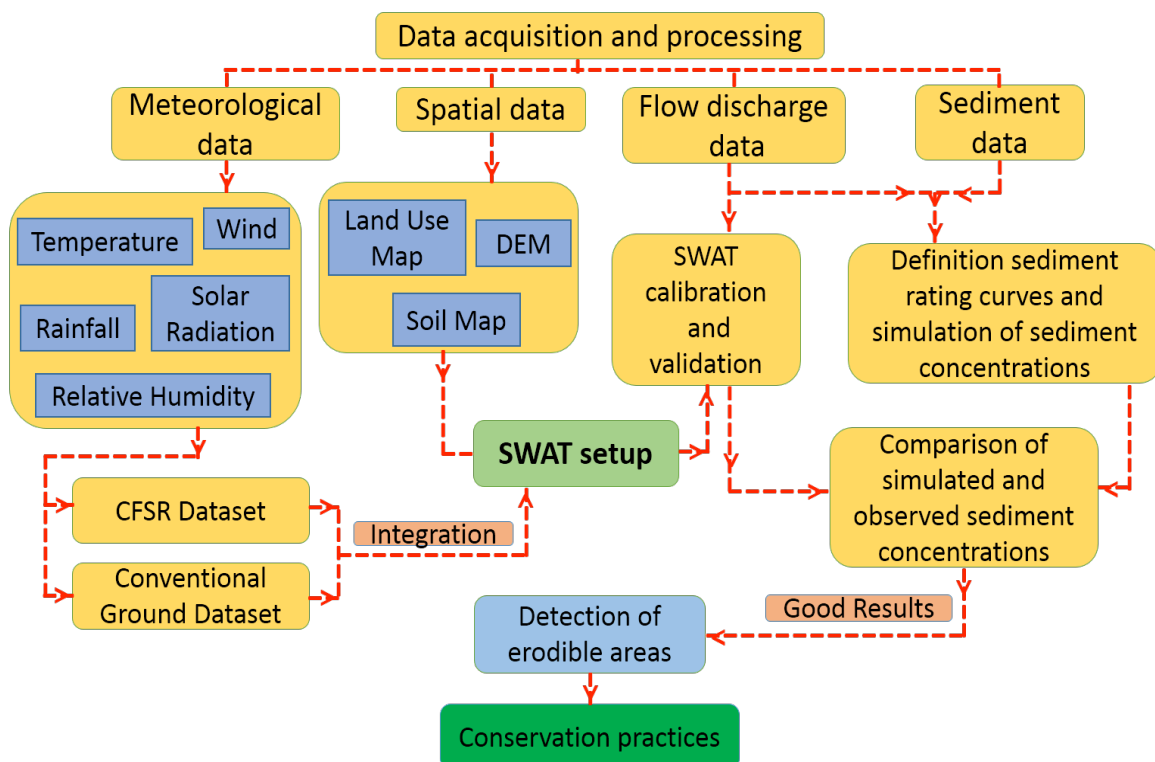


Figure 19. Workflow diagram.

3.1 Input data and SWAT model setup

A common problem to set up hydrological models of the Blue Nile Basin are related to data limitations. In developing countries the distribution of meteorological stations is irregular and dispersed (*Worqlul et al., 2014*). Other weather data problems are

related to measuring gauges; many weather data parameters contain missing data periods, and in several cases erroneous measurements are also possible. Thus, many models are often set up based on limited and incomplete data, which may lead to less reliable models. This lack of hydrological and climatic data has impeded in-depth studies of the hydrology of the Blue Nile Basin (*Tekleab et al., 2011*). The final quality of a hydrological model is highly dependent on the quality of the input data, which in this case has been assessed and processed before its use. Two types of datasets were used in this study: the input data that was used to set up the model, and the evaluation data that was used to calibrate, validate and determine the quality of the models. SWAT requires four types of input data:

- Digital Elevation Model (DEM).
- Land use map.
- Soils map.
- Weather dataset.

A **Shuttle Radar Topographic Mission Digital Elevation Model (SRTM DEM)** from the Consultative Group on International Agricultural Research-Consortium for Spatial Information (CGIAR-CSI) was used to setup the model. This DEM has a resolution of 90 meters, and was used to perform an automatic watershed delineation of the Blue Nile Basin, where the flow direction, flow accumulation and streams network were automatically determined by SWAT.

The second input dataset was a **land use map**, which was obtained from the GIS Portal of the International Livestock Research Institute (ILRI), and corresponds to the year 2004. (<http://data.ilri.org/geoportal/catalog/main/home.page>).

The **soils map** used for these models was developed by the Food and Agriculture Organization of the United Nations (FAO-UNESCO). This world soils map was prepared by FAO and UNESCO at 1:5 000 000 scale (<http://www.fao.org/soils-portal/soil-survey/soil-maps-and-databases/faounesco-soil-map-of-the-world/en/>). The information provided by this map was used in combination with the Harmonized World Soil Database v1.2, a database that combines existing regional and national soil information (<http://www.fao.org/soils-portal/soil-survey/soil-maps-and-databases/harmonized-world-soil-database-v12/en/>).

The last input dataset was the **meteorological information**. Two weather datasets from different sources were used to setup the models. The **first weather dataset** was collected from the National Meteorology Agency of Ethiopia (NMA). The data used for these models correspond to 42 stations distributed in the Blue Nile Basin (*Figure 20*). However, only 15 of these stations are capable of measuring all 5 parameters needed to set up SWAT: rainfall, temperature, relative humidity, solar radiation and wind speed. Moreover, few of these 15 station have available complete and continuous data for the entire period under evaluation (1990-2004). For instance, the collected data for solar radiation was limited to 2 stations only, wind speed was available for 4 stations; only maximum temperature was available for 4 stations, relative humidity was available for 3 stations, and precipitation was available for all 42 stations. Additionally, the quality of this observed data is somehow questionable. Many meteorological stations are more than 10 years old, and their constant technical failure due to the lack of continuous

expert maintenance also questions the quality of the data. Large part of the available ground data has been collected from old stations that could have in many cases malfunctioning, defected and outdated devices. Consequently, using reanalysis datasets, which are multilayer global gridded weather representations, can constitute a good approach (**Rahman, 2016**). Therefore, the **second weather dataset** was the Climate Forecast System Reanalysis (**Figure 20**), a dataset that has been produced by the National Centers for Environmental Prediction (NCEP) (<http://globalweather.tamu.edu/>). CFSR data brings several uncertainties due to its multiple spatial and temporal interpolations (**Dile and Srinivasan, 2014**). It was generated using different assimilation techniques that include satellite radiances, advanced coupled atmospheric, oceanic and land surface modelling components. The global atmosphere resolution of CFSR data is approximately 38km. These atmospheric, oceanic and land surface output products are available at a 0.5°x0.5° latitude and longitude resolution.

For the evaluation of the quality of the SWAT models, monthly flow discharge data and evapotranspiration data were used. The **flow discharge data** was obtained from the Ministry of Water, Irrigation and Electricity of Ethiopia (MWIE) and corresponds to the gauging stations at Kessie and Eldiem at the main stream of the Blue Nile Basin (**Figure 20**). The gauging station at Kessie includes the upper third part of the upper Blue Nile basin (**Shehata, 2016**), while the Eldiem gauging station is located at the border with Sudan and comprises the whole upper Blue Nile basin. For the evapotranspiration analysis, **MODIS data** for the Blue Nile Basin was obtained from the MOD16 Global Terrestrial Evapotranspiration Project (<http://www.ntsug.umd.edu/project/mod16>). The global evapotranspiration data from MOD16 are regular 1 km² land surfaces datasets for the 109.03 million km² of vegetated area in the whole globe at different time interval: 8 days, monthly and annual, from which monthly data generated specifically for the Nile basin was used.

3.1.1 Analysis of the weather datasets, processing and integration

Several previous studies have modeled the entire and also small catchments of the Nile Basin (**Tibebe and Bewket, 2011; Setegn et al. 2008; Setegn et al. 2010; Swallow et al. 2009 and Mulungu et al. 2007**) providing good and meaningful results. However, most of the hydrological models are built for the Lake Tana basin and its sub-basins, Gummara, Ribb, Gilgel Abay and Koga (**Chebud et al., 2009; Setegn et al., 2008, 2010 and Wale, 2008**). **Dessie et al. (2015) and Kebede et al. (2006)** performed a very detailed daily water balance analysis and annual water budget for the Lake Tana basin where the runoff and outflows of ungauged catchment were estimated. **Uhlenbrook et al. (2010)** performed an analysis of the hydrological processes and responses of Gilgel Abay and Koga catchments applying the HBV model. Other studies have modeled the entire Blue Nile Basin, for instance, **Abera et al. (2016)** performed a water budget analysis in the Blue Nile Basin where precipitation, outflow and evapotranspiration analyses were done. **Betrie et al. (2011) and Easton et al. (2010)** also modelled and calibrated the Blue Nile basin using discharge data to estimate sediment yield and erodible areas of the basin, values of the calibrated parameters for flow and sediment were also shown. **Tesemma et al. (2010)** modeled the Blue Nile Basin where the main objective was to perform an analysis of historical trends to improve the understanding of its future conditions. **Dessie et al. (2014)** also performed a runoff and sediment yield

analysis in the Upper Blue Nile, although the main analysis was done at the Lake Tana region. **Tekleab et al. (2011)** also modeled the Upper Blue Nile where an interesting water balance analysis was done and monthly stream flows for several sub-catchments were modeled. However, most of the studies at large scale in the Blue Nile Basin do not provide detailed values for the each of the water balance components of the basin. In many cases literature shows different values for average annual water balance components, these differences are caused mainly by the contrasting input data sources, model configuration and parameterization. Annual rainfall in the Blue Nile Basin is also very variable between years and therefore if the compared models do not correspond to the exact period of times the differences can be large. For instance **Table 8** shows the average annual values for different water balance components in the Blue Nile Basin where the results from **Cherie (2013) and Mengistu (2012)** are different. These models correspond to different periods, however, the validation period used by **Cherie (2013)** is very similar to calibration period used by Mengistu, but the results of both models are still different. In this section the SWAT model has been analyzed from 1990-2004 and considering the above discrepancies the models cannot not totally be compared, although they can be useful as a general reference. Therefore, if input data is used without the respective analyses, models can provide less reliable results. And even small errors in precipitation and temperature can result in considerable inaccuracies and impacts on the models results (**Maraun et al., 2010**). However, since snow melt is not a concern in the Blue Nile Basin, temperature will have very little effect.

Table 8. Average annual water balance components of the upper Blue Nile Basin based on different literature.

Cherie, 2013		
Hydrologic parameters	Calibration period 1976-1982 (mm/year)	Validation period 1992- 1995 (mm/year)
Precipitation	1338	1348
Evapotranspiration	962	960
Revap/shallow aquifer	59	58
Surface runoff	143	151
3.1Return flow	70	38
Transmission losses	9	9
Mengistu et al., 2012		
Hydrologic parameters	Calibration period 1991-1996 (mm/year)	Validation period 1997- 2000 (mm/year)
Precipitation	1422	1547
Evapotranspiration	820.9	816
Groundwater in the shallow aquifer	264.8	302
Surface runoff	314.4	410
Transmission losses	11	12
Groundwater recharge	286	327

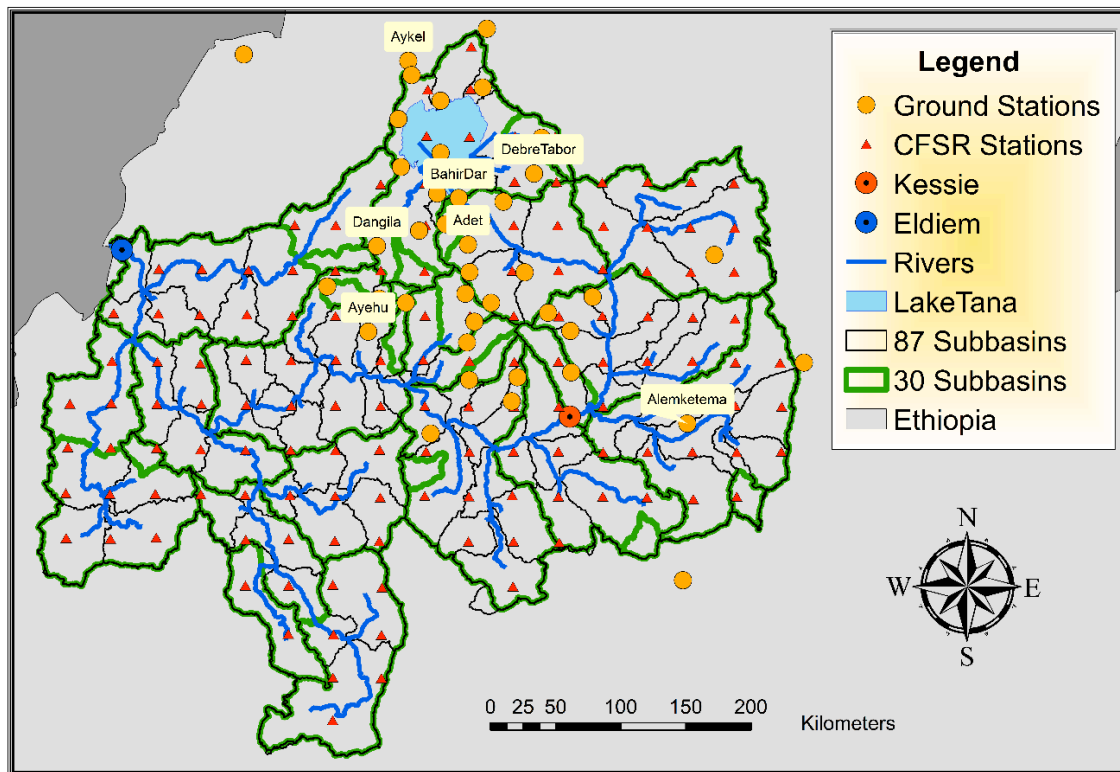


Figure 20. Weather and hydrometric gauging stations in the upper Blue Nile Basin under two discretization levels, 30 and 87 sub-basins (SWAT30 and SWAT87).

Tekleab et al. (2011) and **Uhlenbrook et al. (2010)** checked the data quality of stream flow data in the Blue Nile Basin based on comparisons graphs and additionally a double mass analysis. In this study the weather data quality and consistency of the time series on monthly basis in terms of magnitude and spatial distribution of the five input variables required by SWAT were also analyzed through comparison graphs (**Figure 21, Figure 22, Figure 23 and Figure 24**) to determine the deficiencies of the two datasets (CFSR and Ground datasets) and to form an integrated dataset (**Polanco et al., 2017**).

In the first case, the ground dataset was used without alterations to create the SWAT models. This ground dataset obtained from the NMA corresponds to 42 stations in the Blue Nile Basin, where most of the meteorological stations were located in the eastern part of the watershed (**Figure 20**). Additionally, the data obtained from these stations had several months of missing data, leading to temporal uncertainties (**Polanco et al., 2017**). For the second case, the SWAT models were setup using the CFSR dataset, also without alterations (**Polanco et al., 2017**). This dataset is evenly distributed at 38 km resolution, with over 100 stations available for the Blue Nile Basin, and is temporally continuous (**Figure 20**).

Fuka et al. (2013) utilized CFSR precipitation and temperature data to simulate multiple small catchments in the USA and the Gumara sub-catchment in Ethiopia. These models provided better results than those models using conventional weather data, especially in the cases where the weather gauging stations are more than 10km away from the sub-basin (**Fuka et al., 2013**). However, this is not the case for all watersheds, and after performing a quality check at large scale in the Blue Nile Basin through a

comparison of maps and graphs between the ground and CFSR datasets (**Figure 21, Figure 22, Figure 23 and Figure 24**), it was noticed that not all the weather variables from CFSR are reliable. The precipitation distribution appeared to be underestimated in the eastern region of the Blue Nile Basin and overestimated in the western region (**Figure 21**). The map created from the ground stations (**Figure 22**) showed a precipitation distribution in the western region that is the result of SWAT using the precipitation values from the nearest stations. Two stations in the eastern part, Alemketema and Adet (**Figure 23A, 23B, and Figure 24A, 24B**), showed the underestimation of the CFSR rainfall at the eastern region; and Ayehu (**Figure 23C and Figure 24C**) showed the overestimation of the CFSR rainfall in the western region. For this reason, additional CFSR rainfall stations were not used in the Integrated dataset. However, the graphical and statistical comparisons of the few available stations for relative humidity, temperature and solar radiation showed an acceptable level of agreement between the ground and CFSR datasets. The seasonal behavior and magnitudes of the values for these variables are similar, additionally the 1-1 graphs showed an acceptable degree of matching. For instance, the values for relative humidity for Debre Tabor and Aykel with both datasets show very similar values (**Figure 23D, 23E and Figure 24D, 24E**). The comparisons of maximum temperature for Aykel also showed good degree of matching (**Figure 23G and Figure 24G**), although for Bahir Dar the results were not very good showing a slight underestimation (**Figure 23H and Figure 24H**). The solar radiation comparison at Bahir Dar (**Figure 23I and Figure 24I**) also showed a good agreement between both datasets, although results at Debre Tabor (**Figure 23J and Figure 24J**) showed slightly different results. Another exception was the wind speed data, which in both cases at Adet and Ayehu (**Figure 23K, 23L and Figure 24K, 24L**) was overestimated by the CFSR dataset.

Therefore, these two datasets were integrated to form a third input dataset for SWAT, hereafter called Integrated dataset, with the objective of overcoming their spatial and temporal limitations. **Tekleab et al. (2011) and Uhlenbrook et al. (2010)** filled in missing stream flow data of the Blue Nile Basin using regression analysis, which is also a good approach to fill in missing meteorological values. However in this study, the missing values of the ground dataset refer to complete time series of a specific station and variable. Thus, to create the Integrated dataset, the 42 rainfall stations of the ground dataset were taken as basis, this means that the location of the weather stations of the final Integrated dataset correspond to the location of the 42 rainfall stations of the ground dataset. From there, the missing variables (relative humidity, temperature and solar radiation values) of those 42 rainfall stations were completed by using the variables of their nearest CFSR stations. The Integrated dataset has 42 stations where the data for each variable was combined as follows: the precipitation is formed by 42 rainfall stations taken entirely from the ground dataset; the relative humidity is formed by 3 stations from the ground dataset and 39 stations from the CFSR dataset; the maximum temperature is formed by 4 stations from the ground dataset and 38 stations from the CFSR dataset, the values for the minimum temperature were taken totally from the CFSR dataset; the solar radiation was formed by 2 stations from the ground dataset and 40 stations from the CFSR dataset; no wind speed data was used in the models. However, missing daily values within a variable were completed by the built-in SWAT WXGEN weather generator model (**Sharpley and Williams, 1990**). This Integrated dataset contained more data than the ground dataset, and also provided more reliable precipitation values and distribution than those provided by the CFSR dataset.

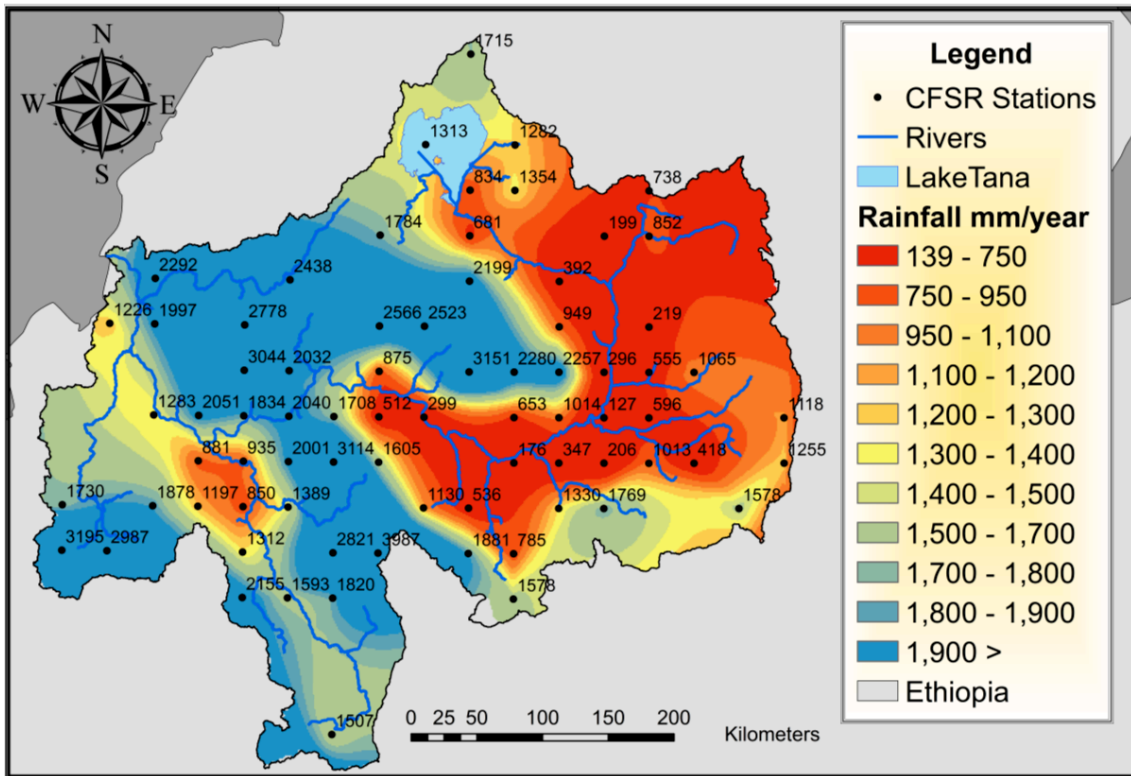


Figure 21. Spatial annual rainfall variation in the upper Blue Nile Basin using the CFSR dataset (Polanco et al., 2017).

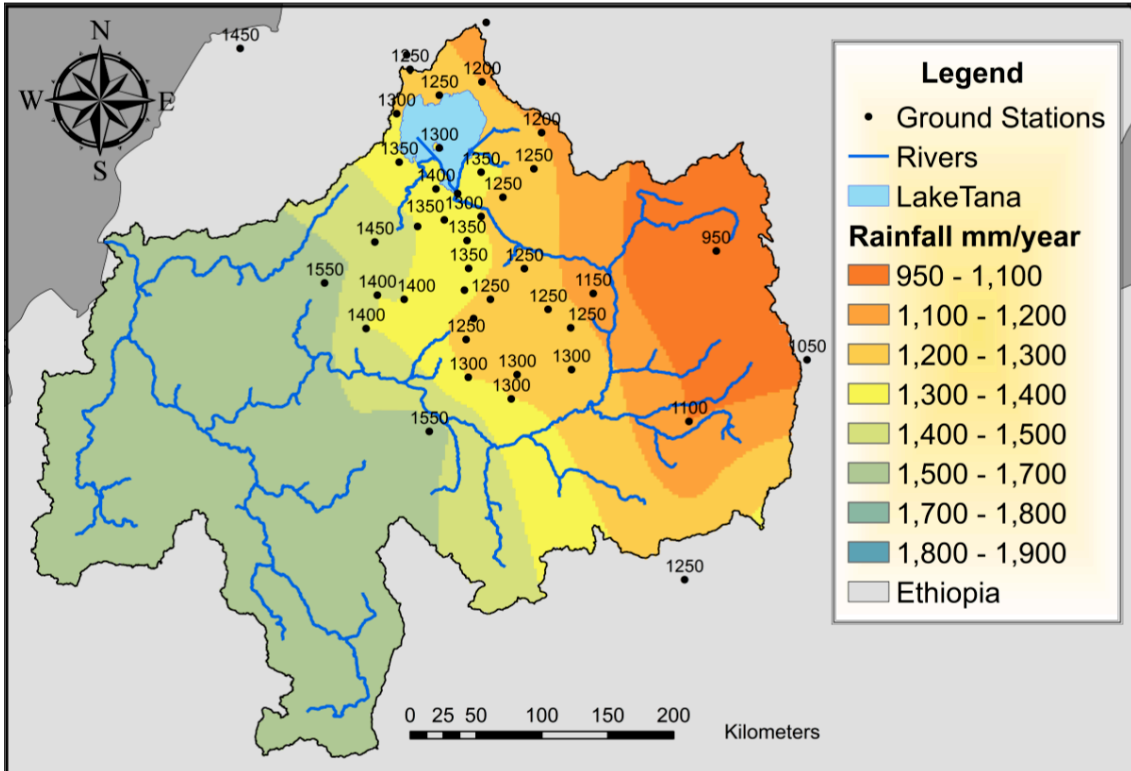


Figure 22. Spatial annual rainfall variation in the upper Blue Nile Basin using the Ground dataset (Polanco et al., 2017).

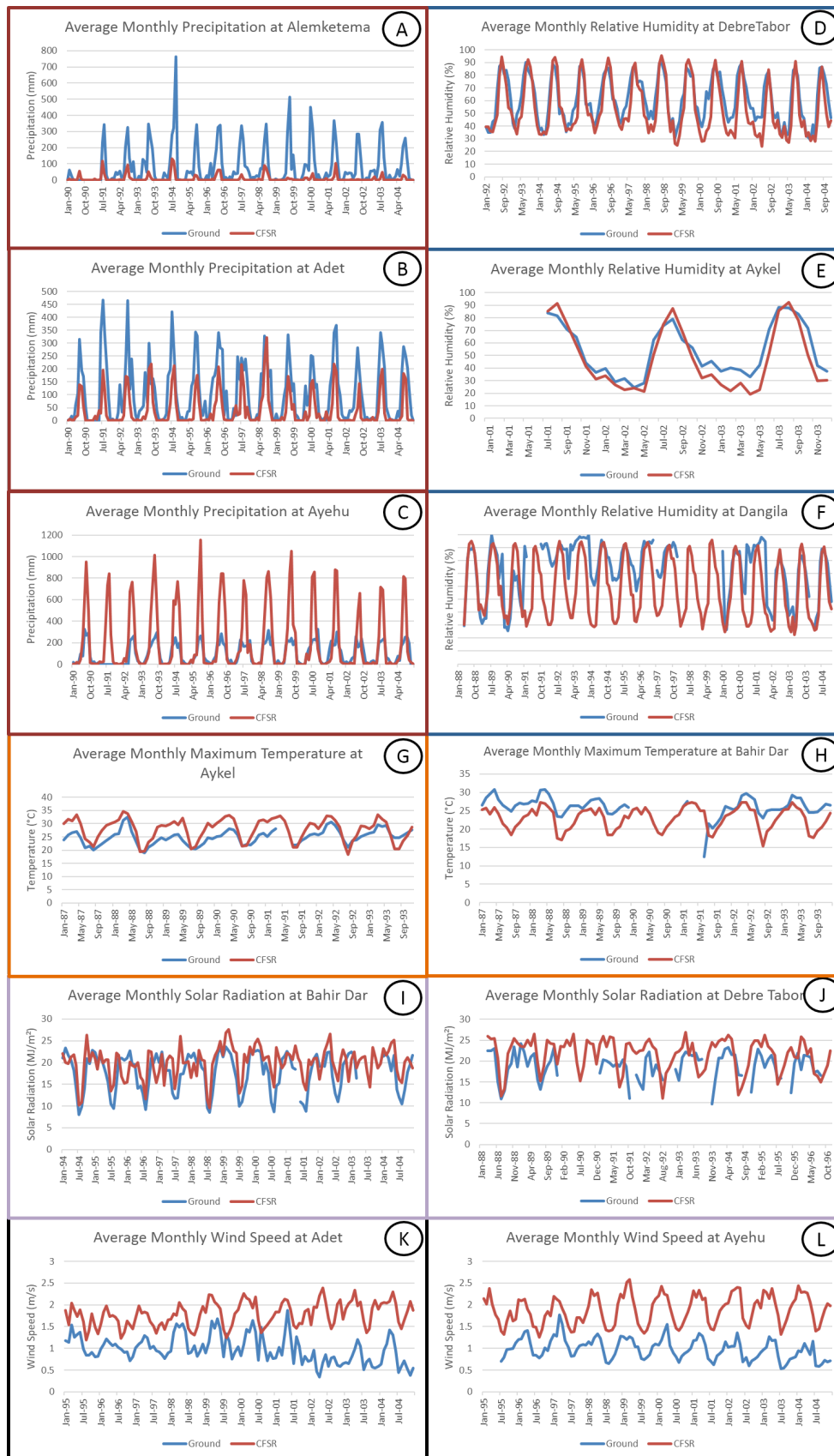


Figure 23. Comparisons between the Ground and CFSR weather datasets. **A, B and C** are average monthly precipitation; **D, E and F** are average monthly relative humidity; **G and H** are average monthly maximum temperatures; **I and J** are average monthly solar radiation; **K and L** are average monthly wind speed (Polanco et al., 2017).

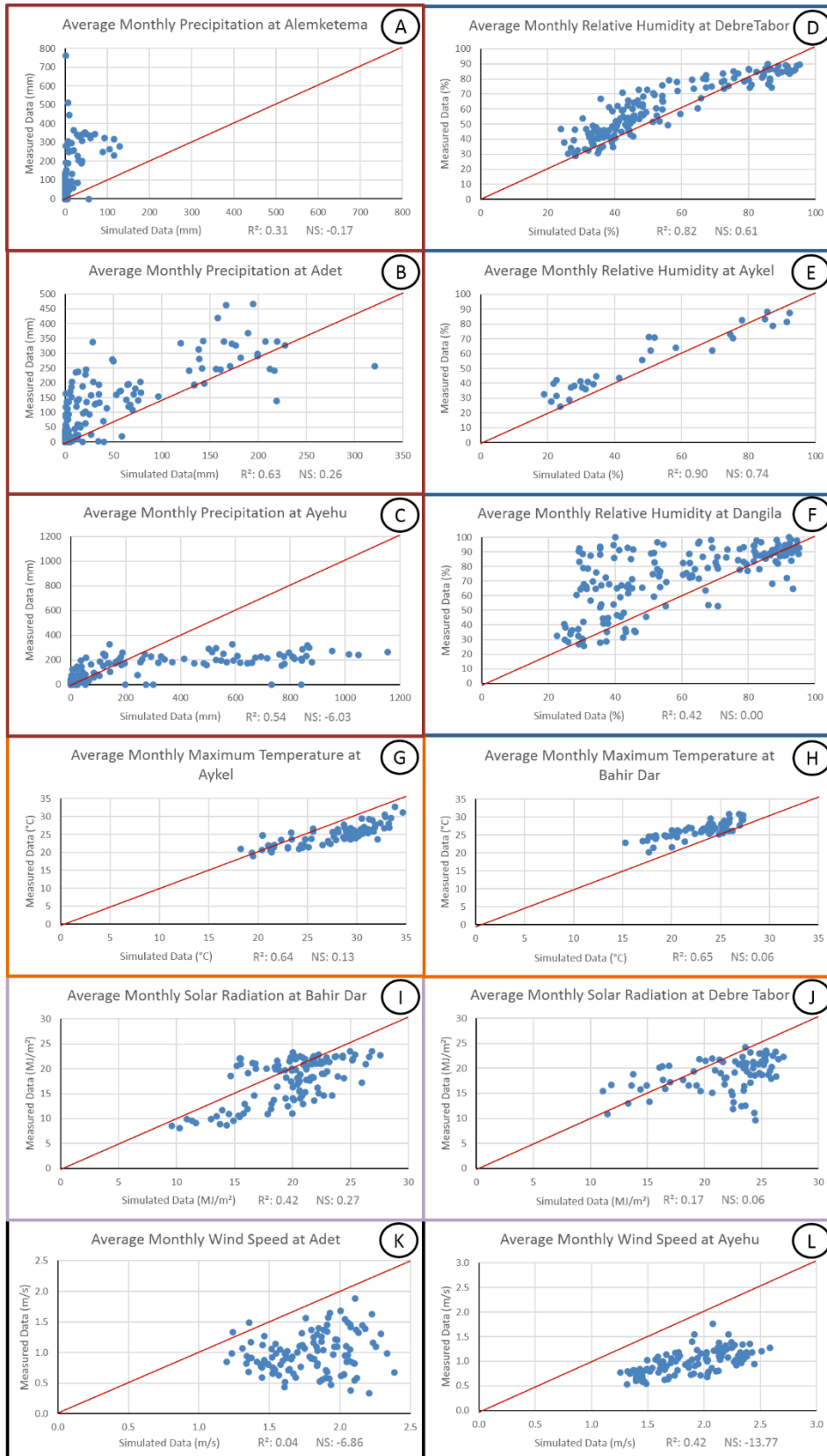


Figure 24. Significance of matching between the Ground and CFSR weather datasets. **A, B** and **C** are average monthly precipitation; **D, E** and **F** are average monthly relative humidity; **G** and **H** are average monthly maximum temperatures; **I** and **J** are average monthly solar radiation; **K** and **L** are average monthly wind speed (Polanco et al., 2017).

3.2 Effects of different sub-basins and HRUs discretization on sediment estimations

Soil erosion is a matter of concern in watershed managements and is one of the most alarming problems being faced in the Blue Nile Basin. Therefore, sediment transport estimations for erosion analyses in this region is one of the most important results that can be obtained from SWAT. However, a comprehensive understanding of how a hydrological model works is an important task that has to be considered before a decision making framework is established based on its results.

Multiple studies have focused their objectives on modelling sediment yields at watersheds outlets, and providing very important information regarding the intensity of the erosion problem in specific sub-catchments, allowing the prioritization of critical areas (Mishra et al. 2007; Asres and Awulachew 2010; Besalatpour et al. 2012; Silva et al. 2012; Chatterjee and Krishna 2013). However, information concerning the effect of the number and size of the sub-basins and HRUs in a hydrological model has rarely been studied.

Often, good calibrations with outflow data can be achieved, and assumptions about the quality of the sediment estimation are done. SWAT calculates all the hydrological processes based on HRUs, which depend on slope classes, soils and land use distribution in the watershed. The HRU area is used to estimate the runoff erosive energy, which is used to calculate sediment yields. Based on the modified rational formula, runoff peaks are the main indicators of erosion. The number and size of HRUs is very flexible and can easily be increased or decreased by defining different thresholds for land use, soil and slope classes. When the threshold for land use, soil and slope classes to create HRUs is defined to 0%, the maximum number of HRUs for the hydrological model is reached. However, this threshold will define only the number of parts with same land use, soil and slope characteristics. For the calculations, SWAT will use all these equal areas within a sub-basin and group them as one HRU. If parts with equal characteristics fall within different sub-basins, they are considered as different HRUs for the calculations. Therefore, creating more sub-basins can still increase the number of total HRUs. However, in this case, the size of each part of an HRU cannot be increased, but only divided or distributed between different sub-basins.

However the number and distribution of HRUs will affect the results of the model. As it will be shown in this study, sediment estimations can significantly vary when different amount of HRUs are considered for the analysis. Sediment loads in SWAT can differ when the HRUs have different sizes, even when the flow discharges estimation remain very similar. Defining the number of sub-basins or HRUs is a critical part for setting up a hydrological model, and having a higher number of sub-basin will not necessarily provide better models. However, increasing the number of sub-basins has been an option that has helped to identify with more precision the location of areas under erosion. Nevertheless, this procedure will still tend to underestimate the total sediment yields (Figure 25). Sediment yield analyses at sub-basin level will not provide an exact location where the erosion is taking place, instead only the total sediment yield of a sub-basin, which in large watersheds will represent several hundreds or thousands kilometers squared. For this reason, an erosion assessment based on HRUs sediment

yields can provide a more accurate location of the erosion and better soil management practices can be proposed. Another factor to consider when creating sub-basin is the weather input data, as this data is processed at sub-basin level and is the most important factor influencing the runoff peaks. Therefore, if not enough weather input data is available in a certain region, having more sub-basins will not provide more reliable results. The HRUs definition has a great impact when it comes to prioritize areas with severe erosion problems and could provide more details of the erosion severity and required control practices. In order to propose effective erosion control practices based on sediment loads obtained from models from ungauged regions, a correct definition of the number of HRUs is necessary.

Chen and Mackay (2004) showed that in SWAT the HRU specific sediment yields (HSSY, t/ha) obtained with MUSLE are non-linearly related to the HRU area. This nonlinearity is undesirable because it makes predictions for HRUs with similar environmental characteristics but different sizes incommensurable, and implies that different spatial delineations of the same basin require different SWAT calibrations (**Chen and Mackay, 2004; Chaplot, 2014**). This sensitivity in the sediment outputs rise several question in ungauged catchments, since different SWAT delineation produces different sediment outputs and will also require different parameterization (**Chen and Mackay, 2004; Chaplot, 2014**). It has been observed that sediment yields have a direct relationship and follows the trend of simulated runoff peaks (**Kumar and Mishra, 2014**). Some studies have shown that decreasing the area of a HRU increases the runoff concentration times leads to lower sediment yields (**Chiang et al., 2014**). The non-linear relation between sediment outputs and HRU size in SWAT (**Figure 25**) is very important phenomenon to be considered in any catchment, especially in those large basins where the aggregation of spatial information and its resolution increases the average size of the model units, in this case the HRUs (**Vigiak et al., 2015**).

This non-linear relationship between HRU sediment yields and area identified by **Chen and Mackay (2004)** is of concern for SWAT sediment modeling in any catchment, but particularly in large basins, where the need for spatial aggregation and the use of low resolution spatial input data inflates the average model unit size. While the original MUSLE can somehow account for the increase in specific sediment yields with size, it cannot consider its decrease (**Vigiak et al., 2015**). However, a threshold between 10 and 50 km² would appear reasonable (**de Vente and Poesen, 2005**), and in agreement with the size for which the original MUSLE had been developed and tested which is up to 40 km² (**Vigiak et al., 2015**).

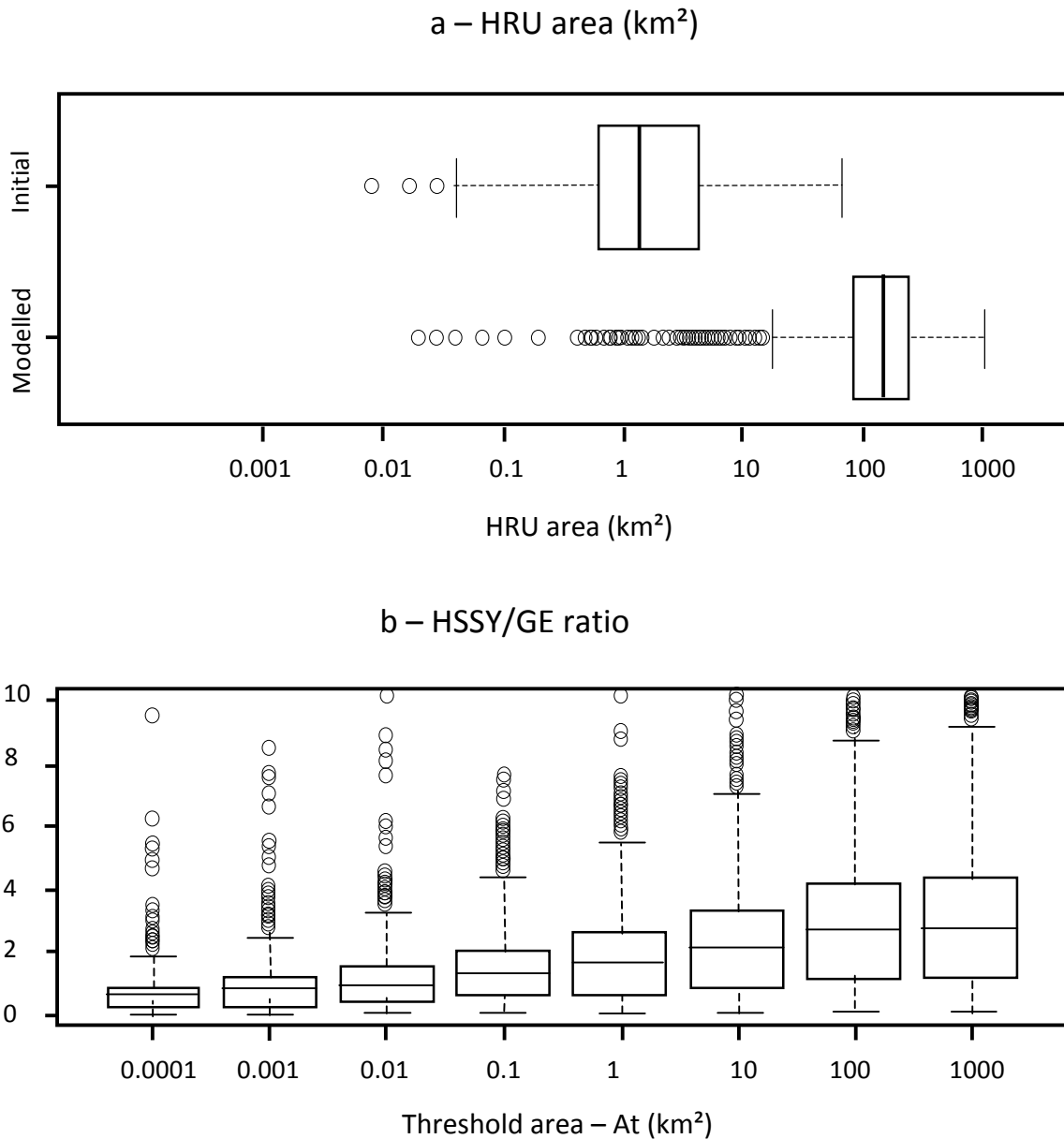


Figure 25. Hydrologic Response Unit (HRU) area distributions and impact of threshold area (A_t) on HRU specific sediment yields. a) Distribution of HRUs area in the Upper Danube Basin derived from the initial GIS inputs overlay (initial), and as modeled using one dominant HRU per sub-basin (modeled); b) ratio of HRU mean annual MUSLE specific sediment yields (HSSY; t/ha/year) to mean annual USLE gross erosion (GE, t/ha/year) for the simulation period (1995–2009) at increasing threshold areas (A_t). The gray lines indicate a ratio of 1, i.e. where HSSY and GE are equal (Vigiak et al., 2015).

This non-linear relationship brings as consequence the fact that sediment estimations cannot be accurately calculated with an area-weighted summation over the total HRUs (**Chen and Mackay, 2004**). In other words the sediment yield is proportional to a specific HRU area raised to the power of 1.12:

$$sed \propto (Area \times Area)^{0.56}$$

Equation (44)

For instance, by using **Equation 44**, if the MUSLE formula were to be applied in a 100 km² watershed using only one HRU the result would be: $100^{1.12} = 173.78$, however, if the same formula were to be applied in the 100km² watershed but with 10 equal-area HRUs the final sediment would result in: $(10^{1.12}) \times 10 = 131.82$. Only by increasing the number of HRUs, this non-linear relationship is causing an underestimation of approximately 24%.

Each separated part of each HRU should provide an independent amount of sediment, which in the end, if added, should provide equal amount of sediment whether they are calculated together or separately in different sub-basins. However, for **Equation 27**, SWAT is using the average HRU slope length instead of the total slope length (**Neitsch et al., 2009**). For instance, a model with different number of HRUs caused by a higher number of sub-basins (HRUs being divided into more HRUs), will sum up larger slope length which generates lower sediment concentrations. SWAT calculates the average of the lengths of these HRUs and use it for L_{slp} on **Equation 27**. Sediment estimations depend on the slope length, longer slope lengths will produce longer overland flow concentration times, t_{ov} , hence longer HRU runoff concentration time (**Equation 26**). If the HRU runoff concentration time is higher; then runoff peaks, which are the maximum indicators of erosive power, will decrease (**Equation 16**), reducing the final sub-basin sediment yield (**Equation 14**). Average slope lengths provide shorter concentration time, therefore, when HRUs are processed independently within different sub-basins the concentration times will keep on increasing, which generates lower sediment yields. This leads to an underestimations of sediment yields. Once the sediment yields are calculated for each HRUs, the sediment transport process in the channel network is a function of aggradations and degradations (**Neitsch et al., 2009**).

3.2.1 Sub-basins selection and description

Initially, with the objective of understanding how the number and size of HRUs affect the sediment concentration and the sediment yield in SWAT, several models of three sub-catchments were compared (**Figure 26**):

- Gumara
- Ribb
- Beressa

The **Gumara** sub-catchment is located nearby the Lake Tana, in the northwestern part of the Blue Nile Basin, 624 km to the north of the capital city Addis Ababa, and has a total area of approximately 1,394 km² (*Ayenew, 2008*). It is shared by four weredas: Fogera, Dera, Farta and Esite under the administration of the regional state Amhara. The rugged and undulated topographic disparity and the variations in altitude of Gumara range between 1780-3750 m.a.s.l. at the high plateau of Guna Mountain with slopes between 20-30% in the high mountainous region in the east and low slopes less than 3% in the low lands (*Nisar, 2016*). Most soils in the Lake Tana basin are derived from the weathered basalt profiles, particularly in Gumara the soils have developed on alluvial sediments (*Mamo et al., 2013*). This topographic conditions have a great impact in the weather, soil and vegetation conditions. Soils in Gumara are mainly dominated by 5 types Haplic Luvisols, Chromic Luvisols, Eutric Vertisols, Eutric Fluvisols, Eutric Leptosols (*FAO-SOTER, 2014*). Its land cover is mainly agriculture, agro-pasture and small farm lots tilled with the traditional ox-drawn plow tool (*Yilma and Awulachew, 2009*). *Mekonnen et al. (2009)* classified the major land cover types as croplands (74%), bushes and shrubs (13%), water (0.1%), grassland (5%), forest (6%) and bare land (2%) while *Mamo (2013)* mentioned that only a small portion of the highlands are forested (less than 1% of the study area) and classified the rest as cultivated land (63.2%), moderately cultivated land (31%), grassland (3.2%), forest (0.36%), urban and built-up (0.063%) and water body (0.059%). In this watershed only one monitoring discharge station exists. Located several kilometers upstream from the Lake Tana at 11°49'59"N and 37°37'59"E. The annual runoff volume of Gumara ranges from 779 Mm³ in 2004 up to 1691 Mm³ in 1996, with an approximate average annual runoff of 1185 Mm³, where the highest peaks occur during July and September and lowest peaks are during December and April (*Nisar, 2016*).

The **Ribb** sub-catchment has an estimated area of approximately 1495 km² and is located in the eastern part of Lake Tana between Latitude 12°0'0"N and longitude 38°0'0"E. Elevation in the watershed ranges from 1772 to 4103 m.a.s.l. The steepest parts are located in the south eastern region of Ribb River catchment, with a continuous decrease of the slope toward its outlet at Lake Tana (*Huber, 2015*). Large areas in the Ribb catchment are used for agriculture with only small parts used for range-grasses. *Setegn (2008)* showed that the most severe erosion conditions are located in the south-eastern part of the catchment. *Betrie et al. (2011) and Easton et al. (2010)* also identified some relative extreme erosion prone areas in the same locations. This catchment has only one meteorological station, Debre Tabor located near its southern border. The dominant soil in the sub-basin are the Eutric Cambisols, sandy soils of brown color with parent metamorphic or volcanic parent material, between 10 and 100 cm deep and consists of medium and fine textured material. In general, cambisols are good for agriculture, therefore are intensively cultivated (*FAO 1986*). This catchment has two types of Eutric Cambisols due to its changing characteristics, for instance hydraulic conductivity (*Huber, 2015*).

The **Beressa** sub-catchment is located in the Jemma River catchment in the southeastern part of the Blue Nile Basin, with an area of approximately 473 km². The Beressa catchment is part of the Amhara region, in the north shoa administrative zone

and in the Basona Werana (*Gasser, 2016*). The elevations of this catchment range between 1710 and 3617 m.a.s.l. The average elevation in the catchment is approximately 2715 m a.s.l. where about 1.6 % of the watershed area is below 2000 m a.s.l., and 81.2 % of the area is below 3000 m a.s.l. The Beressa catchment is mainly dominated by two types of soils, Eutric Cambisols and Pellic Vertisols (*FAO-SORTER, 2014*). Both soils are characterized by containing high amounts of clay (43%-54% of the soil weight in the first layer), and lower amount of silt and sand. Clay are the soil particles which have a diameter less than 0.002 mm. Silt are the particles between 0.002 mm and 0.05 mm, and sand are the particle with diameters between 0.05 and 2.0 mm. Rock is the term for soil particles bigger than 2.0 mm. The northern part of the Beressa catchment is mostly classified as moderately cultivated, whereas the southern part is more extensively cultivated. The very irregular slopes in the northern part of the area do not allow a more intensive agriculture. Debre Birhan city is located between the northern and southern agricultural areas.

The climate in the Beressa catchment is highly dependent on the change of seasons, where 95% of the total annual rainfall happens during July and August, whereas less than 5% of the total rainfall per year occurs during the winter (November, December and January). Due to the topographic characteristics, the Beressa catchment and the area around the city of Debre Birhan belong to the dega climatic zone. In contrast to the Ethiopian climate zones Kolla (Tropical zone) and Woina dega (subtropical zone), the Dega (cool zone) includes the highlands above 2440 meters m.a.s.l. (*Gasser, 2016*).

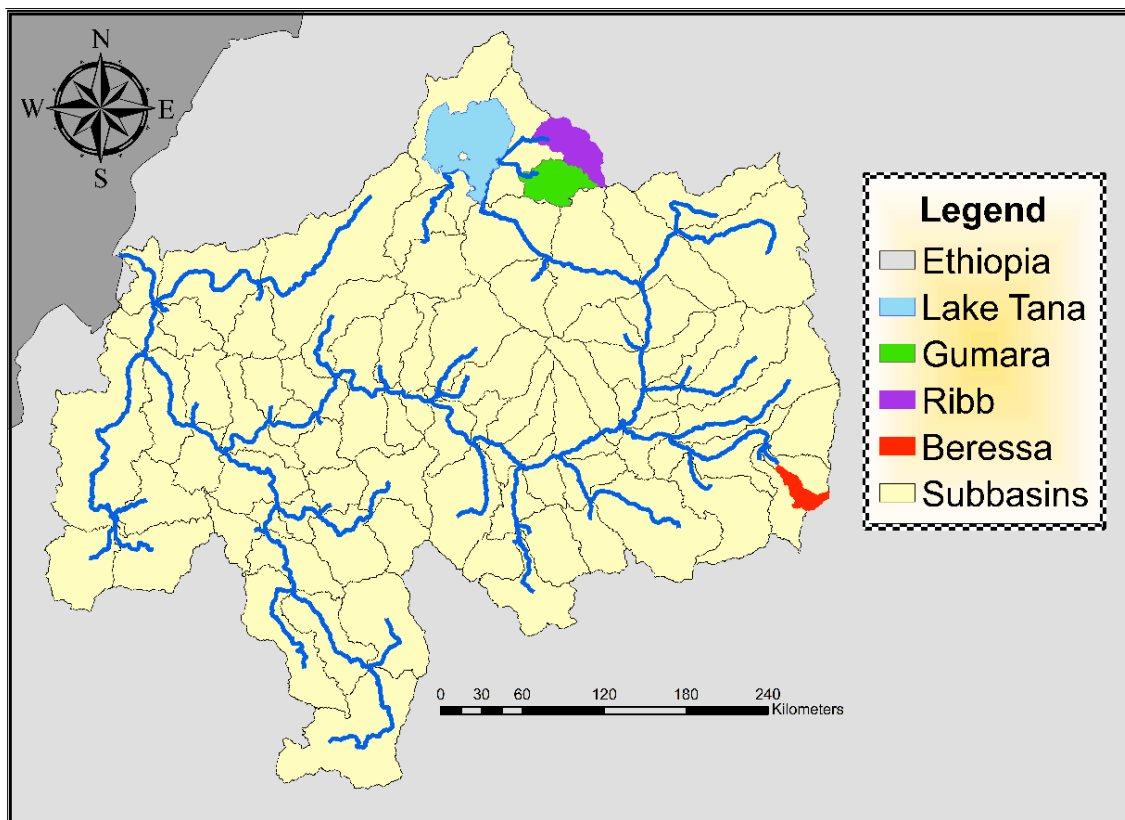


Figure 26. Location of Gumara, Ribb and Beressa sub-catchments in the Blue Nile Basin.

3.2.2 Sub-basin delineations, sediment concentration and sediment yield

These three watersheds were processed using the automatic delineation provided by ArcSWAT, where the flow direction, flow accumulation and streams network were automatically determined by SWAT. Multiple sub-basin delineations were done for each sub-basin (**Table 11, Table 12 and Table 13**). These SWAT models were built from 1988 to 2007, using a 4 years warm-up period (1988-1991). These models of Gumara, Ribb and Beressa helped to understand the effects of using different sub-basins delineation and how the HRUs size influence the runoff peaks and sediment yields.

The land use map for the Gumara catchment was divided into 6 categories: maize, barley, pasture, teff, mixed forest, urban (villages). For the Ribb catchment 6 categories were also defined: Close grown agricultural land, land row crops, generic agricultural land, range brush, range grasses and urban areas (villages). The Beressa catchment was divided into 6 categories as well: bushland, dominantly cultivated, moderately cultivated, pasture, mixed forest and urban (villages).

The HRUs were defined using the 'Multiple HRUs' option under 0% discretization of land use, soil and slope classes over the sub-basin area. This means that the maximum possible number of HRUs based on land use, soil and slope classes was created for all models. However, for each model a different threshold for the sub-basin delineation was chosen, which generated different number of sub-basins. Therefore, although the input datasets and thresholds for the land use, soil and slope classes were the same for all the models, the number of HRUs increased due to a higher number of sub-basins.

For the Gumara catchment 11 models were created, ranging from 1 to 1696 sub-basins and from 71 to 5787 HRUs (**Figure 27, Figure 28 and Table 9**). Ribb catchment was simulated under 11 different models too, ranging from 1 to 1731 sub-basins and from 55 to 5859 HRUs (**Figure 29, Figure 30 and Table 10**). For the Beressa catchment 15 models were created, containing from 7 to 663 sub-basins and from 95 to 2157 HRUs (**Figure 31, Figure 32 and Table 11**). The relationship between the number of subbasins, HRUs and the portion threshold used for each watershed delineation are given in **Table 9, Table 10 and Table 11** for Gumara, Ribb and Beressa, respectively.

Although, the simulated flow discharge of all models remain very similar (**Figures 28C, Figure 30C and Figure 32C**), sediment concentrations and sediment loads are very different between models (**Figures 28A and 28B, Figure 30A and 30B, and Figure 32A and 32B**). Outflows obtained from the models under different number of HRUs continues to show high peaks while the sediment concentrations and sediment loads continue to decrease. The reduction continues to the point where the model containing 5787 HRUs, in the cases of Gumara, provided sediment concentrations lower than 1000 mg/l (**Figure 28A**) while its model with 71 HRUs generated sediment concentrations over 3000 mg/l (**Figure 28A**). This effect is caused by the different slopes lengths used for the calculations. When all HRUs are within a sub-basin, the average slope length will

be used. When the HRUs are within different sub-basins, the HRUs average slope lengths is still used for the calculation, however, in this case the sediment yields of each sub-basin will finally be added, which is the same effect as if the slope lengths of each HRU were added.

This study shows how increasing the number of HRUs (smaller HRUs) also increases the runoff concentration times and reduces the sediment outputs, even when the model calibrations based on flow discharge data remains the same. Having a model that underestimates sediment yields will leave any type of erosion problem totally out control. For instance, the excess of organic or inorganic fertilizers dragged to the water bodies for the agricultural fields product of the runoff process can result in eutrophication (*Setegn et al., 2009*), here the importance of correct sediment yield estimations.

Therefore, defining large number of sub-basins increases the total number of HRUs in a model, and reduces the number of HRUs per sub-basin. This will constantly increase the average slope length and will produce lower sediment concentrations, or vice versa, low number of HRUs could overestimate sediment loads. Although an exact number of sub-basins or HRUs cannot be provided for the Blue Nile Basin, results of these analyses have shown that using a resolution portion between 0.4-1.3% of the total area of a watershed provided less variability in the relationship “number of HRUs-resolution portion” (*Figure 28D, Figure 30D and Figure 32D*).

Table 9. Sub-basins, HRUs and resolution portion for Gumara catchment.

Model	Number of Subbasins	Number of HRUs	Resolution Portion (%)
1	1	71	24.26
2	5	147	16.17
3	19	296	4.04
4	23	356	2.02
5	33	421	1.21
6	51	545	0.81
7	75	717	0.65
8	105	868	0.49
9	161	1149	0.32
10	585	2765	0.08
11	1696	5787	0.02

Table 10. Sub-basins, HRUs and resolution portion for Ribb catchment.

Model	Number of Subbasins	Number of HRUs	Resolution Portion (%)
1	1	55	23.2
2	3	112	15.82
3	13	280	3.95
4	31	492	1.98
5	51	625	1.19
6	75	763	0.79
7	91	880	0.63
8	115	997	0.47
9	160	1226	0.32
10	604	2896	0.08
11	1731	5859	0.02

Table 11. Sub-basins, HRUs and resolution portion for Beressa catchment.

Model	Number of Subbasins	Number of HRUs	Resolution Portion (%)
1	7	95	5.29
2	15	144	2.11
3	54	332	1.06
4	56	350	0.95
5	58	360	0.85
6	60	367	0.79
7	68	405	0.74
8	77	440	0.63
9	83	458	0.58
10	113	596	0.42
11	155	741	0.32
12	215	942	0.21
13	281	1140	0.16
14	436	1590	0.11
15	663	2157	0.06

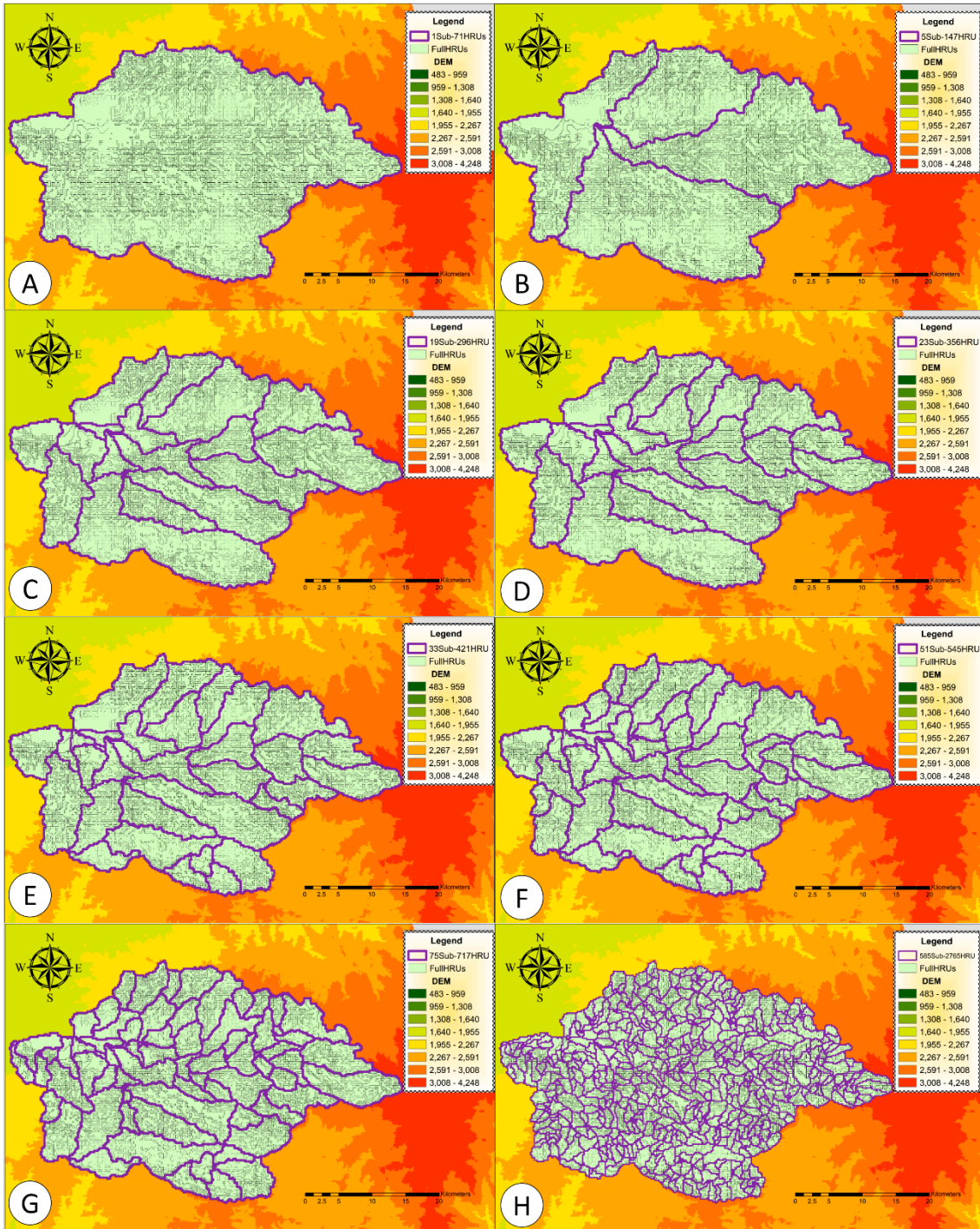


Figure 27. Sub-basins and HRUs distributions at Gumara catchment: **A)** 1Sub-71HRUs, **B)** 5Sub-147HRUs, **C)** 19Sub-296HRUs, **D)** 23Sub-356HRUs, **E)** 33Sub-421HRUs, **F)** 51Sub-545 HRUs, **G)** 75Sub-717HRUs, **H)** 585Sub-2765HRUs.

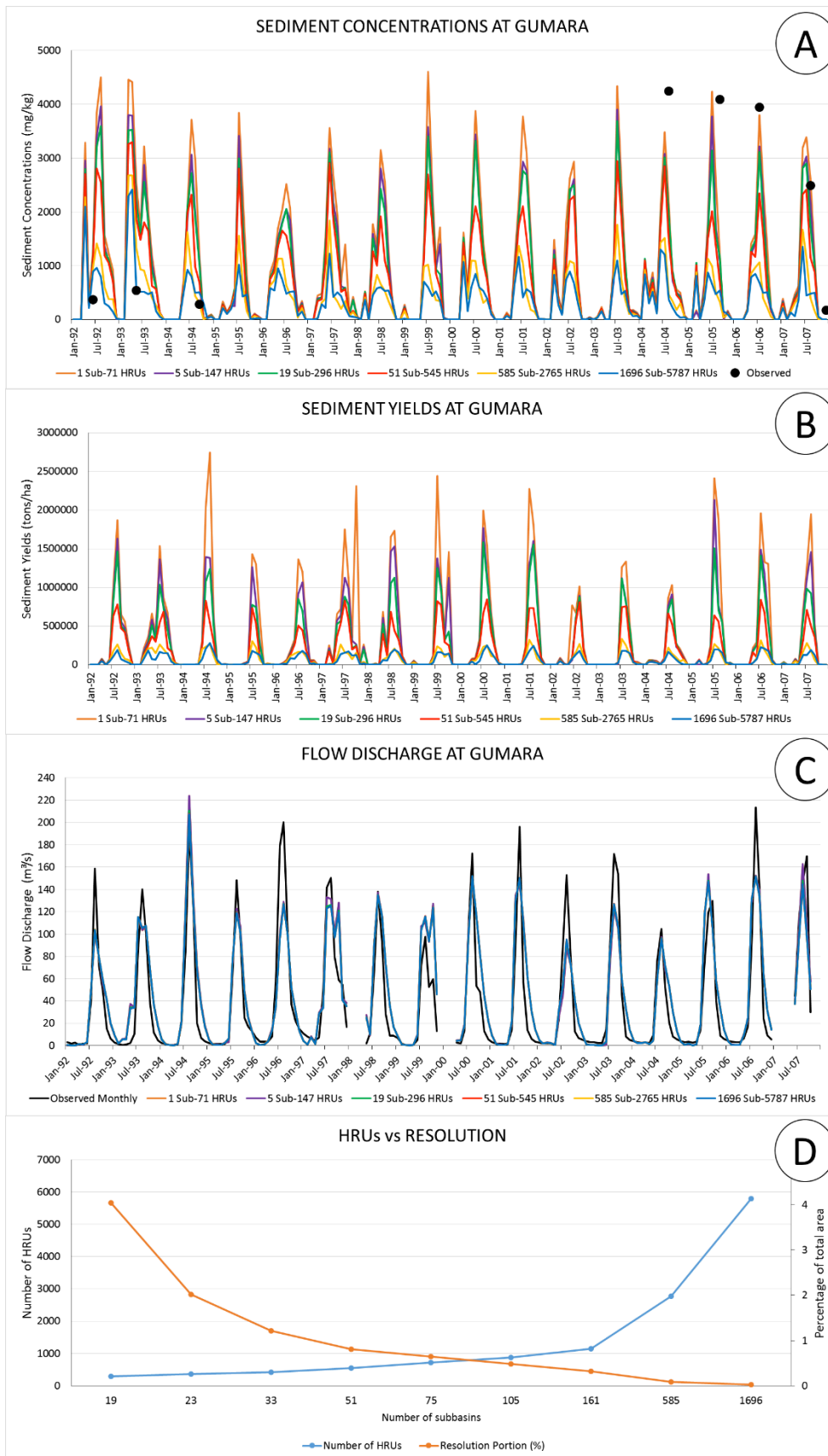


Figure 28. Results at Gumara catchment for the period 1992-2007: **A)** Sediment concentration, **B)** Sediment yield, **C)** Flow discharge, **D)** HRUs vs. resolution.

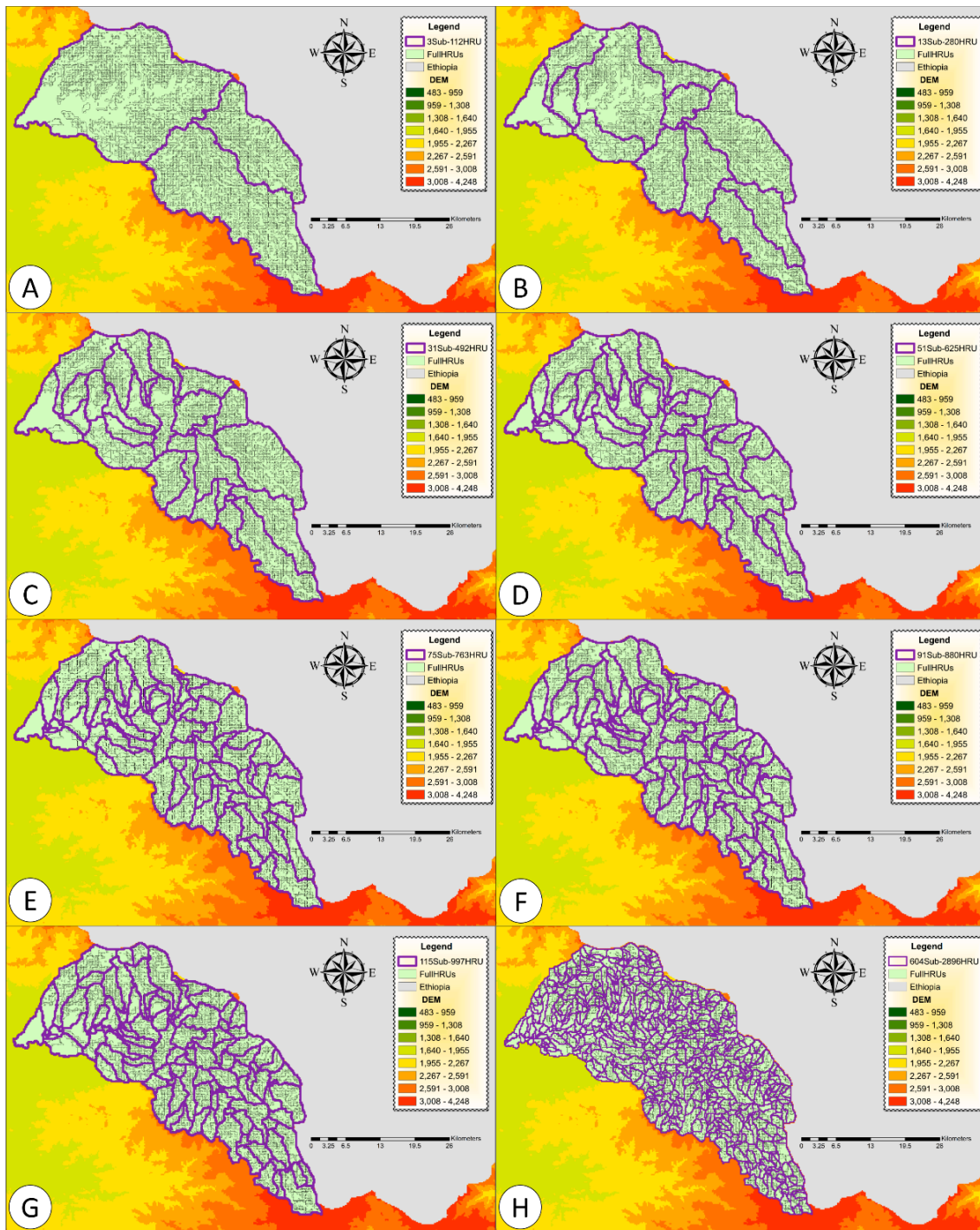


Figure 29. Sub-basins and HRUs distributions at Ribb catchment: **A) 3 Sub-112HRUs, B) 13Sub-280HRUs, C) 31Sub-492HRUs, D) 51Sub-625HRUs, E) 75Sub-763HRUs, F) 91Sub-880 HRUs, G) 115Sub-997HRUs, H) 604Sub-2896HRUs.**

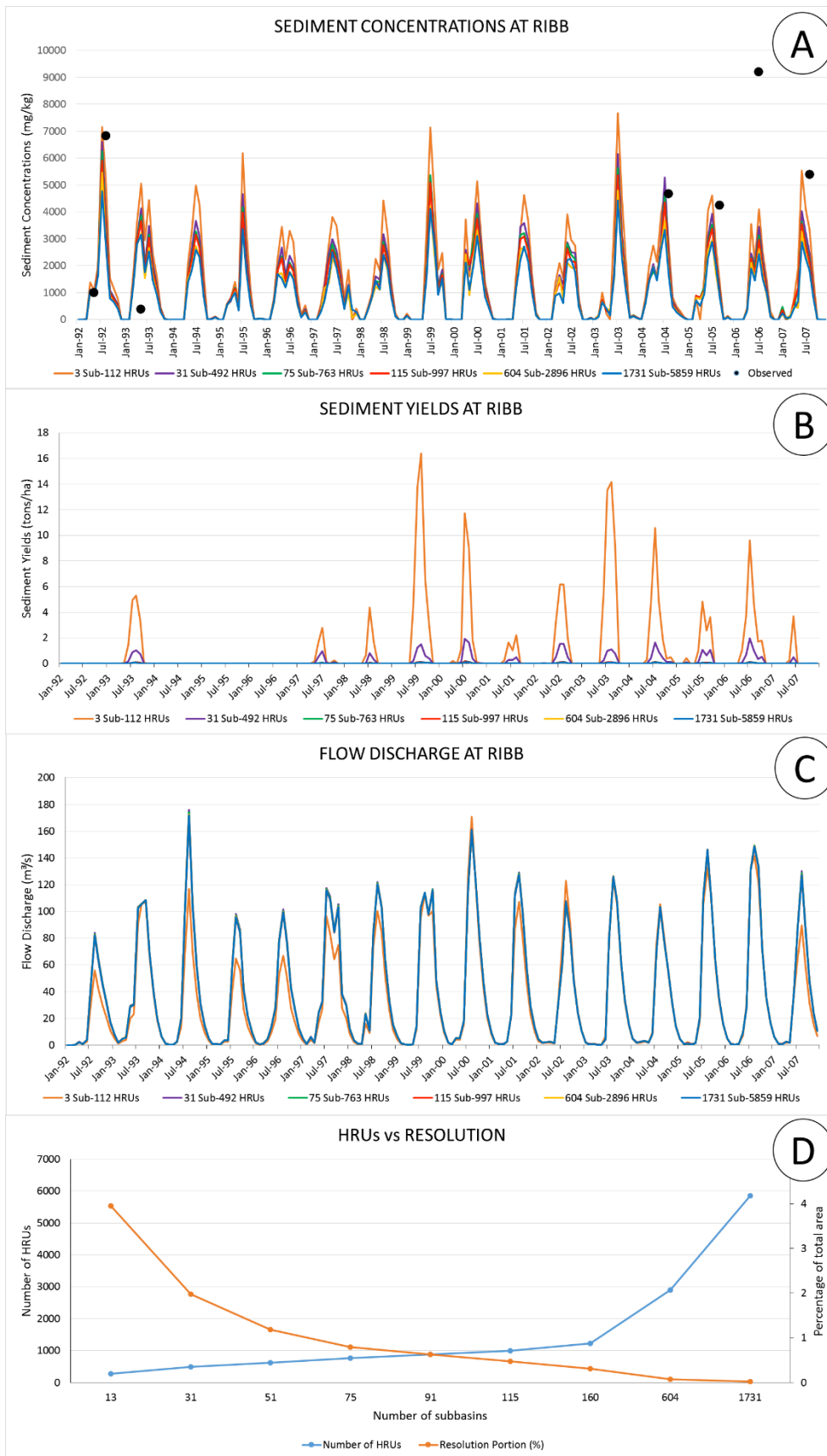


Figure 30. Results at Ribb catchment for the period 1992-2007: **A)** Sediment concentration, **B)** Sediment yield, **C)** Flow discharge, **D)** HRUs vs. resolution.

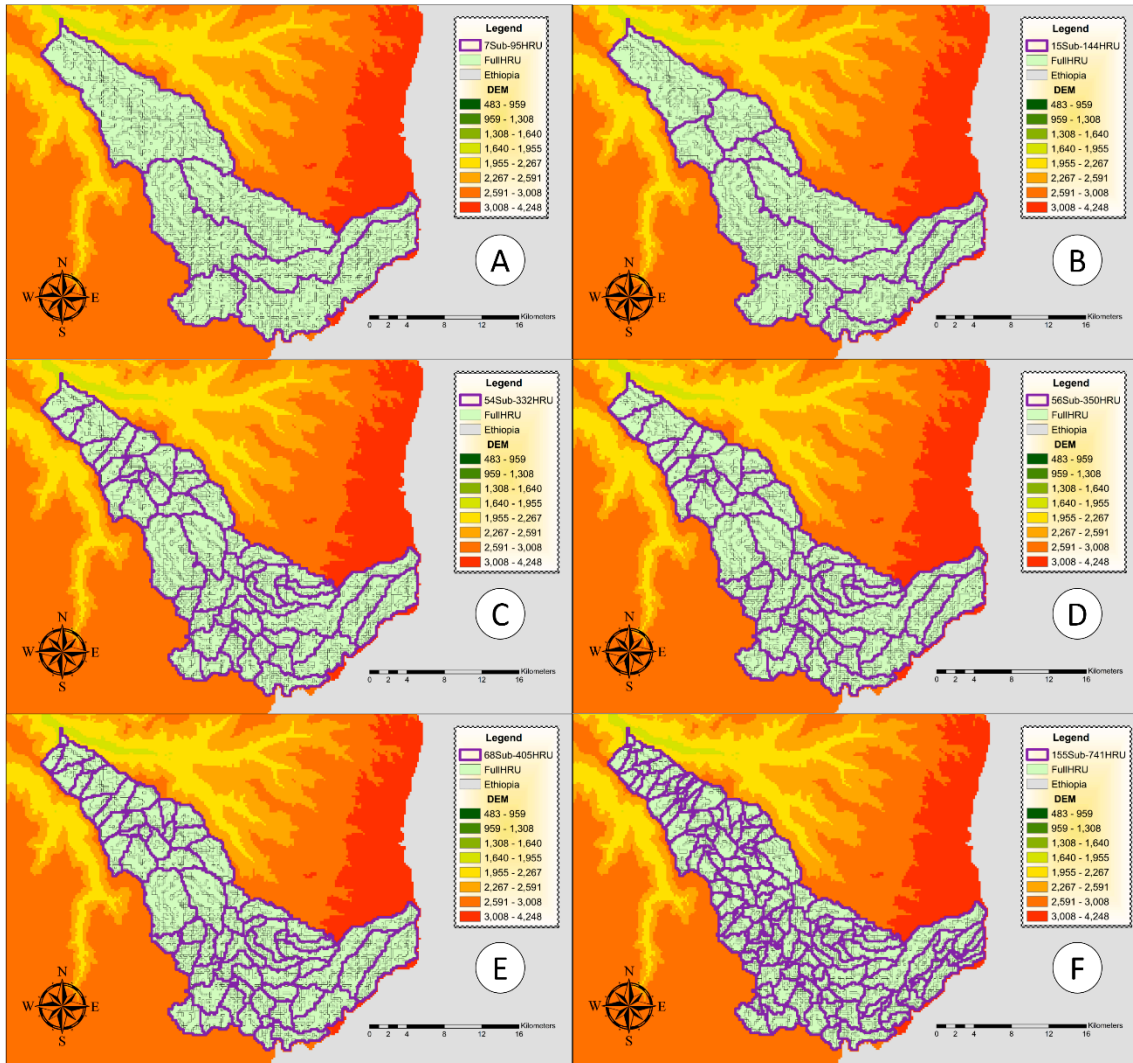


Figure 31. Sub-basins and HRUs distributions at Beressa catchment: **A)** 7Sub-95HRUs, **B)** 15Sub-144HRUs, **C)** 54Sub-332HRUs, **D)** 56Sub-350HRUs, **E)** 68Sub-405HRUs, **F)** 155Sub-741HRUs.

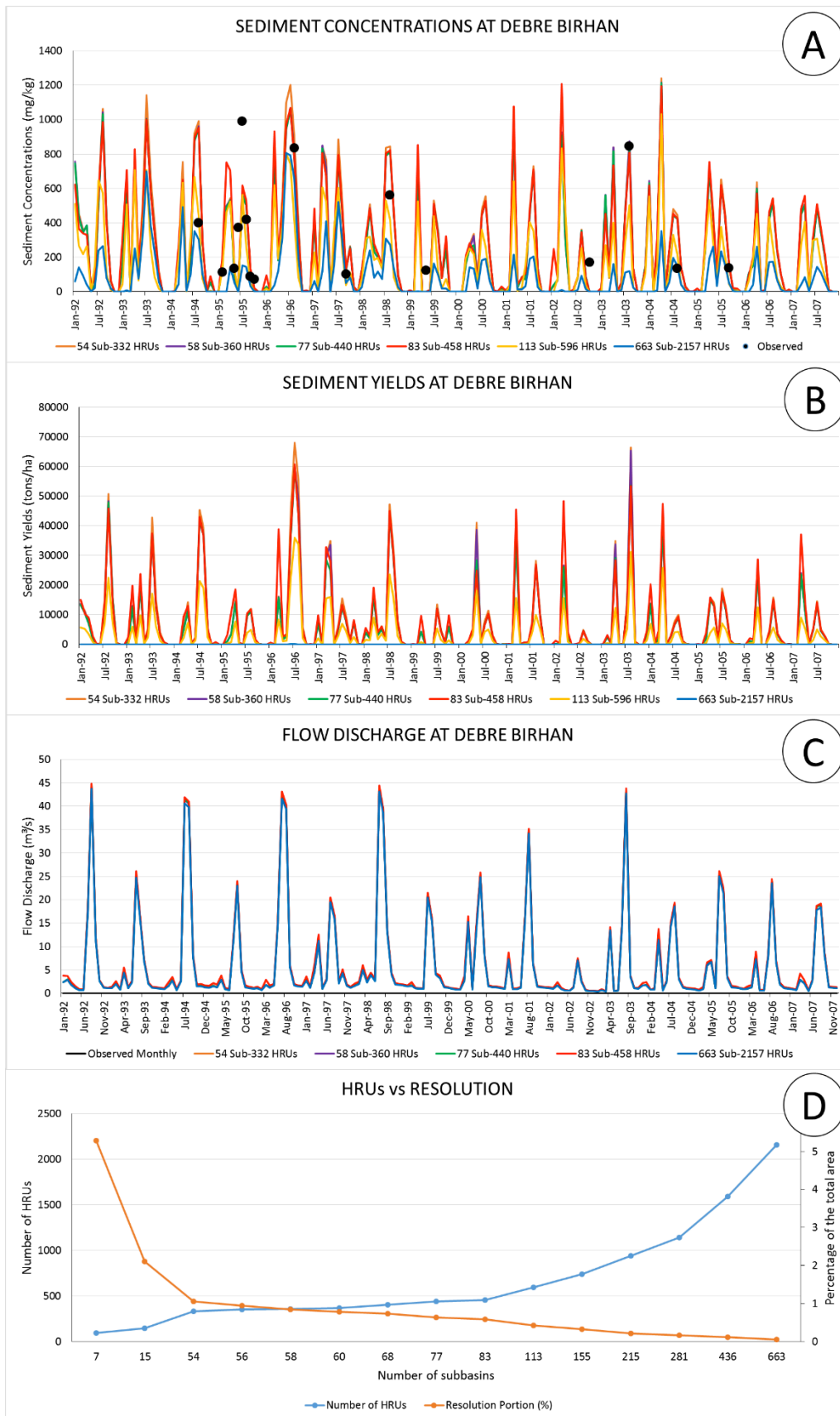


Figure 32. Results at Debre Birhan in the Beressa catchment for the period 1992-2007: **A)** Sediment concentration, **B)** Sediment yield, **C)** Flow discharge, **D)** HRUs vs. resolution.

3.2.3 Sediment concentration rating curves for the Blue Nile Basin

Sediment data in the Blue Nile Basin has rarely been measured and very few data can be found. Only a few measurements have been made during raining season for some years. Thus, hydrological models in this region cannot be accurately calibrated with sediment data, which is also a disadvantage when modeling and analyzing the land degradation problem. Due to this sediment data scarcity multiple methods to estimate sediment loads based on few available measured data have been developed (*Moges et al., 2016*). However, the relationship between sediment load and water discharge is not continuous and constant, especially in the Blue Nile Basin where the sediment concentrations decrease with the progress of the monsoon period (*Moges et al., 2016*). Sediment losses are very difficult to be estimated as it is not linearly bounded to the amount of rainfall as it happens with the runoff (*Moges et al. 2016*). When discharge data has regularly been taken over a certain period of time, then rating curves could be used for estimating sediment loads and concentrations (*Walling, 1990; Horowitz, 2010; Kokpinar et al., 2015; Choi and Lee, 2015; Kheirfam and Vafakhah, 2015*). Several sediment rating curves are available for many different rivers in the world, rating curves specifically for monsoon climates like in the Blue Nile Basin have also been developed by *Moges et al. (2016)*. Rating curves have been used to calibrate and validate models and predict sediment load in the Lake Tana region (*Setegn et al., 2009; Easton et al., 2010; and Moges et al., 2016*). There are multiple ways to convert observed measured discharge and sediment concentrations to rating curves (*Phillips et al., 1999; Horowitz, 2010*). The most common formula used to relate sediment load as result of the relation between sediment concentration and discharge is (*Miller, 1951; Muller and Foerstner, 1968; Phillips et al., 1999; Masoumeh and Mehdi, 2012*):

$$M = a_l Q^b$$

Equation (44)

And the sediment concentration C , can be calculated by dividing the previous equation with the discharge Q :

$$C = a_c Q^{b-1}$$

Equation (45)

where M is the sediment load, Q is the discharge and a_l and b are rating curve parameters determined by regression analysis using observed data (*Gao, 2008*), and $a_c = a_l$.

This sediment load rating curve assumes a unique function of the discharge, also assuming a regular and constant relationship between discharge and sediment concentration (*Gao, 2008*). However, other studies have shown that when observed sediment concentrations are plotted against discharge, a significant scatter around the curve is usually present (*Asselman, 2000; Gao, 2008 and Walling, 1977a*), which proves that other factors additional to discharge also have an influence sediment concentrations. Observed sediment concentrations in streams and rivers of the Blue Nile Basin show a decrease for the same discharge with the progression of the rainy phase (*Guzman et al., 2013 and Tilahun et al., 2013c*). Therefore, this method cannot

be used for predicting sediment concentrations when the sediment concentration decreases throughout the season for a given amount of discharge. Therefore, **Moges et al. (2016)** developed a realistic approach that has been able to determine the decreasing sediment concentration with the progression of the monsoon using the limited available data common in the Ethiopian highlands. **Steenhuis et al. (2009)** and **Tilahun et al. (2013b, c)** adapted the theory originally developed by **Hairsine and Rose (1992)** to include the observed decreasing sediment concentration with the progression of the rainy season in the prediction of sediment concentration. For this reason sediment concentrations have been calculated separately for the rainy monsoon phase and for the dry phase.

Based on the available observed data **Moges et al. (2016)** defined a_c as:

$$a_c = \left[a_t + (a_s - a_t) * \left(\frac{P_e}{P_T} \right) \right] \quad \text{for } P_e < P_T$$

$$a_c = a_s \quad \text{for } P_e \geq P_T$$

Equation (46)

where a_s is the sediment source limiting factor, a_t is the sediment transport limiting factor, P_e is the cumulative effective rainfall (mm) on a particular day, P_T is the threshold cumulative rainfall up to which amount the a_c parameter linearly decreases with cumulative rainfall P_e , and after which the sediment concentration remains at the source limit. Therefore, when P_e is equal to or greater than P_T , the ratio becomes one, which indicates that the sediment concentration is equal to the source limit. The parameters a_c and a_s depend on a number of factors such as slope length, particle size and disposability.

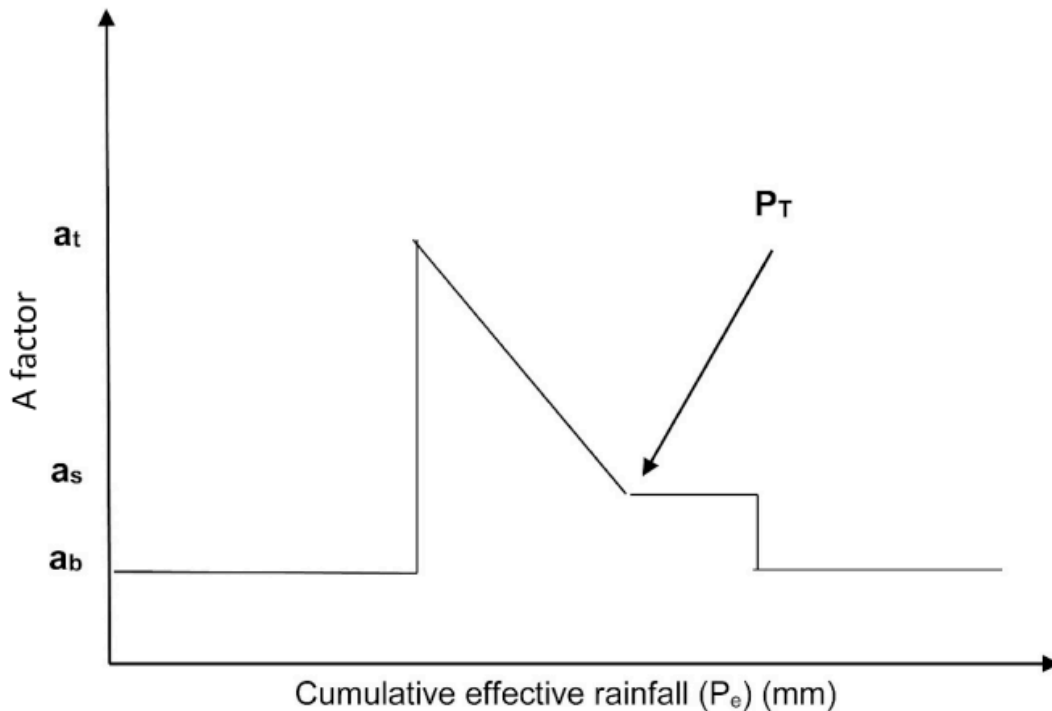


Figure 33. Relationship between sediment concentrations and cumulative effective rainfall (**Moges et al., 2016**).

P_T values are difficult to find and need to be calibrated, however after multiple simulations *Tilahun et al. (2013a, b)* found this value to be approximately 600 mm, which was the value used in this research. The cumulative effective rainfall P_e has been used to replace the “time” parameter because the start of the rainy season varies from year to year and from one location to another within the Blue Nile Basin. To determine P_e , *Moges et al. (2016)* summed the daily effective rainfall, which is equal to precipitation minus the potential evaporation for that day. So, the rainy season starts when the cumulative effective rainfall P_e is greater than 40mm (from observation) and setting each time when P_e is negative to zero. The rainy season in the Blue Nile Basin mostly starts in the beginning of June, however there are some exceptions, for instance in Gilgel Abay starts in mid-May. The rainy season starts earlier in a southern direction. For all of the watersheds the rainy phase ends at the beginning of October. **Figure 33** shows the behavior of the annual cumulative effective rainfall P_e during a year, where the rainy season starts approximately in June and ends in October. As the rainy season advances and precipitation increases the cumulative effective rainfall reaches its maximum peaks usually during the end of August and September, when precipitation decreases, the dry season starts again in October decreasing the cumulative effective rainfall.

If there is a linear relationship between velocity and sediment concentration and the depth of water is small compared to its width, then the exponent b can be set to 1.4 (*Ciesiolka et al., 1995; Yu et al., 1997; Tilahun et al., 2013a, b, c*). Now, by combining **Equation 45** and **Equation 46**, the modified sediment concentration rating curve proposed by *Moges et al. (2016)* for the rainy season can be written as:

$$C = \left[a_t + (a_s - a_t) * \left(\frac{P_e}{P_T} \right) \right] Q^{0.4} \quad \text{for } P_e < P_T$$

$$C = a_s Q^{0.4} \quad \text{for } P_e \geq P_T$$

Equation (47)

The equation to estimate the sediment concentration during the dry monsoon season is:

$$C = a_b Q^{0.4}$$

Equation (48)

Then, the modified load rating curve M for the rainy season can be expressed as:

$$M = \left[a_t + (a_s - a_t) * \left(\frac{P_e}{P_T} \right) \right] Q^{1.4} \quad \text{for } P_e < P_T$$

$$M = a_s Q^{1.4} \quad \text{for } P_e \geq P_T$$

Equation (49)

And for the dry monsoon M can be expressed as:

$$M = a_b Q^{1.4}$$

Equation (50)

With the previous methodology *Moges et al. (2016)* defined sediment rating curves and also provided calibrated values to be used for the sub-catchments in the Lake Tana region (**Table 12**). By applying the same methodology used P_{USLE} factors and slope-length limits for contouring (*Wischmeier and Smith, 1978*). was possible to define the sediment rating curve parameters for other 5 sub-catchments in the upper Blue Nile Basin: Ardy, Azuari, Chena, Muga and Temecha (**Table 13**). In the following chapter, these sediment rating curves were used to estimate sediment concentrations that were then compared with the results provided by SWAT.

Table 12. Calibrated sediment rating curve parameters and the specific dates where the sediment transport ends and the sediment limiting phase starts (*Moges et al. 2016*).

River catchment	A factor calibrated values ($gl^{-1}(mm\ day^{-1})$) ^{-0.4}		A factor for base flow (a_b) ($gl^{-1}(mm\ day^{-1})$) ^{-0.4}	Threshold of effective precipitation (mm)	Date when the a_s starts
	at	as	Ab	PT	
Gilgel Abay	1.6	0.8	0.6	561	15 May
Gumara	5.9	1.5	0.7	574	15 June
Ribb	5.0	0.7	0.2	581	29 May
Megech	2.3	0.3	0.2	588	14 May
Maybar	5.1	0.7	-	598	15 May
Debre Mawi	6.9	1.1	-	599	5 June
Anjeni	3.1	1.8	-	596	27 May

Table 13. Calibrated sediment rating curve parameters for 7 sub-catchments in the upper Blue Nile Basin.

River catchment	A factor calibrated values ($gl^{-1}(mm\ day^{-1})$) ^{-0.4}		A factor for base flow (a_b) ($gl^{-1}(mm\ day^{-1})$) ^{-0.4}	Threshold of effective precipitation (mm)	Date when the a_s starts
	at	as	ab	PT	
Ardy (Metekel-Chagni)	3.2	0.75	0.65	520	June
Azuari (Motta)	4.5	0.68	0.25	534	June
Chena	2.5	0.6	0.6	490	June
Muga	5.7	0.9	0.13	544	June
Temecha	4.8	0.7	0.1	560	June

3.3 Weather datasets vs. sub-basins discretization

This section includes the analyses and comparisons performed with the three weather datasets: CFSR, Ground and the Integrated dataset. The objective of this comparison has been the evaluation of the proposed Integrated dataset, the selection of the most realistic and accurate dataset that will be used to create the final model of the Blue Nile Basin, and selection of the adequate number of sub-basins to be used in the Blue Nile Basin. These three datasets were compared under two models: SWAT30 and SWAT87, models that were divided into 30 and 87 sub-basins, respectively (*Polanco et al., 2017*). This comparison has also helped to understand the effect of the number of sub-basins on the final water balance provided by SWAT. These two delineations were done based on the following criteria:

1. Default resolution portion defined by SWAT: As default value SWAT uses a resolution portion of 2% of the total area to delineate watersheds, which in this cases corresponded to 345,535.84 hectares. By using this value SWAT was able to create enough reaches to define 30 outlets or sub-basins.
2. A proposed resolution portion: Based on the analyses obtained in section 3.2.2, a unique value for the resolution portion cannot be given, however the graphs have shown that values between 0.4-1.3% of the total area provided less variability in the relationship “number of HRUs-resolution portion”. Therefore, a resolution portion of 0.58%, which corresponds to 100,000 hectares, was used to delineate the reaches in the Blue Nile Basin. Based on this delineation 87 sub-basins and 3227 HRUs were created were automatically created.

3.3.1 Parameterization

One of the major constrains in the calibration of hydrologic models is the difficulty of the parameterization of different variables (*Hauhs and Lange, 2008*). The correct combination of the values of the parameters influencing the ground water, runoff and evapotranspiration processes is a key point for the calibration of a hydrological model (*Polanco et al., 2017*). The characterization of watersheds considering their most influential variables is a good approach to determine the predictive capabilities of a model (*McDonnell et al., 2007*). Initially, it is recommended to perform calibrations for annual discharge values, once acceptable results are acquired; a calibration based on monthly values can be performed to achieve more detailed results (*Neitsch et al., 2009*). During a model calibration, a potential value can be assigned for each parameter and for each HRU, which would generate a large number of parameters. However, in SWAT-CUP these values can also be applied as a global modification to estimate parameters by multiplying or adding values. **Table 14** shows the parameterization implemented in this section to calibrate stream flows at Kessie and Eldiem, where r stand for relative values and v for values to be replaced. The same parameterization was applied to SWAT30 and SWAT87 using the 3 datasets.

Calibration of models with wrong parameters values will only produce models with good statistical results but with less realistic representation of the actual properties of the watershed (*Polanco et al., 2017*). Land coverage, soil types and slope have great impact on the total watershed discharge. Therefore, the values of the parameters were modified within the ranges specified by the SWAT Input/Output Documentation 2012

(Arnold et al., 2012). For instance, the available water content of the soils were calibrated in such a way that they did not change the physical properties of the soils. CN2 values were defined within different ranges based on the type of land cover.

Table 14. Parameterization of the SWAT models using the SUFI-2 algorithm for the period 1994-2004 (Polanco et al., 2017).

Parameter	Description	Type of change	Threshold		Fitted value	Ranges of fitted absolute values for the Blue Nile Basin calibration
			Min	Max		
CN2	Curve number for moisture condition II	r	-0.1	0.1	-0.05	60-87
SOL_AWC	Available water capacity of the soil	r	-2	2	1.7	0.095-0.49
ESCO	Soil evaporation compensation factor HRU	v	0.01	1	0.01	0.01
EPCO	Plant uptake compensation factor HRU	v	0.01	1	0.01	1
ESCO	Soil evaporation compensation factor BSN	v	0.01	1	0.01	0.01
EPCO	Plant uptake compensation factor BSN	v	0.01	1	0.01	1
CANMX	Maximum canopy storage	v	0	100	100	57

3.3.2 Effects of different sub-basin discretization levels and rain gauge combinations on the water balance of the upper Blue Nile Basin

After analyzing the results of SWAT30 and SWAT87 under different datasets, it was detected that not only the input data and the parameterization have a critical impact on the water balance, but also the sub-basins distribution (Polanco et al., 2017). Values for the different components of the water balance for the Blue Nile Basin combining SWAT30 and SWAT87 with different datasets are given in Table 17. Values for these hydrological processes based on literature have also been shown on Table 10 (Cherie, 2013 and Mengistu et al., 2012). The uncertainty of the rainfall in the Blue Nile Basin basin is noticeable when models with different sub-basins delineations are compared and show different values (Polanco et al., 2017). Moreover, the average annual precipitation in the Blue Nile Basin also differs between literature (Table 10) and between datasets sources (Table 17). SWAT30 with CFSR data provides an average annual precipitation of 1253 mm, while in SWAT87 the average annual precipitation increases to 1481 mm. This rainfall increase provided by the CFSR dataset is caused by

the number of sub-basins, SWAT87 considers more stations than SWAT30 does (*Polanco et al., 2017*). However, both average annual precipitation values compared to the other two datasets and to the literature could still be within acceptable ranges for Blue Nile Basin.

Table 15. Water balance analysis in the upper Blue Nile Basin for the period 1994-2004 (*Polanco et al., 2017*).

Water balance in the Blue Nile Basin (All values in mm/year)						
Hydrological Component	SWAT30			SWAT 87		
	CFSR Data	Ground Data	Integrated Data	CFSR Data	Ground Data	Integrated Data
Precipitation	1253	1301	1270	1481	1209	1243
Evapotranspiration	729	887	932	848	798	860
Revap/shal. aquifer	27	31	31	27	27	28
Surface runoff	172	167	114	228	166	125
Return flow	274	107	139	307	136	147
Lateral flow	40	50	50	80	73	74
Perc. to deep aquifer	313	199	175	349	168	181
Rechg. deep aquifer	16	10	9	17	8	9

Figure 34 and **Figure 35** show the magnitude and dynamics of the measured and estimated monthly discharge flow at Eldiem under SWAT30 and SWAT87, respectively. The water discharge obtained with the CFSR data is overestimated at Eldiem but it is continuously underestimated at Kessie compared to that provided by the ground and the integrated datasets (**Figure 36 and Figure 37**). Interesting is also to point out the fact that CFSR data only overestimated the flow discharge at Kessie during 1997/98 (*Shehata, 2016*), period that corresponds to the “El Niño” phenomenon (*Melesse et al., 2011*). The flow discharge provided by the CFSR data at Kessie is slightly higher in SWAT87 compare to SWAT30, although in both cases this dataset continues to underestimate the flow discharge. As the precipitation in the watershed changes in magnitude and distribution, the parameterization for the calibration of the models will be different. Therefore, in order to meet good R^2 and NS for the model with a wrong precipitation distribution (in this case the CFSR data), the values of the parameters needed to be modified to unrealistic values (*Polanco et al., 2017*).

The Integrated dataset provided good statistical values for R^2 and NS for both SWAT30 and SWAT87 (**Table 18**). The other models using the ground and CFSR datasets also showed good R^2 results, but very low NS values. Although R^2 is always high in all these models, R^2 is a coefficient that measures only the dynamic of a model, meaning that the models behaved with accuracy matching the seasonality of the rainfalls and dry periods in the Blue Nile Basin (*Polanco et al., 2017*). However, NS is probably a more important factor to be considered as it can be used to quantitatively describe the accuracy of models outputs. Calibrations and validations at Kessie showed good statistical values under SWAT30 and SWAT87 when using the Ground and the Integrated datasets but not with the CFSR dataset (**Figure 36, Figure 37 and Table 17**).

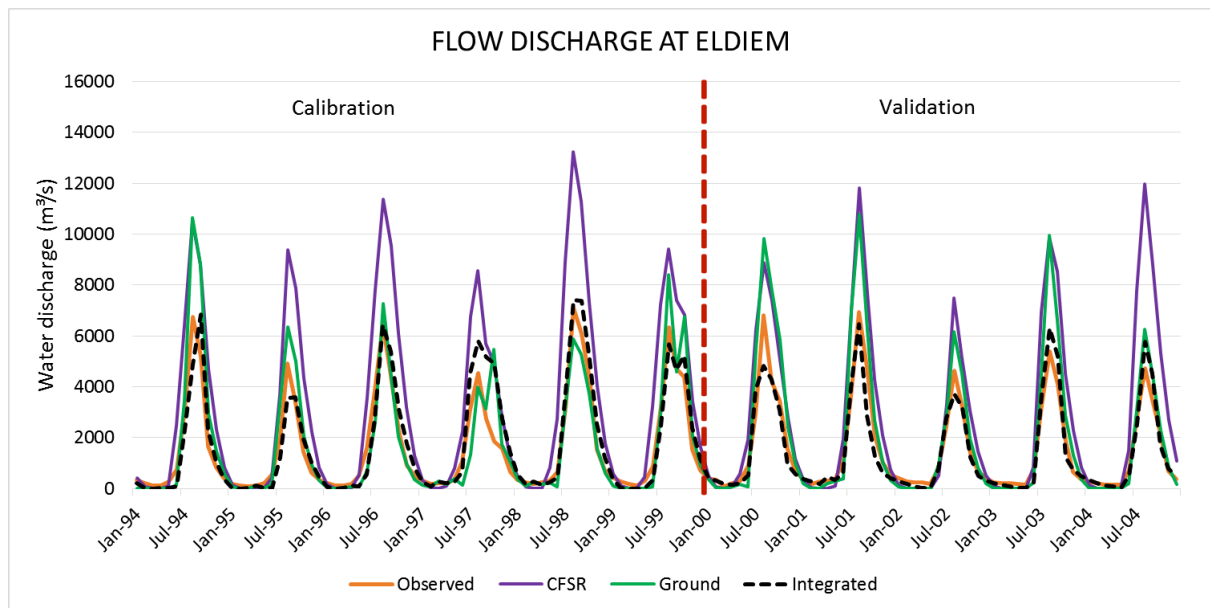


Figure 34. Calibration and validation of SWAT30 at Eldiem. Calibration results achieved R^2 and NS values of: Integrated data: 0.88, 0.84; Ground data: 0.86, 0.74; CFSR data: 0.94, -0.51; respectively. Validation results achieved R^2 and NS of: Integrated data: 0.92, 0.91; Ground data: 0.96, 0.45; CFSR data: 0.92, -0.48; respectively (Polanco et al., 2017).

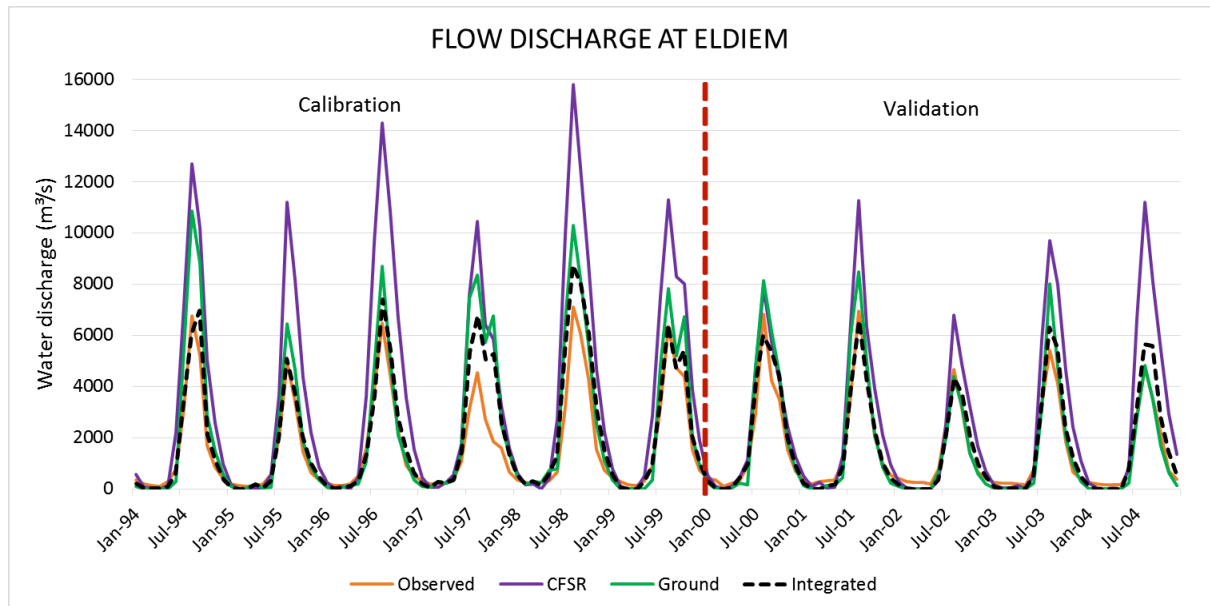


Figure 35. Calibration and validation of SWAT87 at Eldiem. Calibration results achieved R^2 and NS values of: Integrated data: 0.92, 0.80; Ground data: 0.92, 0.43; CFSR data: 0.96, -1.54; respectively. Validation results achieved R^2 and NS of: Integrated data: 0.94, 0.91; Ground data: 0.95, 0.85; CFSR data: 0.89, -0.05; respectively (Polanco et al., 2017).

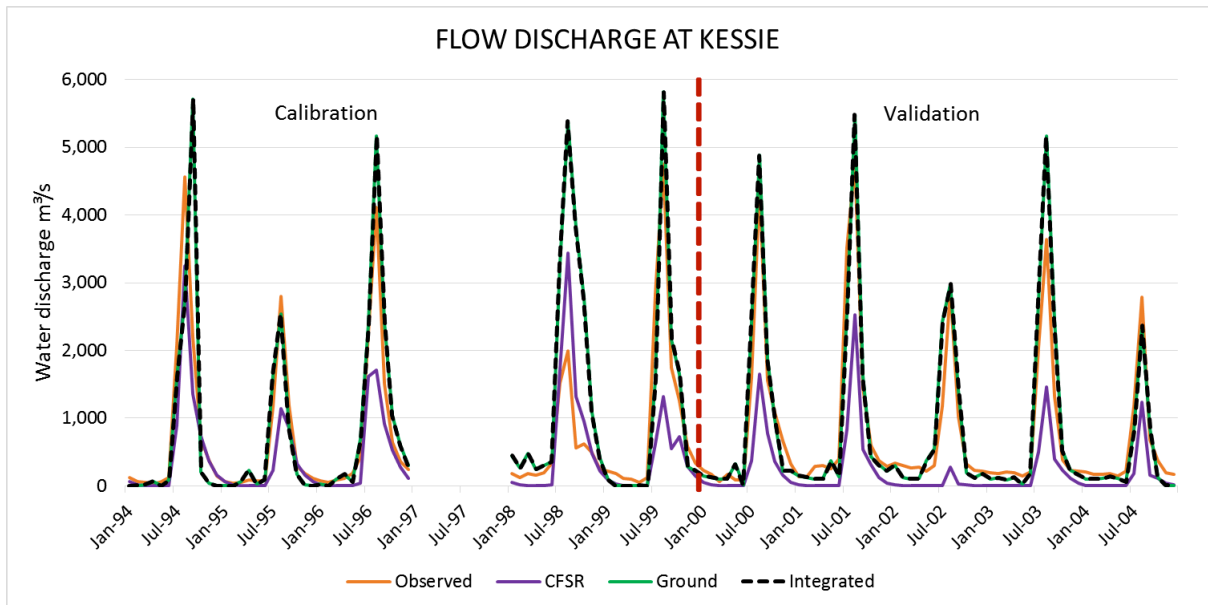


Figure 36. Calibration and validation of SWAT30 at Kessie. Calibration results achieved R^2 and NS values of: Integrated data: 0.74, 0.74; Ground data: 0.74, 0.72; CFSR data: 0.87, 0.46, respectively. Validations results achieved R^2 and NS values of: Integrated data: 0.76, 0.74; Ground data: 0.78, 0.74; CFSR data 0.86, 0.49; respectively (Polanco et al., 2017).

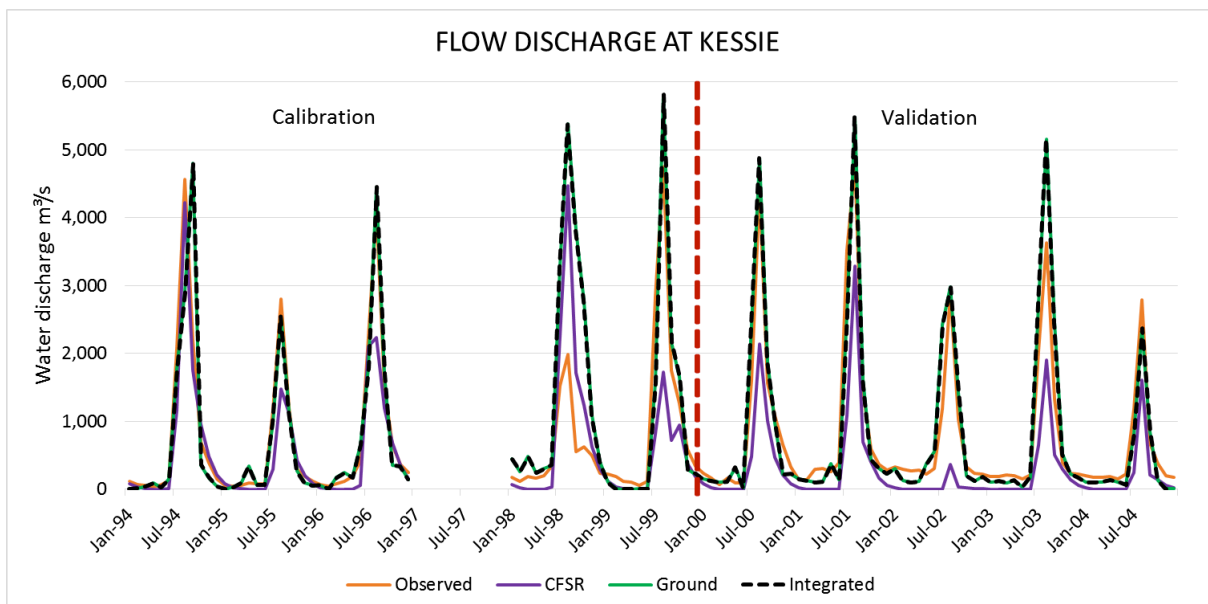


Figure 37. Calibration and validation of SWAT87 at Kessie. Calibration results achieved R^2 and NS values of: Integrated data: 0.77, 0.72; Ground data: 0.77, 0.72; CFSR data 0.77, 0.37; respectively. Validations results achieved R^2 and NS values of Integrated data: 0.78, 0.78; Ground data: 0.80, 0.76; CFSR data 0.74, 0.37; respectively (Polanco et al., 2017).

Table 16. Statistical results for the calibrations and validations with outflow data at Eldiem and Kessie gauging stations (*Polanco et al., 2017*).

		CFSR dataset		Ground dataset		Integrated dataset	
Sub-basins		30	87	30	87	30	87
Eldiem							
Calibration	R²	0.94	0.96	0.86	0.92	0.88	0.92
	NS	-0.51	-1.54	0.74	0.43	0.84	0.80
	p-factor	0.53	0.36	0.66	0.67	0.70	0.77
	r-factor	1.11	0.93	0.83	0.68	0.67	0.54
Validation	R²	0.92	0.89	0.96	0.95	0.92	0.94
	NS	-0.48	-0.05	0.45	0.85	0.91	0.91
Kessie							
Calibration	R²	0.87	0.77	0.74	0.77	0.74	0.77
	NS	0.46	0.37	0.72	0.72	0.74	0.72
	p-factor	0.49	0.57	0.60	0.63	0.60	0.63
	r-factor	0.61	0.71	0.72	0.59	0.72	0.59
Validation	R²	0.86	0.74	0.78	0.80	0.76	0.78
	NS	0.49	0.37	0.74	0.76	0.74	0.78

3.3.3 Average annual evapotranspiration analysis and the effects of different PET methods

The calibration and validation of the models with flow discharge constitute an important part of the quality analysis of a model. Additionally, comparisons with evapotranspiration data could also provide more details to quantify the reliability of hydrological models (*Polanco et al., 2017*). Therefore, evapotranspiration has been another critical factor subject to analysis in this study. Evapotranspiration estimations shown as percentage of the average annual precipitation are frequently given for the Blue Nile Basin. But these percentages would yield totally different amounts depending on the average annual precipitation provided by different weather data sources and different sub-basin discretization (*Polanco et al., 2017*). For instance, the evapotranspiration values in the Blue Nile Basin varied from 729 mm/year in SWAT30 with CFSR data up to 932 mm/year in SWAT30 with the Integrated dataset (*Table 17*).

Actual evapotranspiration data for the Blue Nile Basin was obtained from the MODIS Global Terrestrial Evapotranspiration Project (MOD16), a dataset estimated from land surface by using satellite remote sensing data. It is intended to be used to calculate regional water balances, hence a very important source of data for watershed management and hydrological models analyses. The original MOD16 ET algorithm (*Mu et al., 2007*) was based on the Penman-Monteith equation (*Monteith, 1965*), while the current MOD16 ET has used the improved evapotranspiration algorithm (*Mu et al., 2011*).

In this improved algorithm, the sum of the evaporation from the wet canopy surface, transpiration from the dry canopy surface and evapotranspiration from the soil surface constitute the total daily ET (**Mu et al., 2011**). The formulae for the total daily ET (λE) and potential ET (λE_{POT}) are:

$$\lambda E = \lambda E_{wet_C} + \lambda E_{trans} + \lambda E_{SOIL}$$

Equation (51)

$$\lambda E_{POT} = \lambda E_{wet_C} + \lambda E_{POT_trans} + \lambda E_{wet_SOIL} + \lambda E_{SOIL_POT}$$

Equation (52)

where λE_{wet_C} is the evaporation from the wet canopy surface, λE_{trans} is the transpiration from the dry canopy surface (plant transpiration), λE_{SOIL} is the evaporation from the soil surface, λE_{POT_trans} is the potential plant transpiration, and λE_{SOIL_POT} is the potential soil evapotranspiration.

Previous studies have already shown that the annual ET derived from the MOD16 algorithm are lower than those provided by hydrological models. For instance, **Ruhoff (2013)** detected an underestimation of 21% in the evapotranspiration provided by MOD16 in the Rio Grande basin, Brazil, where the underestimation was mainly caused by the misclassification of the land use. **Sun et al. (2007)** also identify certain disadvantages in the MOD16 evapotranspiration. Nevertheless, a comparison of the SWAT models with satellite evapotranspiration data could help to more accurately identify the level of reliability of the models and could also help to show the performance of the proposed SWAT Error Index (SEI). The models under analysis in this section correspond to the period 1990-2004, however MOD16 ET data is available only for the period 2000-2010. Therefore, the comparison was done only for 5 years, from 2000-2004, corresponding to the validation period of the models.

SWAT models using the ground and Integrated datasets and the Hargreaves equation showed acceptable discharge values and trends compared to the measured discharge data (**Figure 34 and Figure 35**). However, the models overestimated the evapotranspiration values compared to those provided by MOD16 (**Figure 38**). Nevertheless, when using the Penman-Monteith method, the SWAT models using the ground and Integrated datasets provided more similar evapotranspiration values, better R^2 and NS values compared to the values given by the MOD16 evapotranspiration data (**Figure 39**). The best evapotranspiration values compared to the MOD16 data are obtained using the CFSR dataset, this model provided low evapotranspiration values, consequently overestimated the flow discharges (**Figure 34 and Figure 35**).

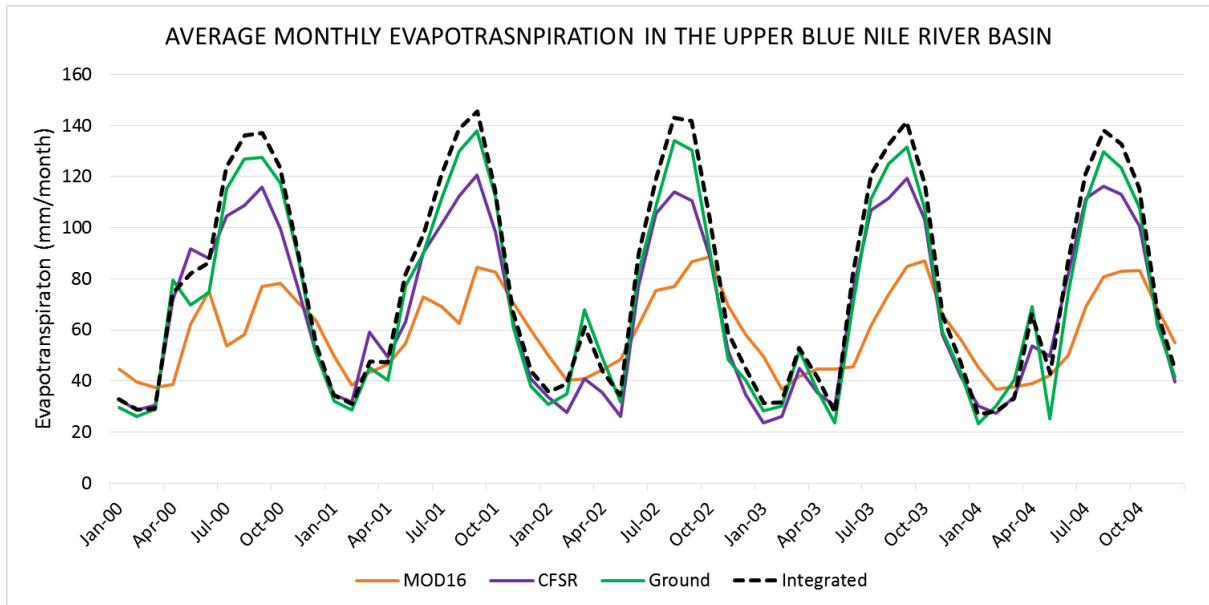


Figure 38. Average monthly evapotranspiration analysis using SWAT87 and the Hargreaves method, with R^2 and NS values of Integrated dataset: 0.63, -2.32; ground dataset: 0.60, -1.32; CFSR dataset: 0.63, -1.20; respectively, compared to the MOD16 data (Polanco et al., 2017).

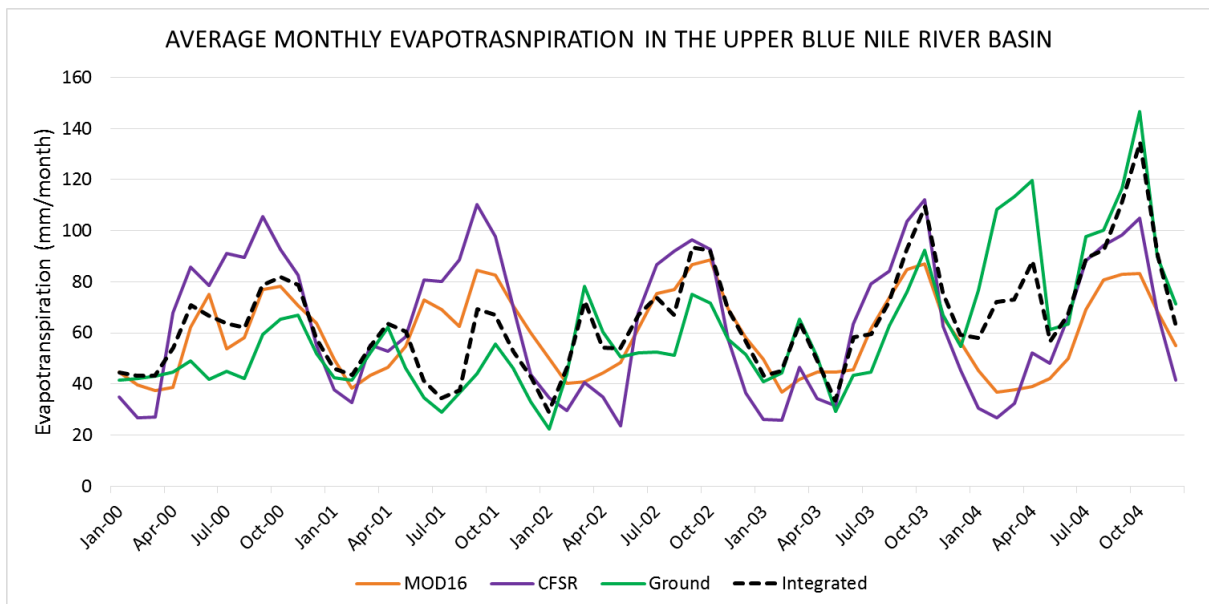


Figure 39. Average monthly evapotranspiration analysis using SWAT87 and the Penman-Monteith method, with R^2 and NS values of Integrated dataset: 0.36, -0.02; ground dataset: 0.34, -0.10; CFSR dataset: 0.74, 0.03; respectively, compared to the MOD16 data (Polanco et al., 2017).

3.4 SWAT Error Index (SEI)

A common problem of hydrological models is the wrong combination of the values of the calibrated parameters, which can also lead to good graphical results, consequently good statistical values, but wrong water balance values (*Polanco et al., 2017*). Therefore, good R^2 and NS values do not always denote the reliability of a model (*Polanco et al., 2017*). R^2 and NS are common statistical parameters used to evaluate and compare time series in hydrological models (*Abbaspour, 2015; De Almeida Bressiani et al., 2015; Dile and Srinivasan, 2014 and Gebremicael et al., 2013*). Additionally, rainfall distribution, parameterization and evapotranspiration are also crucial points to be considered in any hydrological model. Therefore, in this study, after good calibration and validation values for R^2 and NS were achieved using SWAT30 and SWAT87 with the Integrated dataset, and after a comparison between the SWAT ET and MOD16 ET values was completed, an index to quantify the models quality has been introduced, the SWAT Error Index (SEI). This index is intended to be used only as an additional indicator to assess the reliability of the SWAT model, where the relative Root Mean Square Error (rRMSE) was chosen as fitting function (*Polanco et al., 2017*).

Several reliable measured flow discharge datasets are available for rivers, but that is not the case for evapotranspiration data. However, satellite evapotranspiration data is available for most watersheds in the world. Furthermore, the measured discharge dataset and the satellite estimated evapotranspiration dataset do not have the same level of reliability. Therefore, SWAT Error Index uses different weighting values (W_1 and W_2) to define differences in the level of reliability of the datasets, 0.7 for flow discharge and 0.3 for evapotranspiration (*Polanco et al., 2017*). The proposed equation for SEI is as follows:

$$SEI = W_1 \left(\frac{\left(\sqrt{\frac{\sum_{i=1}^n (Q_{oi} - Q_{si})^2}{N}} \right)}{(Q_{o\max} - Q_{o\min})} \right) + W_2 \left(\frac{\left(\sqrt{\frac{\sum_{i=1}^n (ET_{oi} - ET_{si})^2}{N}} \right)}{(ET_{o\max} - ET_{o\min})} \right)$$

Equation (53)

The first part of the equation corresponds to the rRMSE of the values obtained from the discharge data, where, Q_{oi} is the observed discharge data (m^3/s), Q_{si} is the simulated discharge data (m^3/s), $Q_{o\max}$ is the maximum value of the observed discharge data and $Q_{o\min}$ is the minimum value of the observed discharge dataset. The second part of the formula corresponds to the rRMSE achieved from the evapotranspiration data that was obtained from MOD16, where, ET_{oi} is the MOD16 evapotranspiration values, ET_{si} is the SWAT simulated evapotranspiration data, $ET_{o\max}$ and $ET_{o\min}$ are the maximum and minimum values of the MOD16 evapotranspiration data, respectively. W_1 and W_2 are the assigned weighted values for discharge and evapotranspiration, respectively (*Polanco et al., 2017*).

SEI ranges from 0 to $+\infty$, with 0 corresponding to the ideal value. The closer the SEI value of the model is to 0, the model will have a better match with the flow discharge and the evapotranspiration data. Since SEI includes the rRMSE values for discharge and evapotranspiration data, a model with a good SEI results represents a model with a good agreement between these two hydrological processes, which are two important processes influencing the water balance of a watershed. By analyzing the SEI results, the quality of the combination of the parameter used for the calibration could also be evaluated and is less expectable to have a wrong parameterization. SEI was tested for two locations, in the first test was applied to the whole Blue Nile Basin and for second in case was applied in the Ribb sub-catchment of the Lake Tana region (*Polanco et al., 2017*).

4. RESULTS

4.1 Final SWAT model for the upper Blue Nile Basin

The final model for the upper Blue Nile Basin was created based on the statistical results obtained from the previous analyses and meeting the following criteria:

- It has been defined that an optimum model for the Blue Nile Basin should be delineated using a total resolution portion of approximately 0.58% of the total area, which corresponded to 100,000 hectares. Based on this delineation 87 sub-basins were automatically created by SWAT and other 12 sub-basins were manually added to match the outlets of the 7 sub-basins that were used to compare the sediment outputs and other stations used for the discharge calibration, summing up a total of 99 sub-basins.
- By using this delineation percentage the model contains 3466 HRUs, with an average HRU size of 49.8 km², which to certain extent agrees with the area size based on which the MUSLE formulae was developed and tested 40 km² and also with studies performed by *de Vente and Poesen (2005)*, where they mentioned that a threshold between 10 and 50 km² would appear reasonable.
- The model uses the Integrated dataset which provided the most reliable precipitation distribution, water balance values and best statistical results.

The calibration and validation of this model, here after called SWAT99Integrated, was done for 21 years, from 1984 to 2004, dividing the period into two SWAT models using different parameterizations. The first model was run from 1984 to 1993 using a 4 years warm-up period from 1984 to 1987, 4 years calibration period (1988-1991) and 2 years for the validation period (1992-1993). The second model was run from 1990 to 2004 also using a 4 years as warm-up period (1990-1993), 6 years for the calibration (1994-1999) and 5 years for the validation (2000-2004). By performing a hydrological analysis divided into two segments with different parameterization was possible to obtain better fits with the outflow data. The calibration with flow data was mainly done at two stations, Eldiem and Kessie. Although other 7 small sub-catchments were also calibrated where the main objective was the comparison of the sediment concentrations obtained from SWAT with the values obtained from the concentration rating curves (**Figure 40**). **Table 17** shows the main parameters used during the calibration and the reasons why they had to be modified for different periods. Although some causes have to do with changes in precipitation intensities and other meteorological conditions during 1984-2004, other factors influencing the parameterization changes are related to land use, especially the quick expansion of agricultural lands.

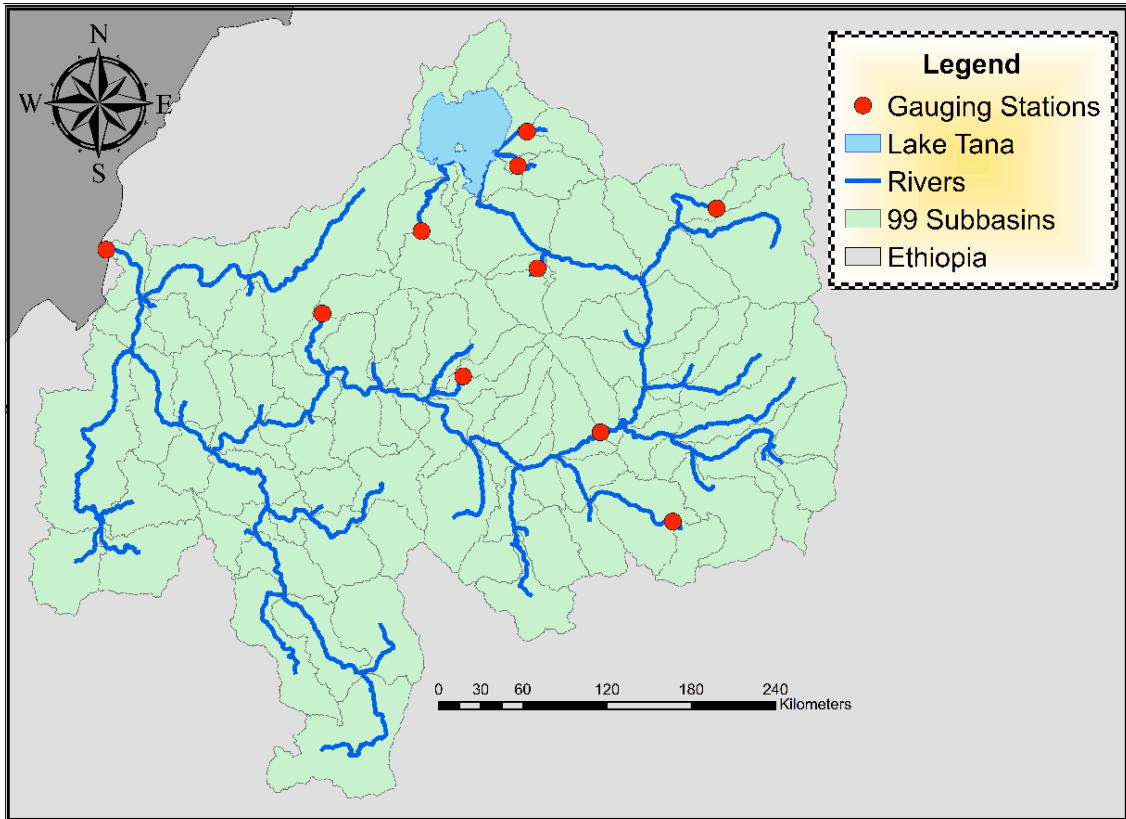


Figure 40. Flow and sediment gauging stations in the upper Blue Nile Basin.

Table 17. Factors influencing the main SWAT parameterization changes for different periods in the upper Blue Nile Basin.

Parameter	Factors influencing the change
CN2	CN2 is highly affected by and represents the type of land use. As it can be seen in Table 18 and Table 20 during the period 1988-1993 CN2 has been lowered while during the period 1994-2004 it has been increased (Table 22 and Table 23), which is also an evidence that agricultural lands have been increasing and with them the soil erosion (Figure 52-55).
ESCO	During 1994-2004 has been decreased which represents that in more regions the top layers cannot satisfy the soil evaporative demand (Table 18 and Table 22). Abandoned agricultural lands that caused soil crusting and cracks have probably caused this water demand increase.
EPCO	This factor has been increased during 1994-2004 (Table 18 and Table 22), also representing that the water demand cannot be met by the top layers and must be satisfied by lower soil layers. This factor also represents the fact that water content in the soils has decreased and plants have required more water for transpiration.

4.1.1 Parameterization, calibration and validation of SWAT at Eldiem and Kessie for the period 1988-1993

For the period 1988-1993, SWAT was initially overestimating the outflows at Eldiem (**Figure 41**), the initial evapotranspiration rate in SWAT99 was 45% and was modified to reach 60%. Therefore the main parameters affecting the evapotranspiration, for instance SOL_AWC, ESCO, EPCO and CANMX, were adapted. CN2 was slightly reduced to match peaks occurring during the rainy seasons. Other parameters controlling the groundwater processes were also modified, GWQMN, GW_REVAP and REVAPM. The calibration was done from 1988 to 1991 and the validation was done for 1992 and 1993. **Table 18** shows all the parameters, ranges and best fitted values used to calibrate and validate the model at Eldiem from 1988 to 1993. The calibration results achieved R² and NS values of 0.79 and 0.76, respectively; while the validation results achieved R² and NS of 0.96 and 0.92, respectively (**Table 19**).

Table 18. Parameterization of SWAT99Integrated using the SUFI-2 algorithm for the period 1988-1993.

Parameter	Description	Type of change	Threshold		Fitted value
			Min	Max	
CN2	Curve number for moisture condition II	r	-0.1	0.1	-0.015
SOL_AWC	Available water capacity of the soil	r	-2	2	1.8
ESCO	Soil evaporation compensation factor HRU	v	0.01	1	0.1
EPCO	Plant uptake compensation factor HRU	v	0.01	1	0.9
ESCO	Soil evaporation compensation factor BSN	v	0.01	1	0.01
EPCO	Plant uptake compensation factor BSN	v	0.01	1	1
CANMX	Maximum canopy storage	v	0	100	100
GWQMN	Deep aquifer percolation fraction	v	0	5000	1875
GW_REVAP	Groundwater “revap” coefficient	v	0.02	0.2	0.1685
REVAPMN	Threshold depth of water in the shallow aquifer for “revap”	v	0	1000	325

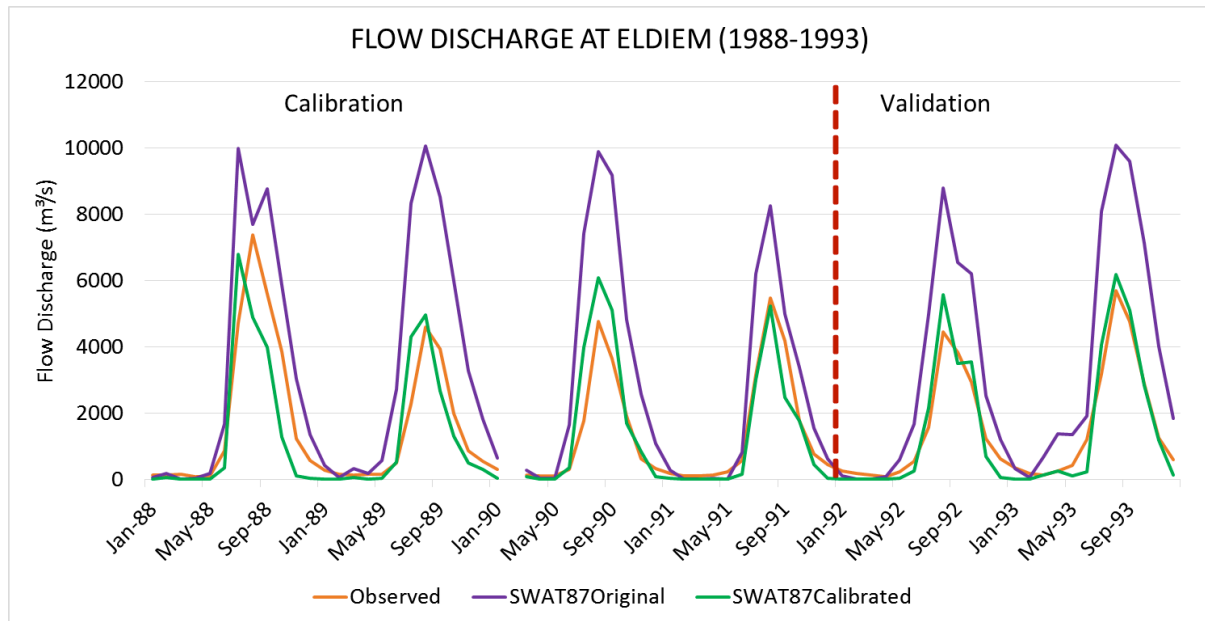


Figure 41. Calibration and validation results at Eldiem with SWAT99Integrated for the period 1988-1993.

Table 19. Statistical results for the calibration and validation with outflow data at the Eldiem gauging station.

Eldiem (1988-1993)		
Calibration	R²	0.79
	NS	0.76
	p-factor	0.80
	r-factor	73
Validation	R²	0.96
	NS	0.92

At the Kessie gauging station, the initial results without calibrations were also overestimated (**Figure 42**). Hence, an adjustment of the parameters was done to improve the statistical results. This calibration was mainly focused on increasing the evapotranspiration rate and reducing runoff. The main parameter used to reduce the peaks was CN2, and for increasing the evapotranspiration were SOL_AWC and the groundwater parameters, ALPHA_BF, GW_DELAY, GWQMN, GW_REVAP and REVAPMN. **Table 20** shows the parameters, their minimum and maximum ranges used for the calibration and their best fitted values for the period 1988-1993. The calibration results at the Kessie gauging station were not as good as in Eldiem, the R² and NS values for the calibrations were of 0.50 and 0.54, respectively; however the results for the validation period were better, achieving R² and NS values of 0.81 and 0.77, respectively (**Table 21**).

Table 20. Parameterization of SWAT99Integrated for the calibration at Kessie for the period 1988-1993.

Parameter	Description	Type of change	Threshold		Fitted value
			Min	Max	
CN2	Curve number for moisture condition II	r	-0.4	0.4	-0.38
SOL_AWC	Available water capacity of the soil	r	-0.3	0.2	0.2
ALPHA_BF	Baseflow alpha factor	v	0	1	0.7
GW_DELAY	Delay time	v	0	500	12.5
GWQMN	Deep aquifer percolation fraction	v	0	5000	575
GW_REVAP	Groundwater “revap” coefficient	v	0.02	0.2	0.1289
REVAPMN	Threshold depth of water in the shallow aquifer for “revap”	v	0	1000	175

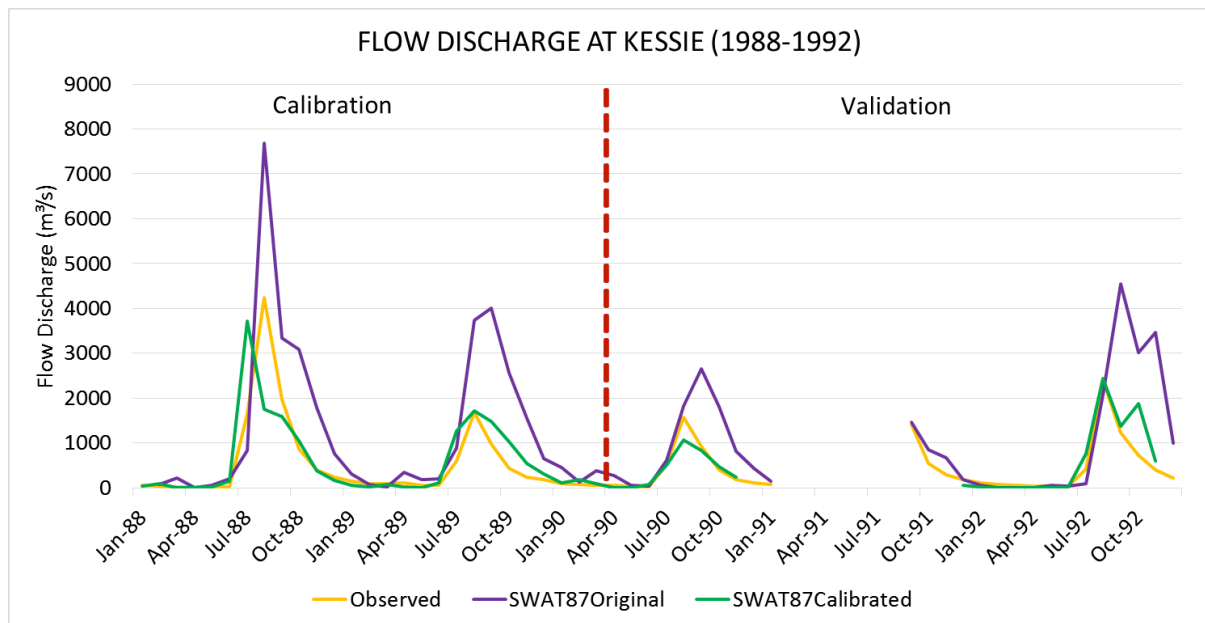


Figure 42. Calibration and validation results at Kessie with SWAT99Integrated for the period 1988-1992.

Table 21. Statistical results for the calibrations and validations with outflow data at the Kessie gauging stations.

Kessie (1988-1993)		
Calibration	R ²	0.50
	NS	0.54
	p-factor	0.77
	r-factor	1.38
Validation	R ²	0.81
	NS	0.77

4.1.2 Parameterization, calibration and validation of SWAT at Eldiem and Kessie for the period 1994-2004

Initially, for this period SWAT99 also overestimated the outflows at Eldiem (**Figure 43**). The initial evapotranspiration rate was approximately 40%, to match the observed values the evapotranspiration was increased to 65%, this means 5% more than the evapotranspiration rate required to calibrate the model from 1988 to 1993. The reason lies mainly on the greater amount of precipitation experienced in the Blue Nile during 1994-2004. **Figure 41** shows that the highest peaks during 1988-1993 before the calibration never surpassed the 10,000 m³/s, while most peaks during 1994-2004 reached the 12,000 m³/s (**Figure 43**). The evapotranspiration rate was increased by incrementing the available water content of the soil through the SOL_AWC parameter. Other parameters that increased the evapotranspiration rate were CANMX, ESCO and EPCO at HRU and basin level. Some parameters controlling the ground water processes were also modified to increase the evapotranspiration rate, these parameters include GWQMN, GW_REVAP and REVAPMN. **Table 22** shows all the parameters, ranges and best fitted values used to calibrate and validate the model at Eldiem from 1994 to 2004. Compared to the previous period (1988-1992), for this calibration the values for ESCO and EPCO at HRU level were modified to 0.01 and 1, respectively. This changed allowed a higher evapotranspiration rate to match the discharge data. Both, calibration and validation achieved very good statistical results. The calibration period was from 1994 to 1999 where the R² and NS values of 0.91 and 0.83 were achieved, respectively. The validation period was from 2000 to 2004 where the R² and NS values of 0.89 and 0.81 were achieved (**Table 23**).

Table 22. Parameterization of SWAT99Integrated for the calibration at Eldiem for the period 1994-2004.

Parameter	Description	Type of change	Threshold		Fitted value
			Min	Max	
CN2	Curve number for moisture condition II	r	-0.1	0.1	0.02
SOL_AWC	Available water capacity of the soil	r	-2	2	1.8
ESCO	Soil evaporation compensation factor HRU	v	0.01	1	0.01
EPCO	Plant uptake compensation factor HRU	v	0.01	1	1
ESCO	Soil evaporation compensation factor BSN	v	0.01	1	0.01
EPCO	Plant uptake compensation factor BSN	v	0.01	1	1
CANMX	Maximum canopy storage	v	0	100	100
GWQMN	Deep aquifer percolation fraction	v	0	5000	1875
GW_REVAP	Groundwater “revap” coefficient	v	0.02	0.2	0.1685
REVAPMN	Threshold depth of water in the shallow aquifer for “revap”	v	0	1000	325

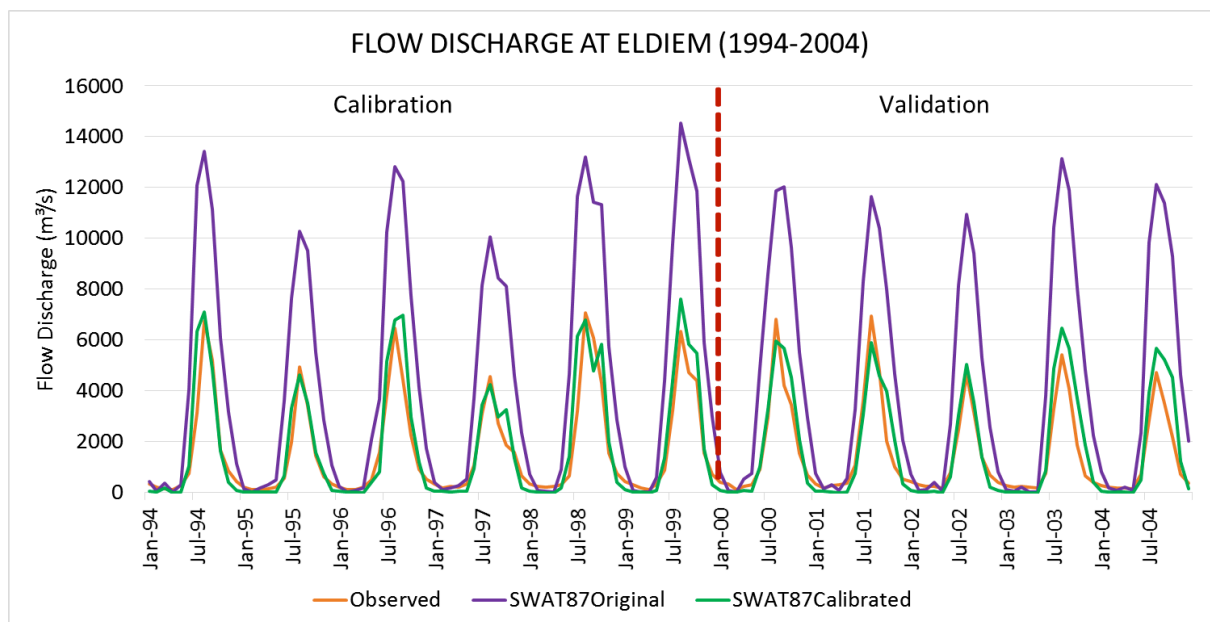


Figure 43. Calibration and validation results at Eldiem with SWAT99Integrated for the period 1994-2004.

Table 23. Statistical results for the calibration and validation with outflow data at Eldiem gauging station.

Eldiem (1994-2004)		
Calibration	R ²	0.91
	NS	0.83
	p-factor	0.87
	r-factor	0.96
Validation	R ²	0.89
	NS	0.81

At the Kessie gauging station, the initial results without calibrations had a good fit with the observed data (**Figure 44**) with a slight underestimation of peaks. Furthermore, a slight adjustment of the parameters was done to improve the statistical results. This calibration was mainly focused on increasing the peaks, as they were underestimated. Compared to the previous period from 1988-1998 where peaks fluctuated from approximately 2,500 m³/s up 7,500 m³/s and the water discharge was continuously overestimated, during 1994-2004 the peaks are more even oscillating at around 3,000 m³/s. The main parameter used was CN2 which absolute value was increased from 71 to 78. The soil available water content (SOL_AWC) was also decreased to reduce the evapotranspiration rate. The other parameters were slightly modified from its original values. **Table 24** shows the parameters used for this calibration. The calibration period was also from 1994 to 1999 and the validation period from 2000 to 2004. The statistical results after calibration were improved achieving R² and NS values of 0.75 and 0.74; and R² and NS values of 0.87 and 0.85, for the calibration and validation periods, respectively (**Table 25**).

Table 24. Parameterization of SWAT99Integrated at Kessie for the period 1994-2004.

Parameter	Description	Type of change	Threshold		Fitted value
			Min	Max	
CN2	Curve number for moisture condition II	r	-0.2	0.2	0.15
SOL_AWC	Available water capacity of the soil	r	-0.2	0.2	-0.03
ALPHA_BF	Baseflow alpha factor	v	0	1	0.725
GW_DELAY	Delay time	v	0	500	12.5
GWQMN	Deep aquifer percolation fraction	v	0	500 0	1625
GW_REVAP	Groundwater “revap” coefficient	v	0.02	0.2	0.0875
REVAPMN	Threshold depth of water in the shallow aquifer for “revap”	v	0	100 0	875

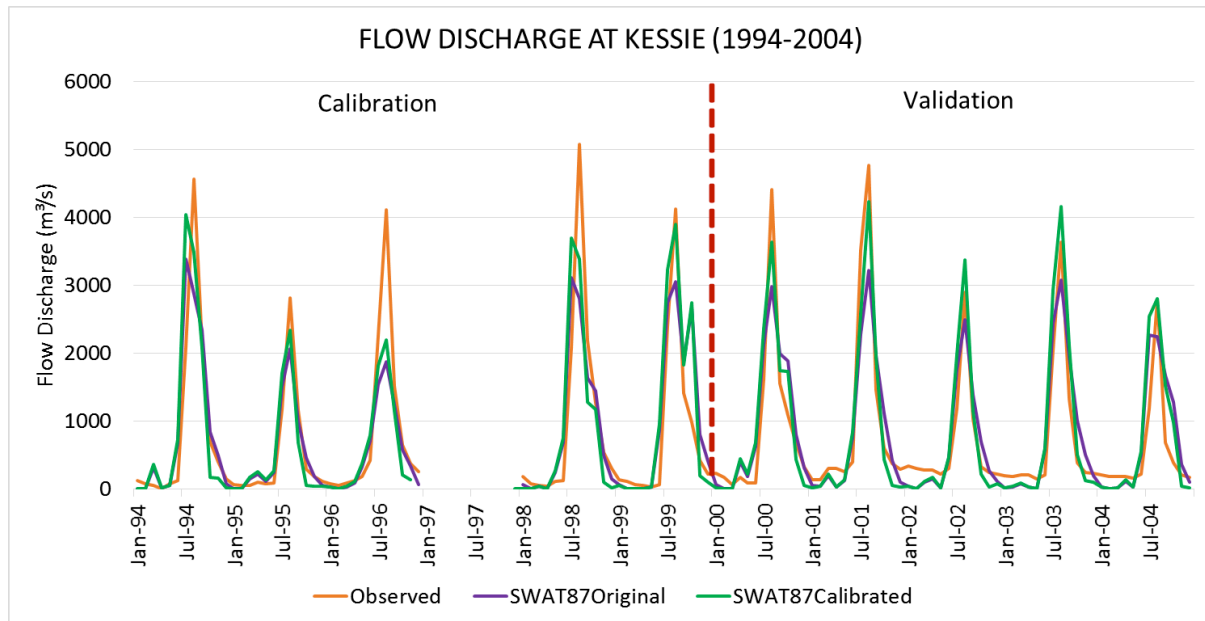


Figure 44. Calibration and validation results at Kessie with SWAT99Integrated for the period 1994-2004.

Table 25. Statistical results for the calibration and validation with outflow data at the Kessie gauging stations.

Kessie (1994-2004)		
Calibration	R²	0.75
	NS	0.74
	p-factor	0.75
	r-factor	0.78
Validation	R²	0.87
	NS	0.85

4.1.3 Calibration and validation of SWAT at several sub-catchments of the Blue Nile Basin for the period 1988-2004

Additional to the main calibration points at Eldiem and Kessie, other 8 small sub-catchments were calibrated using outflow data: Gilgel Abay (**Figure 45**), Ardy (**Figure 46**), Gumara (**Appendix 1**), Ribb (**Appendix 3**), Azuari (**Appendix 5**), Chena (**Appendix 7**), Muga (**Appendix 9**) and Temecha (**Appendix 11**). These 8 stations were selected due to their available measured sediment data. Although their statistical results were not very high they are within satisfactory ranges mostly above 0.5 for R² and NS (**Table 26**).

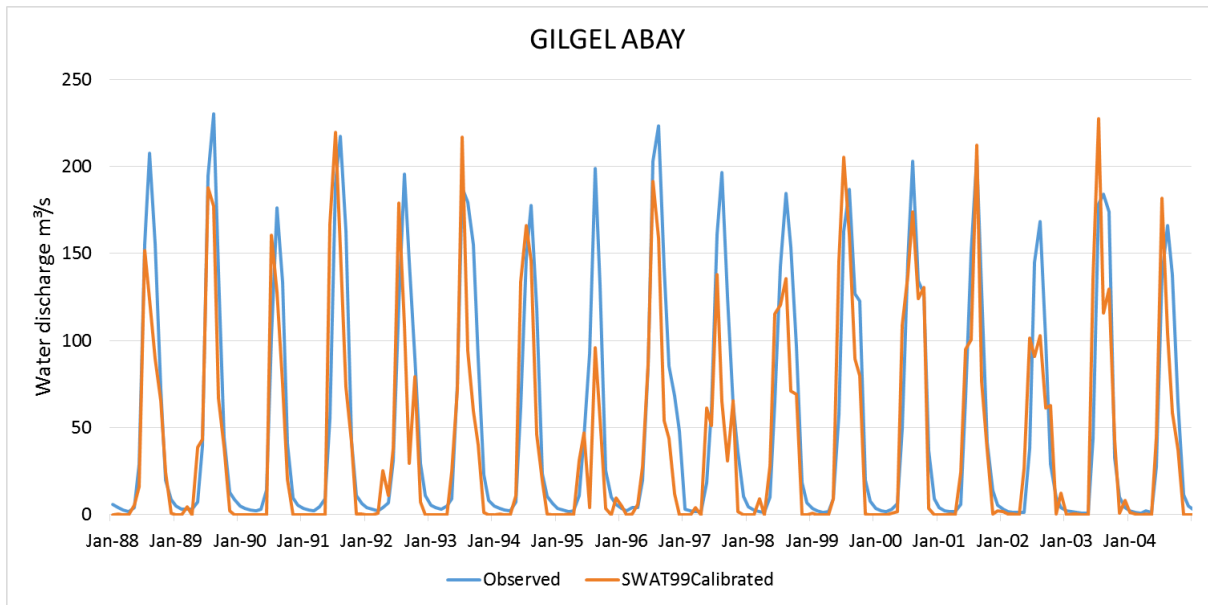


Figure 45. Calibration and validation results at Gilgel Abay with SWAT99Integrated for the period 1988-2004.

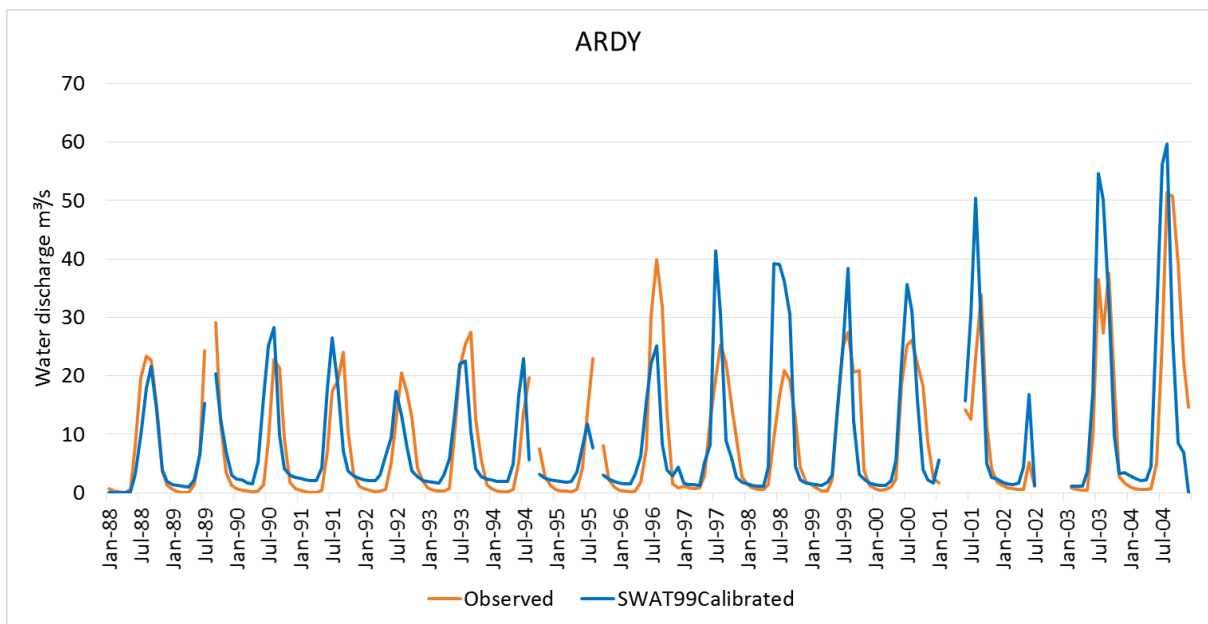


Figure 46. Calibration and validation results at Ardy with SWAT99Integrated for the period 1988-2004.

Table 26. Statistical results for the calibration with outflow data at several sub-catchments in the upper Blue Nile Basin.

Gilgel Abay (1988-2004)			Ardy (1988-2004)		
Calibration	R ²	0.72	Calibration	R ²	0.6
	NS	0.68		NS	0.5
Validation	R ²	0.78	Validation	R ²	0.61
	NS	0.78		NS	0.52
Gumara (1992-2004)			Ribb (2001-2004)		
Calibration	R ²	0.83	Calibration	R ²	0.92
	NS	0.82		NS	0.88
Validation	R ²	0.76	Validation	R ²	0.94
	NS	0.78		NS	0.93
Azuari (1988-2004)			Chena (1996-2004)		
Calibration	R ²	0.61	Calibration	R ²	0.53
	NS	0.53		NS	0.40
Validation	R ²	0.78	Validation	R ²	0.64
	NS	0.51		NS	0.47
Muga (1988-2004)			Temecha (1988-2004)		
Calibration	R ²	0.67	Calibration	R ²	0.68
	NS	0.66		NS	0.46
Validation	R ²	0.7	Validation	R ²	0.7
	NS	0.61		NS	0.57

4.1.4 Parameterization and comparison of SWAT sediment concentrations and sediment rating curves for the period 1988-2004

SWAT has been to certain extent, calibrated with few available sediment concentration values at the Eldiem station, and sediment comparisons were done for other 8 sub-catchments. Continuous sediment data for Eldiem was available for several months during 1993, 2003 and 2004. Results at Eldiem were very good achieving R² and NS values of 0.80 and 0.79, respectively (**Figure 47**). For the rest of stations only few non-continuous sediment concentration sample were available, however the degree of matching between the results provided by SWAT and the results obtained from sediment rating curves are good (**Figure 48, Figure 49, Appendix 2, Appendix 4, Appendix 6, Appendix 8, Appendix 10 and Appendix 12**). These comparison shows that the model somehow provides realistic results.

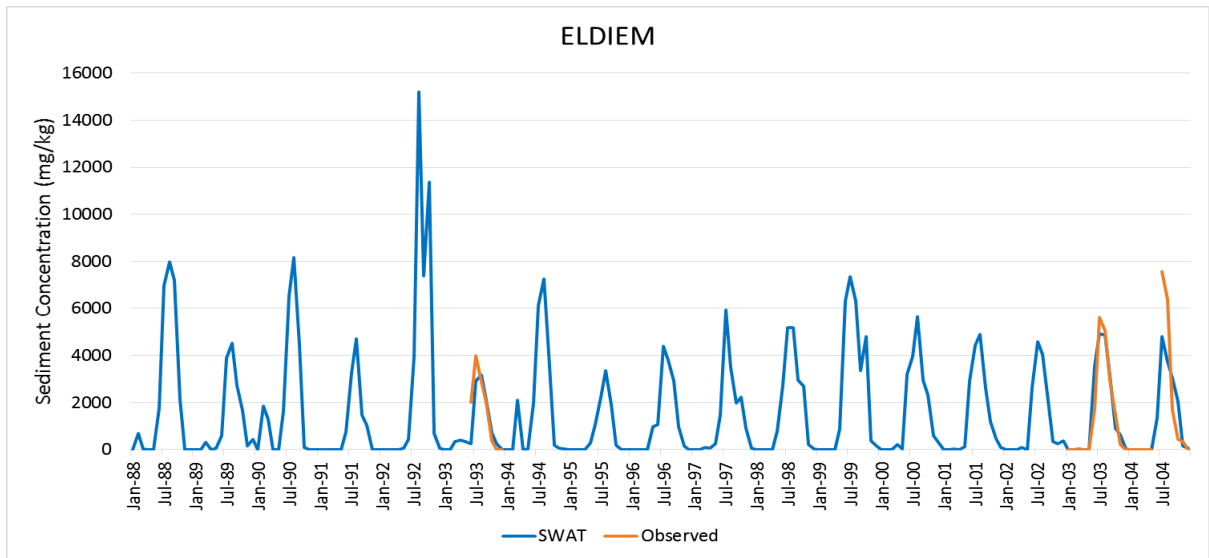


Figure 47. Sediment concentrations (mg/kg) at Eldiem station.

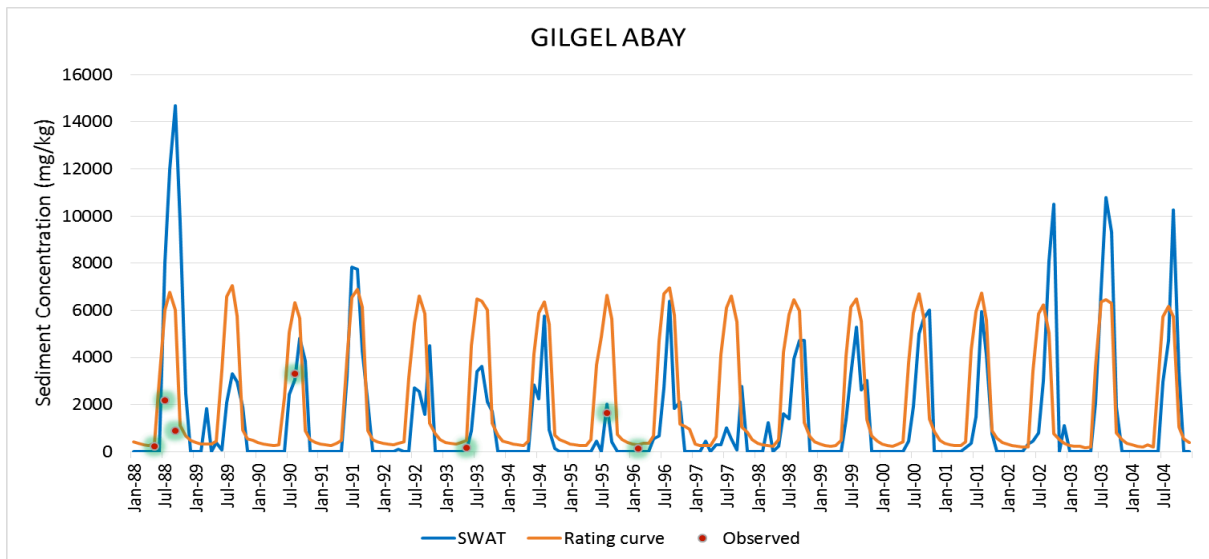


Figure 48. Sediment concentrations (mg/kg) at Gilgel Abay catchment.

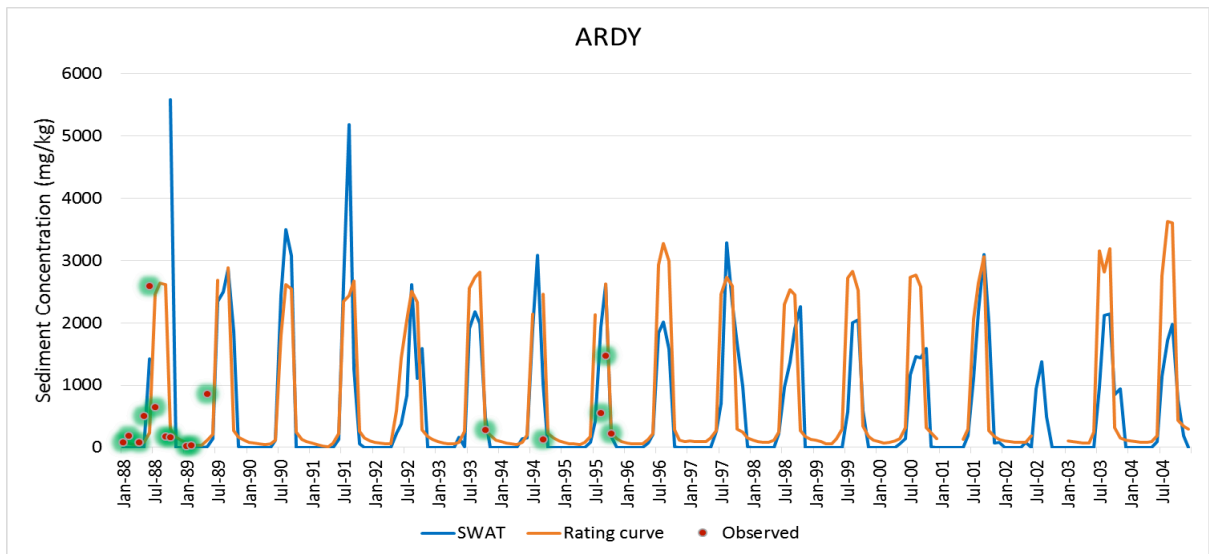


Figure 49. Sediment concentrations (mg/kg) at Ardy catchment.

4.2 Evaluation of SWAT Error Index (SEI)

SEI was tested for two locations, at large scale in the entire Blue Nile Basin and in the Ribb sub-catchment located in the Lake Tana region. The results showed that the behavior and capability of SEI to quantify the level of error of a model through an evaluation of both flow discharge and evapotranspiration estimations is good. For instance, **Table 27** showed that the lower the rRMSE values for water discharge are, rRMSE values for evapotranspiration tends to increase. This is because the flow discharge data is being matched, however the evapotranspiration increases and tends to overestimate those value provided by MOD16 ET. In case that MOD16 ET had a good representation of the evapotranspiration data of a watershed (see second test at Ribb sub-catchment), then the rRMSE values for both discharge and evapotranspiration values should be closer to 0, obtaining lower SEI values. SEI also showed that the models using the integrated datasets are more reliable than the other two datasets, achieving a SEI of 0.29 and 0.27 for SWAT30 and SWAT87, respectively. It also demonstrated that the CFSR dataset is less accurate, with SEI values of 0.4 for both SWAT30 and SWAT87 (**Polanco et al., 2017**).

Table 27. SWAT Error Index results for the upper Blue Nile Basin (**Polanco et al., 2017**).

SWAT30							
Process	Weighting	CFSR Dataset		Ground Dataset		Integrated Dataset	
		rRMSE	Weighted rRMSE	rRMSE	Weighted rRMSE	rRMSE	Weighted rRMSE
Water Discharge	0.7	0.33	0.231	0.17	0.119	0.098	0.068
Evapotranspiration	0.3	0.58	0.174	0.70	0.21	0.75	0.225
SWAT Error Index		0.4		0.33		0.29	
SWAT87							
Process	Weighting	CFSR Dataset		Ground Dataset		Integrated Dataset	
		rRMSE	Weighted rRMSE	rRMSE	Weighted rRMSE	rRMSE	Weighted rRMSE
Water Discharge	0.7	0.37	0.259	0.17	0.119	0.1	0.07
Evapotranspiration	0.3	0.46	0.138	0.58	0.174	0.66	0.198
SWAT Error Index		0.4		0.29		0.27	

The second test was done at the Ribb sub-catchment for the period 2001-2004. The objective have been to show the behavior of SEI in a sub-basin were the MOD16 data provided more reliable results and where the SWAT model was calibrated without compromising the evapotranspiration rate. The calibration with flow discharge data provided good statistical results, where the CFSR dataset achieved R^2 and NS values of 0.81 and 0.75, respectively; and the Ground dataset achieved R^2 and NS values of 0.85 and 0.83, respectively (**Figure 50 and Table 28**). Unlike the SEI test performed for the entire Blue Nile Basin, statistical results obtained from comparing evapotranspiration data in the Ribb sub-catchments are significantly better. The CFSR dataset achieved R^2 and NS values of 0.78 and 0.47, respectively; while the Ground dataset achieved R^2 and NS values of 0.59 and 0.24, respectively (**Figure 51 and Table 28**).

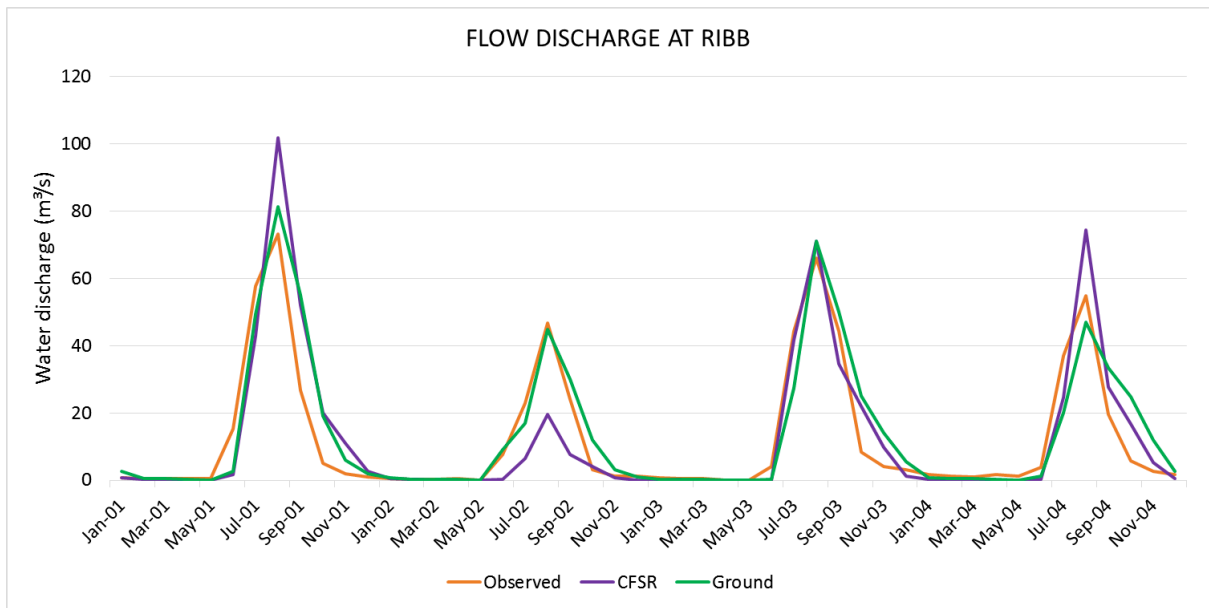


Figure 50. Flow discharge in the Ribb sub-catchment. Calibration with outflow data achieved R^2 and NS values of CFSR data: 0.81, 0.75 and Ground data: 0.85, 0.83; respectively (Polanco et al., 2017).

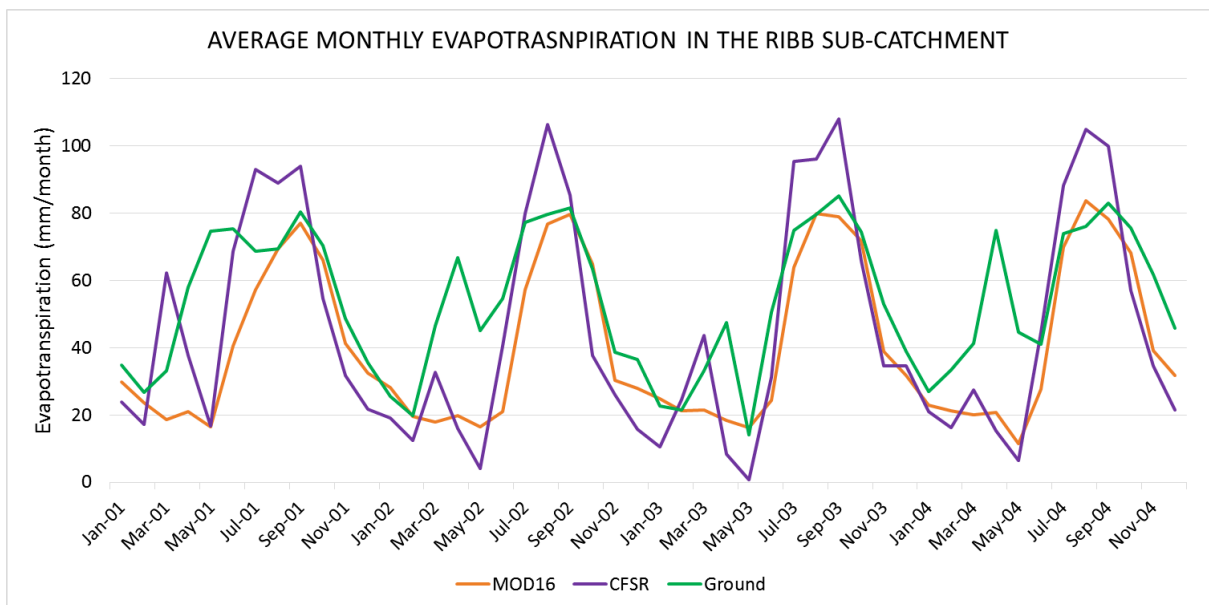


Figure 51. Average monthly evapotranspiration in the Ribb sub-catchment. Statistical results achieved R^2 and NS values of CFSR data: 0.78, 0.47 and Ground data: 0.59, 0.24; respectively, compared to the MOD16 data (Polanco et al., 2017).

SEI showed better values than those obtained from the first test done in the whole Blue Nile Basin. The CFSR dataset provided better R^2 and NS values than the Ground dataset for the evapotranspiration analysis, however the Ground dataset performed better during the calibration with outflow data (**Table 27**). SEI values for both datasets were 0.16, a much better value than those obtained in the first test (**Table 26**). This second test provides a better understanding of how SEI works, it also proved how using reliable evapotranspiration data can improve the SEI values (**Polanco et al., 2017**).

Table 28. Statistical results for the Ribb sub-catchment in the Lake Tana region of the Blue Nile Basin (**Polanco et al., 2017**).

Statistical results for the Ribb sub-catchment									
Process	Weighting	CFSR Dataset				Ground Dataset			
		R^2	NS	rRMSE	Weighted rRMSE	R^2	NS	rRMSE	Weighted rRMSE
Water Discharge	0.7	0.81	0.75	0.13	0.091	0.85	0.83	0.11	0.077
Evapotranspiration	0.3	0.78	0.47	0.23	0.069	0.59	0.24	0.28	0.084
SWAT Error Index		0.16				0.16			

4.3 Erodible areas predicted by SWAT at HRU level

Erosion is a process mainly caused by runoff, therefore, in order to define effective soil management and conservation plans a good understanding of the runoff processes in the Ethiopian highlands is critical (*Bayabil et al., 2010*). *Bayabil et al. (2010)* did an analysis of the effects of the ecology (land cover) and topography (slopes) on the runoff process in the Ethiopian highlands, specifically in the Maybar watershed. Results showed that the topographic factors are more relevant than the ecological factors and concluding that the saturated areas in the lower parts of the hill slopes generated higher runoffs. The upper hill-slopes are usually not saturated zones, they are mainly infiltration zones, thus, the water infiltrates becoming interflows that gently move downhill where the saturated areas are located and higher surface runoff will occur. The phenomena causes more erosion in gently slope areas than it does in the high slopes. To which promoting historical ecological practices to reduce the surface runoff will not alter the hydrological process, however continues to be good mitigation practices. Furthermore, deep rooted trees could additionally help to break up the restrictive layer (hardpan) and improve the water storage in the Blue Nile Basin. The saturated regions expand as the rainstorm progresses (*Hewlett and Hibbert, 1967*) and the amount of runoff per unit increment of precipitation increases with time (*Steenhuis et al., 1995; Liu et al., 2008*), after which it becomes constant (*Steenhuis et al., 2013*).

Soil losses for the Blue Nile basin were estimated at HRU level and grouped based on land use, soil type and slopes (*Table 28*). This table shows how agricultural lands are experiencing the largest soil losses while lands with forest, grass or wheat show lower erosion rates. It can also be seen that the largest and most severe soil losses occur in very high slopes above 25%. And although it was previously mentioned that the saturated areas located in gently slopes are exposed to experience higher surface runoff and with it higher erosion rates, this is only a very distinctive characteristic in this region that also needs further studies and therefore not an event that can be simulated by SWAT, which also brings uncertainties.

Table 29. Soil erosion rates in the Blue Nile Basin grouped by land use, soil type and slope classes for the period 1988-2004.

Land Use	Soil Type	Slope	Soil Loss (t/ha)			
			1988-1990	1991-1995	1996-2000	2001-2004
Agricultural Land-Close-grown	Cambic Arenosols	0-15	19.45	26.37	12.91	12.44
		15-25	70.20	93.90	53.52	49.05
		25-99	131.90	176.42	125.53	98.67
	Chromic Vertisols	0-15	189.37	9.93	23.14	12.83
		15-25	696.99	33.93	73.28	42.60
		25-99	868.60	39.20	83.11	51.85
	Dystric Cambisols	0-15	268.61	6.90	14.90	9.90
		15-25	685.95	19.50	43.45	29.97

		25-99	1310.69	40.22	71.19	60.26	
	Eutric Cambisols	0-15	30.65	12.39	8.24	7.28	
		15-25	126.15	58.51	38.24	32.22	
		25-99	177.32	112.67	65.26	53.88	
	Eutric Fluvisols	0-2	188.06	4.43	8.40	7.42	
	Eutric Nitosols	0-15	66.18	8.95	12.95	7.66	
		15-25	191.15	37.58	48.04	31.30	
		25-99	383.83	65.16	76.42	45.24	
	Eutric Regosols	0-15	39.09	13.50	27.06	20.62	
		15-25	109.62	34.16	67.42	51.78	
	Humic Fluvisols	0-15	252.72	12.94	34.76	15.09	
		15-25	1015.82	50.52	123.77	56.35	
		25-99	954.07	61.55	168.71	63.18	
	Pellic Vertisols	0-15	7.51	3.18	7.72	4.53	
		15-25	37.50	15.44	34.01	20.06	
		25-99	56.89	23.07	44.52	27.35	
	Agricultural Land-Generic	Cambic Arenosols	0-15	21.86	38.60	43.17	30.70
			15-25	67.23	119.13	129.92	90.55
			25-99	120.21	197.37	193.81	135.87
Chromic Vertisols		0-15	67.90	24.42	36.29	25.03	
		15-25	263.64	88.47	129.11	87.77	
		25-99	482.59	123.99	161.91	116.68	
Dystric Cambisols		0-15	101.49	16.67	19.42	14.72	
		15-25	430.10	71.86	85.72	63.98	
		25-99	682.94	130.39	175.60	121.90	
Eutric Cambisols		0-15	42.11	23.80	25.38	20.02	
		15-25	159.31	85.00	82.86	64.71	
		25-99	264.79	158.38	138.32	106.89	
Eutric Fluvisols		0-15	226.68	33.13	28.75	26.66	
		15-25	907.75	130.33	113.39	105.68	
		25-99	1814.63	254.94	221.83	207.60	
Eutric Nitosols		0-15	38.97	22.64	37.93	26.26	
		15-25	189.93	85.23	124.41	89.03	
		25-99	244.81	138.47	219.42	147.99	
Humic Fluvisols		0-15	112.05	30.84	40.44	30.06	
		15-25	461.58	105.13	127.68	98.39	
		25-99	864.19	197.61	246.22	186.06	
Orthic Acrisols		0-15	232.93	35.78	30.92	28.35	
		15-25	524.66	76.76	66.84	61.60	
		25-99	1665.77	239.00	208.16	192.09	
Pellic Vertisols		0-15	0.00	20.10	39.28	23.62	
		25-	0.00	40.91	81.96	47.57	

		9999				
Agricultural Land-Row Crops	Cambic Arenosols	0-15	57.31	30.45	46.78	47.28
		15-25	237.47	118.83	214.20	218.93
		25-99	484.86	228.68	422.06	428.59
	Eutric Cambisols	0-15	86.22	18.29	26.27	23.58
		15-25	269.22	67.30	101.35	90.70
		25-99	432.14	119.39	175.86	156.81
	Eutric Nitisols	0-15	116.57	23.84	35.04	30.23
		15-25	410.85	75.18	106.88	93.46
		25-99	684.60	115.66	186.96	172.01
	Pellic Vertisols	0-15	26.21	0.18	18.40	14.95
		15-25	104.26	0.69	72.93	58.62
		25-99	362.14	2.34	251.92	199.42
Crested Wheatgrass	Eutric Nitisols	0-15	0.00	1.25	1.61	1.87
		15-25	0.00	5.14	6.62	7.44
		25-99	0.00	5.70	7.56	8.28
	Humic Fluvisols	0-15	0.00	2.06	4.88	4.92
		15-25	0.00	7.70	18.67	17.72
		25-99	0.00	10.36	27.39	25.65
Forest- Deciduous	Eutric Nitisols	0-15	0.00	0.08	0.33	0.15
		15-25	0.00	0.27	1.08	0.47
		25-99	0.00	0.35	1.46	0.62
	Humic Fluvisols	0-15	0.00	0.10	0.20	0.12
		15-25	0.00	0.35	0.72	0.40
		25-99	0.00	0.39	0.82	0.45
Forest-Mixed	Cambic Arenosols	0-15	0.38	0.59	0.77	0.32
		15-25	1.35	1.03	2.71	0.97
		25-99	3.34	3.61	6.15	2.39
	Chromic Vertisols	0-15	0.62	0.06	0.23	0.11
		15-25	4.96	0.25	1.00	0.51
		25-99	0.00	0.34	1.88	0.78
	Dystric Cambisols	0-15	0.81	0.03	0.03	0.02
		15-25	3.58	0.11	0.13	0.10
		25-99	4.74	0.15	0.21	0.16
	Eutric Cambisols	0-15	1.53	0.44	0.40	0.18
		15-25	5.98	1.67	0.71	0.60
		25-99	11.28	2.49	1.75	1.08
	Eutric Fluvisols	0-15	13.20	0.42	0.07	0.36
		15-25	73.40	2.52	0.36	2.09
		25-99	119.18	4.54	0.59	3.77
	Eutric Nitisols	0-15	0.62	0.36	0.30	0.12
		15-25	2.92	1.24	1.09	0.43
		25-99	5.38	2.21	1.80	0.61

	Eutric Regosols	0-15	9.89	0.58	0.10	0.46
		15-25	50.20	2.97	0.50	2.47
		25-99	77.00	5.49	0.70	4.34
	Humic Fluvisols	0-15	0.79	0.08	0.12	0.08
		15-25	3.69	0.33	0.48	0.33
		25-99	6.86	0.55	0.82	0.56
	Orthic Acrisols	0-15	1.25	0.07	0.10	0.07
		15-25	5.51	0.27	0.31	0.25
		25-99	7.14	0.34	0.39	0.31
	Pellic Vertisols	0-15	0.55	1.89	0.73	0.17
		15-25	1.16	2.33	1.93	0.32
		25-99	1.65	4.57	2.28	0.50
Pasture	Cambic Arenosols	0-15	0.00	1.21	5.72	4.87
		15-25	0.00	6.24	29.81	24.33
		25-99	0.00	7.49	35.89	28.64
	Eutric Nitosols	0-15	0.46	0.87	4.05	3.30
		15-25	0.54	3.42	15.27	10.94
		25-99	0.00	4.56	25.59	17.98
	Humic Fluvisols	0-15	0.00	0.74	4.18	3.56
		15-25	0.00	1.75	10.07	8.42
		25-99	0.00	2.66	15.71	12.87
Range-Brush	Cambic Arenosols	0-15	1.60	12.42	4.24	1.17
		15-25	6.04	51.05	18.16	3.84
		25-99	9.20	102.66	25.85	5.23
	Chromic Vertisols	0-15	18.15	0.49	0.29	1.14
		15-25	91.18	2.40	1.37	5.74
		25-99	165.96	4.32	2.45	10.56
	Eutric Cambisols	0-15	2.49	3.77	1.58	1.42
		15-25	8.29	11.59	5.29	4.67
		25-99	7.80	33.31	8.02	6.99
	Eutric Nitosols	0-15	1.92	2.40	4.14	0.76
		15-25	5.27	8.57	8.10	2.19
		25-99	2.54	25.23	15.62	2.58
	Humic Fluvisols	0-15	0.00	0.37	1.46	1.03
		15-25	0.00	1.19	4.78	3.31
		25-99	0.00	2.15	9.12	6.20
	Orthic Acrisols	0-15	9.83	0.25	0.19	0.36
		15-25	36.13	0.92	0.70	1.35
		25-99	83.21	2.10	1.61	3.14
Slender Wheatgrass	Eutric Cambisols	0-15	0.00	0.88	0.88	0.78
		15-25	0.00	3.13	3.16	2.74
		25-99	0.00	5.76	6.11	5.09
	Eutric	0-15	0.00	0.34	1.02	0.95

	Nitosols	15-25	0.00	0.80	2.44	2.27
		25-99	0.00	1.38	4.30	3.85
	Humic Fluvisols	0-15	0.00	1.07	1.32	1.10
		15-25	0.00	3.94	4.95	3.94
		25-99	0.00	6.08	8.19	6.16
Wetlands-Mixed	Chromic Vertisols	0-15	0.00	0.23	1.30	1.35
		15-25	0.00	0.83	4.98	4.95
	Eutric Cambisols	0-15	0.06	0.35	1.98	1.49
		15-25	0.19	1.21	8.43	5.51
		25-99	0.24	0.98	9.24	4.41
	Eutric Nitosols	0-15	0.04	0.24	1.16	1.00

From these sediment loads four maps were also created for the period 1988-2004 (**Figure 52, Figure 53, Figure 54 and Figure 55**). These maps show the average annual soil yield for each of the 3466 HRUs and how the erosion problem has evolved during the period under analysis. Maps showed how the erosion problem has significantly increased from 1988 to 2000, although severe erosion reduced in most regions during 2001-2004, for instance in the Beshelo, North Gojam, South Gojam and Beles sub-basins.

Slopes in the North Gojam and Beshelo sub-catchments are very steep mostly over 25% (**Figure 56**). Maps showed that these two catchments and additionally the sub-basin South Gojam have constantly been under severe soil erosion conditions from 1988 to 2004. The upper region of the Beshelo sub-basin has always been experiencing an erosion rate above 50 t/ha/year during 1988-2000, while its lower part has experienced a progressive erosion rate below 20 t/ha/. Most regions in North Gojam and South Gojam sub-basins experienced severe erosion rates over 50 t/ha/year during 1988-2000, but had a significant decrease during 2001-2004. Additional to the very steep slopes, these sub-catchments have two types of soils with high agricultural potential: Eutric Cambisol and Eutric Nitosols, and has been classified as moderately and intensively cultivated with open shrublands (**Figure 7**). The area also have Cambic Arenosol, soil that due to their sandy texture needs careful management practices when used for agricultural purposes.

The Lake Tana region has also experienced a continuous increasing erosions rate and a constant expansion of the agriculture in the surrounding areas of the lake. Although slopes in this region mostly range between 0-25%, the dominant soils are Eutric Cambisols and Eutric Nitosols (**Figure 6**), that due to their fertility have been intensively cultivated under poor land management practices (**Figure 7**). Maps show that the erosion rate during 1988-1990 was over 20 t/ha/year mainly concentrated in the lower Gilgel Abay and Ribb sub-catchments. During the period 1991-1995, the erosion had expanded its boundaries to the upper Gilgel Abay and had become more intensive in both sub-catchments up to more than 50 t/ha/year. During 1996-2000 the erosion in the Ribb catchment is mostly over 20 t/ha/year. Additionally, the erosion in the surrounding areas of Lake Tana had shown an expansion and the erosion in the upper Megech sub-catchment increased from being below 2 t/ha/year until 2000 to

over 20 t/ha/year by 2004. The most significant expansion of erosion in the Lake Tana region was experienced during 2001-2004, where the erosion has almost surrounded the entire Lake Tana. The erosion was expanded and intensified in the lower Ribb and lower Megech sub-catchments, and also in the surrounding areas of Bahir Dar.

The Beles catchment has also experienced a very severe erosion rate between 20-30 t/ha/year during 1988-1990 and even a more severe erosion rate over 50 t/ha/year during 1991-1995. However, the erosion was reduced to rates below 30 t/ha/year during 1996-2004. Soils in the upper Beles are also classified as Eutric Nitisols where the agriculture activity has considered as moderated and with scattered shrubland and open grassland. The lower part of the catchment is covered by Eutric Regosol and Humic Fluvisols with sandy and weakly developed minerals that are considered of low agricultural productivity (**Figure 6**). The land cover in this region is dominated by grasslands, shrublands and small dense woodlands (**Figure 7**).

Slopes in the Dabus catchment are below 15% (**Figure 56**), dominated by Eutric Nitisols and Chromic Vertisols (**Figure 7**). The erosion has been experienced mainly in the western part of the catchment, where Humic Fluvisols with intensive agricultural activity mainly with wooded grasslands show constant erosion rates over 20 t/ha/year. This erosion has shown a continuous expansion to its surrounding areas, where during 1988-1990 Eutric Nitisols in the sub-basin didn't show any erosion at all and for the rest of the period 1991-2004 the erosion increased to over 30 t/ha/year.

Slopes in the Didessa catchment are below 15% (**Figure 56**), and due to the presence of good agricultural soils, Eutric Nitisols, in its upper region (**Figure 6**), part of them have been intensively cultivated, areas with perennial crops cultivation and moderately cultivated constitute the large part of the catchment (**Figure 7**). Therefore, Didessa has also experienced a very fast and intensive erosion rate increase, where no erosion was detected in the upper part of the catchment for the period 1988-1990, however by 1995 the erosion map showed that a large part of the catchment experienced high rates of erosion mostly over 50 t/ha/year and also showing a constant erosion rate for the period 1996-2004. The uppermost region of the catchment covered by forests/perennial crops (**Figure 7**) have suffered erosion rates below 2 t/ha/year.

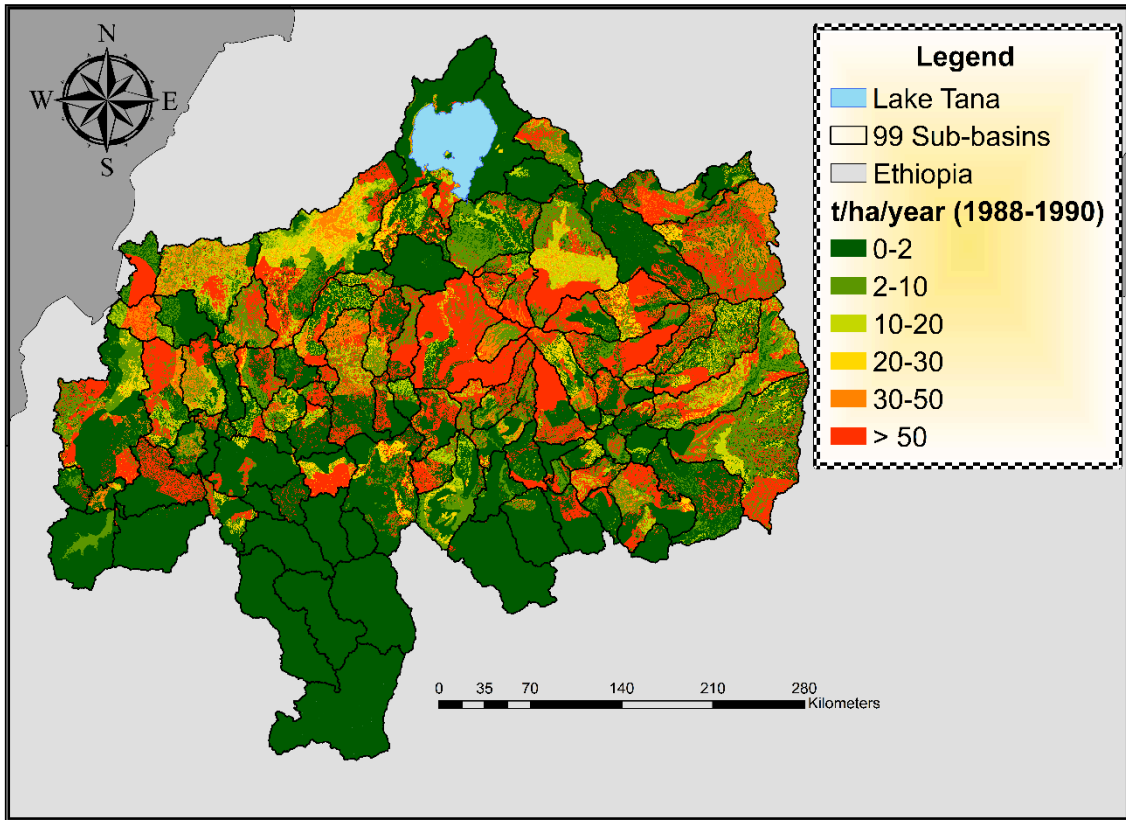


Figure 52. Sediment yield in the upper Blue Nile Basin for the period 1988-1990.

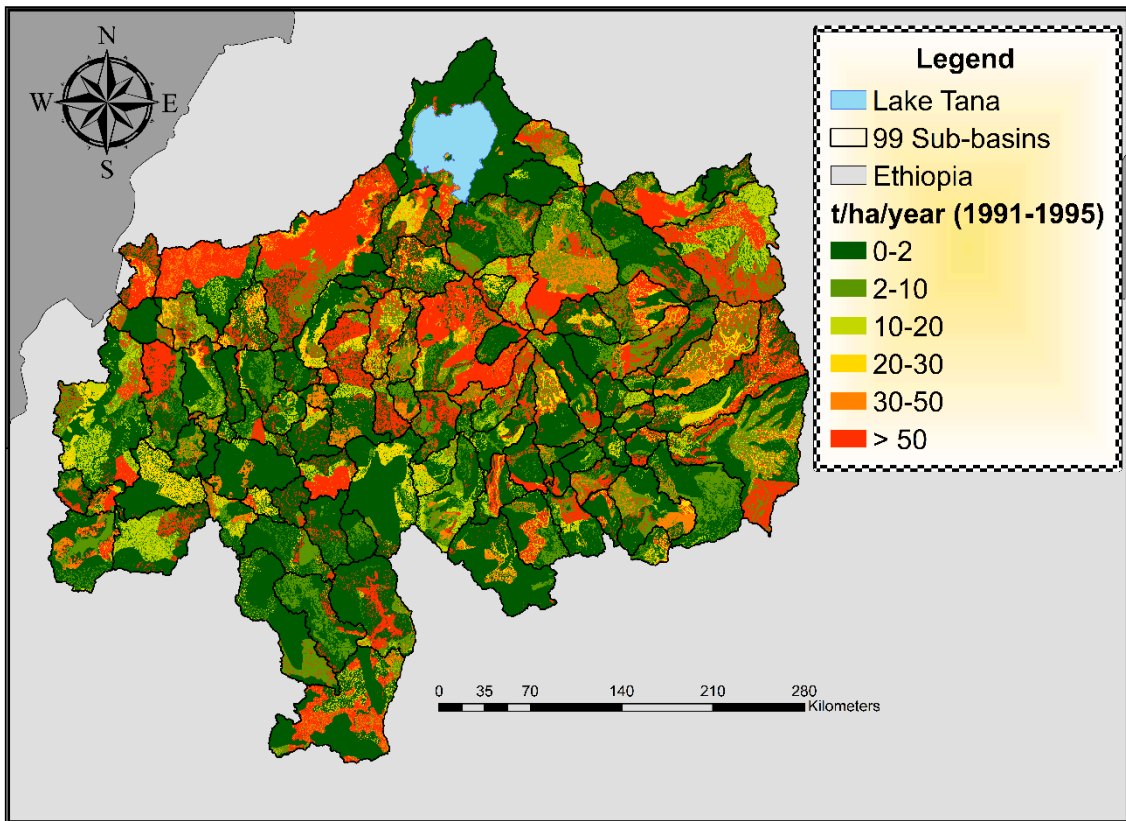


Figure 53. Sediment yield in the upper Blue Nile Basin for the period 1991-1995.

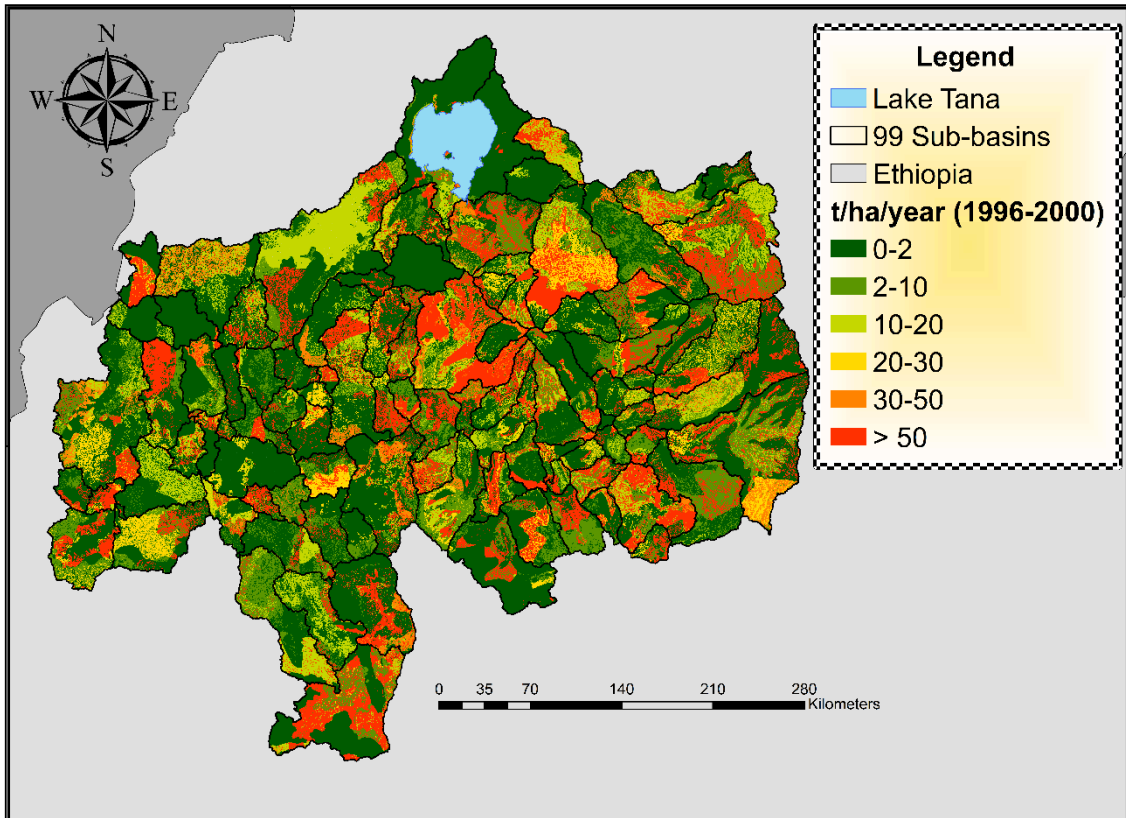


Figure 54. Sediment yield in the upper Blue Nile Basin for the period 1996-2000.

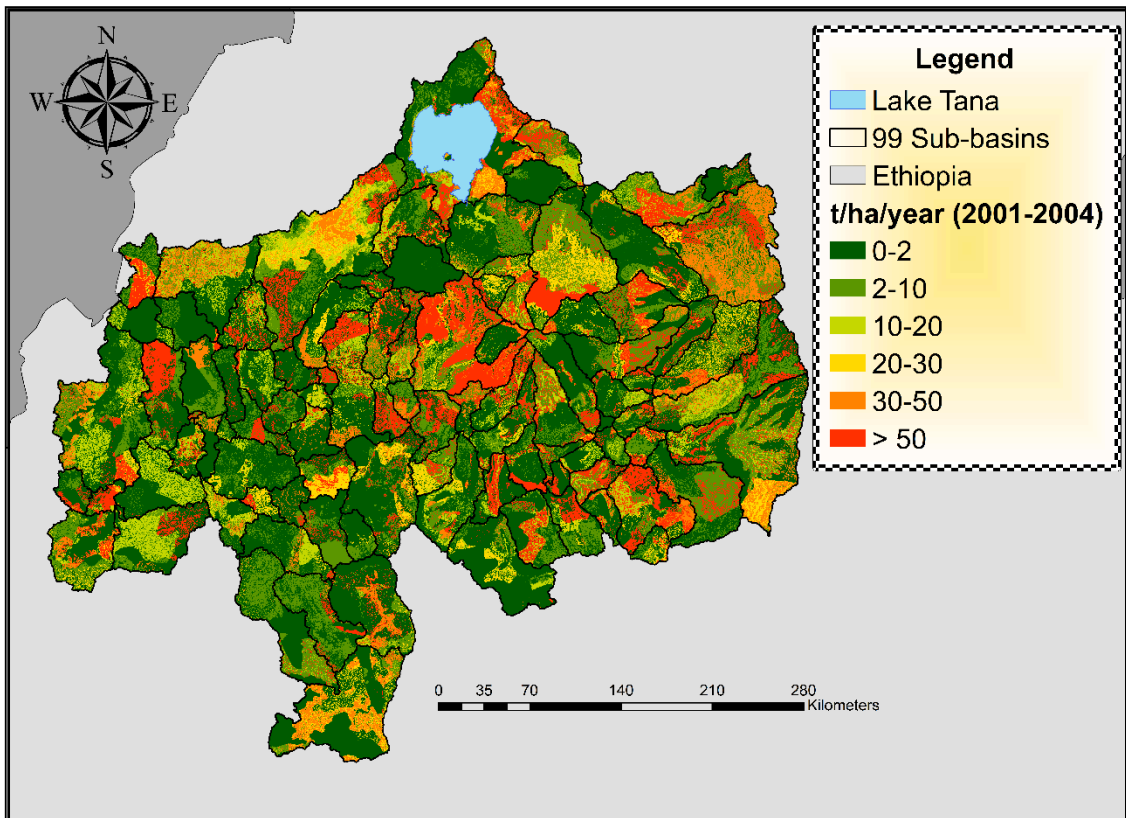


Figure 55. Sediment yield in the upper Blue Nile Basin for the period 2001-2004.

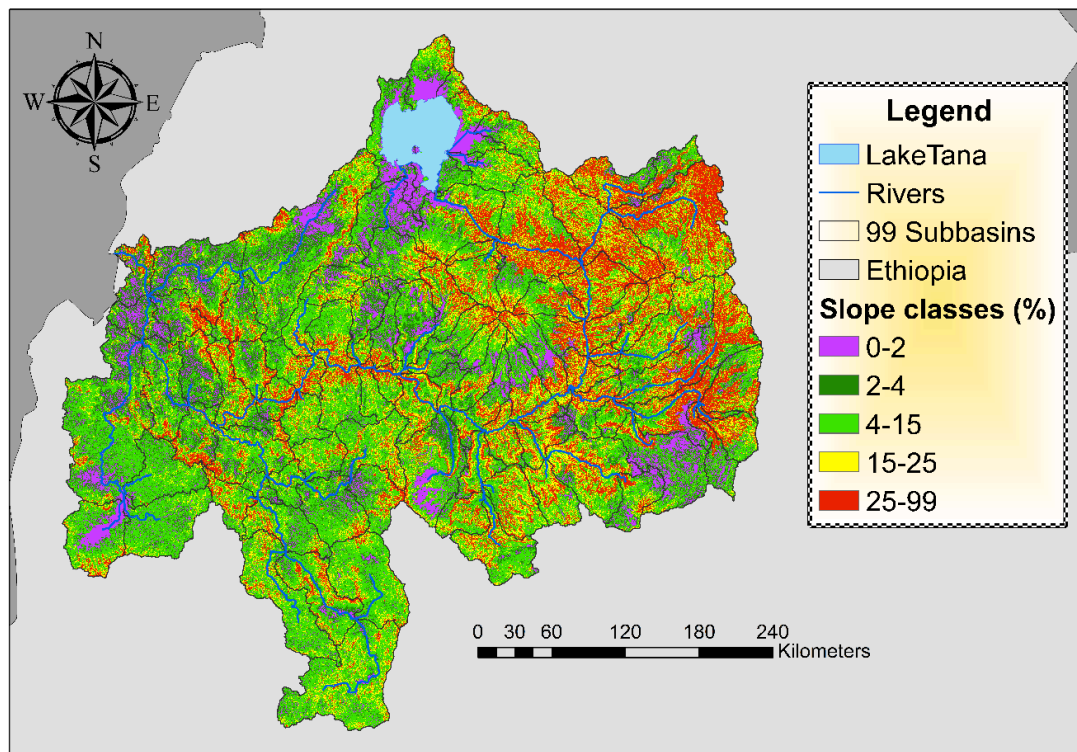


Figure 56. Slope classes in the upper Blue Nile Basin.

Large extensions of land show extremely high erosion rates over 50 t/ha/year, these erodible areas are mostly Nitosols and Cambisols that have been intensively cultivated, and smaller extensions are areas with open grassland and shrublands. Although it is known that erosion rates are very high in the Ethiopian highlands under intensive agricultural activities, **Konnerth (2016)** also mentioned that the remarkably low biomass predicted in SWAT in grasslands, pastures and shrublands can be an important factor causing high sediment yields estimations in these areas. One of the main factors affecting the erosion rates is the rainfall intensity or runoff peaks, which represents the possible potential erosion, however this phenomena is not well represented due to the lack of high resolution rainfall data for the region.

Further comparisons of these results were done with another study done by **Betrie et al. (2011)**, where he presented a soil erosion map for the period 1990-2003 classifying the erosion intensity in four categories (**Figure 57**): low (0-20 t/ha/year), moderate (20-70 t/ha/year), severe (70-150 t/ha/year) and extreme (>150 t/ha/year). **Betrie et al. (2011)** also showed that the erosion rates in several parts of the Beshelo, South Gojam and North Gojam catchments are above 20 t/ha/year. In this study was also possible to detect similar erodible areas at the Beles and Didessa catchments with erosion rates between 20-70 t/ha/year. Results at the Lake Tana where also comparable specially for 2001-2004, where erosion rates in the basin were estimated to be over 30 t/ha/year and in some areas over 50 t/ha/year, whereas **Betrie et al. (2011)** also classifies it from moderate to extreme with rates above 20 and up 150 t/ha/year. **Konnerth (2016)** also simulated the Lake Tana region with more details where the upper regions of Ribb, Gilgel Abay and Gumara showed erosion rates over 30 t/ha/year (**Figure 58**). These results are also comparable with the results obtained from the current model at Ribb and Gilgel Abay, where the erosion rates were also estimated to be mostly over 30 t/ha/year, and an expansion of the erosion to the Megech and lower Ribb sub-catchments during 2001-2004.

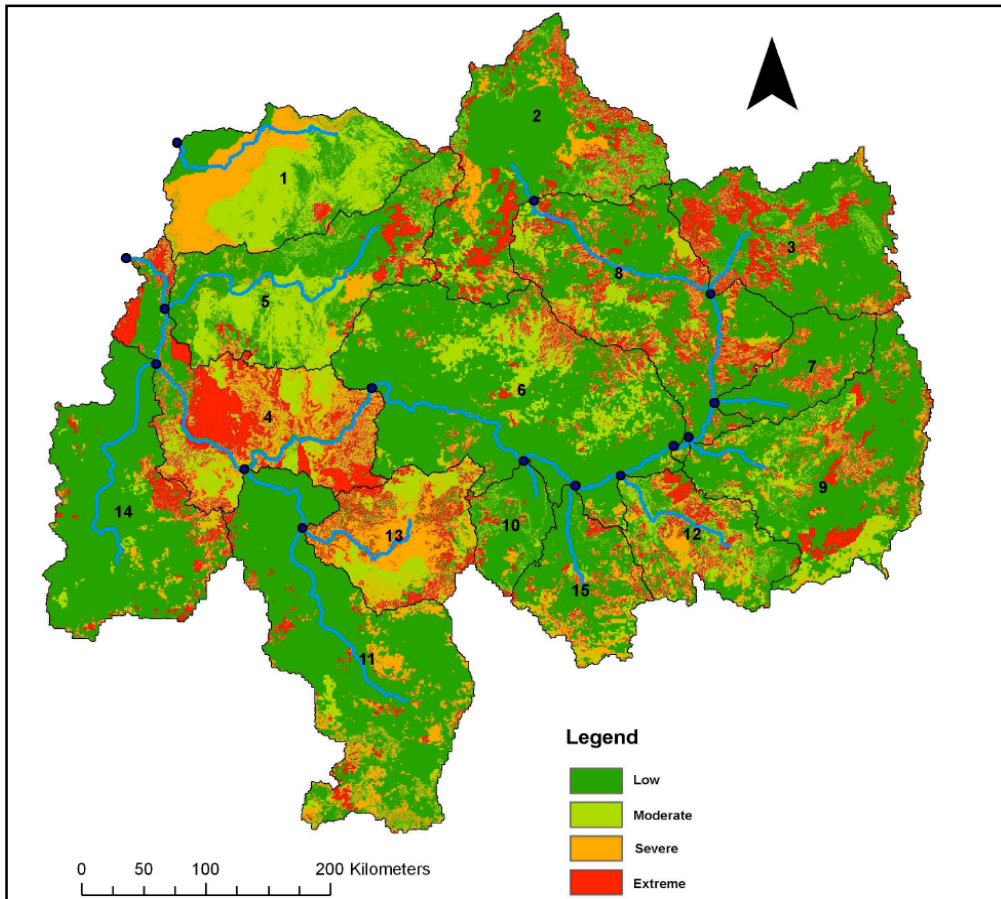


Figure 57. Relative erosion prone areas (predicted sediment yield at each HRU by the SWAT model) for existing conditions in the upper Blue Nile (Betrie et al., 2011).

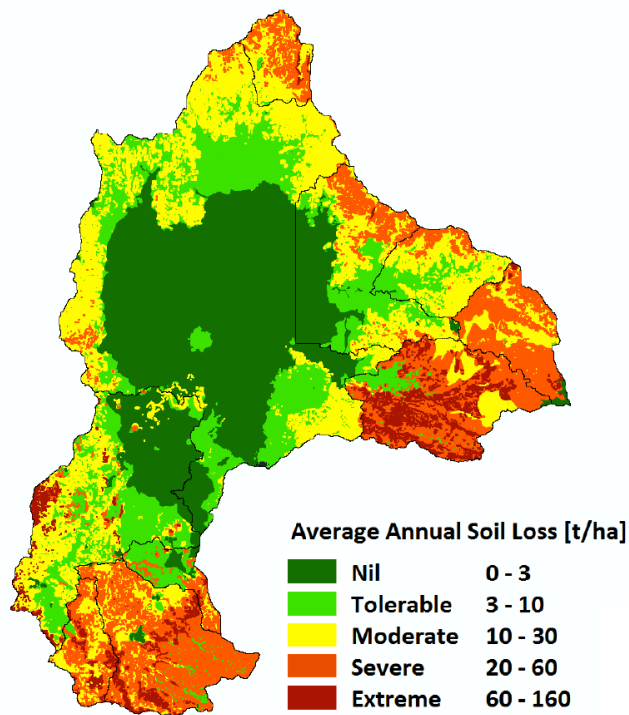


Figure 58. Average annual soil loss estimated by SWAT for Lake Tana basin between 1997 and 2003 (Konnerth, 2016).

However, erosion rates in the Wenbera and Anger sub-catchments differ between both studies, where *Betrie et al. (2011)* showed extremely severe erosion rates between 20-150 t/ha/year, while the current study classifies the erosion in this region as being only mostly over 30 t/ha/year and very small areas above 50 t/ha/year. Results in the Dabus catchment also showed differences, where *Betrie et al.* simulated erosion rates mostly below 20 t/ha/year, while the current study proposes erosion rates mostly between 30-50 t/ha/years

Furthermore, it has to be considered that outputs differences between these models are also caused by the different input data sources, different model setup, and the different parameterization used during the calibration and validation process. For instance, *Betrie et al. (2011)* used rainfall data from 17 ground stations while the current study is using 42 stations obtained from the integration of two datasets. Additionally, the current model has been calibrated at multiple gauging stations which also required the calibration of different parameters for different sub-basins. Furthermore, the current model contains 99 sub-basins and 3466 HRUs, more than those used by *Betrie et al. (2011)*. Or in the model done by *Konnerth (2016)*, where the land use map and the soils map were more detailed than the ones used at large scale in this study. Additionally, *Figure 59* and *Figure 60* show the sediment estimation differences after including the management practices in SWAT through the USLE_P factor.

Table 30. Soil erosion rates in different subbasins of the upper Blue Nile basin.

Sub-basin	Soil loss (t/ha/year)	Soil loss (t/ha/year) (<i>Betrie et al., 2011</i>)
Anger	From 20 to 50	Mostly from 20 to 150
Beles	Mostly >50	Mostly between 20-70
Beshelo	From 20 to >50	From 20 to >150
Dabus	Mostly from 20 to >50	From 20 to 150
Didessa	From 20 to >50	From 20 to 150
Fincha	From 10 to 50	From 20 to 70
Guder	From 30 to >50	From 20 to 150
Jemma	Mostly from 20 to >50	From 20 to 150
Lake Tana	From 20 to >50	Mostly between 20-150
Muger	Mostly from 20 to >50	Mostly between 20-150
North Gojam	Mostly >50	From 20 to 150
South Gojam	Mostly >50	From 20 to 150
Weleka	Mostly from 30 to >50	From 20 to 150
Wenbera	From 20 to 50	Mostly from 70 to 150

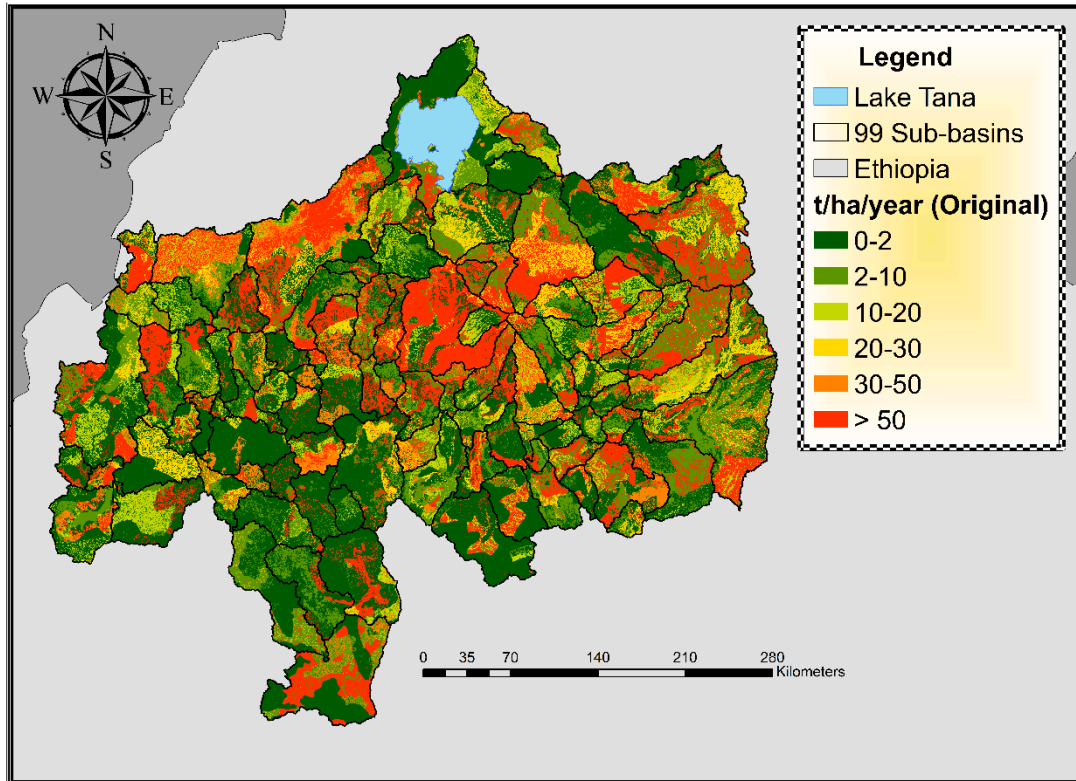


Figure 59. Average annual sediment yield in the upper Blue Nile Basin for the period 1988-2004 without management practices.

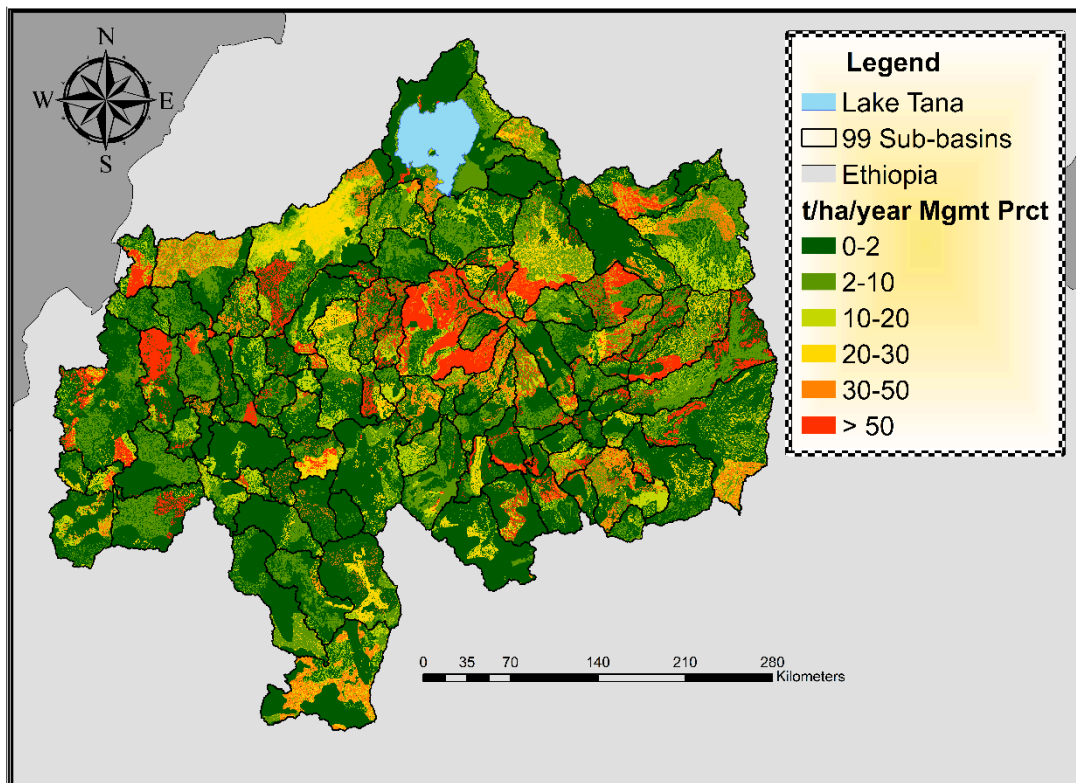


Figure 60. Average annual sediment yield in the upper Blue Nile Basin for the period 1988-2004 with management practices.

4.4 Implications and conservation practices

Conservation practices in SWAT are represented through the USLE_P factor. *Nyssen et al. (2007)* estimated based on field data a USLE_P factor of 0.32 for good stone bunds in the Ethiopian highlands. This value represented well maintained stone bunds. *Naudts (2002)* interviewed farmers in the Tigray high lands of the northern Ethiopia where 90% of the farmers agreed with the efficiency of stone bunds against erosion and the improvement of the soil fertility. While the only relevant disadvantaged has been the attraction of rats (*Nyssen et al., 2007*). *Desta et al. (2005)* also performed on-farm analysis in the Tigray sub-catchment where soil erosion was significantly reduced in a 68%, from 57 t/ha/ year to 18 t/ha/year. After implementing this factor SWAT reduced the average sediment yield from 40 t/ha/year to 12 t/ha/year. Although this practice can significantly help to the reduction of soil loss, *Hengsdijk et al. (2005)* showed that the excess of stone bunds reduce the cropped area, hence the agricultural production. Therefore, the controlled implementation of these is recommended. However, stone bunds can positively affect crop yields on the long term. Other structural management practices to be consider are the filter vegetated strips between cropland and water bodies, terraces that can retain runoff by reducing slope lengths, and also the reduction of channel erosion by constructing small temporary check dams along the river channels to reduce the velocity of concentrated flows.

Another common practice has been the forestation of bare lands, although *Nyssen et al. (2005)* mentioned that forestation of 72% of the area of the catchment is required to reduce soil erosion by only 14%, which requires a lot work compared to the expected outcomes. However, *Descheemaeker et al. (2005)* showed that reforestation could almost eliminate the erosion process in sections with steepest slopes. Other non-structural conservation practices include the incorporation of efficient grasses, fruit and ornamental trees. Additionally, a combination of agroforestry plantations along with some structures for instance the stone bunds could even increase the efficiency for a better soils conservation and agricultural production.

The application of this conservation practices have demonstrated that a sustainable management practices can be applied in the Blue Nile Basin, however, the adequate scenarios and conservation practices can differ largely from one area to another. And although from the agricultural and ecological point of view most of the positive results are given by stone bunds, more research and development of in-situ conservation practices should be done. Additionally, environmental conditions have large variation between different regions within the Blue Nile Basin. Therefore, the combination of multiple conservation practices should be evaluated to define more specific USLE_P values for different regions of the Blue Nile Basin. Furthermore, a combination of Soil and Water Conservation (SWC) practices and structures should be analyzed and incorporated in agricultural production plans.

5. CONCLUSIONS AND RECOMMENDATIONS

5.1 Major findings and limitations of the study

Following the *first objective* of this research, a reliable dataset was created by integrating the CFSR and Ground datasets. The Integrated dataset was able to correctly represent the amount and distribution of precipitation in the upper Blue Nile Basin. Additionally, the Integrated dataset also provided better statistical results during the models calibration and validation, obtaining better R², NS and SEI values. Therefore, it has been proved that the integration of datasets at large scale constitute an effective approach that can compensate certain dataset limitations. However, the data integration should always be supported by statistical analyses to demonstrate that the quality of the data is reliable. During this research phase, it was also found that the statistical results obtained from SWAT30 and SWAT87 were mostly very similar, except the models using the CFSR datasets. The differences were also very noticeable during the water balance analysis, especially in the case of the CFSR dataset. The CFSR dataset has many available stations distributed all over the watershed, hence different delineation will include different number of stations. Therefore, it can be concluded that the number of sub-basin will have a significant effect on the water balance only if large amounts of weather stations are available in a specific watershed, otherwise the number of sub-basin will be irrelevant.

The *second objective* was mainly focused on the analysis of the effects of the number of sub-basins and HRUs on the sediment estimations in SWAT. During this phase it was proved that the average slope lengths used by SWAT will easily change under different HRU amounts and can dramatically change the sediment estimations. This phenomena will significantly impact the runoff concentration times of the HRUs causing a reduction of the sediment yield when the size of HRUs decreases. This causes large uncertainties in the sediment load estimations even when a good calibration with flow discharge data is achieved. Furthermore, this research proposed a threshold for the resolution portion of the total area used for the delineation. It was observed that the largest variation between the number of sub-basins and HRUs are portions smaller than 0.40% and larger than 1.3% of the total area. Therefore, any resolution portion within this range should provide reliable sediment estimations. However, this resolution portion was specifically defined for the upper Blue Nile Basin, hence further studies should be done if applied in other watersheds. Nevertheless, sediment estimations will always be simulated with some level of uncertainties in the Blue Nile Basin due to the complexity of these processes and the lack of observed measured data.

Furthermore, this research also proposed the use of sediment rating curves to estimate sediment concentrations that were very helpful to compare the results obtained from SWAT. The results from SWAT and the sediment rating curves were compared with the few available measured data, where both results showed realistic values. Therefore, potential of sediment rating curves should not be underestimated and should always be considered as a very important approach to generate sediment concentration values that can be used to compare the results provided by hydrological models.

The **third objective** aimed to propose the SWAT Error Index (SEI) as an additional tool to express the level of error of SWAT models. SEI was successfully tested in the entries upper Blue Nile Basin and also in the Ribb sub-catchment. After its evaluation, SEI showed to be a very useful additional method that could help to develop models that can provide a better representation of the water balance of a watershed. SEI also showed that the Integrated dataset successfully achieved better and more reliable results than the Ground and CFSR datasets separately. However, further tests and improvements should be done to this index, specifically for the definition of the weighted values for the discharge and evapotranspiration components.

5.2 Contributions and final conclusions of the research

The final erosion analyses performed in the upper Blue Nile Basin showed how dangerous soil losses can be for the agricultural production. Although general conservations practices that could be implemented in the Blue Nile Basin were mentioned, correct values for USLE_P can only be correctly defined through in-site studies and based on detailed understanding of the problems of specific sub-catchments. Additionally, specific conservation practices should be defined for different sub-catchments in the Blue Nile Basin, for instance the rehabilitation of soil, rainfall harvesting, diversification of the crops, encouraging the use of drought resistant crop varieties, breed seeds that use water efficiently, reforestation, and improvements in the irrigated agricultural systems and water use efficiency.

Environmental processes in the Blue Nile Basin are complex and irregular during different seasons and also very contrasting in different regions of the watershed. Therefore, obtaining accurate results and proposing management and conservation practices that can be put in practice is very difficult. However, with the proposal of an adequate threshold to define sub-basins in the upper Blue Nile Basin, the integration of a more reliable weather dataset and the development of sediment rating curves for multiple sub-catchments, this dissertation has accomplished the main objective of creating, calibrating and validating a reliable SWAT model for the upper Blue Nile Basin. This research has also presented a small step further for the evaluation of SWAT models with the proposal of the SWAT Error Index (SEI). The methodology applied in this research can certainly provide a better criteria that can help modelers to consider multiple factors before modelling watersheds, consequently better models that can provide more reliable results can be achieved.

5.3 Discussions and new research fields

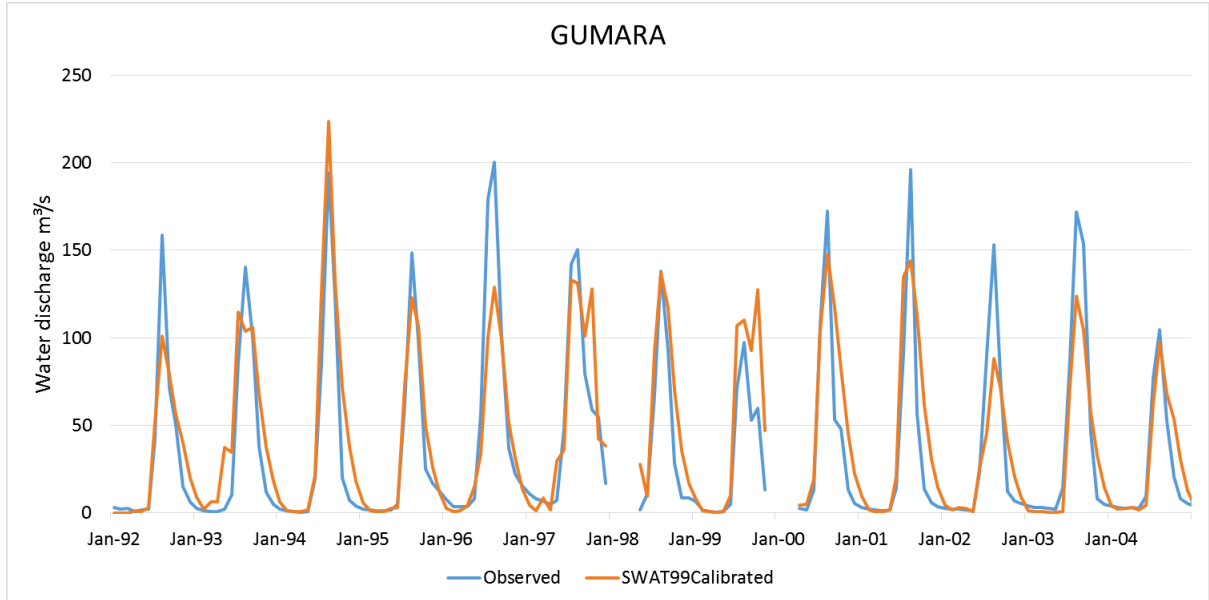
Hydrological processes were successfully simulated and based on the statistical results obtained from the calibrations and validations with flow discharge data, and comparisons with the few available sediment measurements, it can be said that SWAT is able to simulate both processes correctly. However, it is worthwhile to mention the high levels of uncertainty that model might constitute, especially when several important hydrological processes are highly reliant on very sensitive parameters like CN and SOL_AWC, different parameterization may be required for different time periods within

the same catchment, furthermore, alongside with the fact that sediment estimations cannot be calibrated due to the lack of measured data, they are highly reliant on two sensitive parameters SPCON and SPEXP.

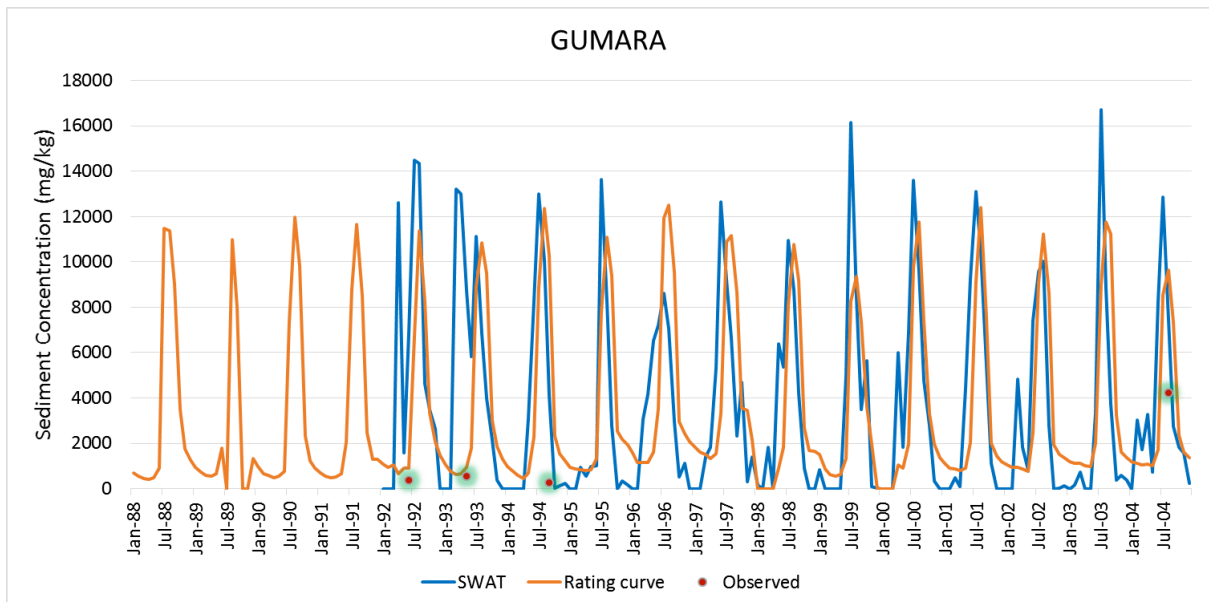
Although results in this study appear to be within realistic ranges and up to some extent provided important information about the current condition of the watershed and also helpful details to improve the management of the watershed, it is also important to mention that multiple gaps still remain for further improvements and new research fields. For instance, one of the most significant degradation problems in the Blue Nile are the deep and wide gully formations. Gullies are continuously expanding at alarming rate and drastically damaging agricultural areas (*Daba et al., 2003*). Even when these gully developments are very severe especially in regularly saturated lower lands, these formations cannot be simulated in SWAT therefore its impacts have not been mentioned in this research. Further studies should be done on gully formations, their impacts and possible rehabilitation practices, additionally potential codes can also be developed and integrated in SWAT to simulate gully formation.

Another important segment that has also left room for new researches is the exact identification of erodible areas. Although HRUs are a good approach to identify small erodible regions, SWAT is drifted to estimate the largest amount of erosion in very high slopes which to certain extent seems reasonable. However, other studies have mentioned that these high slope areas are simply infiltration areas where the runoff is not very strong causing low erosion rates, and therefore mentioning that the lower saturated areas experience stronger runoffs hence higher erosion rates. This theory also requires further research and could also be interesting identifying if this is a particular case in the Blue Nile basin or if it applies to every watershed. Additionally, this saturated-areas effect cannot be simulated by either, including this extension in SWAT could also help to model watershed process with more accuracy.

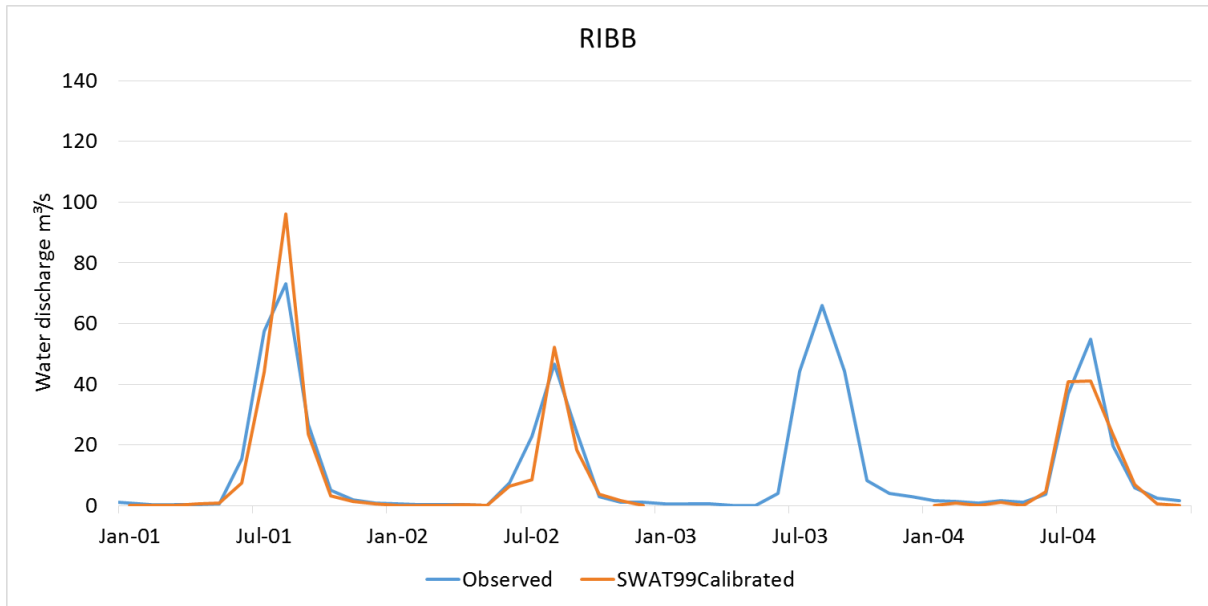
APPENDICES



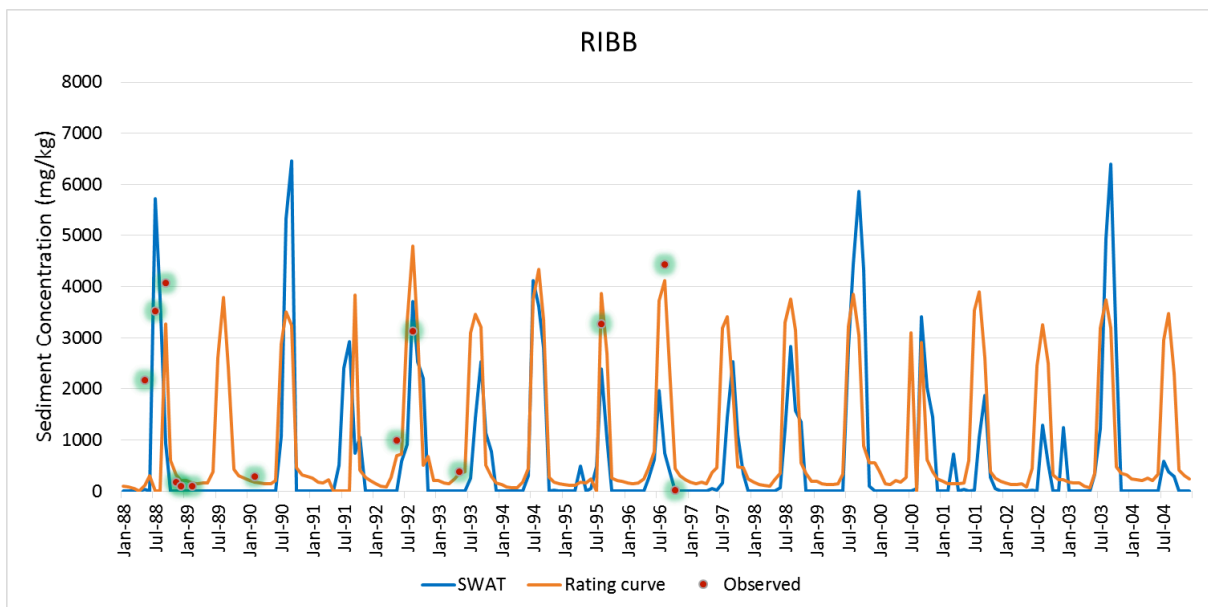
Appendix 1. Calibration and validation results at Gumara with SWAT99 Integrated for the period 1992-2004. Statistical results achieved R^2 values of 0.83 and 0.76 for the calibration and validation, respectively; and NS values of 0.82 and 0.78 for the calibration and validation, respectively.



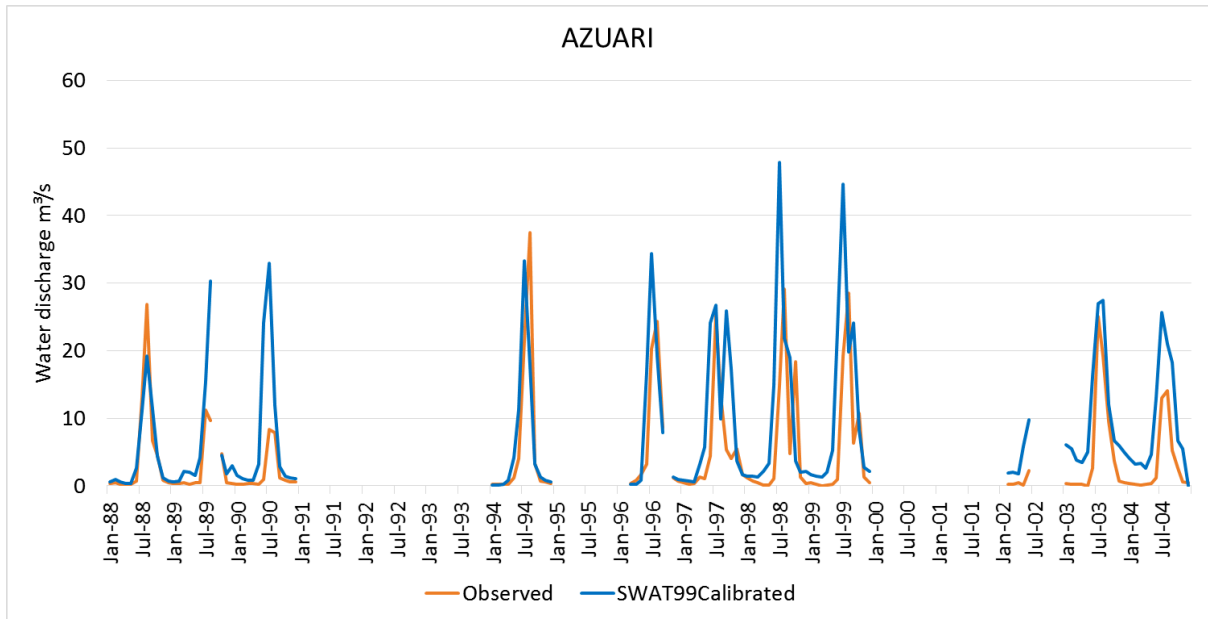
Appendix 2. Sediment concentrations (mg/kg) at Gumara catchment.



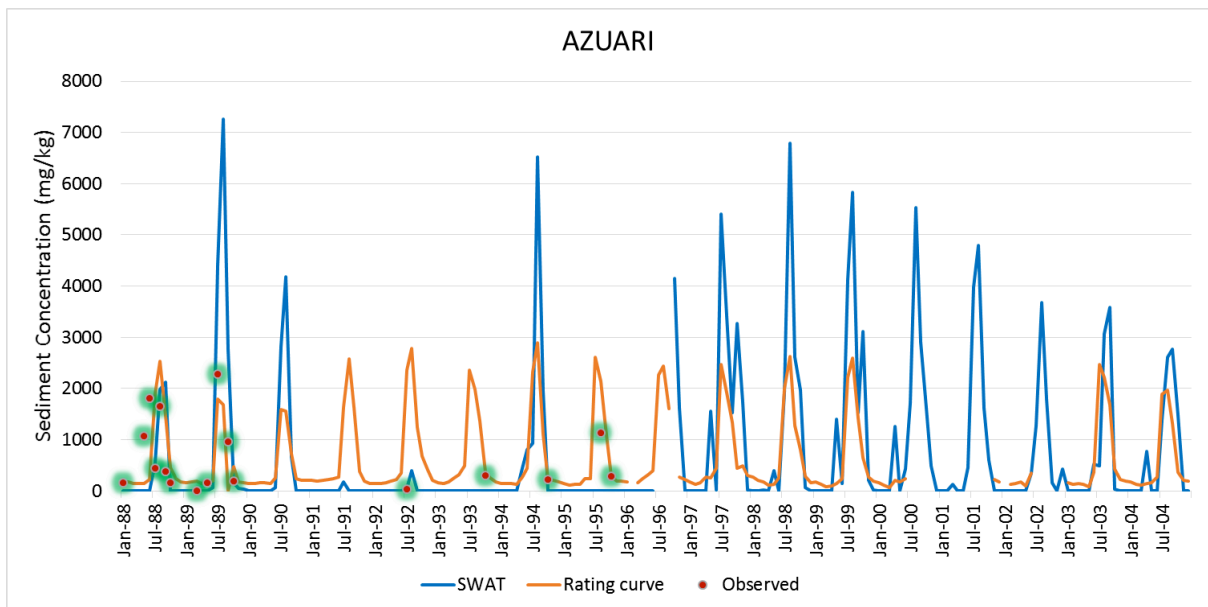
Appendix 3. Calibration and validation results at Ribb with SWAT99Integrated for the period 2001-2004. Statistical results achieved R^2 values of 0.92 and 0.94 for the calibration and validation, respectively; and NS values of 0.88 and 0.93 for the calibration and validation, respectively.



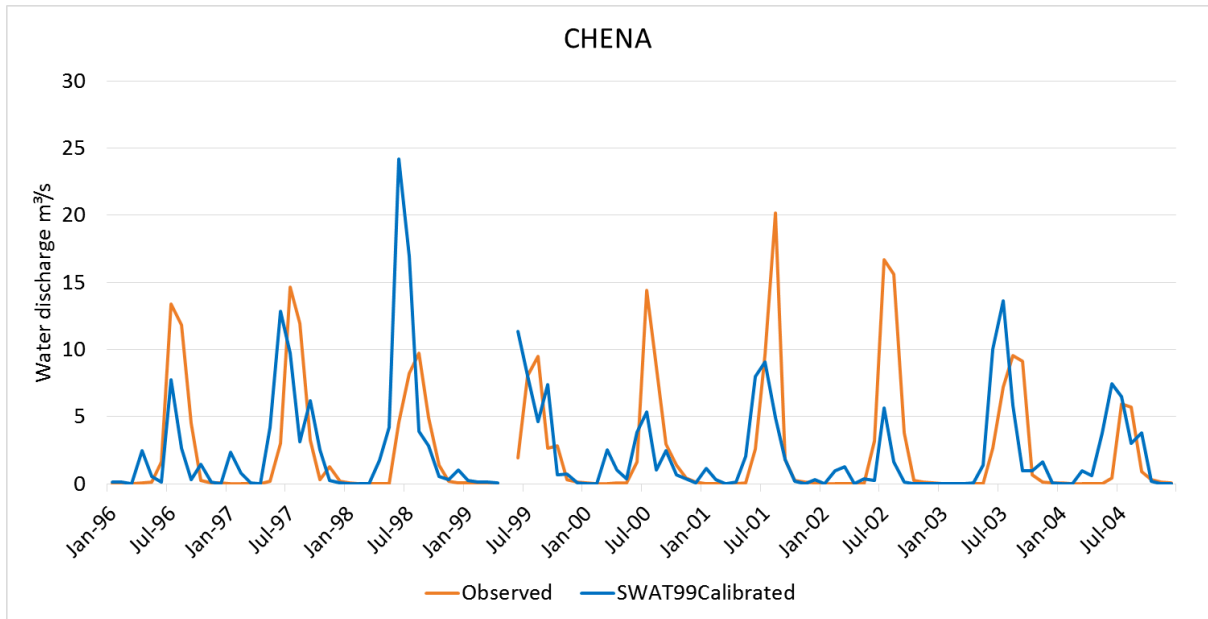
Appendix 4. Sediment concentrations (mg/kg) at Ribb catchment.



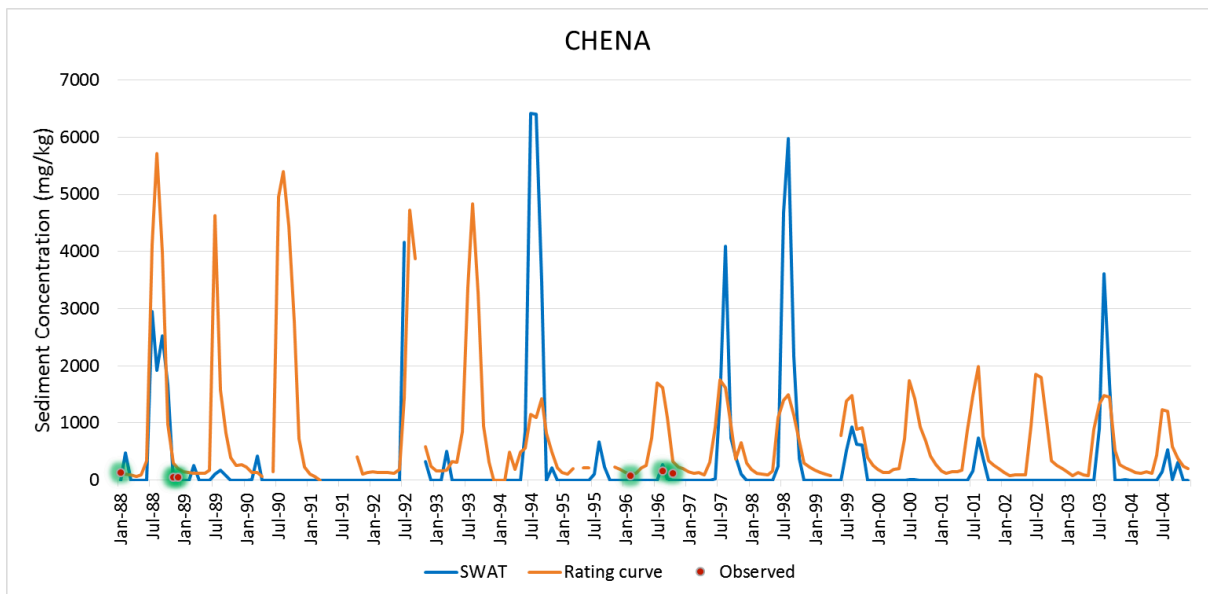
Appendix 5. Calibration and validation results at Azuari with SWAT99Integrated for the period 1988-2004. Statistical results achieved R^2 values of 0.61 and 0.78 for the calibration and validation, respectively; and NS values of 0.53 and 0.51 for the calibration and validation, respectively.



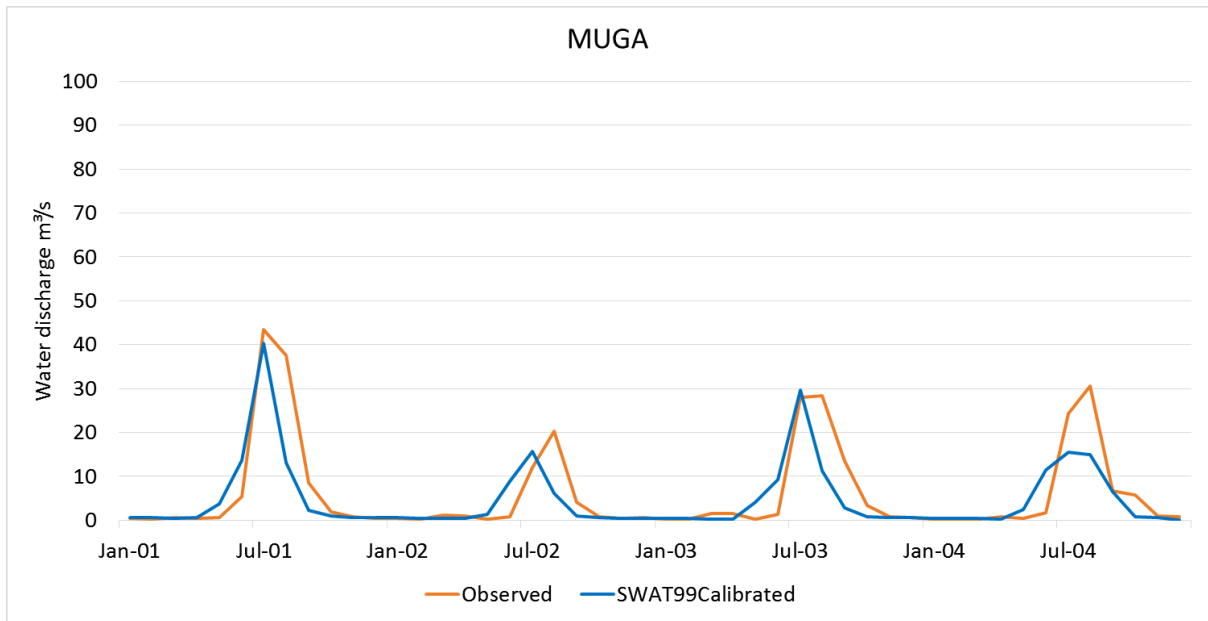
Appendix 6. Sediment concentrations (mg/kg) at Azuari catchment.



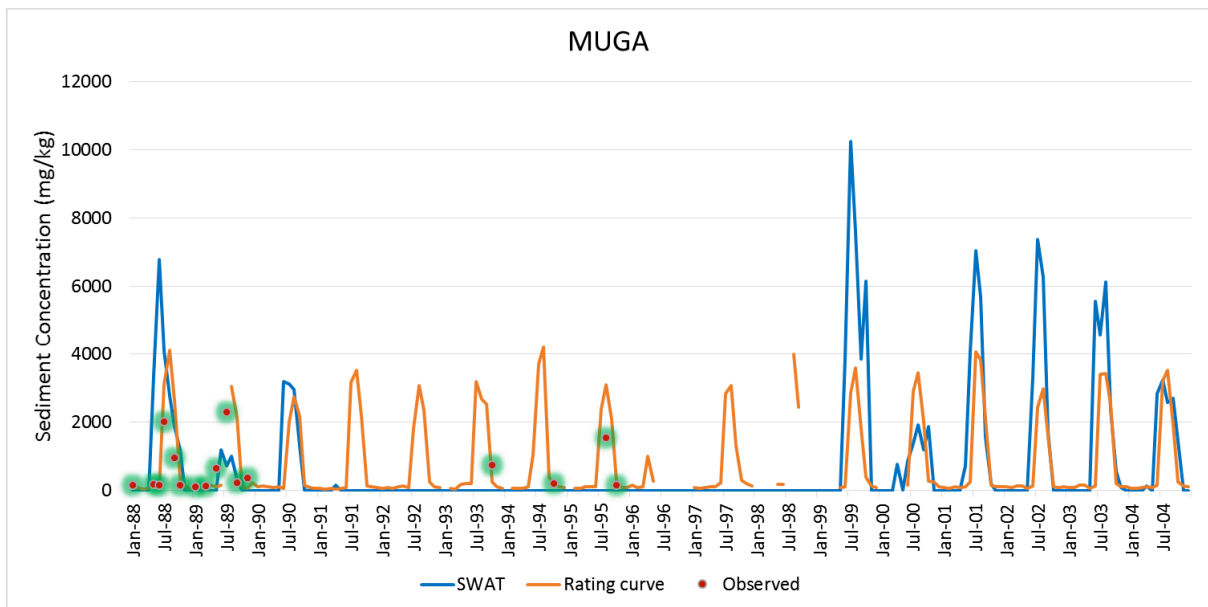
Appendix 7. Calibration and validation results at Chena with SWAT99Integrated for the period 1996-2004. Statistical results achieved R^2 values of 0.53 and 0.64 for the calibration and validation, respectively; and NS values of 0.40 and 0.47 for the calibration and validation, respectively.



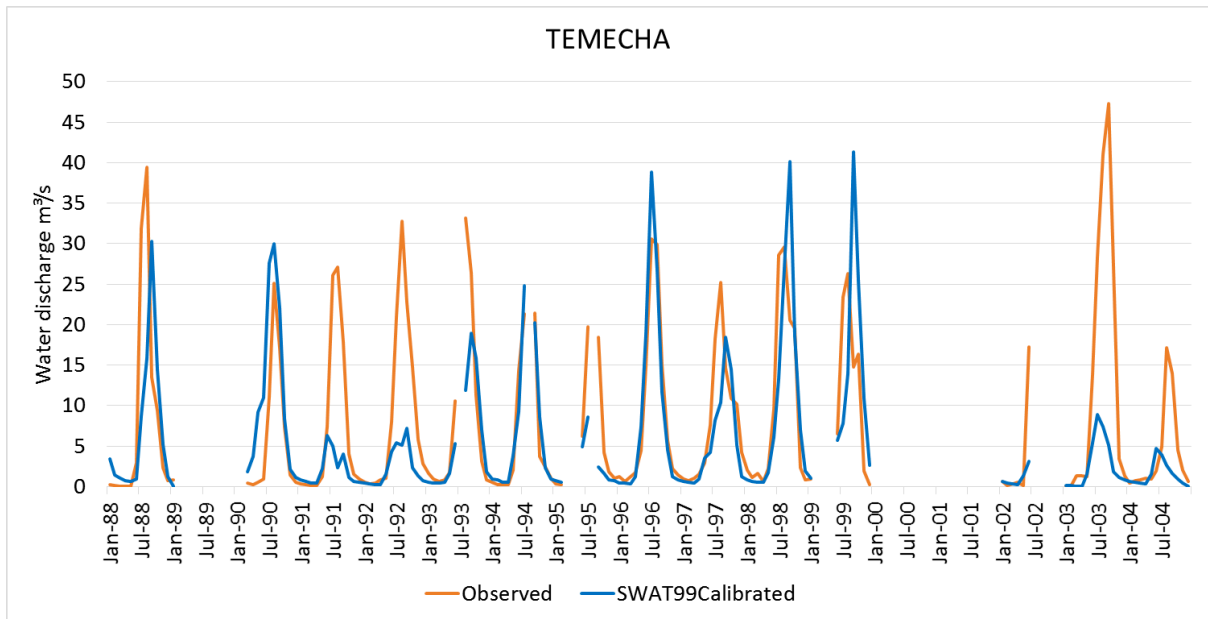
Appendix 8. Sediment concentrations (mg/kg) at Chena catchment.



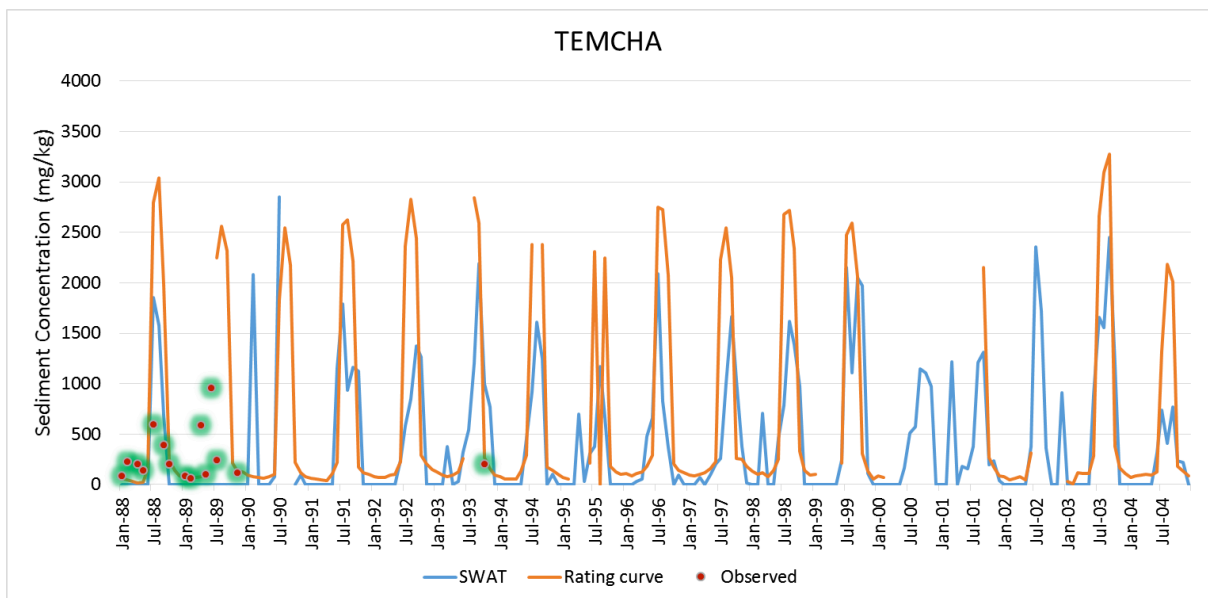
Appendix 9. Calibration and validation results at Muga with SWAT99Integrated for the period 2001-2004. Statistical results achieved R^2 values of 0.67 and 0.7 or the calibration and validation, respectively; and NS values of 0.66 and 0.61 for the calibration and validation, respectively.



Appendix 10. Sediment concentrations (mg/kg) at Muga catchment.



Appendix 11. Calibration and validation results at Temecha with SWAT99 Integrated for the period 1988-2004. Statistical results achieved R^2 values of 0.68 and 0.7 for the calibration and validation, respectively; and NS values of 0.46 and 0.57 for the calibration and validation, respectively.



Appendix 12. Sediment concentrations (mg/kg) at Temcha catchment.

ID	NAME	LAT	LONG	Elevation	Name	1980	1981	1982	1983	1984	1985	1986	1987	1988	1989	1990	1991	1992	1993	1994	1995	1996	1997	1998	1999	2000	2001	2002	2003	2004	2005
1	p114366	11.635	37.746	2292	Arb- Gebeya(Dera)																										
2	p114367	12.768	37.625	2961	Ambagiorgis																										
3	p114368	11.264	37.492	2216	Adet																										
4	p114369	9.896	37.086	2179	Finchaa																										
5	p114370	10.956	30.509	1642	Chagni																										
6	p114371	12.419	37.045	1929	Chandiba																										
7	p114372	10.296	37.465	2050	Debre Alias																										
8	p114373	10.296	37.465	2050	D. Markos																										
9	p114374	11.586	38.015	2667	Debretabor																										
10	p114375	10.657	38.167	2505	Debre work																										
11	p114376	11.256	36.84	2122	Dangila																										
12	p114377	13.151	37.898	2847	Debark																										
13	p114378	12.194	37.049	1806	Delgi																										
14	p114379	10.562	37.494	2040	Dembecha																										
15	p114380	11.964	36.914	1826	Dengay ber																										
16	p114381	11.783	37.561	1943	Dera Hamusite																										
17	p114382				Ebinat																										
18	p114383	10.85	37.602	3018	Feresbet																										
19	p114384	10.75	38.065	2687	FELGEBIRHAN																										
20	p114385	10.849	36.885	2310	Gimjabet Mariam																										
21	p114386	12.238	37.299	1820	Gorgora																										
22	p114387	9.037	38.736	2456	Gundil																										
23	p114388	9.037	38.736	2456	Gundowoin																										
24	p114389	10.897	36.967	2502	Kessa																										
25	p114390	10.934	37.484	2352	Kidamaja																										
26	p114391	10.964	38.273	3138	Laybir																										
27	p114392	10.871	38.269	2624	Mertuelmariam																										
28	p114393	11.474	37.284	1970	Meshenti																										
29	p114394	12.954	36.157	717	Metema																										
30	p114395	11.078	37.877	2444	Motta																										
31	p114396	11.07	37.514	2636	Quarit																										
32	p114397	12.74	35.51	530	Abbay Sheleko																										
33	p114398	12.767	35.602	535	Addis Zemen																										
34	p114399	10.63333	36.6	1725	Ayehu																										
35	p114400	12.48	37.03	2150	Aykel																										
36	p114401	11.59	37.388	1811	Bahir Dar new																										
37	p114402	11.59	37.388	1811	Bahir Dar old																										
38	p114403	11.59	37.388	1811	Bahir Dar syn																										
39	p114404	12.33333	37.236	2000	Chuahit																										
40	p114405	11.873	37.226	1795	Deke Estifanos																										
41	p114406	11.7	37.51	1900	Dera Hamusite																										
42	p114407	12.26	37.54	1500	Enfiraz																										
43	p114408	10.99861	36.89833	2540	Enjibara																										
44	p114409	11.75	38.33	2700	Gassay																										
45	p114410	12.50556	37.40833	1967	Gondar																										
46	p114411	12.74	35.51	530	Gummera																										
47	p114412	10.57	37.04	2540	Gundil																										
48	p114413	10.927	36.604	1952	Kidamaja																										
49	p114414	11.382	37.389	2100	Kimbaba																										
50	p114415	12.165	37.636	1818	Koga																										
51	p114416	12.1	36.1	1920	Kunzila																										
52	p114417	11	37.13	2690	Sekela																										
53	p114418	10.83	37.0125	2570	Tillili																										
54	p114419	11.309	37.038	1900	Wetet Abay																										
55	p114420	10.33333	38.17	1852	Yetmen																										
56	p114421	11.727	37.217	1800	Zege																										
57	p114422				Shahura																										
58	p114423	9.037	38.736	2456	Shindi																										
59	p114424	11.49	37.588	1625	Tis Abbay																										
60	p114425	9.037	38.737	2456	Wote Abbay																										
61	p114426				Wanzave																										
62	p114427	11.922	37.699	1848	Woreta																										
63	p114428	10.651	37.520	2466	Yechereka																										
64	p114429	10.154	37.747	2327	Yejubie																										
65	p114430	10.328	37.808	2458	Yetmen																										

Appendix 13. Rainfall data availability for the upper Blue Nile Basin.

ID	NAME	LAT	LONG	Elevation	Name	1980	1981	1982	1983	1984	1985	1986	1987	1988	1989	1990	1991	1992	1993	1994	1995	1996	1997	1998	1999	2000	2001	2002	2003	2004	2005
1	p114398	12.767	35.602	535	Addis Zemen																										
2	p114368	11.264	37.492	2216	Adet																										
3	p114400	12.480	37.030	2150	Aykel																										
4	p114403	11.590	37.388	1811	Bahir Dar new																										
5	p114402	11.59	37.388	1811	Bahir Dar old																										

Appendix 14. Temperature data availability for the upper Blue Nile Basin.

ID	NAME	LAT	LONG	Elevation	Name	1980	1981	1982	1983	1984	1985	1986	1987	1988	1989	1990	1991	1992	1993	1994	1995	1996	1997	1998	1999	2000	2001	2002	2003	2004	2005
1	p114368	11.264	37.492	2216	Adet																										
2	p114399	10.633	36.600	1725	Ayehu																										
3	p114400	12.480	37.030	2150	Aykel																										
4	p114403	11.590	37.388	1811	Bahir Dar Syn																										
5	p114370	10.956	30.509	1642	Chagni																										
6	p114376	11.256	36.840	2122	Dangila																										
7	p114373	10.296	37.465	2050	Debre Markos																										
8	p114374	11.586	38.015	2667	Debre Tabor																										
9	p114410	12.506	37.408	1967	Gondar																										
10	p114395	11.078	37.877	2444	Motta																										
11	p114431	11.737	38.469	3135	Nefas																										

Appendix 15. Relative humidity data availability for the upper Blue Nile Basin.

ID	NAME	LAT	LONG	Elevation	Name	1980	1981	1982	1983	1984	1985	1986	1987	1988	1989	1990	1991	1992	1993	1994	1995	1996	1997	1998	1999	2000	2001	2002	2003	2004	2005
1	p114368	11.264	37.492	2216	Adet																										
2	p114400	12.480	37.030	2150	Aykel																										
3	p114403	11.590	37.388	1811	Bahir Dar Syn																										
4	p114370	10.956	30.509	1642	Chagni																										
5	p114376	11.256	36.840	2122	Dangila																										
6	p114373	10.296	37.465	2050	Debre Markos																										
7	p114374	11.586	38.015	2667	Debre Tabor																										
8	p114410	12.506	37.408	1967	Gondar																										
9	p114395	11.078	37.877	2444	Motta																										

Appendix 16. Solar radiation data availability for the upper Blue Nile Basin.

Number	Name	LAT	LONG	Elevation	Name	1980	1981	1982	1983	1984	1985	1986	1987	1988	1989	1990	1991	1992	1993	1994	1995	1996	1997	1998	1999	2000	2001	2002	2003	2004	2005
1	p114370	10.956	30.509	1642	Chagni																										
2	p114368	11.264	37.492	2216	Adet																										
3	p114403	11.590	37.388	1811	Bahir Dar Syn																										
4	p114399	10.633	36.600	1725	Ayehu																										
5	p114432	10.698	37.176	1996	Mankush																										
6	p114374	11.586	38.015	2667	Debra Tabor																										
7	p114376	11.256	36.840	2122	Dangila																										
8	p114395	11.078	37.877	2444	Motta																										
9	p114375	10.657	38.167	2505	Debre Werk																										
10	p114373	10.296	37.465	2050	Debre Markos																										

Appendix 17. Wind speed data availability for the upper Blue Nile Basin.

ID	Ground Dataset				CFSR Dataset			
	NAME	LAT	LON	Elevation	NAME	LAT	LONG	Elevation
1	p114366	11.635	37.746	2292	p117378	11.709	37.813	2054
2	p114367	12.768	37.625	2961	p126375	12.645	37.5	2417
3	p114368	11.264	37.492	2216	p114375	11.396	37.5	2169
4	p114369	9.896	37.086	2179	p98372	9.835	37.188	2414
5	p114370	10.956	30.509	1642	p111366	11.084	36.563	1716
6	p114371	12.419	37.045	1929	p123369	12.33	36.875	1131
7	p114372	10.296	37.465	2050	p101375	10.147	37.5	1851
8	p114373	10.296	37.465	2050	p101375	10.147	37.5	1851
10	p114375	10.657	38.167	2505	p108381	10.772	38.125	2472
12	p114377	13.151	37.898	2847	p126378	12.645	37.813	2032
13	p114378	12.194	37.049	1806	p123372	12.33	37.188	1836
14	p114379	10.562	37.494	2040	p105375	10.46	37.5	2222
15	p114380	11.964	36.914	1826	p120369	12.021	36.875	1826
16	p114381	11.783	37.561	1943	p117375	11.709	37.5	1833
18	p114383	10.85	37.602	3018	p108378	10.772	37.813	3012
19	p114384	10.75	38.065	2687	p108381	10.772	38.125	2472
20	p114385	10.849	36.885	2310	p108369	10.772	36.875	2184
21	p114386	12.238	37.299	1820	p123372	12.33	37.188	1836
22	p114387	9.037	38.736	2456	p92388	9.211	38.75	2498
23	p114388	9.037	38.736	2456	p89388	8.899	38.75	2138
25	p114390	10.934	37.484	2352	p111375	11.084	37.5	2730
27	p114392	10.871	38.269	2624	p108384	10.772	38.438	2021
28	p114393	11.474	37.284	1970	p114372	11.396	37.188	2068
29	p114394	12.954	36.157	717	p126363	12.645	36.25	747
30	p114395	11.078	37.877	2444	p111378	11.084	37.5	2730
31	p114396	11.07	37.514	2636	p111375	11.084	37.5	2730
33	p114398	12.767	35.602	535	p126356	12.645	35.625	520
35	p114400	12.48	37.03	2150	p126369	12.645	36.875	1610
36	p114401	11.59	37.388	1811	p111375	11.709	37.5	1833
37	p114402	11.59	37.388	1811	p111375	11.709	37.5	1833
38	p114403	11.59	37.388	1811	p111375	11.709	37.5	1833
40	p114405	11.873	37.226	1795	p114400	12.021	37.188	1784
42	p114407	12.26	37.54	1500	p123375	12.33	37.5	1794
53	p114418	10.83	37.0125	2570	p108372	10.772	37.188	2207
55	p114420	10.33333	38.17	1852	p105381	10.46	38.125	2532
56	p114421	11.727	37.217	1800	p117372	11.709	37.188	1811
58	p114423	9.037	38.736	2456	p89388	8.899	38.75	2138
59	p114424	11.49	37.588	1625	p114378	11.396	37.5	2169
60	p114425	9.037	38.737	2456	p89384	8.899	38.438	2101
63	p114428	10.651	37.520	2466	p108375	10.772	35.7	2111
64	p114429	10.154	37.747	2327	p101378	10.147	37.813	2244
65	p114430	10.328	37.808	2458	p101378	10.147	37.813	2244

Appendix 18. Geographic coordinates of the ground stations and its respective CFSR stations used in the Integrated dataset.

Location No.	Station Number	River/Lake	Site	1980	1981	1982	1983	1984	1985	1986	1987	1988	1989	1990	1991	1992	1993	1994	1995	1996	1997	1998	1999	2000	2001	2002	2003	2004	2005
2	111002	GELGEL A.	MARAWI																										
3	111003	KOGA	MERAWI																										
5	111005	RIBB	Nr. Addis																										
6	111006	GUMMERA	BAHIR DAR																										
9	111009	UPPER RIB	ON D.TABO																										
10	111011	LAKE TANA	BAHIR DAR																										
14	111016	GEMERO	Nr.Maksegnit																										
16	111018	GARNO	Nr. Infra																										
17	111019	EZANA	BAHIRDAR																										
19	111021	AMEN	DANGILA																										
33	112017	MUGA	DEJEN																										
34	112018	AZUARI	Nr.Mota																										
35	112019	TIGDAR	Nr.Unde Woin																										
43	112030	TEME	Nr.Mota																										
44	112031	SUHA	Nr.Bichena																										
49	112037	SEDIE	Nr. Mota																										
50	112038	YEDA	Nr.Amber																										
51	112039	CHENA	ISTAY																										
56	113008	CHEMOGA	Nr.DEBRE																										
58	113012	GUDLA	DEMBECHA																										
59	113013	BIRR	Nr.Jigga																										
60	113014	TEMCHA	DEMBECHA																										
61	113015	LEZA	JIGA																										
63	113019	FETAM	TILILE																										
64	113023	DURA	METEKEL																										
66	113028	DONDOR	METEKEL																										
67	113029	ARDY	Nr.Metek																										
69	113033	QUASHINI	Nr. Addis Kiddame																										
74	113039	BOGENA	LUMAME																										
75	113040	MISSINI	KOSSOBER																										
102	116005	MAIN BELES	BRIDGE																										
106	113035	AYO	Nr.Kosso																										
116	116004	SILGEL BELES	Nr. Mandu																										
120	-	BIRBIR	YUBDO																										
121	-	BEKO	NRTEPI																										
122	-	BARO	MASHA																										
123	-	BARO	GAMBELLA																										
124	-	ATAYE	ATAYE																										
125	-	BITINWOHA	Nr. TEPI																										
126	-	BORKENA	Nr. Kombolcha																										
127	-	BORKENA	Swampoutlet																										
128	-	CHERECHA	CHANKA																										
129	-	ELIKKEI	Nr. SUPPI																										
130	-	GÄCHTEB	MIZANTEFERI																										
131	-	GEBÄ	Nr. SUPPI																										
132	-	GELDA	Nr. Ambessame																										
133	-	GENGI	GECHA																										
134	-	GILO	PIGNUDO																										
135	-	GUMERO	GORE																										
136	-	JARRA	JARRA																										
137	-	KETO	CHANKA																										
138	-	KORICHE	KILTU KARA																										
139	-	KUNI	CHANKA																										
140	-	LAH	FINOTÉ SALAM																										
141	-	MEGECH	AZEZO																										
142	-	MERDEFA	Nr. Alem Trefi																										
143	-	METI	Nr. Dembidolo																										
144	-	OUWA	GULISO																										
145	-	ROBI	ROBIT																										
146	-	SORE	Nr.Metu																										
147	-	UKA	UKA																										
148	-	WENKA	ISTAY																										

Appendix 19. Flow discharge data availability for the upper Blue Nile Basin.

LIST OF REFERENCES

Abate, M., Nyssen, J., Steenhuis, T., Moges, M., Tilahun, S., Enku, T., and Adgo, E.: Morphological changes of Gumara River channel over 50 years, Upper Blue Nile basin, Ethiopia. *Journal of Hydrology*, 525, 152-164. <http://dx.doi.org/10.1016/j.jhydrol.2015.03.044>, 2015.

Abbaspour, K. C.: SWAT-CUP: SWAT calibration and uncertainty programs-A user manual, Tech. rep., Swiss Federal Institute of Aquatic Science and Technology, Eawag, Dübendorf, Switzerland, 2015.

Abbaspour, K. C., Jonson, C. A. and van Genuchten, M. T.: Estimating Uncertain Flow and Transport Parameters Using a Sequential Uncertainty Fitting Procedure. Madison: Soil Science Society of America, 2004.

Abera, W., Formetta, G., Brocca, L., and Rigon, R.: Water budget modelling of the Upper Blue Nile basin using the JGrass-NewAge model system and satellite data, *Hydrol. Earth Syst. Sci. Discuss.*, doi:10.5194/hess-2016-290, in review, 2016.

Abteu W., Melesse A. M., Dessalegne T.: El Niño Southern Oscillation link to the Blue Nile River Basin hydrology, *Hydrological Processes*, Volume 23, Issue 26, Pages 3653–3660, DOI: 10.1002/hyp.7367, 30 December 2009.

Ali, M., Sterk, G., Seeger, M., Boersema, M., and Peters, P.: Effect of hydraulic parameters on sediment transport capacity in overland flow over erodible beds, *Hydrol. Earth Syst. Sci.*, 16, 591-601, doi:10.5194/hess-16-591-2012, 2012.

Allen, R. G., Pereira, L.S., Raes D. and Smith, M.: Crop Evapotranspiration: Guidelines for computing crop water requirements, FAO Irrigation and Drainage Paper No. 56, Food and Agriculture Organization, Land and Water, Rome, Italy, 1998.

Althoff, I. and Förch, G.: Water Balance Modelling in the Southern Ethiopian Rift Valley: the example of Bilate River Catchment. Centre for International Capacity Development CICD Series, Universität Siegen, Vol. 3, 2009.

Arnold, J. G., Kiniry, J. R., Srinivasan, R., Williams, J. R., Haney, E. B. and Neitsch, S.L.: Soil & Water Assessment Tool, Input/Output documentation, version 2012, Texas Water Resources Institute, 246-248, 2012.

Arnold, J. G., Srinivasan, R., Muttiah, R. S. and Williams, J. R.: Large Area Hydrologic Modeling And Assessment Part I: Model Development. *JAWRA Journal of the American Water Resources Association*, 34: 73–89. doi:10.1111/j.1752-1688.1998.tb05961.x, 1998.

Asselman, N. E. M.: "Fitting and Interpretation of Sediment Rating Curves." *Journal of Hydrology* 234 (3–4): 228–48. doi:10.1016/S0022-1694(00)00253-5, 2000.

Asselman, N. E. M.: "Suspended Sediment Dynamics in a Large Drainage Basin: The River Rhine." *Hydrological Processes* 13 (10): 1437–50. doi:10.1002/(SICI)1099-1085(199907)13:103.0.CO;2-J, 1999.

Asres, M. T. and Awulachew, S. B.: SWAT based runoff and sediment yield modeling: a case study of the gumera watershed in the Blue Nile basin. *Ecohydrol Hydrobiol* 10:191–200, 2010.

Awulachew, S. B.; Merry, D. J.; Kamara, A. B.; van Koppen, B.; Penning de Vries, F.; Boelee, E.; Makombe, G.: Experiences and opportunities for promoting small-scale/micro irrigation and rainwater harvesting for food security in Ethiopia. Colombo, Sri Lanka: International Water Management Institute (IWMI). 91p. (IWMI Working Paper 98), 2005.

Awulachew, S. B., Yilma, A. D., Loulseged, M., Loiskandl, W., Ayana, M., Alamirew, T.: Water Resources and Irrigation Development in Ethiopia. Colombo, Sri Lanka: International Water Management Institute. 78p. (Working Paper 123), 2007.

Ayenew, Y.: Rainfall-Runoff Modelling for Sustainable Water Resources Management: The Case of Gumara Watershed, Ethiopia (Master). Addis Ababa University, 2008.

Barati, R.: Parameter estimation of nonlinear Muskingum models using Nelder-Mead Simplex algorithm, *Journal of Hydrologic Engineering*, 16(11): 946-954, 2011.

Bastidas, L. A., Gupta, H. V. and Sorooshian, S.: Emerging paradigms in the calibration of hydrologic models, *Mathematical Models of Large Watershed Hydrology*, Water Resources Publications, LLC, Englewood, CO, USA, 1, pp.25-56, 2002.

Bayabil, H. K., Tilahun, S. A., Collick, A. S., Yitaferu, B., and Steenhuis, T. S.: Are runoff processes ecologically or topographically driven in the (sub) humid Ethiopian highlands? The case of the Maybar watershed, *Ecohydrology*, 3, 457–466, 2010.

Bekele Y., Nata T. and Bheemalingswara K.: Preliminary Study on the Impact of Water Quality and Irrigation Practices on Soil Salinity and Crop Production, Gergera Watershed, Atsbi-Wonberta, Tigray, Northern Ethiopia, *MEJS*, Volume 4 (1):29-46, 2012.

Besalatpour, A., Hajabbasi, M. A., Ayoubi, S., and Jalalian A.: Identification and prioritization of critical sub-basins in a highly mountainous watersheds using SWAT model. *J Soil Sci* 1:58–63, 2012.

Betrie, G.D., Mohammed, Y. A., Van Griensven, A., and Srinivasan. R.: Sediment management modelling in the Blue Nile Basin using SWAT model. *Hydrol. Earth Syst. Sci.*, 15, 807–818, doi: 10.5194/hess-15-807, 2011.

Beven, K. J.: Rainfall-runoff modelling: The primer 2nd Edition, ISBN 978-0-470-71459-1, Wiley-Blackwell, January 2012.

Beven, K. J. and Binley, A. M.: The future of distributed models: model calibration and uncertainty prediction. *Hydrological Processes*, 6(3), 279-298. DOI:10.1002/hyp.3360060305, 1992.

Beven, K.J. and Kirkby M.J.: Towards a simple physically-based variable contributing model of catchment hydrology. *Hydrologic Sciences Bulletin*. 24(1), 43-69, 1979.

Block, J. P., Strzepek, K. and Rajagopalan, B.: Integrated Management of the Blue Nile Basin in Ethiopia, Hydropower and Irrigation Modeling, IFPRI Discussion Paper 00700, International Food Policy Research Institute, May, 2007.

Campbell, F. B. and H. A. Bauder.: "A Rating-Curve Method for Determining Silt Discharge of Streams." Transactions, American Geophysical Union 21: 603–7. doi:10.1029/TR021i002p00603, 1940.

Chandra, P., Patel, P.L., Porey, P. D. and Gupta, I. D.: Estimation of sediment yield using SWAT model for Upper Tapi basin, ISH Journal of Hydraulic Engineering, 2014.

Chaplot, V.: Impact of spatial input data resolution on hydrological and erosion modeling: recommendations from a global assessment. Phys. Chem. Earth 67–69, 23–35, 2014.

Chatterjee, S. and Krishna, S. A. P.: Geospatial assessment of soil erosion vulnerability at watersheds level in some sections of the upper Subarnarekha river basin Jharkhand India. Environ Earth Sci 71:357–374, 2013.

Chebud, Y. A., Melesse, A. M.: Modelling lake stage and water balance of Lake Tana, Ethiopia, Hydrol. Process. 23, 3534-3544, 2009.

Chen, E. and Mackay, D. S.: Effects of distribution-based parameter aggregation on a spatially distributed agricultural nonpoint source pollution model. J. Hydrol. 295, 211–224, 2004.

Cherie, N. Z.: Downscaling and Modeling the Effects of Climate Change on Hydrology and Water Resources in the Blue Nile Basin, Ethiopia, PhD Thesis University of Kassel, Germany, 2013.

Chiang, L. C. and Yuan, Y.: NHDPlus dataset, watershed subdivision and SWAT model performance. Hydrol. Sci. J. <http://dx.doi.org/10.1080/02626667.2014.916408>, 2014.

Chiang, L. C., Yuan, Y., Mehaffey, M., Jackson, M., Chaubey, I.: Assessing SWAT's performance in the Kaskaskia River watershed as influenced by the number of calibration stations used. Hydrol. Process. 28, 676–687. <http://dx.doi.org/10.1002/hyp.9589>, 2014.

Choi, S. U. and Lee, J.: Assessment of total sediment load in rivers using lateral distribution method, J. Hydro Environ. Res., 9, 381–387, doi:10.1016/j.jher.2014.06.002, 2015.

Ciesiolka, C. A., Coughlan, K. J., Rose, C. W., Escalante, M. C., Hashim, G. M., Paningbatan, E. P., and Sombatpanit, S.: Methodology for a multi-country study of soil erosion management, Soil Technol., 8, 179–192, 1995.

Colby, B. R.: Relationship of sediment discharge to streamflow. US Geol. Survey Open File Report, 1956.

Conacher, A. J. and Jeanette Conacher.: Rural land degradation in Australia. Oxford University Press, 1995.

Conway, D.: A water balance model of the Upper Blue Nile in Ethiopia, Hydrological Sciences Journal, 42:2, 265-286, DOI: 10.1080/02626669709492024, 1997.

Conway, D.: The Climate and Hydrology of the Upper Blue Nile River, The Geographical Journal, Vol. 166, No. 1, pp. 49-62, March, 2000.

Costard, F., Forget, F., Mangold, N. and Peulvast, J. P.: Formation of recent martian debris flows by melting of near-surface ground ice at high obliquity. Science 295, 110–

113, 2002.

Crawford, C.G.: LOADEST2 Version 1.101: Single Station Version of LOADEST, a Program to Calculate Mean River Loads at 149 Coastal National Stream Quality Accounting Network (NASQAN) Stations. 5957 Lakeside Boulevard, Indianapolis, Indiana 46278: USGS in Cooperation with the National Oceanic and Atmospheric Administration, 1998.

Daba, S., Rieger, W., and Strauss, P.: Assessment of gully erosion in eastern Ethiopia using photogrammetric techniques, CATENA, Volume 50, Issues 2-4, Pages 273-291, 1 January 2003, [https://doi.org/10.1016/S0341-8162\(02\)00135-2](https://doi.org/10.1016/S0341-8162(02)00135-2), 2003.

De Almeida Bressiani, D., Srinivasan, R., Jones, C. A., and Mendiondo, E. M.: Effects of different spatial and temporal weather data resolutions on the stream flow modeling of a semiarid basin, Northeast Brazil, Int. J. Agr. Biol. Eng., 8, 1-16, doi:10.3965/j.ijabe.20150803.970, 2015.

de Vente, J., Poesen, J.: Predicting soil erosion and sediment yield at the basin scale: scale issues and semi-quantitative models. Earth Sci. Rev. 71, 95-125, 2005.

Derib, S.: Balancing water availability and water demand in the Blue Nile: A case study of Gumara watershed in Ethiopia (Ph.D). University of Bonn, Germany, 2013.

Descheemaeker, K., Nyssen, J., Rossi, J., Poesen, J., Mitiku Haile, Moeyersons, J., Deckers, J.: Sediment deposition and pedogenesis in exclosures in the Tigray Highlands, Ethiopia. Geoderma, in press, doi:10.1016/j.geoderma.2005.04.027, 2005.

Dessie, M., Verhoest, N. E. C., Pauwels V. R. N., Adgo, E. Deckers, J., Poesen, J., Nyssen, J.: Water balance of a lake with floodplain buffering: Lake Tana, Blue Nile Basin, Ethiopia, Journal of Hydrology, Volume 522, Pages 174-186, 2015.

Dessie, M., Verhoest, N. E. C., Pauwels, V. R. N., Admasu, T., Poesen, J., Adgo, E., Deckers, J. and Nysse, J.: Analyzing runoff processes through conceptual hydrological modelling in the Upper Blue Nile Basin, Ethiopia, Hydrol. Earth Syst. Sci., 18, 5149-5167, doi:10.5194/hess-18-5149-2014, 2014.

Desta, G., Nyssen, J., Poesen, J., Deckers, J., Mitiku Haile, Govers, G., Moeyersons, J.: Effectiveness of stone bunds in controlling soil erosion on cropland in the Tigray Highlands, Northern Ethiopia. Soil Use and Management, 2005.

Dile, Y. T. and Srinivasan, R.: Evaluation of CFSR climate data for hydrologic prediction in data-scarce watersheds: an application in the Blue Nile River Basin. JAWRA Journal of the American Water Resources Association, 50(5), 1226-1241, doi:10.1111/jawr.12182, 2014.

Duan, N.: Smearing estimate: a nonparametric retransformation method. J. American Statistical Association, 78(383), 605-610, 1983.

Duan, Q.; Gupta, H.V.; Sorooshian, S.; Rousseau, A.N. and Turcotte R.: Calibration of Watershed Models, American Geophysical Union, Washington, DC, USA, 2003.

Eberhart, R. and Kennedy, J.: "A new optimizer using particle swarm theory." Micro Machine and Human Science, 1995. MHS'95., Proceedings of the Sixth International Symposium on. IEEE, 1995.

Easton, Z. M., Fuka, D. R., White, E. D., Collick, A. S., Biruk, A. B., McCartney, M., Awulachew, S. B., Ahmed, A. A., and Steenhuis, T. S.: A multi basin SWAT model analysis of runoff and sedimentation in the Blue Nile, Ethiopia, *Hydrol. Earth Syst. Sci.*, 14, 1827–1841, doi:10.5194/hess-14-1827-2010, 2010.

Ellison, W.D.: Studies of raindrop erosion. *Agric. Eng.* 25: 131-181, 1944.

Emam, R. A., Kappas, M., Hoang Khanh Nguyen, L. and Renchin, T.: Hydrological Modeling in an Ungauged Basin of Central Vietnam Using SWAT Model, *Hydrol. Earth Syst. Sci. Discuss.*, doi:10.5194/hess-2016-44, 2016.

ENTRO: Water Atlas of the Blue Nile Sub-Basin, Draft Report, Eastern Nile Technical Regional Office (ENTRO), Ethiopia, 2006.

Ethiopian Agricultural Research Organization (EARO): Annual Report of Soil Department, Addis Ababa, Ethiopia, 1988.

FAO: Agro-climatic Resource Inventory for Land use Planning. Ethiopia. Technical Report 2. AG: DP/ETH/78/003, Rome, 1984a.

FAO: Assistance to Land use Planning in Ethiopia. Land use, Production Regions and Farming Systems Inventory. Technical Report 3. AG: DP/ETH/78/003. Rome, 1984b.

FAO: Ethiopian highland reclamation study: Ethiopia. Rome, Food and Agriculture Organization of the United Nations, 1986.

FAO: Land use and Production Systems. Assistance to land use planning, Ethiopia Technical Report 4, AG: DP/ETH/781003, Rome, 1984c.

FAO: Provisional Soil Map of Ethiopia. Land Use Planning Project. Addis Ababa, Ethiopia, Ministry of Agriculture (MoA) 2000. Agroecological Zonations of Ethiopia. Addis Ababa, Ethiopia, 1984d.

FAO: Salt-Affected Soils and their Management, *FAO Soils Bulletin* 39, 1988.

FAO: World reference base for soil resources 2014: International soil classification system for naming soils and creating legends for soil maps. *World Soil Resources Report*, 2014.

Farres, P.: "The dynamics of rainsplash erosion and the role of soil aggregate stability." *Catena* 14(1-3): 119-130, 1987.

Ferguson, R. I.: "Accuracy and Precision of Methods for Estimating River Loads." *Earth Surface Processes and Landforms* 12 (1): 95–104. doi:10.1002/esp.3290120111, 1987.

Ferguson, R.I.: River Loads Underestimated by Rating Curves. *Water Resour. Res.* 22(1), 74–76, 1986.

Folle, F., Dalzell, B. and Mulla, D.: Evaluation of Best Management Practices (BMPs) in Impaired Watersheds Using the SWAT Model, Department of Soil, Water and Climate University of Minnesota, USA, 2007.

Fuka D. R., Walter M. T., MacAlister C., Degaetano A. T., Steenhuis T. S., Easton Z. M.: Using the Climate Forecast System Reanalysis as weather input data for watershed models, *Hydrol. Process.*, 28, pages 5613–5623, doi: 10.1002/hyp.10073, 2014.

Fullen, M. A. and Reed, A. H.: Rill erosion on arable loamy sands in the West Midlands of England, *Catena supplement*, 85-96, 1987.

Gao, P.: Understanding watershed suspended sediment transport, *Progress in Physical Geography*, 32, 243–264, 2008.

Garcia, M. and Parker, G.: Entrainment of bed sediment into suspension. *Journal of Hydraulic Engineering*, 117(4), 414-435. DOI: 10.1061/(ASCE)0733-9429(1991)117:4(414), 1991.

Gasser, W.: Simulation of erosion of ungauged subcatchments in the Blue Nile Basin, Master's Thesis, Technische Universität München, Munich, Germany, 2016.

Gassman, W. P., Reyes, M. R., Green, C. H. and Arnold, J. G.: The soil and water assessment tool: historical development, applications, and future research direction, *T. ASABE*, 50, 1211-1250, 2007.

Gebremicael, T. G., Mohamed, Y. A., Betrie, G. D., van der Zaag, P., and Teferi, E.: Trend analysis of runoff and sediment fluxes in the Upper Blue Nile basin: A combined analysis of statistical tests, physically-based models and landuse maps, *J. Hydrol.*, 482, 57–68, doi:10.1016/j.jhydrol.2012.12.023, 2013.

Griensven, A., Ndomba, P., Yalew, S., and Kilonzo, F.: Critical review of SWAT applications in the upper Nile basin countries, *Hydrol. Earth Syst. Sci.*, 16, 3371–3381, 2012.

Gupta, H. V., Sorooshian, S. and Yapo, P. O.: Status of auto-matic calibration for hydrologic models: Comparison with multilevel expert calibration, *J. Hydrologic Eng.*, 4(2): 135-143, 1999.

Guzman, C. D., Tilahun, S. A., Zegeye, A. D., and Steenhuis, T. S.: Suspended sediment concentration–discharge relationships in the (sub-) humid Ethiopian highlands, *Hydrol. Earth Syst. Sci.*, 17, 1067–1077, doi:10.5194/hess-17-1067-2013, 2013.

Hairsine, P. B. and Rose, C.W.: Modeling water erosion due to overland flow using Physical principles 1. Sheet flow, *Water Resour. Res.*, 28, 237–243, 1992.

Hargreaves, G. H. and Samani, Z. A.: Estimating potential evaporation. *J. Irrig. Drain. Eng.-ASCE*, 108(3), 225-230, 1982.

Hargreaves, G. H. and Samani, Z. A.: Reference crop evapotranspiration from temperature. *Applied Engineering in Agriculture* 1:96-99, 1985.

Hassan, A.: Water Balance Model for the Eastern Nile Basin, Final Report Volume I (Main Report), Eastern Nile Planning Model (ENPM) Project, Dhaka, October, 2012

Hauhs, M. and Lange, H.: Classification of runoff in headwater catchments: A physical problem?, *Geography Compass*, 2(1), 235–254, 2008.

HEC (Hydrologic Engineering Center): Flow Transitions in Bridge Backwater Analysis, US Army Corps of Engineers, Davis, CA, pp.71, 1995.

Hengsdijk, H., Meijerink, G., Mosugu, M.: Modelling the effect of three soil and water conservation practices in Tigray, Ethiopia. *Agric. Ecosyst. Environ.* 105, 29–40, 2005.

Heusch B.: Aménagement de terroir: techniques de lutte contre l'érosion. CNEARC

Montpellier, 199 p., 1988.

Hewlett, J. D. and A.R. Hibbert: Factors affecting the response of small watersheds to precipitation in humid areas. In W.E. Sopper and H.W. Lull, editors, *Forest hydrology. Proceedings of the international symposium on forest hydrology*. Penn State Univ., University Park, PA. p. 275–290, 1967.

Hickin, E. J.: *River Geomorphology*. Wiley, 1995.

Horowitz, A. J.: A quarter century of declining suspended sediment fluxes in the Mississippi River and the effect of the 1993 flood, *Hydrol. Process.*, 24, 13–34, 2010.

Horowitz, A. J.: “An Evaluation of Sediment Rating Curves for Estimating Suspended Sediment Concentrations for Subsequent Flux Calculations.” *Hydrological Processes* 17 (August): 3387–3409, 2003.

Hu, B., Wang, H., Yang, Z. and Sun, X.: “Temporal and Spatial Variations of Sediment Rating Curves in the Changjiang (Yangtze River) Basin and Their Implications.” *Quaternary International* 230 (1–2): 34–43, 2011.

Huber, H.: Investigation of Hydrologic Response Unit (HRU) Discretization for Erosion Modelling with SWAT in the Upper Blue Nile Basin, Master’s Thesis, Technische Universität München, Munich, Germany, 2015.

Hudson, N.W.: *Soil Conservation*, Batsford, London, 320 p., 1973.

Jha, M., Gassman, P.W., Secchi, S., Gu, R. and Arnold, J.: Effects of watershed subdivision on SWAT flow, sediment and nutrient predictions. *J. Am. Water Resour. Assoc.* 40, 811–825, 2004.

Jones, A., Breuning-Madsen, H., Brossard, M., Dampha, A., Deckers, J., Dewitte, O., Gallali, T., Hallett, S., Jones, R., Kilasara, M., Le Roux, P., Micheli, E., Montanarella, L., Spaargaren, O., Thiombiano, L., Van Ranst, E., Yemefack, M. and Zougmore, R.: *Soil Atlas of Africa*. European Commission, Publications Office of the European Union, Luxembourg, 2013.

Julien, P.Y. and Simons, D.B.: *Sediment Transport Capacity of Overland Flow*. s.l., American Society of Agricultural Engineers, Transactions of the ASAE, 1985. pp. 755–762. Vol. 28, 1985.

Kabir, M.A., Dutta, D. and Hironaka, S.: Estimating sediment budget at a river basin scale using a process-based distributed modelling approach. *Water Resour Manage* 28:4143–4160, 2014.

Kebede, S., Travi, Y., Alemayehu, T., and Marc, V.: Water balance of Lake Tana and its sensitivity to fluctuations in rainfall, Blue Nile basin, Ethiopia, *J. Hydrol.*, 316, 233–247, 2006.

Kheirfam, H. and Vafakhah M.: Assessment of some homogeneous methods for the regional analysis of suspended sediment yield in the south and southeast of the Caspian Sea, *J. Earth Syst. Sci.*, 124, 1247–1263, doi:10.1007/s12040-015-0604-7, 2015.

Knisel, W. G.: *CREAMS. A field-scale model for chemicals, runoff and erosion from agricultural management systems*, USDA Conservation Research Report, 640 pp. 1980.

Kokpinar, M. A., Altan-Sakarya, A. B., Kumcu, S. Y., and Gogus, M.: Assessment of

sediment yield estimations for large watershed areas: a case study for the Seyhan, Demirkopru and Hirfanli reservoirs in Turkey, *Hydrol. Sci. J.*, 60, 2189–2203, doi:10.1080/02626667.2014.959954, 2015.

Konnerth, I.: SWAT for Assessing Negative Impacts of Erosion in Lake Tana Basin, Master's Thesis, Technische Universität München, Munich, Germany, August, 2016.

Kumar, S. and Mishra, A.: Critical Erosion Area Identification Based on Hydrological Response Unit Level for Effective Sedimentation Control in a River Basin. *Water Resour Manage* (2015) 29:1749-1765, 2014.

Kuczera, G. and Parent, E.: Monte Carlo assessment of parameter uncertainty in conceptual catchment models: the Metropolis algorithm, *Journal of Hydrology* 1(1), 69-85. DOI: 10.1016/S0022-1694(98)00198-X, 1998.

Legates, D. R. and McCabe, G. J.: "Evaluating the use of "goodness-of-fit" measures in hydrologic and hydroclimatic model validation." *Water resources research* 35.1 (1999): 233-241, 1999.

Leopold, L. B., and Thomas Maddock.: *The Hydraulic Geometry of Stream Channels and Some Physiographic Implications*. PP - 252. United States Geological Survey. <http://pubs.er.usgs.gov/publication/pp252>, 1953.

Liu, B. M., Collick, A. S., Zeleke, G., Adgo, E., Easton, Z. M. and Steenhuis, T. S.: Rainfall-discharge relationships for a monsoonal climate in the Ethiopian highlands. *Hydrol. Processes* 22:1059–1067. doi:10.1002/hyp.7022, 2008.

Lyon, S.W., Walter, M.T., Gerard-Marchant, P., and Steenhuis, T.S.: Using a topographic index to distribute variable source area runoff predicted with the SCS curve-number equation. *Hydrological Processes*. 18, 2757-2771, 2004.

Luk, S.: "Effect of soil properties on erosion by wash and splash." *Earth Surface Processes* 4(3): 241-255, 1979.

Makombe, G., Kelemework, D. and Aredo, D.: A comparative analysis of rainfed and irrigated agricultural production in Ethiopia, *Irrig Drainage Syst*, 21: 35. doi:10.1007/s10795-007-9018-2, 2007.

Makombe, G.; Namara, R.; Hagos, F.; Awulachew, S. B.; Ayana, M.; Bossio, D.: A comparative analysis of the technical efficiency of rain-fed and smallholder irrigation in Ethiopia. Colombo, Sri Lanka: International Water Management Institute. 37p. (IWMI Working Paper 143), 2011.

Malunjkar, V. S., Shinde, M. G., Ghotekar, S. S. and Atre, A. A.: Estimation of Surface Runoff using SWAT Model. *International Journal of Inventive Engineering and Sciences (IJIES)* ISSN: 2319–9598, Volume-3 Issue-4, March, 2015.

Marshall, L.; Nott, D. and Sharma A.: A comparative study of Markov chain Monte Carlo methods for conceptual rainfall-runoff modeling, *Water Resour. Res.*, 40, W02501, doi:10.1029/2003WR002378, 2004.

Mamo, M. K. and K. Jain, M.: Runoff and Sediment Modeling Using SWAT in Gumera Catchment, Ethiopia. *Open Journal of Modern Hydrology*, 03(04), 196-205. <http://dx.doi.org/10.4236/ojmh.2013.34024>, 2013.

Maraun, D., Wetterhall, F., Ireson, A. M., Chandler, R. E., Kendon, E. J., Widmann, M., Brienen, S., Rust, H. W., Sauter, T., Themeßl, M., Venema, V. K. C., Chun, K. P., Goodess, C. M., Jones, R. G., Onof, C., Vrac, M., and Thiele-Eich, I.: Precipitation downscaling under climate change: Recent developments to bridge the gap between dynamical models and the end user, *Reviews of Geophysics*, 48, doi:10.1029/2009RG000314, 2010.

Masoumeh, R. and Mehdi, F.: Estimating Suspended sediment concentration by a neural differential evolution (NDE) and comparison to ANFIS and three ANN Models, *Disaster Adv.*, 5, 346–359, 2012.

McClellan, T.; Deenik, J.; Singleton, P.: Soil Nutrient Management for Maui County, University of Hawaii, College of Tropical Agriculture and Human Resources (CTAHR), 2016.

McDonnell, J. J., Sivapalan, M., Vache, K., Dunn, S., Grant, G., Haggerty, R., Hinz, C., Hooper, R., Kirchner, J., Roderick, M. L., Selker, J. and Weiler, M.: Moving beyond heterogeneity and process complexity: a new vision for watershed hydrology, *Water Resour. Res.*, 43, 1-6, 2007.

McMahon, T. A., Finlayson, B. L. and Gippel, C. J.: *Stream Hydrology: An Introduction for Ecologists*. John Wiley and Sons, 2004.

Me, W., Abell, J. M., and Hamilton, D. P.: Effects of hydrologic condition on SWAT model performance and parameter sensitivity for a small, mixed land use catchment in New Zealand, *Hydrol. Earth Syst. Sci.*, 19, 4127-4147, doi:10.5194/hess-19-4127-2015, 2015.

Meade, R. H. and Moody, J. A.: “Causes for the Decline of Suspended-Sediment Discharge in the Mississippi River System, 1940–2007.” *Hydrological Processes* 24 (1): 35–49. doi:10.1002/hyp.7477, 2010.

Mekonnen, M. A., Wörman, A., Dargahi, B. and Gebeyehu, A.: Hydrological modelling of Ethiopian catchments using limited data. *Hydrol. Process.*, 23: 3401–3408. doi:10.1002/hyp.7470, 2009.

Melesse, A. M., Abtew, W., Setegn, S. G., and Dessalegne, T.: Hydrological Variability and Climate of the Upper Blue Nile River Basin. In A. M. Melesse (Ed.), *Nile River Basin: Hydrology, Climate and Water Use*, 2011.

Mengistu, D. T. and Sorteberg, A.: Sensitivity of SWAT simulated streamflow to climatic changes within the Eastern Nile River basin, *Hydrol. Earth Syst. Sci.*, 16, 391-407, doi:10.5194/hess-16-391-2012, 2012.

Miller, C. R.: Analysis of flow-duration, sediment-rating curve method of computing sediment yield, Denver, US Bureau of Reclamation, 55 pp., 1951.

Minnesota Department of Agriculture: Conservation Practices. Minnesota Department of Agriculture. [Online] 2016. [Cited: October 12, 2016.] <http://www.mda.state.mn.us/protecting/conservation/practices/contourstrip.aspx>, 2016.

Miserez, A.: Soil erodibility and mapping in different hydrological land systems of Lake Tana basin, Ethiopia, MSc thesis study, Department of Soil and Water Management, KULeuven, Leuven, Belgium, 2016.

Mishra, A., Kar, S. and Singh, V. P.: Prioritizing structural management by quantifying the effect of LULC on watershed runoff and sediment yield. *Water Resour Manage* 21:1899–1913, 2007.

MoA (Ministry of Agriculture): Natural Resources Management Directorates, Small-Scale Irrigation Situation Analysis and Capacity Needs Assessment, Addis Ababa, Ethiopia, 2011.

Moges, M. A., Zemale, F. A., Alemu, M. L., Ayele, G. K., Dagneu, D. C., Tilahun, S. A., and Steenhuis, T. S.: Sediment concentration rating curves for a monsoonal climate: upper Blue Nile, *SOIL*, 2, 337-349, doi:10.5194/soil-2-337-2016, 2016.

Monteith, J. L.: "Evaporation and environment." *Symp. Soc. Exp. Biol.* Vol. 19. No. 205-23, 1965.

Morehead, M. D., Syvitski, J. P., Hutton, E. W. H., and Peckham, S. D.: "Modeling the Temporal Variability in the Flux of Sediment from Ungauged River Basins." *Global and Planetary Change* 39 (1–2): 95–110. doi:10.1016/S0921-8181(03)00019-5, 2003.

Morgan, R. P. C.: *Soil Erosion and Conservation*. 2nd ed. Longman, London, 1995.

Moriasi, D. N., Arnold, J. G., Van Liew, M. W., Bingner, R. L., Harmel, R. D., and Veith, T. L.: Model evaluation guidelines for systematic quantification of accuracy in watershed simulations, *T. ASABE*, 50, 885–900, 2007.

MoWR (Ministry of Water Resources): *Irrigation Development Strategy (Component of the Water Sector Development Strategy)*. Draft Report, Addis Ababa, Ethiopia, 2001.

Mu, Q., Heinsch, F. A., Zhao, M. and Running, S.W.: Development of a global evapotranspiration algorithm based on MODIS and global meteorology data. *Remote Sensing of Environment*, 111, 519–536, 2007.

Mu, Q., Zhao, M. and Running, S. W.: Improvements to a MODIS global terrestrial evapotranspiration algorithm. *Remote Sensing of Environment*, 115, 1781–1800, 2011.

Mueller, G. and Foerstner, U.: General relationship between suspended sediment Concentrations and water discharge in the Alpenrhein and some other rivers, *Nature*, 217, 244–245, 1968.

Mulungu, D. M. M. and Munishi, S. E.: Simiyu river catchment parameterization using SWAT model, *J. Phys. Chem. Earth A/B/C*, 32, 1032–1039, 2007.

Nash, J. E. and Sutcliffe, J. V.: River flow forecasting through conceptual models, Part I: A discussion of principles, *Journal of Hydrology* 10(3), pp.282–290, 1970.

Naudts, J.: *Les Hautes Terres de Tembien, Tigre', Ethiopie; Re'sistance et limites d'une ancienne civilisation agraire; Conse'- quences sur la de'gradation des terres. Me'moire pre'sente' en vue de l'obtention du Diplo'me d'Agronomie Tropicale*. CNEARC, Montpellier, 147 pp., 2002.

Nearing, M., Foster, G., Lane, L., and Finkner, S.: A process-based soil erosion model for USDA-Water Erosion Prediction Project technology, *T. Am. Soc. Agr. Biol. Eng.*, 32, 1587–1593, 1989.

Neitsch, S. L., Arnold, J.G., Kiniry, J.R. and Williams, J. R.: *Soil and Water Assessment Tool, Theoretical Documentation Version 2009*, Grassland, Soil and Water Research

Laboratory and Blackland Research Center, Texas, 2009.

Nisar, Z.: Hydrological and Sediment Modelling of the Gumera Catchment using SWAT and SHETRAN, Master's Thesis, Technische Universität München, Munich, Germany, 2016.

Nyssen, J., Haregeweyn, N., Descheemaeker, K., Desta, G., Vancampenhout, K., Poesen, J., Haile, M., Moeyersons, J., Buytaert, W., Naudtsf, J., Deckers, J., Govers, G.: Comment on "Modelling the effect of soil and water conservation practices in Tigray, Ethiopia", *Agric. Ecosyst. Environ.* 105, 29–40, 2005.

Nyssen, J., Poesen, J., Desta, G., Vancampenhout, K., D'aes, M., Yihdego, G., Govers, G., Leirs, H., Moeyersons, J., Naudts, J., Haregeweyn, N., Haile, M. and Deckers, J.: Interdisciplinary on-site evaluation of stone bunds to control soil erosion on cropland in Northern Ethiopia." *Soil and Tillage Research*, Volume 94, Issue 1, Pages 151–163, 2007.

Parsakhoo, A., Hosseini, S.A., Lotfallan, M. and Jalilvand, H.: Soil loss and displacement by heavy equipment in forest road sub grading projects. *Int J Sediment Res* 24:227–235, 2009.

Peters-Kümmerly, B.E.: Untersuchungen u"ber Zusammensetzung und Transport von Schwebstoffen in einigen Schweizer Flu"ssen. *Geographica Helvetica* 28, 137–151, 1973.

Phillips, J. M., Webb, B. W., Walling, D. E., and Leeks, G. J. L.: Estimating the suspended sediment loads of rivers in the LOIS study area using infrequent samples, *Hydrol. Process.*, 13, 1035– 1050, 1999.

Pimentel, D., Harvey, C., Resosudarmo, P., Sinclair, K., Kurz, D., McNair, M., Crist, S., Shpritz, L., Fitton, L., Saffouri, R. and Blair, R.: Environmental and economic costs of soil erosion and conservation benefits. *Science* 267: 1117–1123, 1995.

Polanco, E. I., Fleifle, A., Ludwig, R., and Disse, M.: Improving SWAT model performance in the upper Blue Nile Basin using meteorological data integration and subcatchment discretization, *Hydrol. Earth Syst. Sci.*, 21, 4907-4926, <https://doi.org/10.5194/hess-21-4907-2017>, 2017.

Pye, K.: *Sediment Transport and Depositional Processes*. Blackwell Scientific Publication, 1994.

Rahman, H.: Potential Climate Change Impacts on Hydrology and Water Resources of the Upper Blue Nile River Basin, Ethiopia, Master's Thesis, Technische Universität München, Munich, Germany, August, 2016.

Ritter, J.: *Soil Erosion – Causes and Effects*, FACTSHEET, ISSN 1198-712X, Queen's Printer for Ontario, October, 2012.

Roth, L. and Lemann, T.: Comparing CFSR and conventional weather data for discharge and soil loss modelling with SWAT in small catchments in the Ethiopian Highlands, *Hydrol. Earth Syst. Sci.*, 20, 921–934, 2016.

Ruhoff, A. L., Paz, A. R., Aragao, L. E. O. C., Mu, Q., Malhi, Y., Collischonn, W., Rocha, H. R. and Running, S. W.: Assessment of the MODIS global evapotranspiration algorithm using eddy covariance measurements and hydrological modelling in the Rio Grande basin, *Hydrological Sciences Journal – Journal des Sciences Hydrologiques*, 58 (8), 2013.

Santhi, C., Arnold, J. G., Williams, J. R., Dugas, W. A., Srinivasan, R. and Hauck, L. M.: Validation of the SWAT model on a large river basin with point and nonpoint sources, *Journal of the American water resources association*, Vol. 37, No. 5, October, 2001.

Setegn, S. G., Darfahi, B., Srinivasan, R., and Melesse, A. M.: Modeling of sediment yield from Anjeni-gauged watershed, Ethiopia using SWAT model, *J. Am. Water Resour. Assoc.*, 46, 514–526, doi:10.1111/j.1752-1688.2010.00431.x, 2010.

Setegn, S. G., Srinivasan, R. and Dargahi, B.: Hydrological Modelling in the Lake Tana Basin, Ethiopia Using SWAT Model, *Open Hydrol. J.*, 2, 49–62, 2008.

Setegn, S. G., Srinivasan, R., Dargahi, B., and Melesse, A. M.: Spatial delineation of soil erosion vulnerability in the Lake Tana Basin, Ethiopia, *Hydrol. Process.*, 23, 3738–3750, doi:10.1002/hyp.7476, 2009.

Setegn, S. G., Srinivasan, R., Melese, A. M., and Dargahi, B.: SWAT model application and prediction uncertainty analysis in the Lake Tana Basin, Ethiopia. *Hydrological processes* *Hydrol. Process.*, 24, 357–367, 2010.

Sharpley, A. N. and Williams, J. R.: EPIC-Erosion Productivity Impact Calculator, 1. Model Documentation, 1990.

Shehata, O.: Identifying spatial and temporal uncertainties of CFSR data by averaging gridded values in the Upper Blue Nile River Basin, Ehtiopia, Bachelor's Thesis, Technische Universität München, Munich, Germany, 2016.

Sichingabula, Henry M.: "Factors Controlling Variations in Suspended Sediment Concentration for Single-Valued Sediment Rating Curves, Fraser River, British Columbia, Canada." *Hydrological Processes* 12 (12): 1869–94. doi:10.1002/(SICI)1099-1085(19981015)12:123.0.CO;2-G, 1998.

Silva R.M., Montenegro S. M. G. L. and Santos C. A. G.: Integration of GIS and remote sensing for estimation of soil loss and prioritization of critical sub-catchments: a case study of Tapacura catchment. *Nat Hazards* 62:953–970, 2012.

Sivapalan, M.: Pattern, process and function: Elements of a unified theory of hydrology at the catchment scale, *Encyclopedia of Hydrological Sciences*, edited by: Anderson, M. G., John Wiley & Sons, Ltd., 2006.

SKYbrary Aviation Safety: Inter Tropical Convergence Zone (ITCZ) - Skybrary.aero, from [http://www.skybrary.aero/index.php/Inter_Tropical_Convergence_Zone_\(ITCZ\)](http://www.skybrary.aero/index.php/Inter_Tropical_Convergence_Zone_(ITCZ)), 2016.

Steenhuis, T. S., Collick, A. S., Easton, Z. M., Leggesse, E. S., Bayabil, H. K., White, E. D., Awulachew, S. B., Adgo, E., and Ahmed, A. A.: Predicting Discharge and Erosion for the Abay (Blue Nile) with a simple model, *Hydrol. Process.*, 23, 3728– 3737, 2009.

Steenhuis, T. S., Hrnčíř, M., Poteau, D., Romero Luna, E. J., Tilahun, S. A., Caballero, L. A. Guzman, C. D., Stoof, C. R., Šanda, M., Yitaferu, B., and Císlerová, M.: A Saturated Excess Runoff Pedotransfer Function for Vegetated Watersheds. *Vadose Zone J.* 12. doi:10.2136/vzj2013.03.0060, 2013.

Steenhuis, T.S., Winchell, M., Rossing, J., Zollweg, J.A., and Walter, M.F.: SCS runoff equation revisited for variable-source runoff areas. *Journal of Irrigation and Drainage Engineering*. 121(3), 234-238, doi:10.1061/(ASCE)0733-9437,1995.

Syvitski, J. P., Morehead, M. D., Bahr, D. B. and Mulder, T. "Estimating Fluvial Sediment Transport: The Rating Parameters." *Water Resources Research* 36 (9): 2747–60. doi:10.1029/2000WR900133, 2000.

Sun, Z., Wang, Q., Ouyang, Z., Watanabe, M., Matsushita, B. and Fukushima, T.: Evaluation of MOD16 algorithm using MODIS and ground observational data in winter wheat field in North China Plain, *Hydrol. Process.* 21, 1196–1206, 2007.

Swallow, B. M., Sang, J. K., Nyabenge, M., Bundotich, D. K., Duraiappah, A. K., and Yatich, T. B.: Tradeoffs, synergies and traps among ecosystem services in the Lake Victoria basin of East Africa, *Environ. Sci. Pol.*, 12, 504–519, doi:10.1016/j.envsci.2008.11.003, 2009.

Tanveer, A., Ghulam, N., Boota, M. W., Fiaz, H., Azam, M. I., Jun, J. H., Faisal, M.: Uncertainty analysis of runoff and sedimentation in a forested watershed using sequential uncertainty fitting method, *Sciences in Cold and Arid Regions*, 8(4): 297–310, 2016.

Tekleab S., Uhlenbrook S., Mohamed Y., Savenije H. H. G., Temesgen M., and Wenninger J.: Water balance modeling of Upper Blue Nile catchments using a top-down approach, *Hydrol. Earth Syst. Sci.*, 15, 2179–2193, 2011.

Tesemma, Z. K., Mohamed, Y. A. and Steenhuis, T. S.: Trends in rainfall and runoff in the Blue Nile Basin: 1964–2003. *Hydrol. Process.*, 24: 3747–3758. doi:10.1002/hyp.7893, 2010.

Thodsen, H., Hasholt, B. and Pejrup, M.: Transport of phosphorous, wash load and suspended sediment in the River Varde Å in Southwest Jutland, Denmark. In: *Sediment Transfer through the Fluvial System (Proc. Moscow Symposium, August 2004)*, 466–473. IAHS Pub.288, IAHS Press Wallingford, UK, 2004.

Thomas, R. B.: "Monitoring Baseline Suspended Sediment in Forested Basins: The Effects of Sampling on Suspended Sediment Rating Curves." *Hydrological Sciences Journal* 33 (5): 499–514. doi:10.1080/02626668809491277, 1988.

Tibebe, D. and Bewket, W.: Surface runoff and soil erosion estimation using the SWAT model in the Keleta watershed, Ethiopia, *Land Degrad. Develop.*, 22, 551–564, doi:10.1002/ldr.1034, 2011.

Tilahun, S. A., Mukundan, R., Demisse, B. A., Engda, T. A., Guzman, C. D., Tarakegn, B. C., Easton, Z. M., Collick, A. S., Zegeye, A. D., Schneiderman, E. M., Parlange J. Y., and Steenhuis, T. S.: A Saturation Excess Erosion Model, *T. Am. Soc. Agr. Biol. Eng.*, 56, 681–695, 2013a.

Tilahun, S. A., Guzman, C. D., Zegeye, A. D., Ayana, E. K., Collick, A. S., Yitaferu, B., and Steenhuis, T. S.: Spatial and Temporal Patterns of Soil Erosion in the Semi-humid Ethiopian Highlands: A Case Study of Debre Mawi Watershed. In *Nile River Basin: Ecohydrological Challenges, Climate Change and Hydropolitics*, 149–163, edited by: Melesse, A. M., Abtew, W., and Setegn, G. S., Springer International Publishing Switzerland, 2013b.

Tilahun, S. A., Guzman, C. D., Zegeye, A. D., Engda, T. A., Collick, A. S., Rimmer, A., and Steenhuis, T. S.: An efficient semi-distributed hillslope erosion model for the subhumid Ethiopian Highlands, *Hydrol. Earth Syst. Sci.*, 17, 1051–1063, doi:10.5194/hess-17-

1051-2013, 2013c.

Torri, D., M. Sfalanga and Chisci, G.: Threshold Conditions for Incipient Rilling. Bryan, R.B. (ed). Rill Erosion: Processes and Significance. Catena Supplement 8. W. Germany:Catena Verlag. 97-105, 1987.

Tran, V. T. T.: AN ANALYSIS OF THE SUSPENDED SEDIMENT RATING CURVE PARAMETERS IN THE UPPER MISSISSIPPI RIVER BASIN AT THE MONTHLY AND ANNUAL LEVELS, Trace: Tennessee Research and Creative Exchange, University of Tennessee, Knoxville, August, 2014.

Uhlenbrook, S., Mohamed, Y., and Gagne, A. S.: Analyzing catchment behavior through catchment modeling in the Gilgel Abay, Blue Nile Basin, Ethiopia, *Hydrol. Earth Syst. Sci.*, 14, 2153–2165, doi:10.5194/hess-14-2153-2010, 2010.

Van Griensven, A. and Bauwens, W.: Multi-objective auto-calibration of semidistributed water quality models, *Water Resources Research* 39 (12): 1348, DOI: 10.1029/2003WR002284, 2003.

Van Griensven, A. and Meixner, T.: Methods to quantify and identify the sources of uncertainties for river basin water quality models. *Water Science and Technology*, 53(1): 51-59, 2006.

Van Liew, M. W., and Garbrecht, J.: HYDROLOGIC SIMULATION OF THE LITTLE WASHITA RIVER EXPERIMENTAL WATERSHED USING SWAT, Volume 39, Issue 2, 10.1111/j.1752-1688.2003.tb04395.x, Pages 413–426, April 2003.

Vigiak, O.; Malagó, A.; Bouraoui, F.; Vanmaercke, M.; Poesen, J.: Adapting SWAT hillslope erosion model to predict sediment concentrations and yields in large Basins. *Science of the Total Environment* 538: 855-875, 2015.

Vrugt, J. A., Gupta, H. V.; Bouten, W. and Sorooshian, S.: A Shuffled Complex Evolution Metropolis algorithm for optimization and uncertainty assessment of hydrologic model parameters, *Water Resour. Res.*, 39, 1201, doi:10.1029/2002WR001642, 8, 2003.

Wale, A.: Hydrological balance of Lake Tana Upper Blue Nile Basin, Ethiopia, Enschede, Netherlands, 2008.

Wang, H. and Sun, F.: Impact of LUCC on Streamflow using the SWAT model over the Wei River Basin on the Loess Plateau of China, *Hydrol. Earth Syst. Sci. Discuss.*, doi:10.5194/hess-2016-332, in review, 2016.

Walling, D. E.: Assessing the accuracy of suspended sediment rating curves for a small basin, *Water Resour. Res.*, 13, 531–538, 1977a.

Walling, D.E.: Limitation of the rating curve technique for estimating suspended sediment loads, with particular reference to British rivers. In: *Erosion and Solid Matter Transport in Inland Waters (Proc. Paris Symposium, July 1977)*, 34–48. IAHS Pub. 122. IAHS Press Wallingford, UK, 1977b.

Walling, D.E.: Suspended sediment and solute response characteristics of the river Exe, Devon, England. In: DavidsonArnott R., Nickling W. (Eds.), *Research in fluvial systems*. Geoabstracts, Norwich, pp. 169–197, 1978.

Walling, D. E.: Suspended Sediment and Soluble Yield from a Small Catchment prior to Urbanization. In Gregory, K.J and Walling, D.E (eds) *Fluvial Processes in Instrumented Watersheds*. Institute of British Geographers Special Publication 6, IBG, 1974.

Walling, D. E. and Quine, T. A.: Calibration of caesium-137 measurements to provide quantitative erosion rate data, *Land Degrad. Develop.*, 2, 161–175, 1990.

Walling, D. E. and Webb, B.W.: “The Reliability of Rating Curve Estimates of Suspended Sediment Yield: Some Further Comments.” *Sediment Budgets* IAHS Publication No. 1974: 337–50, 1988.

Walling, D.E. and Webb, B.W.: The reliability of suspended sediment load data. *IAHS Publ.*, 133, 177–194, IAHS Press Wallingford, UK, 1981.

Werfring, A.: Typology of irrigation in Ethiopia. A thesis submitted to the University of Natural Resources and Applied Life Sciences, Vienna. Institute of Hydraulics and Rural Water Management, in partial fulfillment of the degree of Diplomingeieur, 2004.

Williams, J. R.: Sediment-yield prediction with universal equation using runoff energy factor. Present and Prospective Technology for Predicting Sediment Yield and Sources: Proceedings of the Sediment Yield Workshop 1975, USDA Sedimentation Lab., Oxford, November 28–30, 1972. ARS-S-40. 244–252, 1975.

Wischmeier, W. H., Johnson, C. B. and Cross, B. V.: A soil erodibility nomograph for farmland and construction sites. *s.l., Journal of Soil and Water Conservation*, 1971. pp. 189-193. Vol. 26, 1971.

Wischmeier, W. H. and Smith, D. D.: Predicting rainfall-erosion losses from cropland east of the Rocky Mountains: guide for selection of practices for soil and water conservation. Washington, D.C., Agricultural Research Service, 1965.

Wischmeier, W. H. and Smith, D. David: Predicting rainfall erosion losses, a guide to conservation planning. Washington, D.C., Science and Education Administration, Agriculture handbook, 1978. Vol. 537, 1978.

Worqlul, A. W., Maathuis, B., Adem, A. A., Demissie, S. S., Langan, S., and Steenhuis, T. S.: Comparison of rainfall estimations by TRMM 3B42, MPEG and CFSR with ground-observed data for the Lake Tana basin in Ethiopia, *Hydrol. Earth Syst. Sci.*, 18, 4871–4881, doi:10.5194/hess-18-4871-2014, 2014.

Yang, D.W., Kanae, S., Oki, T., Koike, T. and Musiak, K.: Global potential soil erosion with reference to landuse and climate changes. *Hydrol Process* 17:2913–2928, 2003.

Yang, G., Chen, Z., Yu, F., Wang, Z., Zhao, Y. and Wang, Z.: “Sediment Rating Parameters and Their Implications: Yangtze River, China.” *Geomorphology, Monsoon Rivers of Asia*, 85 (3–4): 166–75. doi:10.1016/j.geomorph.2006.03.016, 2007.

Yang, J., Reichert, P., Abbaspour, K. C.: Hydrological modeling of the Chaohe Basin in China: Statistical model formulation and bayesian inference. *Journal of Hydrology*, 340: 167-182. doi:10.1016/j.jhydrol.2007.04.006, 2007.

Yazew E.: Development and management of irrigated lands in Tigray, Ethiopia. PhD thesis, UNESCO/IHE Institute for Water Education, Delft, the Netherlands, 265 pp., 2005.

Yilma, A. D. and Awulachew, S. B.: Characterization and atlas of the Blue Nile Basin and its sub basins. In: Improved water and land management in the Ethiopian highlands: its impact on downstream stakeholder's dependent on the Blue Nile. Intermediate Results Dissemination Workshop. International Livestock Research Institute (ILRI), Addis Ababa, Ethiopia.5-6 February 2009. Summary report, abstracts of papers with proceedings on CD-ROM: Colombo, Sri Lanka: International Water Management Institute (IWMI). p1-236, 2009.

Young, R. A., Onstad, C., Bosch, D., and Anderson, W. P.: AGNPS: A nonpoint-source pollution model for evaluating agricultural watersheds, *J. Soil Water Conserv.*, 44, 168–173, 1989.

Yu, B., Rose, C. W., Ciesiolka, C. A., Coughlan, K. J., and Fentie, B.: Toward a framework for Runoff and soil loss prediction using GUEST technology, *Aust. J. Soil Res.*, 35, 1191–1212, 1997.

Zhang, L., Dawes, W. R. and Walker G. R.: Predicting the effect of vegetation changes on catchment average water balance, *Tech. Rep.99/12 Coop. Res. Cent. Catch. Hydrol.*, Canberra, 1999.

Zhang, P., Liu, R., Bao, Y., Wang, J., Yu, W. and Shen, Z.: Uncertainty of SWAT model at different DEM resolutions in a large mountainous watershed. *Water Res.* 53, 132–144, 2014.

Zhang, W., Wei, X., Zheng, J., Zhu, Y. and Zhang, Y.: “Estimating Suspended Sediment Loads in the Pearl River Delta Region Using Sediment Rating Curves.” *Continental Shelf Research* 38 (April): 35–46. doi:10.1016/j.csr.2012.02.017, 2012.